

**Aus dem Institut für Tierpathologie
des Fachbereichs Veterinärmedizin
der Freien Universität Berlin**

und

**dem Fachgebiet 17 für Influenzaviren und weitere Viren des
Respirationstraktes des Robert Koch - Instituts**

**AAV-vector based vaccines for pandemic viruses:
Evaluation of broadly reactive responses against
influenza A viruses and SARS-CoV-2**

Inaugural-Dissertation

zur Erlangung des Grades
einer Doktorin der Veterinärmedizin
an der
Freien Universität Berlin

vorgelegt von

Sandra Stelzer

Tierärztin aus Hagen

Berlin 2024

Journal-Nr.: 4436

**Gedruckt mit Genehmigung des Fachbereichs Veterinärmedizin
der Freien Universität Berlin**

Dekan: Univ.-Prof. Dr. Uwe Rösler
Erster Gutachter: Univ.-Prof. Dr. Achim Gruber
Zweiter Gutachter: PD Dr. Thorsten Wolff
Dritter Gutachter: PD Dr. Christoph Gabler

Deskriptoren (nach CAB-Thesaurus):

influenza a virus, severe acute respiratory syndrome coronavirus 2,
immune response, pandemics, vaccination, vaccines, antibodies

Tag der Promotion: 10.04.2024

Meiner Familie und Uwe

“The road and the tale have both been long, would you not say so? The trip has been long and the cost has been high... but no great thing was ever attained easily. A long tale, like a tall Tower, must be built a stone at a time.”

— Stephen King, The Dark Tower

Table of Content

Table of Content	IV
List of Figures	VII
List of Tables	IX
Abbreviations/Definitions	X
1 Introduction.....	1
2 Literature Review	3
2.1 Current and past pandemics – One Health paradigms with major impact	3
2.2 Influenza viruses	4
2.2.1 Taxonomy	4
2.2.2 Morphology and replication	7
2.3 SARS-CoV-2	11
2.3.1 Taxonomy of human coronaviruses	11
2.3.2 Morphology and replication	15
2.4 The immune system.....	18
2.4.1 Immunity to IAV.....	24
2.4.2 Immunity to SARS-CoV-2	28
2.5 AAV-vectors	32
2.5.1 AAV-vectors as vaccines	35
2.6 Mouse models in influenza A virus and vaccine research	38
2.7 Research objectives and aim of study.....	40
3 Material and Methods.....	42
3.1 Material	42
3.1.1 Mouse models.....	42
3.1.2 Cell lines.....	42
3.1.3 Viruses	42
3.1.4 Plasmids	44
3.1.5 Primers	45
3.1.6 Antibodies.....	46
3.1.7 Bacteria	47
3.1.8 Enzymes.....	47
3.1.9 Kits	47
3.1.10 Consumables and Equipment	48
3.1.11 Buffers and Media	49
3.1.12 Pharmaceuticals.....	52
3.1.13 Chemicals.....	52

3.1.14	Software	55
3.2	Methods	56
3.2.1	Cloning of pAAV-vector plasmids	56
3.2.2	Verification of the pAAV-plasmids	58
3.2.3	Production of recombinant AAV-vectors	62
3.2.4	Laboratory animal work	65
3.2.5	Methods for the immunological and virological evaluation of samples	68
3.2.6	IAV-specific immunological and virological methods	70
3.2.7	SARS-CoV-2-specific immunological and virological methods	72
3.2.8	Statistics	73
4	Results	74
4.1	Influenza	74
4.1.1	AAV-HA/NP immunization results in a more broadly reactive antibody response than can be achieved with WIV immunization alone	75
4.1.2	AAV-H3 is immunogenic in mice after intranasal application and induces virus strain-specific antibodies	79
4.1.3	AAV-HA/NP immunization results in a different pattern of Fcγ-receptor activation compared to WIV-immunization	80
4.1.4	AAV-H3 induces virus strain-specific FcγR-responses	82
4.1.5	Neutralizing and hemagglutination inhibition titers display virus-strain specificity after immunization with AAV-HA/NP and WIV	83
4.1.6	Neutralizing and hemagglutination inhibition titers display virus-strain specificity after immunization with AAV-HA and AAV-H3	84
4.1.7	Induction of antibodies against the hemagglutinin stalk	84
4.1.8	Mucosal antibodies were induced in the respiratory tract after immunization with AAV-HA/NP and AAV-H3 immunization	84
4.1.9	Induction of T-cell responses	87
4.1.10	AAV-HA/NP prime-boost immunization protected mice against homologous, heterologous and heterosubtypic challenge	88
4.1.11	AAV-H3 immunization protected mice from challenge with X31	93
4.2	SARS-CoV-2	96
4.2.1	Design and in vitro evaluation of AAV-S-RBD of SARS-CoV-2 wildtype and VOCs	96
4.2.2	AAV-S-RBD immunization results in different patterns of titer development in different mouse strains	100
4.2.3	Immunogenicity of AAV-S-RBD with variant receptor-binding domains	105

4.2.4	Mucosal antibody response to the AAV-S-RBD vaccine in lung homogenates and nasal washes	106
4.2.5	Immunization with AAV-S-RBD BA.2 results in broadly reactive FcγRI-activating responses	107
4.2.6	Neutralizing titers of variant AAV-S-RBDs	109
4.2.7	T-cell responses against SARS-CoV-2 wildtype and different variant receptor-binding domains.....	109
5	Discussion	111
5.1	Influenza A	112
5.1.1	Antigens, vectors, mouse model and application routes	113
5.1.2	Immunogenic properties of AAV and WIV vaccination	115
5.2	SARS-CoV-2	123
5.2.1	Design and <i>in vitro</i> evaluation of an AAV-S-RBD vaccine.....	123
5.2.2	Immunogenicity of the AAV-S-RBD vector vaccine	126
5.3	Perspective and Outlook	131
6	Summary	133
7	Zusammenfassung.....	135
8	Bibliography.....	137
9	Appendix	183
10	List of Publications	189
10.1	Oral Presentations	189
10.2	Poster Presentations	189
11	Acknowledgements/Danksagung	190
12	Funding Sources	192
13	Conflict of Interest.....	192
14	Rights and permissions	192
15	Declaration of independence	193

List of Figures

Figure 1: Pandemic timeline	3
Figure 2: Phylogenetic tree of the hemagglutinin genes of influenza A virus subtypes	5
Figure 3: Schematic presentation of cross-species transmission of influenza A viruses	6
Figure 4: Schematic representation of an influenza A virus virion and electron micrographs of different influenza A virus strains.....	7
Figure 5: Schematic of the hemagglutinin trimer in complex with the ligand LSTc	8
Figure 6: Replication cycle of influenza A viruses	9
Figure 7: Schematic of influenza A virus nucleoprotein with bound RNA	10
Figure 8: Taxonomy of human coronaviruses.....	12
Figure 9: Nextstrain clade scheme of SARS-CoV-2 variants of concern.....	15
Figure 10: SARS-CoV-2 structure	16
Figure 11: Schematic representation of the full-length SARS-CoV-2 spike protein	17
Figure 12: SARS-CoV-2 spike protein in different conformational states	18
Figure 13: The IgG antibody molecule.....	21
Figure 14: Human Fcγ-receptors	23
Figure 15: Schematic representation of Adeno-associated virus vectors	32
Figure 16: FcγR reporter cell assay.....	69
Figure 17: Immunization schedule for the evaluation of AAV-vector vaccines against influenza A viruses	74
Figure 18: Quality control of AAV-vectors for influenza A virus antigens.....	75
Figure 19: Phylogenetic tree of influenza A viruses used for serological analysis.....	76
Figure 20: Immunization with AAV-HA/NP, but not WIV results in a broadly reactive antibody response	78
Figure 21: Immunization with AAV-HA and AAV-H3 results in a strain-specific antibody response	79
Figure 22: Immunization with AAV-HA/NP results in a different FcγR-activation profile than WIV immunization	81
Figure 23: Immunization with AAV-HA and AAV-H3 results in strain-specific FcγR-responses	83
Figure 24: Induction of antibodies towards the hemagglutinin stalk	85
Figure 25: IgA antibodies were induced against homologous, heterologous and heterosubtypic virus in the respiratory tract after AAV-HA/NP immunization, and against X31 after AAV-H3 immunization	86
Figure 26: No CD4 and CD8 T-cell responses against influenza A antigens were detected .	87

Figure 27: AAV-HA/NP prime-boost immunization protected mice from homologous, heterologous and heterosubtypic challenge	89
Figure 28: Viral challenge: Weight loss and lung virus titers	91
Figure 29: Clinical scores differed from control groups after Cal/7/09pdm and X31, but not after PR8 challenge in immunized mice.....	92
Figure 30: Design of the AAV-S-RBD vector	96
Figure 31: Quality control of the AAV-S-RBD vectors	97
Figure 32: The Dual-AAV-vector system for the SARS-CoV-2 S-Protein	98
Figure 33: Receptor-binding domain variant proteins demonstrated binding to ACE2 <i>in vitro</i>	100
Figure 34: Immunogenicity of the AAV-S-RBD vector varied in different mouse strains.....	101
Figure 35: Antibodies induced after immunization with the AAV-S-RBD wt vector showed neutralizing activity against SARS-CoV-2.....	102
Figure 36: <i>In vivo</i> immunogenicity evaluation of varying immunization schemes with the AAV-S-RBD wt vector in BALB/c mice did not result in antibody induction	104
Figure 37: Immunization with the AAV-S-RBD BA.2 vector resulted in strong antibody titers against SARS-CoV-2 wt, Beta, Delta and BA.1 variants.....	105
Figure 38: No mucosal antibody responses to immunization with the AAV-S-RBD variant vaccines could be detected	107
Figure 39: Immunization with the AAV-S-RBD BA.2 vector resulted in strong FcγRI-activating responses against wt, Beta and Delta S1-domain, but not against BA.1	108
Figure 40: Immunization with AAV-S-RBD BA.2 resulted in neutralizing titers against SARS-CoV-2 Omicron BA.1, BA.2 and BA.5 variants, but not against others	109
Figure 41: No antigen-specific T-cells were detected after immunization with the AAV-S-RBD wt and variant vectors	110
Figure 42: Differences in the spike protein of the SARS-CoV-2 Omicron variants BA.1, BA.2 and BA.5	129
Figure 43: Gating strategy for intracellular cytokine staining for CD4 and CD8 T-cells	183
Figure 44: Fractions of CD4 ⁺ and CD8 ⁺ cells of CD3 ⁺ cells in miced immunized with influenza A antigens	184
Figure 45: Hemagglutinin amino acid sequences of influenza A viruses H1N1 Cal/7/09pdm and PR8 and H3N2 Aichi/2/1968.....	185
Figure 46: Nucleoprotein amino acid sequences of influenza A viruses H1N1 Cal/7/09pdm and PR8 and H3N2 Aichi/2/1968.....	186
Figure 47: Data on first PR8 challenge	187
Figure 48: Data on second PR8 challenge	188

List of Tables

Table 1: SARS-CoV-2 variants of concern as defined in the different nomenclature systems	13
Table 2: SARS-CoV-2 variant of concern mutations in the S1 subunit of the spike protein ...	14
Table 3: Composition of SDS-PAGE gels	60
Table 4: Lethal doses of IAV used for mouse infections	66
Table 5: Hemagglutination inhibition and neutralizing titers are virus strain-specific	83
Table 6: Hemagglutination inhibition and neutralizing titers are virus strain-specific after AAV-HA and AAV-H3 immunization	84
Table 7: Splicing donor sites of the S-RBD constructs used in this thesis.....	125
Table 8: IgG antibody titers, FcγR-activating titers, and PRNT ₅₀ titers of the AAV-S-RBD immunizations	130

Abbreviations/Definitions

AAV	adeno-associated virus
ACE2	angiotensin-converting enzyme 2
ADCC	antibody-dependent-cellular cytotoxicity
ADCP	antibody-dependent-cellular phagocytosis
ADE	antibody-dependent enhancement
APC	antigen presenting cell
Ca/7/09pdm	influenza virus A/California/7/2009pdm (H1N1)
CD	cluster of differentiation
CMV	cytomegalovirus
COVID-19	coronavirus disease 2019
DNA	desoxyribonucleic acid
<i>E. coli</i>	<i>Escherichia coli</i>
ECDC	European Centre for Disease Prevention and Control
E-protein	envelope protein of SARS-CoV-2
ELISA	enzyme-linked immune sorbent assay
FcγR	Fcγ-receptor
GFP	green-fluorescent protein
GV-SOLAS	Gesellschaft für Versuchstierkunde/Society for Laboratory Animal Science
HA	hemagglutinin of IAV
HAT	human airway trypsin-like protease
HPAI	highly pathogenic avian influenza
i.m.	intramuscularly
i.n.	intranasally
IAV	influenza A virus
IFN γ	interferon gamma
Ig	immunoglobulin
IL	interleukins
ITR	inverted terminal repeats
LAIV	live-attenuated vaccine
LSTc	sialylneolacto- <i>N</i> -tetraose c
M1	matrix Protein 1 of IAV
M2	matrix Protein 2 of IAV
MERS-CoV	Middle East respiratory syndrome coronavirus

MHC.....	major histocompatibility complex
M-protein.....	membrane protein of SARS-CoV-2
MN assay.....	microneutralization assay
mRNA.....	messenger RNA
NA.....	neuraminidase of IAV
NEP.....	nuclear export Protein of IAV
NHP.....	non-human primates
NK cells.....	natural killer cells
NP.....	nucleoprotein of IAV
N-protein.....	nucleocapsid protein of SARS-CoV-2
NS1.....	non-structural protein 1 of IAV
Nsp.....	non-structural protein
NTD.....	N-terminal domain
PA.....	polymerase acid of IAV
PB1.....	polymerase basic 1
PBS.....	phosphate buffered saline
PB2.....	polymerase basic 2
PFU.....	plaque forming unit
PHEIC.....	public health emergency of international concern
PR8.....	influenza virus A/Puerto Rico/8/1934 (H1N1)
PRNT ₅₀	plaque reduction neutralization assay (50% plaque reduction)
QIV.....	quadrivalent inactivated vaccine
RdRp.....	RNA-dependent RNA polymerase of IAV
RNA.....	ribonucleic acid
RNP.....	ribonucleoprotein complex of IAV
s.c.....	subcutaneously
SARS-CoV.....	severe acute respiratory syndrome coronavirus
SARS-CoV-2.....	severe acute respiratory syndrome coronavirus type 2
sgRNA.....	subgenomic RNA
S-protein.....	spike glycoprotein of SARS-CoV-2
S-RBD.....	receptor-binding domain of SARS-CoV-2
STIKO.....	Ständige Impfkommission
TCID ₅₀	50% tissue culture infectious dose
TIV.....	trivalent inactivated vaccine

TMPRSS2.....	transmembrane protease serine subtype 2
TNF α	tumor necrosis factor alpha
TRS.....	transcription regulatory sequence
vg.....	viral genomes
VOC.....	variant of concern
vRNA.....	viral RNA
WHO.....	World Health Organization
WIV.....	whole inactivated virus

1 Introduction

The severe acute respiratory syndrome coronavirus type 2 (SARS-CoV-2) and influenza A viruses (IAV) are significant public health concerns.

Influenza viruses cause seasonal waves, while SARS-CoV-2 triggered a pandemic in 2020, which is still ongoing. The World Health Organization (WHO) has terminated the public health emergency of international concern (PHEIC) in May 2023, stating that the virus has established itself in the population causing regular waves.

For influenza viruses, first vaccines have been available for wider use since 1945, but their composition needs to be re-assessed and the vaccine must be re-administered on a yearly basis due to drift processes of the virus. Research focuses on the development of a universal influenza vaccine, which is not dependent on the everchanging parts of the surface glycoprotein hemagglutinin (HA). These efforts are still ongoing.

Since the start of the SARS-CoV-2 pandemic, research and vaccine development progressed in record time, having the first licensed vaccines ready by the end of 2020. In the course of the pandemic, variants of the initial virus have emerged. The further they progressed from the original virus, the more they showed immune evasion, so by now it has been stated that the wildtype strain should be left out of updated vaccine formulations. In this thesis, an adeno-associated virus (AAV) – vector is evaluated as a vaccine vector for both abovementioned viruses.

In the context of developing a broadly reactive influenza vaccine, this vector system has already been shown to be a promising candidate. AAV-vector vaccines have also been in development for SARS-CoV-2, but none has reached market-level authorization yet.

The object of this thesis is 1) the immunological evaluation of AAV-vectors delivering different IAV antigens as a vaccine against influenza viruses in a mouse model of influenza and 2) the design and assessment of an AAV-vector vaccine targeting the receptor-binding domain of SARS-CoV-2 (AAV-S-RBD).

For this evaluation, a bivalent AAV-HA + AAV-NP (AAV-HA/NP) vaccine was used, investigating a possible synergistic effect to induce a broadly reactive immune response. It should further be assessed, if priming with an AAV-vector vaccine could have an enhancing effect, similar to a natural influenza infection or the immunization with a live-attenuated vaccine, on the induction of a broadly reactive immune response compared to priming with an inactivated vaccine. Additionally, the immunogenicity of an AAV-vector carrying a group 2 HA (AAV-H3) was evaluated, and further assessed, if a broader immune response could be achieved by the combination of group 1 and 2 HAs (AAV-HA/H3).

The AAV-S-RBD vaccine was designed and evaluated *in vitro* before its immunological properties were assessed *in vivo*. As the pandemic progressed, the vector was adapted to emerging variants of concern (VOC) of SARS-CoV-2 and cross-reactivity was assessed.

2 Literature Review

2.1 Current and past pandemics – One Health paradigms with major impact

During the 20th century, there have been five documented pandemics, meaning the outbreak of an infectious disease over multiple countries or continents, leading to great socioeconomic losses and challenges to public health. Four of these pandemics were due to IAV subtypes, namely H1N1 (1918), H2N2 (1957), H3N2 (1968) and H1N1 (2009) (Palese 2004; McCullers 2016; Yang et al. 2022). The fifth pandemic, caused by SARS-CoV-2, was declared in March 2020 by the WHO, who ended the PHEIC recently in May 2023, but the pandemic is still ongoing (Figure 1).

These pandemics all have a zoonotic origin, meaning that those infectious diseases originated in animals and crossed over to humans. Zoonoses appear to emerge more and

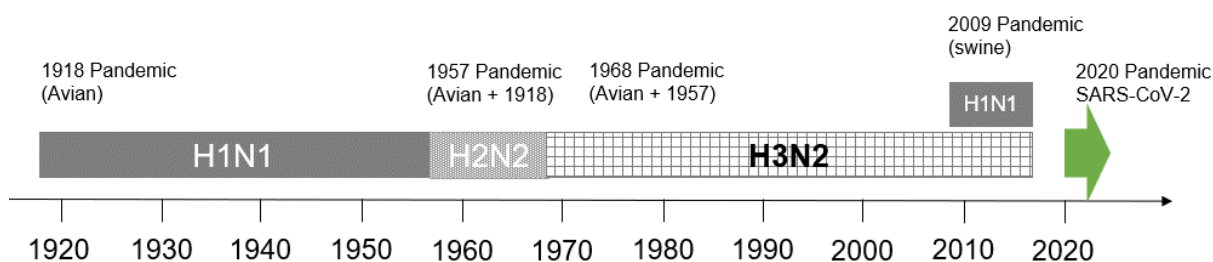


Figure 1: Pandemic timeline

Four of the five pandemics in the 20th century have been caused by influenza A viruses. The 1957 and 1968 were reassortants, whereas the H1N1 viruses came directly from animal reservoirs. The fifth pandemic is still ongoing and has been caused by SARS-CoV-2. Own illustration based on Palese (2004), McCullers (2016), Yang et al. (2022) and WHO (2023c).

more frequently, because natural habitats of animals and human territories are becoming more interconnected and intensive animal husbandry and wildlife trade are extending, accompanied by environmental degradation (Jones et al. 2008; Jones et al. 2013; Smith et al. 2014; Everard et al. 2020; Kenyon 2020).

The 1918 H1N1 virus had an avian origin, the 1957 H2N2 was a reassortant of the 1918 H1N1 and an avian virus, the 1968 H3N2 was a reassortant of the previous strain as well, and the 2009 H1N1 originated in swine (McCullers 2016).

The origin of SARS-CoV-2 has been discussed and studied intensely, but the exact transmission route leading up to the pandemic is not known. On the other hand, it is known that bats are the natural reservoir hosts for Alpha- and Beta-coronaviruses (Yang et al. 2022). Most likely there was a zoonotic event, where the virus crossed over from an intermediate host animal to humans at the Huanan market late in 2019 (Kenyon 2020; Pekar et al. 2022).

Seasonal IAV can infect up to 20% of the global population and up to 650,000 deaths are reported worldwide, 72,000 of those only in the WHO European Region (WHO 2023b).

SARS-CoV-2, as of August 2023, has caused more than 769 million cases worldwide and more than 6.95 million reported deaths (WHO 2023c).

Thus, the IAV and SARS-CoV-2 pandemics are paradigms for One Health problems that can have a major impact on public health and economies and need to be met with a One Health approach, integrating measures not only from human medicine, but also veterinary medicine, as well as environmental interventions (Ludwig et al. 2014; Kenyon 2020). To be able to better respond to future pandemics, or even prevent them, this multi-level approach needs to be applied.

2.2 Influenza viruses

2.2.1 Taxonomy

Influenza viruses belong to the family of *Orthomyxoviridae* (Kuhn et al. 2021). They have a segmented negative-sense, single-stranded RNA genome. Until today, four genera have been identified, namely *Alpha-*, *Beta-*, *Gamma-* and *Delta*influenzaviruses with the respective species *Influenza A*, *B*, *C* and *D virus* (Kuhn et al. 2021). Influenza A, B and C viruses are known to cause disease in humans (Paules and Subbarao 2017; Uyeki et al. 2022).

Influenza D viruses are the most recently discovered Influenza viruses and have primarily been found in cattle as their reservoir (Hause et al. 2014). Periodical spillover to other mammalian and poultry species has been found, without evidence of replication (Su et al. 2017; Liu et al. 2020).

Influenza C viruses have also been found in pigs, dogs and cattle and rare cases of human to swine transmission have been reported (Sederdahl and Williams 2020). Infection is mostly asymptomatic in adults but can be dangerous for young children (Matsuzaki et al. 2006).

Influenza B viruses mostly infect humans but have also been found in marine mammals like seals (Osterhaus et al. 2000).

For influenza B viruses, two antigenically distinct lineages, B/Yamagata, and B/Victoria, have been defined (Rota et al. 1990; Nerome et al. 1998). During the SARS-CoV-2 pandemic, B/Yamagata has disappeared completely, and it remains to be determined whether it can re-emerge (WHO 2022a).

Influenza A viruses have the broadest host range and the highest pandemic potential. Their natural reservoir are wild birds, specifically waterfowl, but they can infect different mammalian species in addition to humans, like pigs, horses, or dogs (Figure 3) (Webster

et al. 1992; Yoon et al. 2014).

There have been different virus subtypes identified for IAV due to the composition of their surface glycoproteins hemagglutinin (HA) and neuraminidase (NA). To date there are 18 antigenically distinct HA (H1-18) and 11 NA (N1-11) subtypes described (Wu et al. 2014; Hutchinson 2018; Long et al. 2019). The HA and NA subtypes can additionally be divided into 2 groups each, depending on their amino acid sequence (HA groups displayed in Figure 2), whereas the bat-derived NAs (N10 and N11) do not fit in either of the groups. Not all subtypes can infect every susceptible species equally well or can pass it on productively (Figure 3). The subtypes H17N10 and H18N11 have only been found in bats (Tong et al. 2012; Tong et al. 2013).

Both, influenza A and B viruses evolve to escape existing immunity. In this way, they can cause seasonal epidemics annually. This evolutionary process occurs via point mutations in the HA and NA epitopes, leading to amino acid substitutions, insertions, or deletions, which results in antigenic drift (Krammer et al. 2018; Uyeki et al. 2022).

Another process, which occurs in IAV due to their segmented genome and their ability to infect a broad range of different hosts, is called antigenic shift. If two or more antigenically distinct IAV subtypes infect the same host, those viruses can go through the process of reassortment. Such events can potentially lead to new variants with pandemic potential, when the genes for the surface glycoproteins in human-adapted strains are exchanged. Reassortment processes most commonly happen at the close human-animal interface and are not predictable (Krammer et al. 2018; Uyeki et al. 2022).

In addition to the abovementioned pandemics, influenza A and B viruses circulate in the human population and cause seasonal epidemics. The subtypes that currently exist in humans are H1N1 and H3N2. H1N1 circulated after the 1918 pandemic until 1957, when it was temporarily replaced, but re-emerged in 1977, until it was replaced by the novel H1N1

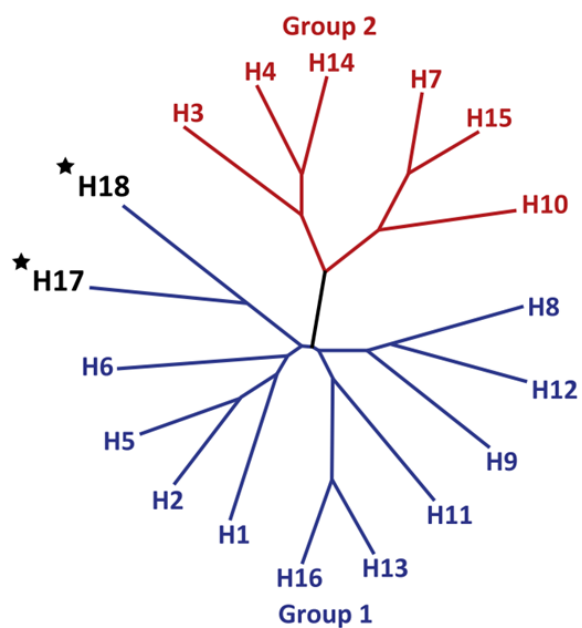


Figure 2: Phylogenetic tree of the hemagglutinin genes of influenza A virus subtypes

Displayed is the phylogenetic tree of IAV hemagglutinin (HA) molecules, which can be categorized into two groups: group 1 (in blue) and group 2 (in red). H17 and H18 are bat derived HA, which belong to group 1 (reproduced from Wu et al. (2014), image rights in chapter 14).

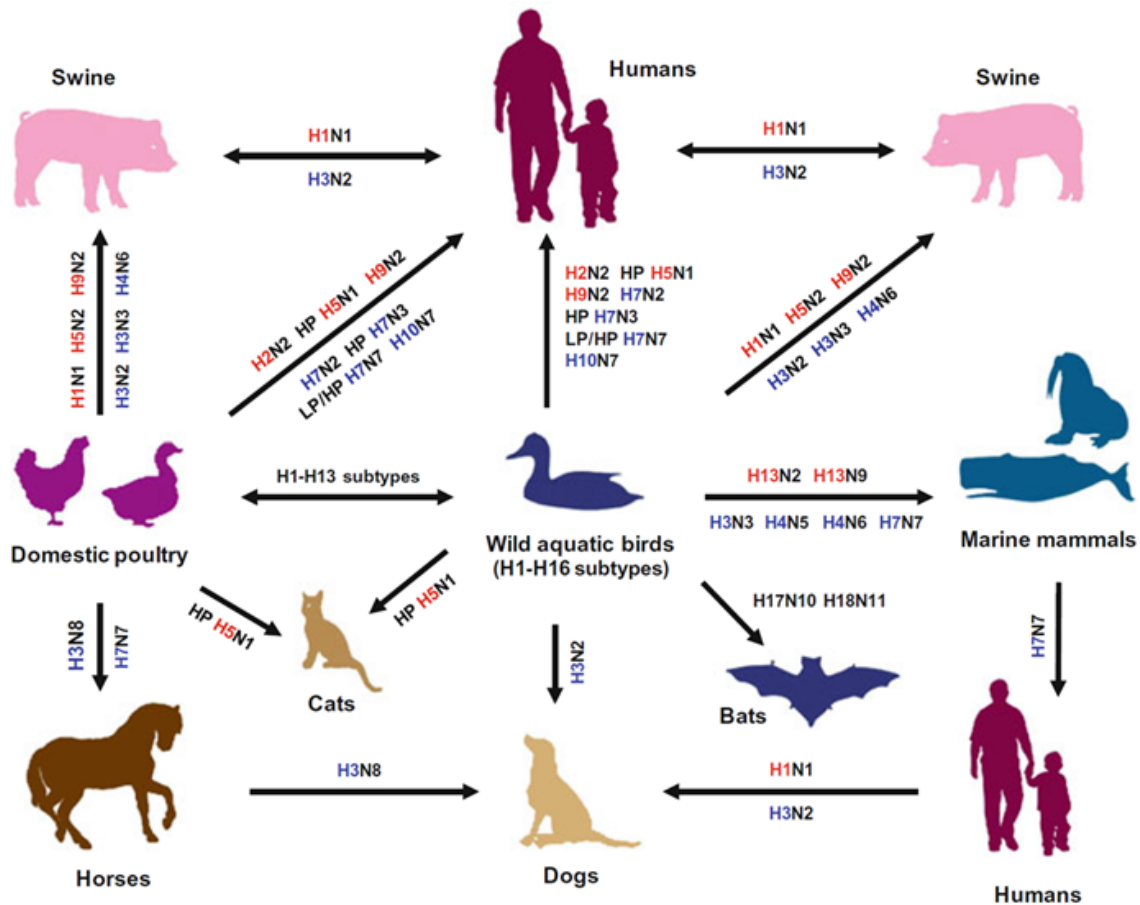


Figure 3: Schematic presentation of cross-species transmission of influenza A viruses

Aquatic birds naturally are the principal reservoirs for influenza A viruses including horses, cats, dogs, marine animals, domestic poultry, pigs, bats, and humans. Group 1 HA subtypes are represented in red and group 2 HA subtypes are represented in blue (reproduced from Yoon et al. (2014), image rights in chapter 14).

pandemic strain of 2009 (Figure 1). H3N2 has been co-circulating with H1N1 since the 1968 pandemic (Palese 2004; McCullers 2016). Those infections are directly transmitted from person to person via aerosols or droplets.

Regularly, human infections with avian or swine IAV are reported in people closely working or living with infected animals. Avian influenza virus infections with H5 or H7N9 subtypes often display a severe clinical course, with a higher case fatality rate than seasonal influenza (Li et al. 2014). For subtypes H7N7 and H9N2 the course is usually mild (Jonges et al. 2014). Swine influenza subtypes are H1N1, H1N2 and H3N2 and mainly cause mild disease as well.

Since October 2022 there has been a high number of incidences of highly pathogenic avian influenza (HPAI) with an H5-HA of clade 2.3.4.4.B (Friedrich-Loeffler-Institut 2023). The current events can be classified as a panzootic, as many different avian and mammalian species have reportedly been severely affected (Friedrich-Loeffler-Institut 2023). Human

cases are still very rare and the risk of zoonotic events appears to be still low (ECDC 2023). A moderate risk, however, exists for people who are occupationally exposed to infected poultry or mammals (ECDC 2023).

2.2.2 Morphology and replication

Influenza viruses are enveloped viruses, containing segmented, single-stranded, negative-sense RNA (Krammer et al. 2018). The viral particles are pleomorphic and can have a spherical, elliptical, or filamentous shape, with a diameter of 80-120 nm (spherical), or a length of up to 20 μm (filamentous) (Harris et al. 2006; Bouvier and Palese 2008; Noda 2011). A schematic representation of IAV and electron micrographs depicting the pleomorphic nature of IAV are represented in Figure 4.

The genome of influenza A and B viruses is segmented into eight segments, while the genome of influenza C and D viruses is divided into seven segments (Nakatsu et al. 2018). Those segments are numbered from the longest to the shortest segment. Four of these segments only encode for one viral protein, while the others can also carry the information

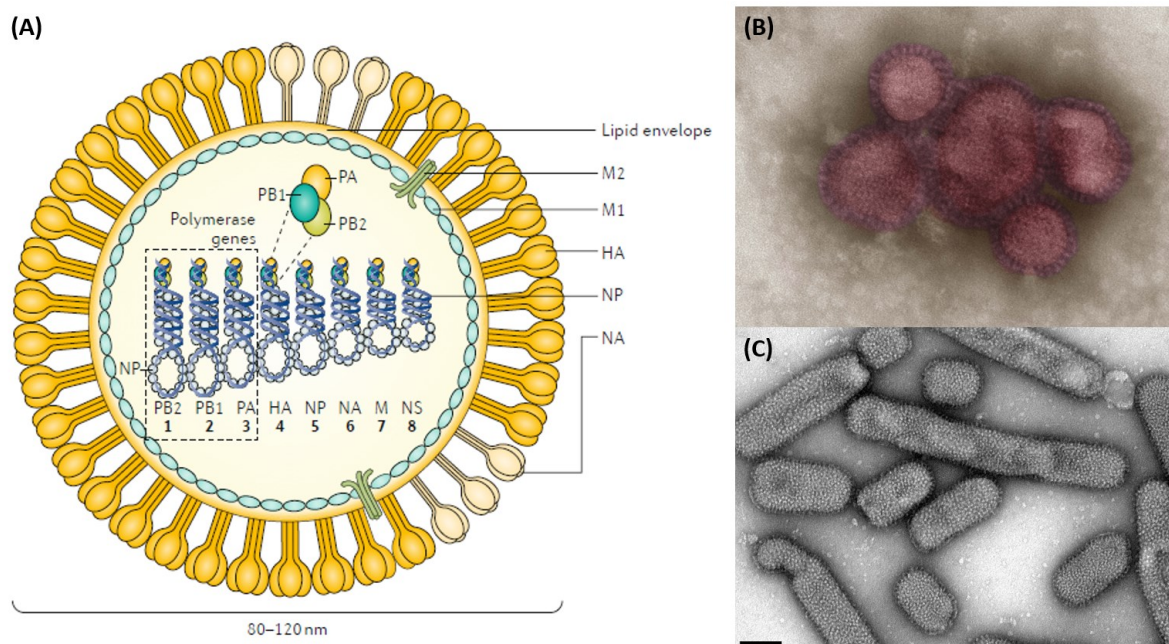


Figure 4: Schematic representation of an influenza A virus virion and electron micrographs of different influenza A virus strains

(A) This schematic depicts the location of the viral proteins of an IAV virion. The lipid membrane contains the HA, NA and M2 proteins. The inner part of the virion is lined by the M1 protein, encasing the viral RNA genome consisting of eight segments, organized in complexes with the PA, PB1, PB2 and NP proteins (reproduced from Krammer et al. (2018), image rights in chapter 14). **(B)** An electron micrograph of Influenza virus A/California/7/2009 (H1N1), colouring, negative staining, Transmission electron microscopy (TEM). Initial magnification x 85,000 (reproduced from Holland and Bannert, image rights in chapter 14). **(C)** An electron micrograph of Influenza A virus Berlin/H1N1 (Orthomyxoviruses). Negative staining, transmission electron microscopy (TEM). Bar = 100 nm (reproduced from Bannert and Möller, image rights in chapter 14).

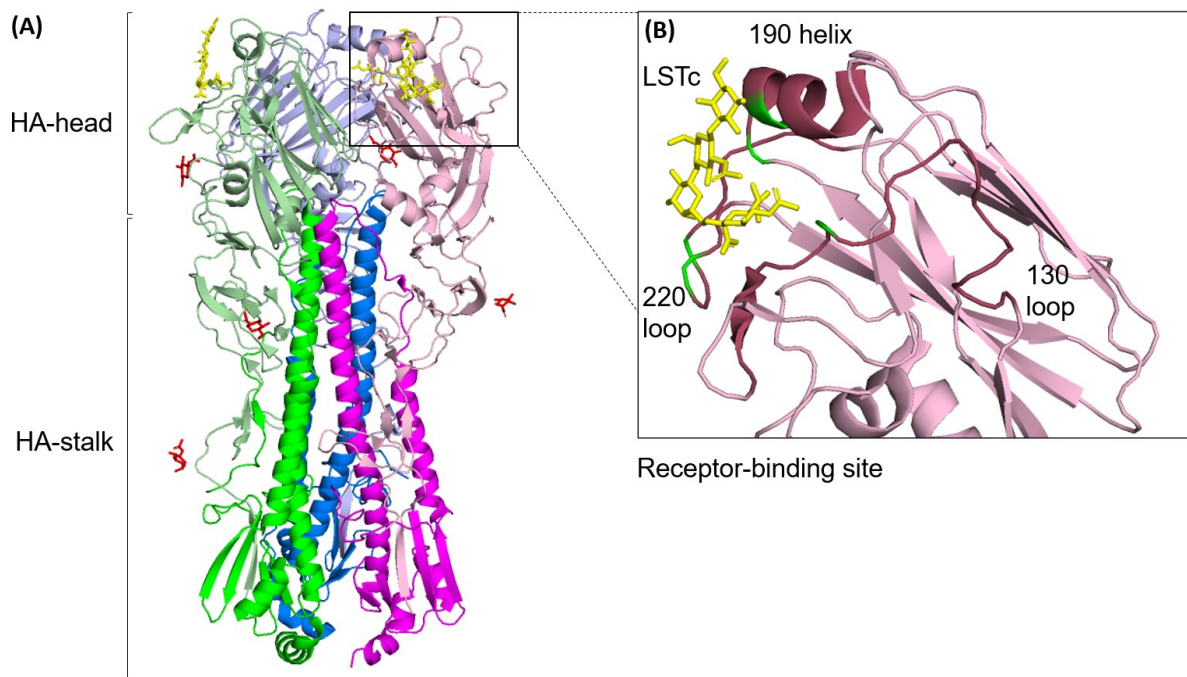


Figure 5: Schematic of the hemagglutinin trimer in complex with the ligand LSTc

(A) Structure of the trimeric HA, HA1 subunits in pale colors, HA2 subunits in the corresponding bright colors. Glycan residues on the subunits in red. (PDB: 3UBE)

(B) Receptor-binding site, main structures in dark red, dominant interaction residues in green. The ligand LSTc is depicted in yellow (Xu et al. 2012; NCBI 2023). (Own illustration generated in PyMOL from the given PDB template) LSTc: Sialylneolacto-N-tetraose c

for other proteins, depending on the virus species.

The viral membrane of IAV contains the HA, NA and matrix proteins (M2), with the HA being the most abundant of the three (Zebedee and Lamb 1988; Bouvier and Palese 2008; Hutchinson et al. 2014). The layer below the outer membrane is comprised of the major matrix protein (M1). In the viral core, the nuclear export protein (NEP) and the ribonucleoprotein complex (RNP) are located. The RNP contains the RNA segments, which are coated with the nucleoprotein (NP) and bound to the viral RNA-dependent RNA polymerase (RdRp) consisting of the subunits polymerase acid (PA), polymerase basic 1 (PB1) and polymerase basic 2 (PB2) (Noda et al. 2006). Another component of the virion is the non-structural protein 1 (NS1), which is thought to be multifunctional, but with a very low abundance in the virion (Hutchinson et al. 2014).

For replication, the viral HA must bind its receptor on the host cell (Figure 5). Sialic acid containing glycans (sialoglycans) on cell surface glycoproteins and glycolipids function as such receptors (Rogers and Paulson 1983; Thompson et al. 2019). Between host species, IAV display a difference in binding-specificity to the sialoglycans. While human IAV preferably bind to α 2-6-linked glycan (NeuAca2-6Gal) receptors found throughout the human upper respiratory tract, avian IAV bind to α 2-3-linked (NeuAca2-3Gal) receptors, which are located in the avian intestinal tract (Thompson et al. 2019; Liu et al. 2023). In

humans, α 2-3-linked sialic acid can be found in the lower respiratory tract, which is a reason for the limited capacity of avian influenza to spread between humans, but also for severe respiratory disease being caused by some avian IAV of the H5 subtype (Shinya et al. 2006; van Riel et al. 2006).

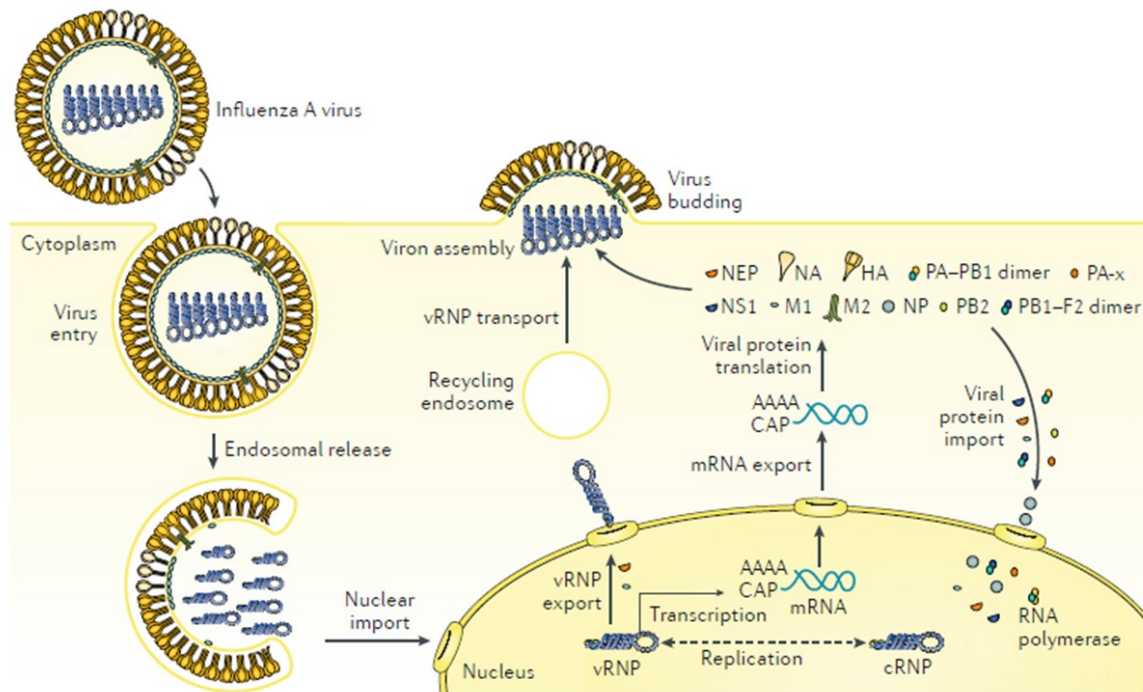


Figure 6: Replication cycle of influenza A viruses

Viral particles attach to the sialoglycans on the cell surface and enter the cells in endosomes before the viral membrane fuses with the endosomal membrane and the viral genome is released and transported to the nucleus. Here, the viral genome is transcribed and replicated by the viral RNA-dependent RNA polymerase (RdRp). Translation of the viral proteins takes place in the cytoplasm. Finally, new virions are assembled and bud from the plasma membrane (reproduced from Krammer et al. (2018), image rights in chapter 14).

When the HA has attached to the host cell receptor, internalization of the virion starts either via clathrin-coated pits, or through macropinocytosis (Matlin et al. 1981; de Vries et al. 2011) (Figure 6). Either way, the endosome containing the virion is then trafficked and acidified, leading to fusion of the viral membrane with the endosomal membrane. Fusion is mediated by the HA2 subunit, which forms the fusion peptide after cleavage of the HA0 precursor protein into the HA1 and HA2 subunits (Chen et al. 1998). Cleavage is necessary for the virus to be infective and is performed by trypsin-like host cell proteases in the human respiratory tract, such as HAT or TMPRSS2, recognizing the cleavage site containing a single arginine in most HA subtypes (Steinhauer 1999). In the HPAI subtypes H5 and H7, the cleavage site is altered, containing a polybasic signal, which makes them susceptible to cleavage by subtilisin-like proteases such as furin, which are ubiquitously expressed throughout the body (Stieneke-Grober et al. 1992; Steinhauer 1999), leading to enhanced

infectivity and pathology. Cleavage, however, does not instantaneously lead to the full dissociation of the HA protein, as the two subunits remain connected via disulfide bonds (Stieneke-Grober et al. 1992; Chen et al. 1998). Simultaneously, acidification also results in the opening of the pH-sensitive M2 ion channel, lowering the pH inside the virion as well (Pinto and Lamb 2006).

This process results in the disruption of the M1 layer and the release of the RNPs into the host cell cytoplasm (Helenius 1992). This is followed by their transport into the nucleus, in which transcription and replication of the viral genomic RNA can take place. The RdRp needs a 5'-capped primer to initiate transcription of viral RNA into mRNA. For this purpose, the PA endonuclease function cleaves these 5'-cap structures from nascent host cell RNA polymerase II transcripts (Dias et al. 2009). This process is called "cap-snatching" (Dias et al. 2009; Reich et al. 2014). On the 3' end, the viral mRNAs carry a poly-A-tail, due to a uridine-rich region in the viral RNA (vRNA) template (Poon et al. 1999). Once the vRNA is transcribed into mRNA, the host cell machinery continues with the translation process in the cytosol (Dou et al. 2018). Once the viral proteins are translated, they trans-localize depending on the signals they carry. Proteins that support transcription and replication of vRNA, e.g., PBA, PB1, PB2, NEP, M1 and NP, are transported to the nucleus (Smith et al. 1987; Wu and Pante 2009). Proteins designated for the viral membrane (HA, NA, M2) are synthesized and modified in the rough endoplasmic reticulum, meaning that the HA receives N-glycosylations and palmitoylations (Hebert et al. 1995; Veit et al. 2013). The membrane proteins are also assembled into their respective oligomers, e.g., a trimer for HA and tetramers for NA and M2 (Copeland et al. 1986; Leser and Lamb 2005; Dou et al. 2018). They are then trafficked through the trans-Golgi network to finally be accumulated in cholesterol-rich regions in the apical plasma membrane, the so-called "lipid rafts" (Leser and Lamb 2005). Replication of the viral genome does also depend on host cell factors. The final negative sense vRNA designated for the new virions is synthesized from a positive sense complementary RNA not containing the abovementioned 5' cap, which had been transcribed from the original vRNA template (Vreede et al. 2004; Fodor 2013). Host proteins from the ANP32 family are involved in this process

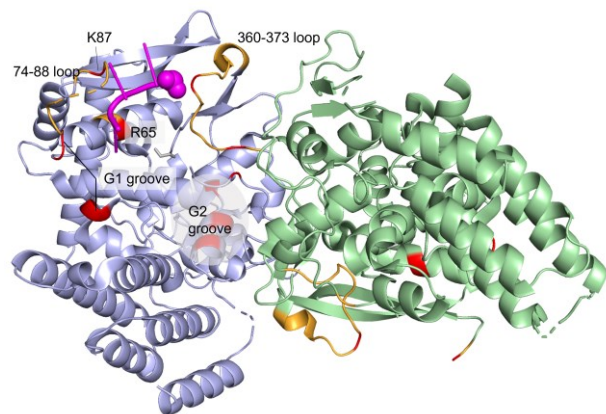


Figure 7: Schematic of influenza A virus nucleoprotein with bound RNA

Structure of a homodimer of the nucleoprotein (NP) in light blue and green. RNA is displayed in pink. The main structures are highlighted in orange with the main functional residues labelled in red. (PDB: 7DXP) (Tang et al. 2021). Own illustration generated in PyMOL from the given PDB template.

(Peacock et al. 2019; Zhu et al. 2023). It is assembled to RNPs with the newly synthesized proteins that had been transported to the nucleus (Dou et al. 2018) (RNA bound to NP in Figure 7). These new RNPs are exported from the nucleus in association to CRM1, which is mediated by M1 and NEP (Neumann et al. 2000; Lakdawala et al. 2016). They are finally trafficked in vesicles containing Rab11 (Amorim et al. 2011; Eisfeld et al. 2011; Lakdawala et al. 2016) to the lipid rafts in the plasma membrane already containing the viral membrane proteins, thereby masking their trans-localization signal to not be trafficked back to the nucleus again (Wu and Pante 2009). Now, mediated by M1, packaging of the new virions occurs (Brunotte et al. 2014). Importantly, vRNA segments are labeled with segment-specific genome-packaging signals located in the noncoding and terminal coding regions of the 3' and 5' ends to ensure that only one copy of each segment is included in the new virion (Goto et al. 2013). For the budding of the new virions to take place, the sialidase activity of NA has to prevent the HA from binding to host cell sialoglycans (Palese et al. 1974; Rossman and Lamb 2011).

2.3 SARS-CoV-2

SARS-CoV-2 is the etiological agent responsible for the coronavirus disease 2019 (COVID-19) that emerged in December 2019 (Zhou et al. 2020a). The related pandemic was declared in March 2020 by the WHO (Carvalho et al. 2021). Initially, an unprecedented worldwide public health response has been put in place, including the unified global implementation of non-pharmaceutical interventions, wide funding of research with faster publication processes and record-time development of vaccines. The virus has shown a high rate of mutation, with new variants emerging quickly, leading to enhanced transmissibility compared to the original strain.

SARS-CoV-2 is transmitted via aerosols and droplets, which are expelled by asymptomatic and symptomatic infected persons. The spread via asymptomatic people and its rather long incubation period led to the pandemic development, in contrast to SARS-CoV.

2.3.1 Taxonomy of human coronaviruses

The family of the *Coronaviridae* belongs to the order of the *Nidovirales* and contains the subfamily of *Orthocoronavirinae*, which encompasses the genera *Alpha-*, *Beta-*, *Delta-* and *Gammacoronavirus* (Corman et al. 2018; Coronaviridae Study Group of the International Committee on Taxonomy of 2020). While Alpha- and Betacoronaviruses are known to infect several mammalian species, Delta- and Gammacoronaviruses infect birds.

Currently, seven human coronaviruses are known, which belong to either the Alpha- or Betacoronaviruses (Figure 8) (Fung and Liu 2019). The endemic coronaviruses HCoV-229E (Hamre and Procknow 1966) and HCoV-NL63 (van der Hoek et al. 2004) are

Alphacoronaviruses, while HCoV-OC43 (McIntosh et al. 1967) and HCoV-HKU1 (Woo et al. 2005) are Betacoronaviruses. Those four are usually referred to as the common cold coronaviruses and mainly cause mild upper and lower respiratory tract infections (Su et al. 2016).

The epidemic Middle East respiratory syndrome coronavirus (MERS-CoV) (Zaki et al. 2012) and SARS-CoV (Drosten et al. 2003) and the pandemic SARS-CoV-2 (Zhu et al. 2020) are Betacoronaviruses, MERS-CoV belonging to the subgenus *Merbecovirus*, while SARS-CoV and SARS-CoV-2 are sarbecoviruses (Coronaviridae Study Group of the International Committee on Taxonomy of 2020).

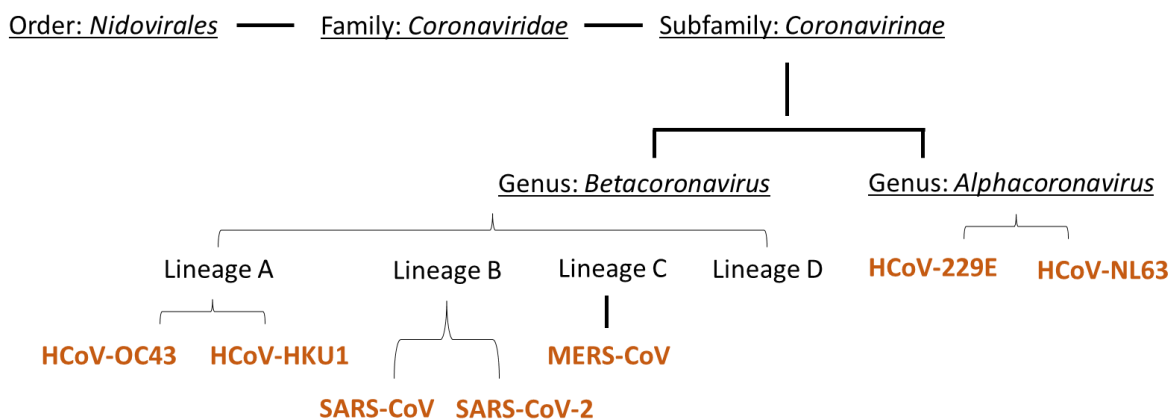


Figure 8: Taxonomy of human coronaviruses

The seven known human coronaviruses belong to the order of *Nidovirales*, the family of *Coronaviridae*, the subfamily of *Coronavirinae* and the two genera of *Betacoronavirus* and *Alphacoronavirus*. The seven known human coronaviruses are displayed in orange. Own illustration based on Fung and Liu (2019).

2.3.1.1 Variants of Concern (VOC) of SARS-CoV-2

Like other viruses, SARS-CoV-2 also evolves over time while it circulates in the human population. Especially RNA viruses are prone to accumulate point mutations because of the low-fidelity RNA-dependent RNA polymerase (Rehman et al. 2020), even though coronaviruses have an exoribonuclease with proofreading capability (Minskaia et al. 2006). Another important mechanism for coronavirus evolution is recombination (Lai and Cavanagh 1997; Bobay et al. 2020).

Due to the high rate of viral dissemination, replication and prevalence, new viral variants emerged quickly over the course of the pandemic until now. Genome alterations mainly occur in the gene coding for the spike glycoprotein (S-protein), which is responsible for receptor binding and cell entry and is a target for neutralizing antibodies. Changes in the receptor-binding domain (S-RBD) and the N-terminal domain (NTD) thus can lead to an increased fitness for the virus due to a higher affinity to the receptor and immune escape (Harvey et al. 2021; McLean et al. 2022).

Of those emerging variants, the WHO defines variants of concern (VOC) and variants of interest (VOI). VOCs are defined by an increase in transmissibility and virulence and thereby decreasing effectiveness of public health measures (WHO 2022b). WHO nomenclature for those variants uses the Greek Alphabet and has been developed to also suit a non-scientific audience, to aid efficient communication to the public (WHO 2022b). For scientific purposes, there are established nomenclature systems by GISAID (GISAID 2021), Nextstrain (Hadfield et al. 2018) and Pangolin (Rambaut et al. 2020a) for tracking genetic lineages of SARS-CoV-2 (Table 1).

WHO label	Pangolin lineage	GISAID clade	Nextstrain clade	Date of earliest documentation
Alpha	B.1.1.7	GRY	20I (V1)	September 2020
Beta	B.1.351	GH/501Y.V2	20H (V2)	May 2020
Gamma	P.1	GR/501Y.V3	20J (V3)	November 2020
Delta	B.1.617.2	G/478K.V1	21A, 21I, 21J	October 2020
Omicron	B.1.1.529	GR/484A	21K, 21L, 21M, 22A, 22B, 22C, 22D	November 2021

Table 1: SARS-CoV-2 variants of concern as defined in the different nomenclature systems

Own table adapted from WHO (2022b).

The first notable mutation in the spike protein receiving attention was the amino acid change D614G, which was detected more frequently since April 2020 and replaced the ancestral virus worldwide (Yurkovetskiy et al. 2020; Plante et al. 2021). Studies indicated that it presented an advantage for infectivity and transmissibility (Hou et al. 2020; Korber et al. 2020; Volz et al. 2021). Conformational changes leading to a higher fraction of the “open” state of the spike protein, but not an increased binding affinity have been described (Yurkovetskiy et al. 2020).

After the emergence of single mutations, lineages containing more mutations appeared in late 2020 and subsequently from then on (Table 2). The first VOC defined by the WHO was the Alpha variant (B.1.1.7.), which was first documented in September 2020 in the UK (Rambaut et al. 2020b). Of its 27 mutations, 8 are located in the gene encoding for the S-protein, with one of those, N501Y, in the S-RBD. N501Y has been shown to result in the highest increases in ACE2 affinity (Starr et al. 2020). The deletions in the NTD could be associated with immune escape or increased infectivity (McCarthy et al. 2021; Meng et al.

	Subunit 1					C	
	SP (1–13)	N-terminal domain (14–305)	306–330	Receptor-binding domain (311–527)	CTD1 (528–590)		CTD2 (591–680)
Alpha		69/70Δ, Y144Δ		N501Y	A570D		P681H
Beta		L18F, D80A, D215G, L242H†, 242/244Δ†, R246I		K417N, E484K, N501Y			
Gamma		L18F, T20N, P26S, D138Y, R190S		K417T, E484K, N501Y		H655Y	
Delta		T19R, 156/157Δ, R158G		L452R, T478K			P681R
Omicron†		A67V, 69/70Δ, T95I, G142D, 143/145Δ, 211Δ, 214EPE, L212I		G339D, S371L, S373P, S375F, K417N, N440K, G446S, S477N, T478K, E484A, Q493R, G496S, Q498R, N501Y, Y505H	T547K	H655Y, N679K	P681H

Table 2: SARS-CoV-2 variant of concern mutations in the S1 subunit of the spike protein

Omicron data is based on BA.1

Reproduced from McLean et al. (2022), image rights in chapter 14.

2021), while the substitution in position 681, which is close to the furin cleavage site between the S1 and S2 domains, has been shown to improve cell entry and transmissibility (McCarthy et al. 2021; Peacock et al. 2021). N501Y has arisen convergently in different lineages, Alpha, Beta and Gamma (Harvey et al. 2021). The Beta variant (B.1.351) was first sampled in May 2020 in South Africa, but only gained importance in December 2020, when it started to expand rapidly (Tegally et al. 2021; WHO 2022b). It harbors 19 mutations, including K417N, E484K and N501Y in its S-RBD, which are associated with immune evasion (McLean et al. 2022). The Gamma variant was first described in November 2020 in Brazil (Faria et al. 2021; WHO 2022b), with 31

mutations in total and ten of those in the S-protein gene. It has mutations at the same positions in the S-RBD as Beta, but differs in position 417, with the substitution K417T (Faria et al. 2021).

The Delta variant appeared in October 2020 in India (WHO 2022b). It contains six mutations in the spike protein, including P681R, like Alpha. In the S-RBD it has two mutations, L452R and T478K, which have not been detected in the former VOCs. L452R is linked to increased binding affinity and immune escape (Li et al. 2020).

Currently, the Omicron variant is circulating worldwide. It was first documented in November 2021 (WHO 2022b). It displays the largest number of mutations seen until today, most of them in the S-gene, especially in the S-RBD region (McLean et al. 2022) (Table 2). So far, several sublineages have been described. The most recent subvariants described are XBB.1.5., XBB.1.16 and BQ.1, with the two XBB variants originating from the BA.2 lineage and BQ.1 from the BA.5 lineage (CoVariants 2022).

The source of emergence of Omicron is not clear, but interestingly, phylogenetic analyses show, that the common predecessor of Omicron and the other variants dates back to mid-2020 (Hadfield et al. 2018; Nextstrain 2022). The Nextstrain clade schema shows Omicron having the same predecessor as Alpha and Gamma, while Beta and Delta have diverged earlier (Figure 9).

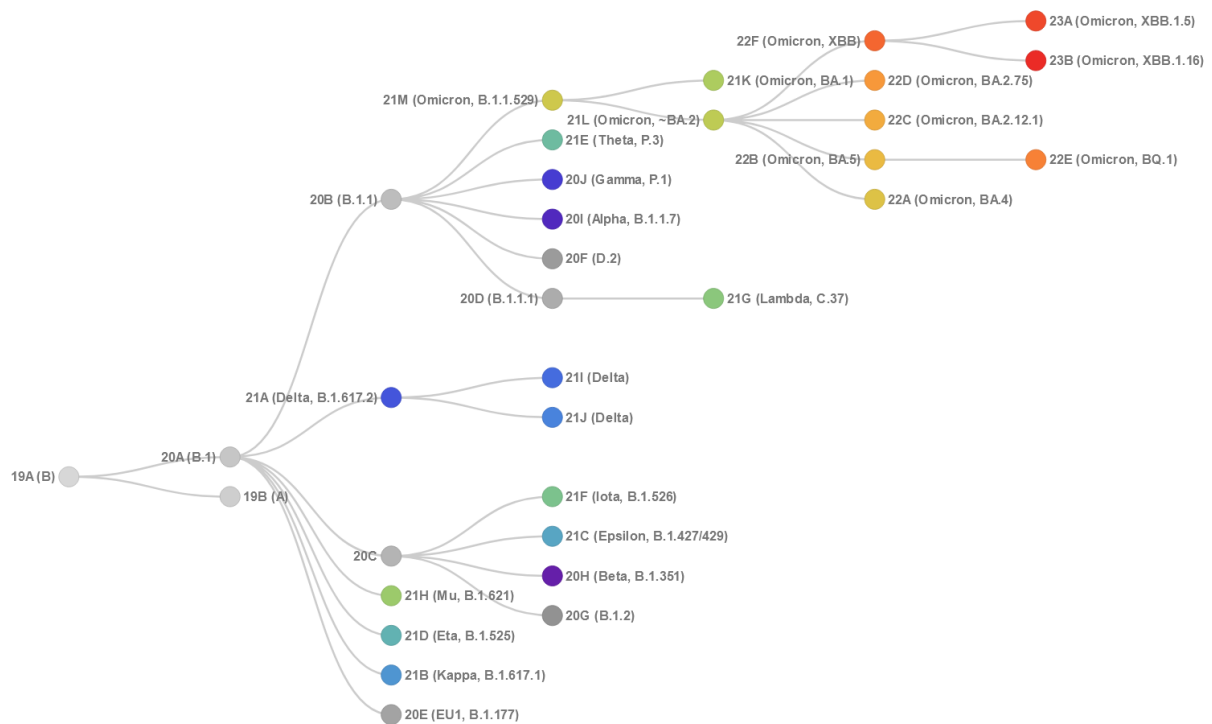


Figure 9: Nextstrain clade scheme of SARS-CoV-2 variants of concern

Image reproduced from CoVariants.org:

(Hadfield et al. 2018; CoVariants 2022; Nextstrain 2022), image rights in chapter 14.

2.3.2 Morphology and replication

Coronavirus particles are enveloped and contain a non-segmented, single-stranded and positive-sense RNA genome. They have the largest and most complex replicating RNA genome, with a size of up to 32kb (Denison et al. 2011), which is enclosed by the nucleocapsid protein (N). The viral membrane contains three proteins, the spike protein (S), membrane protein (M) and envelope protein (E). S, M, E and N are the structural proteins of the virus (Siu et al. 2008; Hartenian et al. 2020; Jamison et al. 2022) (Figure 10). The homotrimeric spike glycoprotein mediates cell entry through a specific host cell receptor and has two domains, S1 and S2 (Figure 11). There is a cleavage site between S1 and S2, and another one at S2'. The S-RBD is located in the S1 subunit (Jackson et al. 2022) (Figure 11). The S-protein trimer of SARS-CoV-2 presents in different conformational states, generally the open and closed conformation (Figure 12) (Gur et al. 2020; Pramanick et al. 2021). These definitions relate to the position of the S-RBD. In the closed conformation, all S-RBDs are in the down position, covering the S2-domains, while in the open conformation at least one S-RBD is in the up position. Here, binding to the host cell receptor, but also to antibodies, is favored (Berger and Schaffitzel 2020; Yin et al. 2022; Lee et al. 2023).

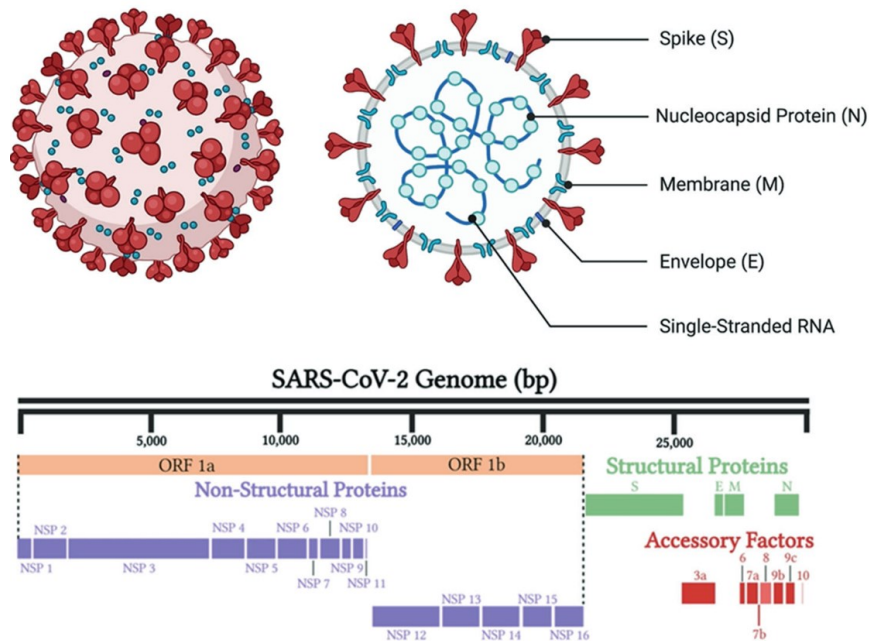


Figure 10: SARS-CoV-2 structure

Depicted here are the components of the SARS-CoV-2 virion (above) and the genome structure (below). The membrane contains the S-, M- and E-proteins, while the N-protein is located inside in complex with the RNA. The SARS-CoV-2 genome encodes for non-structural (purple) and structural proteins (green), as well as accessory factors (red). Image reproduced from Jamison et al. (2022), image rights in chapter 14.

For SARS-CoV-2, like for SARS-CoV and HCoV-NL63, the receptor is ACE2 (Hoffmann et al. 2020). MERS-CoV utilizes the dipeptidyl-peptidase 4 (DPP4) as its receptor and many Alphacoronaviruses use aminopeptidase N (APN) (Fehr and Perlman 2015; V'Kovski et al. 2021). The M-glycoprotein, which is responsible for organizing viral components into virions, spans the membrane three times, which allows it to interact with the other membrane proteins laterally and with the RNA and N-protein through the C-terminal domain. It is the most numerous membrane protein of the virion (Siu et al. 2008; Fehr and Perlman 2015). The N-protein packages and encapsidates the RNA genome (Siu et al. 2008). The E-protein is the least abundant protein, but its depletion has shown to have strong negative effects on virus growth and particle formation. It is a viroporin, forming ion channels in the host cell membrane (Siu et al. 2008; Mukherjee et al. 2020).

Besides the structural proteins, the coronavirus genome encodes for 16 non-structural proteins (nsps) in two open reading frames (ORF1a and 1b), which make up two-thirds of the viral genome. Either a shorter polyprotein is translated (pp1a), including nsp1-11, or the longer pp1ab is translated, to produce nsp1-16. This is regulated via a frameshift strategy, where a stop codon is either read or bypassed. Nsp1-11 are involved in regulation of the host immune response and act as cofactors for replication and transcription, while the nsps encoded by ORF1b are the core components of replication and transcription.

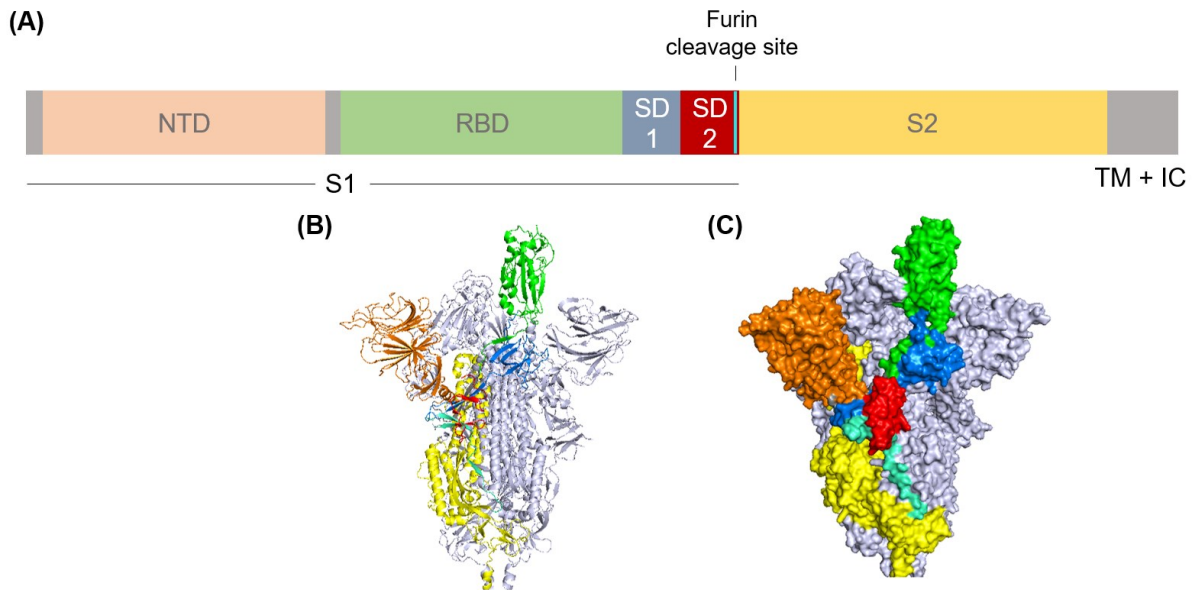


Figure 11: Schematic representation of the full-length SARS-CoV-2 spike protein

(A) Schematic representation of the SARS-CoV-2 spike protein (S-protein) domains in one subunit; NTP: N-terminal domain, RBD: Receptor-binding domain, SD 1/2: subdomain 1 and 2, TM + IC: Transmembrane anchor and intracellular tail. (B) Crystal structure of the S-protein trimer and (C) corresponding surface representation with the S-RBD in the up position (PDB: 7DK3); colors correspond to the schematic in (A), in (B) and (C) only one subunit is colored, the other two are in grey. Own illustrations, (A) based on Jackson et al. (2022), (B) and (C) generated in PyMOL from the given PDB template.

There needs to be a stoichiometric balance between these components for the virus to maintain optimal conditions for infectivity and replication (Hartenian et al. 2020; Finkel et al. 2021; Jamison et al. 2022).

For replication, SARS-CoV-2 needs to enter the host cell via binding to its receptor ACE2. As mentioned above, other coronaviruses utilize different receptors. The S1 subunit containing the receptor-binding domain mediates receptor binding, while the transmembrane S2 subunit, which contains heptad repeat regions and the fusion peptide, mediates fusion with the host cell membrane. This requires cleavage at the S2' site by TMPRSS2. If there is no TMPRSS2, the virus-ACE2 complex can also be internalized by the host cell and be cleaved by cathepsins. In both ways, viral RNA is released into the cytosol of the host cell (Jackson et al. 2022). After the release, the viral replication and transcription complex (RTC) is established, expressing the nsps as described above. Genomic replication is initiated by the synthesis of a negative-sense copy of the full genome, which then functions as a template for the new positive-sense genomes, which then can be packaged into new virions. Simultaneously, nested sets of subgenomic RNAs (sgRNAs) are produced through the process of discontinuous transcription, which is a characteristic of the *Nidovirales*, from the one third of the genome, which encodes for the structural and accessory proteins (Hartenian et al. 2020; V'Kovski et al. 2021; Jackson et

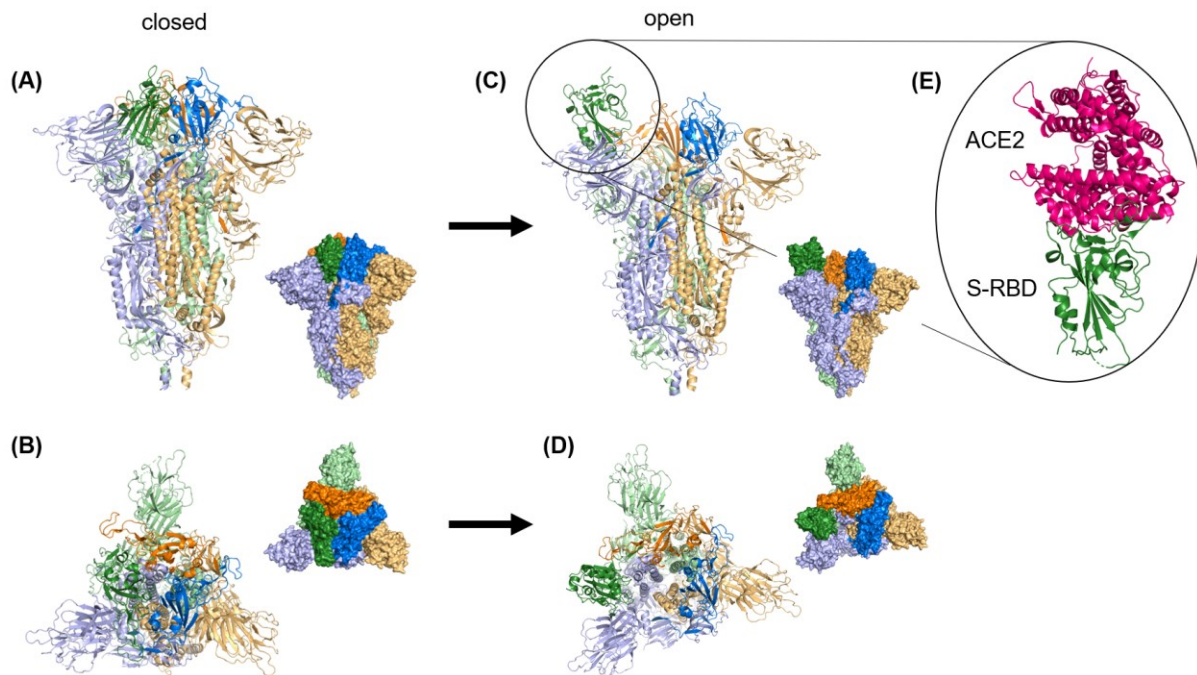


Figure 12: SARS-CoV-2 spike protein in different conformational states

(A) Crystal structure of the spike protein (S-protein) trimer in the closed conformation, corresponding surface representation in the lower right corner, receptor-binding domains (S-RBD) in brighter colors (B) top view of the closed S-protein trimer, surface representation on the right (C) Crystal structure of the open S-protein trimer with one S-RBD (green) in the up position (D) corresponding top view to C (E) Crystal structure of the S-RBD (green) binding to ACE2 (pink) (PDB: A+B: 7DF3, C+D: 7DK3, E: 6VW1). Own illustrations generated in PyMOL from the given PDB templates.

al. 2022). In this process, 3' co-terminal negative-sense sgRNAs are produced as templates for the 5' co-terminal subgenomic mRNAs. This is facilitated by transcription regulatory sequences (TRSs). One TRS-leader (TRS-L) sequence is located at the 5' end of the genomic RNA, while there are also TRS-body (TRS-B) sequences 5' of every ORF along the genome, except ORF1a and ORF1b. Due to complementary sequences between the newly synthesized TRS-B sequence and the TRS-L, the transcription complex can jump from any TRS-B to the TRS-L and continue transcription from that point. The negative-strand sgRNAs now serve as templates for the expression of the structural and accessory proteins. After translation, those proteins transit through the ER-to-Golgi intermediate compartment (ERGIC), where they engage with encapsidated genomic RNA, resulting in budding in vesicles. From those, the new virions are released (Hartenian et al. 2020; V'Kovski et al. 2021).

2.4 The immune system

When a potential pathogen, like a virus, enters the body, in the case of IAV or SARS-CoV-2 via the respiratory tract, an orchestrated response of the host defense mechanisms is

initiated. This is true for all mammals, with some species-specific differences that need to be kept in mind. Also, most main mechanisms are true for avian species as well, but there are also important differences (Sharma 1997). Here, the description focuses on the mammalian adaptive immune response to pathogens.

The first line of defense are the physical and chemical barriers of the body (Riera Romo et al. 2016).

The following immune response is a combination of the innate and the adaptive immune mechanisms (Medzhitov and Janeway 2000; Parkin and Cohen 2001).

The unspecific innate immune response sets in immediately after a pathogen, foreign to the body, is being recognized (Medzhitov and Janeway 2000). This recognition relies solely on general molecular patterns of pathogens and does not require a previous exposure to the antigen to become effective (Muzio et al. 2000). Cells of the innate immune system are neutrophils, macrophages and natural killer (NK) cells (Turvey and Broide 2010).

The adaptive immune response is antigen-specific, meaning that it recognizes specific parts of proteins of the specific pathogen (Parkin and Cohen 2001). While this response is more beneficial, it takes longer to form and requires a previous exposure to the pathogen (Parham 2015). After a first encounter, it takes one to two weeks to effectively respond, while after a repeated exposure, the response sets in after about three days already (Bröker et al. 2019). In the process of forming the specific response, gene rearrangements take place (Parham 2015). The cells of the adaptive immune response are B-cells and T-cells. T-cells can be further differentiated into subclasses, the two most important ones being T-Helper cells (Th-cells) and cytotoxic T-cells (Tc-cells) (DeWitt et al. 2015; Kumar et al. 2018).

Those two defense mechanism do not stand separately from each other, but they closely interact. In the following description, the focus lies on the adaptive immune response, thus parts of the innate immune response will not be discussed in detail. However, it should not be disregarded that the innate response is essential for the development of the adaptive immune response.

Cells of the adaptive immune system

All immune cells originate from hematopoietic stem cells, which is a pluripotent stem cell, being able to give rise to any type of blood cell (Spangrude et al. 1988; Ghosn et al. 2012). Several signaling checkpoints determine the faith of differentiation. Adaptive immune cells arise from the common lymphoid progenitor, which can also differentiate into dendritic or NK cells (Parham 2015). Immune cells can be distinguished via surface markers, the so called "Cluster of Differentiation" (CD), numbered in order of identification, not in a functional pattern (Bröker et al. 2019).

B-cells are named after their origin in the *bursa fabricii* in birds, or the bone marrow in mammals. They carry class II major histocompatibility complex (MHC) molecules, which allows them to present antigen to T-cells after activation (Parham 2015). The transmembrane B-cell receptor (BCR) is composed of a membrane bound antibody molecule linked with an intracellular signaling unit to stimulate the activation of the cell. One B-cell only has one type of specific BCR and only produces antibodies with the same specificity (Parham 2015). Plasma cells are B-cells after activation which produce antibodies, and memory B-cells can be reactivated to become plasma cells with the re-appearance of a previously encountered antigen (Parkin and Cohen 2001).

T-cells are named after their localization of maturation in the thymus (Dalmaso et al. 1963; Kumar et al. 2018). T-cells have T-cell receptors (TCR), which can recognize antigen presented to them bound to an MHC molecule on an antigen presenting cell (APC). Th-cells are CD4-positive and receive antigen via MHC II molecules, while Tc-cells are CD8-positive and require presentation of antigen via MHC I molecules (DeWitt et al. 2015). Th-cells coordinate the immune response and activate B-cells (Kumar et al. 2018). There are different subclasses of Th-cells, which can impact the immune response, depending on the dominant subclass, e.g., Th1-cells dominate for intracellular pathogens, while Th2-cells are more prominent in reactions against non-phagocytatable pathogens (e.g. ectoparasites or worms) and chronic disease (Romagnani 1999). Th17-cells are most active against extracellular pathogens and Treg-cells down-regulate the immune response (Chatila 2005).

Besides the bone marrow and the thymus, the lymphatic system with the lymph vessels and lymph nodes is essential for the transport and maturation of immune cells (Hampton and Chtanova 2019). The spleen also has regions with T- and B-cells, like the periarteriolar lymphoid sheath (PALS) for T-cells and the marginal zone with B-cell follicles (Lewis et al. 2019).

The Major Histocompatibility Complex

As mentioned above, the MHC molecules are important for antigen presentation. Human MHC are also called human leucocyte antigen (HLA) (Parham 2015; Bröker et al. 2019).

Class I MHC are expressed by almost all nucleated cells. Thus, they are not found on red blood cells, but also not on sperm cells and neurons (Parham 2015).

Class II MHC are expressed by APCs, like macrophages, dendritic cells, and B-cells (Parham 2015).

The MHC genes are usually tightly linked and stay together when they are passed on to offspring. This block of MHC genes is called haplotype. The combination of haplotypes in offspring gives rise to new combinations and increases fitness and resistance against

disease. In inbred mouse strains, there is no variability in haplotypes anymore, so they are all histocompatible with each other (Cuppen 2005).

Antigen presentation

When a pathogen enters the body, professional APCs phagocytize or endocytose the pathogen and its peptides are then presented on the MHCs.

Antigen presentation is different in the MHC classes. On MHC I, peptides bind best with 9 amino acids, as they are slightly bending out of the groove, presenting the middle of the peptide (Parham 2015). On MHC II, peptides can be 13 to 18 amino acids long and rather lie flat in the cleft (Parham 2015).

The antigens on the MHC II are recognized by Th-cells, leading to their activation. Tc-cells on the other hand, recognize all foreign antigens on MHC I, leading to the death of those cells (Bröker et al. 2019).

Immunoglobulins

Immunoglobulins (Ig) are usually referred to as antibodies and are one of the most important features of the adaptive immune response beside the cellular components. They are proteins produced by plasma cells, recognizing specific peptides of a previously encountered pathogen (Parham 2015; Bröker et al. 2019). They label their specific antigen, so that phagocytes can eliminate infected cells or antigen complexes.

The Y-shaped molecule consists of two identical heavy chains (~100 kDa) and two identical light chains (~50kDa), each containing a variable and a constant region. They are held together by covalent disulfide bonds and weak interactions. The constant regions form the stem (or F_c) of the antibody, and the variable regions for the antigen binding domain (or F_{ab}) (Figure 13).

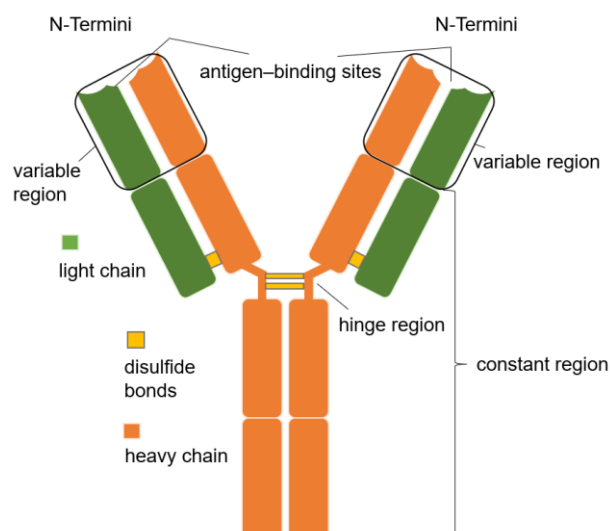


Figure 13: The IgG antibody molecule

The antibody molecule consists of two light chains (green) and two heavy chains (orange), connected via disulfide bonds (yellow).

The N-terminal F_{ab} region is variable and binds to the antigen, while the constant F_c region is located at the C-terminus. Own illustration based on Parham (2015).

There are five classes of antibodies, that differ in function and conformation.

The first antibody class expressed by B-cells is the IgM antibody. Its monomeric form is usually membrane bound and when secreted, it forms pentamers. It activates the innate complement system (Parham 2015).

IgD antibodies are also usually membrane bound and aid the recognition by naïve B-cells. The most abundant and important antibody class are the IgG antibodies. They are soluble and are secreted in large amounts by plasma cells after antigen recognition. In humans, there are four IgG subclasses, while in mice there are three (Dekkers et al. 2017). Their different functions are expressed differentially in specific situations (Vidarsson et al. 2014). IgG1 and IgG3 enhance inflammation during Th1-responses. IgG2 is only mildly inflammatory and dominates during Th2-responses. IgG4 activates an intermediate response and is the only subclass that does not activate complement.

IgA antibodies are mainly found in the mucosa and are mostly secreted as a dimer.

IgE antibodies are secreted as a defense against parasites and are involved in the allergic response.

Immunoglobulins are produced by B-cells. The number of possible antibodies in any one individual are vast, but one single B-cell can only synthesize antibodies with a single antigen-binding region. Thus, B-cells undergo constant negative selection processes in the bone marrow, to eliminate B-cells recognizing self-antigen, or they undergo apoptosis when they don't encounter a suitable antigen. When a B-cell recognizes a fitting antigen, i.e. a pathogen, and an activating Th-cell further stimulates it, it starts to divide and produce antibodies in large numbers. Activated naïve B-cells undergo class switching, meaning that they switch from producing IgM antibodies to producing IgG antibodies. This process takes about one week. Activation usually happens in the cortex of lymph nodes, where subsequently a germinal center forms. In those germinal centers, affinity maturation of the B-cell takes place, meaning that clones of the original B-cell, that bind the antigen more effectively, are positively selected. Those have undergone the process of somatic hypermutation, in which single point mutations are introduced at high rates into the genes encoding for the antigen-binding region, and thus creating clones with higher or lower affinity to the antigen (Parham 2015).

Signaling

To communicate with one another, immune cells utilize different ways of signaling.

They either transfer information via direct cell to cell contact, e.g. Th-cell and APCs communicate via the MHC II receptor, or they use pathways via chemical signals, like cytokines, e.g. chemokines and interleukins (IL). Those cytokines orchestrate the process of inflammation. A plethora of different molecules has been identified, which can be

classified by the use of certain receptors and on their participation in specific immune responses, i.e., if they act on cells of the adaptive or innate response, or if they have pro- or anti-inflammatory properties (Turner et al. 2014).

There are three main receptor types for signaling: the immunoglobulin receptors and type I and II receptors.

The most prominent ligands for the Ig receptor belong to the IL-1 family, which play a central role in the pro-inflammatory responses and are secreted by different cell types like macrophages, B cells and DCs (Dinarello 2009).

Type I receptors are the largest class of immune-related signal systems, with shared signal transduction chains. Their common gamma chain for example is shared between IL-2, IL-4, IL-7 and others (He et al. 1995), while the common Beta chain is used by IL-5, IL-3 and GM-CSF (Woodcock et al. 1994). IL-2 is produced by T-cells and facilitates proliferation and activation of activated B- and T-cells (Turner et al. 2014).

Type II receptors are the second largest immune-related receptor class and are used, among others, by IFN γ , which is a major inflammatory signal. IFN γ is produced by T-cells and activates anti-viral responses, macrophage activity, MHC I and II expression on cells and neutrophil and monocyte function.

Fc γ -Receptors

Antibodies binding to pathogens can serve as ligands for receptors present on immune cells, such as dendritic cells, macrophages, monocytes, B cells, NK cells or neutrophils (Keeler and Fox 2021). The interaction is facilitated via the fragment crystallizable (Fc)

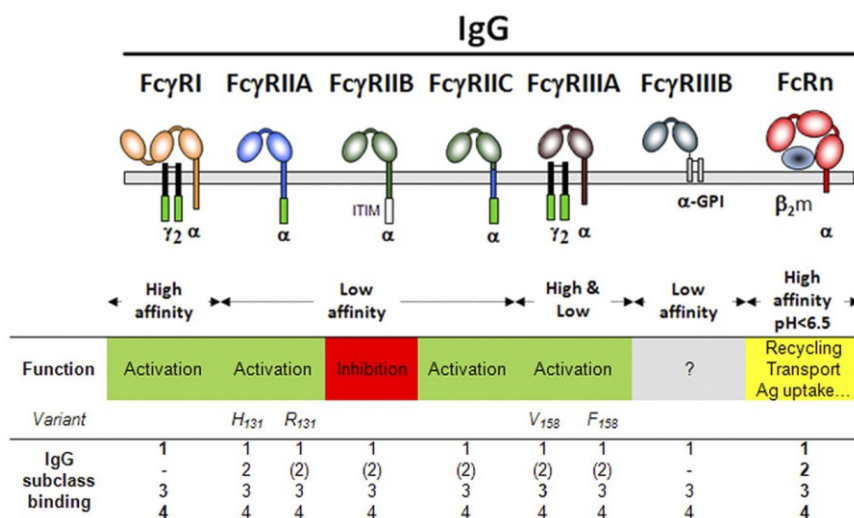


Figure 14: Human Fc γ -receptors

IgG receptors are either associated with activating (ITAM, green) or inhibition (ITIM, white) motifs. IgG subclasses have different binding affinities to the receptors (lower table; high binding affinity in bold, plain low binding, in parentheses very low binding and – indicates no binding). Image reproduced from Bruhns (2012), rights in chapter 14.

region of the antibody and can result in distinct effector functions (Keeler and Fox 2021). The most abundant antibody isotype present in plasma is IgG, which is detectable by Fc gamma receptors (FcγRs) (Keeler and Fox 2021). Such effector functions can result in the clearance of infected cells via antibody-dependent-cellular cytotoxicity (ADCC) or antibody-dependent-cellular phagocytosis (ADCP) (Fonseca et al. 2018). On the other hand, the Fc-FcγR interaction can result in antibody-dependent enhancement (ADE) of the disease, when not clearance of the virus is enhanced, but an easier entry into the cells expressing the receptor, as it has been observed for dengue virus (Balsitis et al. 2010; Halstead et al. 2010).

FcγRs can be distinguished into type I and type II receptors, that bind the IgG Fc domain in either the open (type I) or closed (type II) conformation (Bournazos et al. 2009; Sondermann et al. 2013; Pincetic et al. 2014). Thus, the conformational state of the Fc domain can lead to different immunological outcomes (Pincetic et al. 2014). The six human (hFcγRI, IIA, IIB, IIC, IIIA, IIIB) and four murine (FcγRI, IIB, III, IV) type I FcγRs can further be distinguished by their potential to exhibit activating or inhibiting effector functions (Bruhns 2012; Keeler and Fox 2021).

The activating receptors (hFcγRI, IIA, IIC, IIIA, IIIB and murine FcγRI, III, IV) contain an immunoreceptor tyrosine-based activation motif (ITAM), while the inhibitory receptors (hFcγRIIB and murine FcγRIIB) contain an immunoreceptor tyrosine-based inhibition motif (ITIM) (Figure 14) (Bruhns 2012; Rosales and Uribe-Querol 2013).

Those receptors are usually co-expressed on multiple cell types, combining activating and inhibitory signals, resulting in a fine-tuned initiation of cell functions (Boruchov et al. 2005; Nimmerjahn and Ravetch 2008). Furthermore, the receptors have different binding-capacities for the distinct IgG subclasses (Bruhns 2012).

These downstream antibody effector functions need to be considered when implementing vaccination strategies or therapeutics (Nimmerjahn and Ravetch 2008; Pincetic et al. 2014).

Fc receptor function has been associated with protection against disease, including influenza and SARS-CoV-2, highlighting the importance of antibody functions besides neutralization (Jegaskanda 2018; Richardson and Moore 2021).

2.4.1 Immunity to IAV

2.4.1.1 Immune response to and immunity induced by natural IAV infection

The primary target cells of IAV are airway and alveolar epithelial cells (Shinya et al. 2006; van Riel et al. 2010). As mentioned above, the first line of defense against a pathogen is the unspecific innate immune response. The virus is recognized through pathogen

associated molecular patterns (PAMPs), which activate pathogen recognition receptors (PRRs) (Cao 2016). Most important in IAV infection is the retinoic acid-inducible gene-1 protein (RIG-I), recognizing intracellular ssRNA and transcriptional intermediates of IAV (Opitz et al. 2007; Iwasaki and Pillai 2014). Its activation leads to cytokine production and further downstream antiviral reactions. Cells of the innate immune system in the lungs initiate the first antiviral responses. For example, alveolar macrophages phagocytose infected cells and thus, limit viral spread and take part in the regulation of the following adaptive response (Tumpey et al. 2005). Dendritic cells migrate from the site of infection to the draining lymph node and present IAV antigen to T-cells, initiating the adaptive immune response (Hintzen et al. 2006).

Tc-cells are activated, either by Th1-cells or independently, and induce apoptosis in infected cells (La Gruta and Turner 2014). Their granzyme A has been shown to also cleave viral and host cell proteins involved in viral protein synthesis (Andrade 2010; van Domselaar and Bovenschen 2011). These virus-specific Tc-cells are more directed against conserved proteins, like NP, M1 and PA, and last up to two years in mice (Valkenburg et al. 2012; Grant et al. 2016). Memory T-cells alone, however, are not capable of protecting mice from heterosubtypic IAV infection (Rangel-Moreno et al. 2008).

Th2-cells activate and promote the B-cell response. As described above, during the life cycle of IAV, not all viral proteins are similarly abundant and thus, not equally accessible to immune cell receptors.

HA is the immunodominant protein of IAV, as it is the most abundant surface protein and responsible for binding to the host cell receptor. Antibodies targeting the receptor-binding site are defined as a correlate of protection (Hobson et al. 1972). The importance of antibodies against the HA head is their strong neutralizing and hemagglutination inhibition activity (Ohmit et al. 2011; Memoli et al. 2016). These effects are achieved by blocking of the interaction either via steric hindrance or direct binding of the antibody to the receptor-binding pocket (Schmidt et al. 2015; Krammer 2019).

Natural infection has shown to induce antibody responses focused on the globular head of HA (Krammer 2019). This type of response, however, although shown to be very long lived, is rather strain-specific, as the HA head is prone to continuous changes due to antigenic drift. Antibodies against the more conserved HA-stalk domain, which have the potential to also inhibit virus entry, are only prevalent at very low levels. Thus, if an individual encounters an IAV of a strain that has drifted away far enough from the strain that person had originally been infected with, there will be no sufficient level of protection. Due to this, IAV can cause yearly epidemics with severe outcomes.

Furthermore, antibodies against NA that inhibit its function have also been identified as a correlate of protection (Couch et al. 2013; Monto et al. 2015; Memoli et al. 2016). It is far

less immunostimulatory than HA, but antibodies are prevalent and present for a long time (Rajendran et al. 2017).

Antibodies against internal IAV antigens like NP, are detectable after infection, but at very low levels and they do not seem to contribute to antibody-mediated protection.

The mucosal immune response to natural infection most likely targets the same proteins but might produce more broadly reactive antibodies due to a higher avidity of the dimeric form of secreted IgA antibodies (Suzuki et al. 2015; Krammer 2019).

An important concept that needs to be considered when looking at immunity to influenza viruses is the original antigenic sin (OAS). It describes that the exposure to a certain strain of IAV in early years shapes the immune response to following IAV infections and vaccinations with drifted strains later in life (Krammer 2019). The classic OAS concept indicates, that the imprint that had been made by the original strain leads to a boosting effect, that is mainly directed against the shared epitopes between both strains, and not so much against the drifted regions in the new strain (Francis 1960; Krammer 2019). This is not fully understood yet but could be utilized to create more efficient vaccination concepts. Especially for H3N2 strains, which have undergone a greater antigenic evolution than H1N1 strains, the memory B-cell response seems to have a strong shaping effect on the immune response after vaccination (Auladell et al. 2022).

2.4.1.2 Current influenza vaccines, vaccine response and alternative vaccination strategies

Vaccination is the most important tool available to prevent the seasonal flu and to reduce the severity outcome of the seasonal epidemics. Current vaccines, however, are only 10-60% effective, due to vaccine mismatch with the actual circulating strain (Krammer and Palese 2015; Paules et al. 2017; Paules et al. 2018).

The composition of the vaccine is evaluated and updated, if necessary, every year by the WHO for the Northern and Southern hemispheres based upon monitoring of the currently circulating virus strains. This prediction is made six to nine months in advance to the next flu season, during which the vaccines can be manufactured. The long timespan leaves sufficient possibility for the virus to change until the vaccines are administered. As current vaccines are mainly produced in embryonated chicken eggs, egg adaptation of the vaccine seed virus can further reduce effectiveness (Raymond et al. 2016; Zost et al. 2017). In the 2014-15 season, the H3N2 strain in the vaccine only had a 13% effectiveness against the actual circulating strain, leading to a high morbidity and mortality especially in the elderly (Paules et al. 2018).

Currently, intramuscularly administered trivalent or quadrivalent (TIV or QIV) split virus or viral subunit vaccines are used most commonly, including two IAV strains (H1N1 and

H3N2) and one or two IVB strains (Victoria and Yamagata) (Soema et al. 2015; Paul-Ehrlich-Institut 2022). In Germany, the Standing Committee on Vaccination (Ständige Impfkommision, STIKO) recommends the use of the QIV vaccine since 2018 (STIKO 2018).

The abovementioned formulations follow the use of whole inactivated virus (WIV) or split vaccines when they show to have an acceptable level of adverse effects (al-Mazrou et al. 1991; Barberis et al. 2016). All inactivated vaccine preparations available today are equally immunogenic and safe (Beyer et al. 1998; Beyer et al. 2011).

There are also live-attenuated influenza vaccines (LAIV), which are being administered via a nasal spray, following the natural route of infection (Soema et al. 2015). This has shown to induce mucosal responses, which inactivated vaccines are not capable of doing (Tosh et al. 2008; Soema et al. 2015). They have shown to be more beneficial in children older than two years, but only limited in non-naïve adults (Ohmit et al. 2006; Belshe et al. 2007). The protection that is achieved by vaccination is not only dependent on the degree of matching between circulating and vaccine strains, but can also be influenced by prior influenza exposure, vaccination history, age and comorbidities (Paules et al. 2018).

Strikingly, a cohort study evaluating the relationship between preexisting anti-HA antibodies and preexisting CD4 T-cells specific for H1 and H3 and the B- and T-cell responses to vaccination with commercial vaccines, found a negative relationship between the abundance and expansion of CD4 T-cells after vaccination, as well as an inverse relationship between preexisting anti-HA antibodies and CD4 T-cell and B-cell responses to vaccination (Moritzky et al. 2023).

Overall, currently available vaccines are an important public health measure, but have some important drawbacks as outlined above. Thus, new vaccination strategies are needed to overcome these.

A target for a universal or broadly protective influenza vaccine was identified by the National Institute of Allergy and Infectious Diseases (NIAID) as: “A vaccine with $\geq 75\%$ protection against symptomatic disease caused by group 1 and 2 influenza A viruses lasting ≥ 12 months in all populations” (Paules et al. 2018).

The aim for broad protection needs new approaches in antigen design and delivery. As neutralizing antibodies are directed towards the HA-head, new additional correlates of protection would have to be defined for broadly reactive immune responses, as those employ different modes of action. The conserved stalk domain (Krammer and Palese 2013) or conserved epitopes in the head (Wu and Wilson 2018) of the HA have been identified as possible targets, as well as the NA (Eichelberger et al. 2018), the ectodomain of the M2 protein (Schepens et al. 2018), or the NP, which has been shown to induce a strong T-cell response (Zheng et al. 2014; Clemens et al. 2018; Leroux-Roels et al. 2023).

Alternative delivery platforms include among others viral vectors or mRNA. Suitable viral vector platforms that have been studied intensely for influenza A antigens are the Modified Vaccinia virus Ankara (MVA) (Antrobus et al. 2012; Lillie et al. 2012; Altenburg et al. 2014) or Adenoviruses (Gurwith et al. 2013; Antrobus et al. 2014). The mRNA technology has recently gained momentum during the COVID-19 pandemic and has also been applied to influenza A antigens. A multivalent mRNA vaccine encoding for 20 different HA antigens was recently shown to confer protection against matched and mismatched virus strains in mice and ferrets (Arevalo et al. 2022).

Modes of action important for broadly reactive immunity are ADCC via Fc γ -receptors (Jegaskanda et al. 2013b; Jegaskanda et al. 2013c; DiLillo et al. 2014; Jegaskanda et al. 2014), CD8 T-cell responses (Zheng et al. 2014; Paules et al. 2017) and complement-dependent cytotoxicity (Terajima et al. 2011). Important to note is, that the standard TIV was shown to not induce or prime cross-reactive ADCC and Tc-cell responses de novo, in contrast to natural infection (Jegaskanda et al. 2013a).

2.4.2 Immunity to SARS-CoV-2

2.4.2.1 Immune response to and immunity induced by natural SARS-CoV-2 infection

SARS-CoV-2 enters the body, just like IAV, through the respiratory tract and replicates in the upper and lower airway epithelia (Sette and Crotty 2021). Here, it is also subjected to the initial innate immune response. As described above, one group of main effector molecules of the innate response are interferons. SARS-CoV-2 has been shown to effectively evade and block this particular response, leading to a less efficient and delayed innate and subsequently adaptive immune response (Arunachalam et al. 2020; Bastard et al. 2020; Blanco-Melo et al. 2020; Laing et al. 2020; Kasuga et al. 2021). A short temporal delay in innate response is associated with so-defined asymptomatic or mild disease (Oran and Topol 2020), while an impaired or far delayed innate response has shown to lead up to severe or fatal disease (Hadjadj et al. 2020; Galani et al. 2021). In the latter case, the virus can replicate to high numbers without being stopped by innate and adaptive responses until it reaches high viral loads. Without an effective adaptive response and a high viral load, eventually the innate response attempts to control the infection with an overshooting response, leading to excessive lung pathology. Additionally, the few T-cells available are over-reactive, adding to the inflammatory effect. This phenomenon is referred to as “cytokine storm” and can lead to severe conditions such as acute lung injury (ALI), systemic inflammatory response syndrome (SIRS) and acute respiratory distress syndrome (ARDS) (Song et al. 2020).

The adaptive humoral immune response to SARS-CoV-2 is mainly directed towards to S-protein (Merad et al. 2022). Antibodies against the S-RBD can neutralize the virus by blocking interaction with the receptor (Zohar and Alter 2020). Fewer antibodies with neutralizing activity are directed against the NTD (Piccoli et al. 2020). As described above, SARS-CoV-2 VOCs have mutations mainly in the S-RBD, resulting in escape from neutralizing antibodies (Merad et al. 2022).

Cellular immune responses are directed against multiple antigens, including structural and nonstructural viral proteins (Rydzynski Moderbacher et al. 2020). Generally, the presence of virus-specific T-cells has been associated with milder disease (Liao et al. 2020; Sekine et al. 2020; Zhou et al. 2020b).

From other coronaviruses it is known that the protective effect of the immune response may wane rather quickly, only lasting less than one year, enabling reinfections with the same virus (Edridge et al. 2020). For SARS-CoV-2 this seems to be the case as well. Neutralizing antibody responses, the correlate of protection, peak within the first weeks after infection, but subsequently decline quickly (Cromer et al. 2021; Muecksch et al. 2021), while cellular responses last longer (Zuo et al. 2021). A recent meta-analysis found no significant differences in the clinical pattern or severity of primary infections and reinfections, suggesting that natural immunity is not long-lasting in COVID-19 patients (Deng et al. 2023a). However, the duration of protection against reinfection after a SARS-CoV-2 infection is not fully understood yet and more research is needed.

The emergence of antigenically distinct immune-escape VOCs has led to continuous waves of infection and reinfections. Reinfections with the Omicron VOC occur at a higher frequency than with previous VOCs (Burkholz et al. 2023). Also, Omicron reinfections after initial Omicron infection are happening over a shorter time span than after primary infection with an earlier VOC (Burkholz et al. 2023). Omicron is also known to inhibit MHC I expression and upregulation, leading to evasion of recognition by CD8 T-cells (Moriyama et al. 2023). This evidence suggests that SARS-CoV-2 continues to develop more immune escape and inhibiting features, leading to a less efficient and less durable humoral and cellular immune response after natural infection.

As for IAV, the phenomenon of immune imprinting, or original antigenic sin, is also discussed for SARS-CoV-2. Evidence suggests that prior infection or vaccination with the original Wuhan-Hu-1 strain shapes the immune response to subsequent variants or vaccinations with altered antigen (Roltgen et al. 2022). On the other hand, it has been found, that immunity to seasonal coronavirus spike proteins has no negative effect on immunity after mRNA vaccination against SARS-CoV-2 in mice (Amanat et al. 2023). These findings need to be further investigated to implement them into research for new vaccines.

2.4.2.2 Current SARS-CoV-2 vaccines and vaccine response

The emergence of SARS-CoV-2 and the COVID-19 pandemic have led to an unprecedented public health response including the fast development of vaccines. By February of 2023, current vaccines have approximately saved more than 20 million lives (Callaway 2023). As of March 2023 (most recent update), the “COVID-19 – Landscape of novel coronavirus candidate vaccine development worldwide” of the WHO lists 183 vaccines in clinical development and 199 vaccines in pre-clinical development (WHO 2023a).

As the main vaccine antigen, the S-protein of the original Wuhan-Hu-1 strain was used on different vaccine platforms (Patel et al. 2022). Because of the emergence of the VOCs, there are also bivalent vaccines on the market by now, additionally including the Omicron BA.1 or BA.4/5 S-proteins as an antigen.

The first two vaccines to receive a conditional authorization in the EU were based on mRNA, namely Comirnaty[®] (BioNTech/Pfizer) and Spikevax[®] (Moderna). These two vaccines are still available, meanwhile also in the bivalent formulation. They induce high titers of neutralizing antibodies, activate T-cell responses and overall decrease disease severity and spread (Jackson et al. 2020; Walsh et al. 2020; Kalimuddin et al. 2021; Rotshild et al. 2021; Sahin et al. 2021).

One downside to them is that they need to be stored at a temperature of -80°C until application, which hinders distribution and shipping to remote places (Echaide et al. 2023). The formulation should also be revised to shift the response away from the Th17 activation (Echaide et al. 2022; Echaide et al. 2023).

Two other vaccines based on an adenoviral vector platform were also authorized early on and broadly distributed. Compared to the mRNA vaccines, the adenoviral vaccines, especially Vaxzevria[®] by AstraZeneca, were found to cause increased levels of severe side effects, like thrombosis with thrombocytopenia syndrome (TTS), immunothrombocytopenia (ITP) and in rare cases also cerebral venous sinus thrombosis (CVST) or splanchnic vein thrombosis (SVT) (Greinacher et al. 2021b; Kowarz et al. 2022). It was found that autoantibodies against platelet factor 4 (PF4) played a role in this condition (Greinacher et al. 2021a). In reference to the condition heparin-induced thrombocytopenia (HIT), the term vaccine-induced immune thrombotic thrombocytopenia (VITT) was established (Kowarz et al. 2022).

It was also found, that in addition to the membrane bound immunogenic S-protein, which was delivered via the Ad5-vector, smaller, soluble fragments of the spike protein were also produced (Kowarz et al. 2022). These resulted in immune aggregates in the brain sinuses causing the thrombotic events. This was explained with the finding that by codon-

optimization, additional splicing donor and acceptor sites had been introduced into the S-gene. The vector contains DNA, which undergoes the regular splicing process of the cell, which viral RNA would not. This is why the genes of cytosolic RNA-viruses like SARS-CoV-2 are not laid out for splicing.

Those complications usually occurred in people younger than 60 years of age, so that in Germany the distribution of the vaccine was first limited to the age group above-60 years, before Vaxzevria[®] was fully suspended (RKI 2021). The other adenoviral vaccine by Janssen (JCOVDEN) is still available, but also only for the above-60 age group (RKI 2021). In other parts of the world, other vaccines were licensed, like the whole inactivated virus-vaccine COVAXIN[®] in India, or the vaccines by Sinopharm in China (BIBP-CorV and WIBP-CorV, both WIV-vaccines).

Most vaccines were able to prevent symptomatic infection and severe or critical disease (Grana et al. 2022), but are more efficient in preventing severe disease than milder cases (Yang et al. 2023). Vaccine efficiency decreased with time after the last dose and was higher after subsequent booster doses (Link-Gelles et al. 2023; Yang et al. 2023). Against the Omicron VOC, primary immunization with either mRNA or adenoviral vaccines showed only limited protection against symptomatic disease, which could be increased with an mRNA booster dose, but this also decreased over time (Andrews et al. 2022). A third booster dose of mRNA vaccine was shown to enhance neutralization capacity against Omicron (Muik et al. 2022b), but the current subvariant XBB shows an even further enhanced immune escape ability (Brandolini et al. 2023). The bivalent booster vaccines were recommended by the German STIKO in October 2022 (RKI 2022). They have shown to reduce hospitalization and death and were also effective against the BQ.1-BQ.1.1 and XBB-XBB.1.5 subvariants (Lin et al. 2023).

Overall, these first vaccines were a valuable tool to prevent severe disease and death in the first years of the pandemic, but due to the limitations described above, especially in the context of new subvariants emerging continuously, new vaccines need to be developed (Al-Fattah Yahaya et al. 2023; Marks et al. 2023). The goal is to induce a long-lasting protection, which covers a broad range of SARS-CoV-2 variants, and maybe even a broader class of coronaviruses (Callaway 2023). Protection should not only prevent infection, but also transmission of the virus (Callaway 2023; Marks et al. 2023). Additionally, the formulation of the following vaccines should be improved to lower the risk of side effects and be more effective at lower doses (Morens et al. 2023).

One potential new approach are intranasal vaccines, that mimic the route of natural infection and can induce mucosal antibodies, which could prevent or reduce infection (Morens et al. 2023). Some candidate vaccines have already been proven to be superior to the current approaches in mice and hamsters, resulting in high levels of neutralizing

antibodies, a robust T-cell response, and inhibition of replication of the virus in the respiratory tract (Deng et al. 2023b; Nouailles et al. 2023). An intranasal Omicron booster vaccine after intramuscular immunization also showed improved results in providing an effective mucosal and systemic immune response (Wang et al. 2023).

Another approach is the use of different vaccine epitopes. Immunodominant T-cell epitopes that are conserved in VOCs have been found to be outside of the S-protein (Shafqat et al. 2022). Furthermore, broadly neutralizing antibodies have been identified against a conserved area of the S-RBD (He et al. 2022). Those antibodies proved to be protective against diverse SARS-like coronaviruses (He et al. 2022).

2.5 AAV-vectors

Adeno-associated viruses (AAV) have first been described by Atchison et al. (1965), when they were conducting research on simian adenoviruses and found them as a contamination. They were described as particles, that were antigenically different from the adenoviruses and could only replicate in their presence (Atchison et al. 1965; Hoggan et al. 1966).

Since then, they have come a long way and have proven to be a valued tool as vectors, mostly for gene therapy, but also as vaccine vehicles.

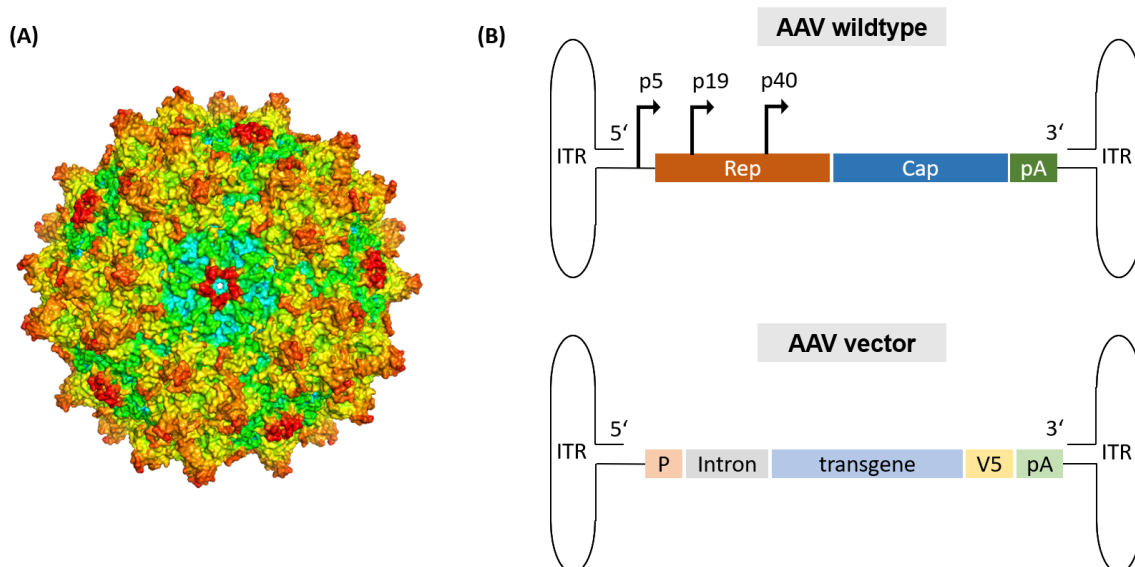


Figure 15: Schematic representation of Adeno-associated virus vectors

(A) AAV9 vector capsid represented as a 3D model (PDB: 7MT0, color-gradient b-factor, own illustration generated in PyMOL). **(B)** schematic of the Adeno-associated virus (AAV) genome of the wildtype (upper panel) and vector (lower panel). In the wildtype genome the replication (rep) and capsid (cap) genes are present, p9, p19 and p40 indicate the promoters and pA the termination signal. The AAV-vector genome contains the promoter (P), Intron, transgene, V5-tag and pA-signal. Own illustration based on Daya and Berns (2008) and Kwon and Schaffer (2008).

AAV belong to the family of *Parvoviridae* and to the genus of *Dependoparvovirus* (Muzyczka and Berns 2001; Sant'Anna and Araujo 2022). They are replication defective and depend on helper viruses, e.g. adenoviruses or herpesviruses for replication in mammalian cells (Carter 2004). AAV have a single-stranded DNA genome of ~4.7 kb in size, encoding for three open reading frames, the rep (replication), cap (capsid) and aap (assembly), which can result in at least eight gene products (Srivastava et al. 1983; Sonntag et al. 2010; Naso et al. 2017). Positive and negative DNA strands are equally sufficient for packaging and infection (Samulski et al. 1987; Zhong et al. 2008; Zhou et al. 2008). The coding sequences are flanked by inverted terminal repeats (ITRs), which serve as the starting point of replication and as a packaging signal (Hauswirth and Berns 1977; Samulski and Muzyczka 2014). Their capsid is 25nm in diameter, arranged in a $T = 1$ icosahedral symmetry and consists of 60 capsid subunits (Figure 15) (Sonntag et al. 2010). Those 60 subunits are a combination of the three expressed cap gene proteins VP1, VP2 and VP3 in a stoichiometric ratio of 1:1:10, resulting from alternative splicing and translation initiation from a nonconventional ACG codon (Becerra et al. 1988; Cassinotti et al. 1988; Trempe and Carter 1988). The rep gene encodes for the four proteins required for viral genome replication and packaging, Rep78, Rep68, Rep52, Rep40 (Figure 15) (Naso et al. 2017). The assembly-activating protein is encoded by the aap gene and is suggested to provide a scaffolding function during capsid assembly (Naumer et al. 2012). For infection, AAV either bind to heparan sulfate proteoglycan (HSPG), or N- or O-linked sialic acid on the cell surface as their primary receptor (Summerford and Samulski 1998; Perabo et al. 2006; Vance et al. 2015). Fibroblast growth factor receptor 1 (FGFR1), $\alpha_v\beta_5$ integrin, hepatocyte growth factor receptor (HGFR), the laminin receptor (LamR), epidermal growth factor receptor (EGFR) and the platelet-derived growth factor receptor Beta (PDGFRB) have been identified as secondary receptors, depending on the serotype (Qing et al. 1999; Summerford et al. 1999; Vance et al. 2015). For cell entry, the type I transmembrane protein KIAA0319L has been identified as a universal AAV receptor (AAVR) (Pillay et al. 2016).

After binding to the receptors, AAV are internalized either via clathrin-coated pits or endocytosis (Bartlett et al. 2000). Helper function of adenoviruses is only necessary for early gene expression, not for entry or passage through the cell (Ferrari et al. 1996; Bartlett et al. 2000). AAV uses the cells microtubule network to reach the perinuclear region to deposit the DNA (Xiao and Samulski 2012), before it is imported to the nucleus via the nuclear pore complex, small GTPase Ran and cellular karyopherins (Nicolson and Samulski 2014). The genome can either be integrated into chromosome 19 or remain extrachromosomal as episomes (Deyle and Russell 2009). AAV can enter the lytic stage characterized by genome replication, viral gene expression and virion production in the

presence of helper genes, like adenoviral E1a, E1b, E2a, E4 and VA RNA or the DNA polymerase, helicase and other necessary components for transcription of herpesviruses (Carter 2004; Daya and Berns 2008). Otherwise, they can develop latency (Daya and Berns 2008). Other helper viruses have been described as well, e.g. hepatitis B virus (HBV) (Hosel et al. 2014) or human bocavirus 1 (Wang et al. 2017).

Antibodies against AAV are highly prevalent in humans and non-human primates, distinguishing them into different serotypes assigned to six clades (A-F) or classifying them as clones (AAV3-5, ch.5, rh.8) (Gao et al. 2004; Weitzman and Linden 2011). Overall, more than 100 genomic species have been identified, which belong to AAV1-9 (Gao et al. 2004; Mitchell et al. 2009). AAV serotypes 2, 3 and 5 were isolated from humans, while serotype 4 was identified in non-human primates and the origin of AAV1 and 6 is unclear, as it has been isolated from both sources (Gao et al. 2002). Depending on their capsid, those serotypes demonstrate different tissues tropisms (Mitchell et al. 2009).

AAV harbor some favorable features, which have led to their wide use as vectors for gene delivery in humans. They are non-pathogenic, making them safe for the use in humans (Berns and Linden 1995). When they are used as vectors, all viral genes can be deleted, resulting in a high efficiency of delivering the transgene, while the immunogenicity is reduced further, and safety is enhanced (Kwon and Schaffer 2008). They can deliver the transgene to dividing and non-dividing cells in various tissues (Fisher et al. 1997; Gao et al. 2002), depending on the cell tropism of the serotype (Wu et al. 2006).

Downsides include the broadly pre-existing immunity in the human population to multiple serotypes (Erles et al. 1999; Cottard et al. 2004; Calcedo et al. 2009), their limited packaging size (Dong et al. 1996; Wu et al. 2010) and the inefficiency of delivering the transgene in high concentration only to specific cell populations (Kwon and Schaffer 2008). Three AAV-vector based drugs have been approved for the purpose of gene therapy, one targeting the LPL gene with an AAV1-based vector injected into the thigh muscle (Glybera[®]), another one targeting the RPE65 gene with an AAV2-based vector injected into the retina (Luxturna[®]) (Bennett et al. 2016) and Zolgensma[®] for spinal muscular atrophy, underlining their safety. Unfortunately, due to the high cost of the treatment, Glybera[®] has already been withdrawn from the market, five years after having been approved (Senior 2017).

While for the use in gene therapy the host immune response towards the vector and the transgene is unwanted (Barnes et al. 2019; Lotfinia et al. 2019; Rabinowitz et al. 2019), there needs to be an immune response against the transgene for the purpose of using the vectors as vaccines (Nieto and Salvetti 2014). The capsid, however, should ideally not be subjected to a neutralizing, pre-existing immune response and, for vaccines, should be able to be delivered repeatedly, if needed as a booster dose (Nieto and Salvetti 2014).

Especially, the response of Tc-cells, lysing cells expressing non-self antigen on MHC I receptors, would be unfavourable, as this would attenuate transgene expression (Barnes et al. 2019; Rabinowitz et al. 2019). Importantly, also in commonly used animal models, neutralizing antibodies against AAV1, 2, 6 and 9 were found, even in mice purchased directly from a commercial breeder (Rapti et al. 2012).

Successful efforts have been made to engineer the AAV-vector capsid to hinder the immune response towards them (Lee et al. 2005; Maguire et al. 2012), to create variants resistant to neutralization, while simultaneously improving targeted delivery to specific tissues or cells (Hudry et al. 2016; Meliani et al. 2017), or to find alternative application routes circumventing neutralization (Limberis and Wilson 2006; Gray et al. 2013).

2.5.1 AAV-vectors as vaccines

AAV-vectors have been evaluated for the use as vaccines against various viruses, including IAV (Xin et al. 2001; Lin et al. 2009; Sipo et al. 2011; Fiddeke 2016; Demminger et al. 2020), SARS-CoV (Du et al. 2006; Du et al. 2008b; Du et al. 2008c) and recently also SARS-CoV2 (Zabaleta et al. 2021; Liao et al. 2022; Liu et al. 2022; Qin et al. 2022; Wu et al. 2022; Zabaleta et al. 2022; Zhao et al. 2022; Tong et al. 2023).

2.5.1.1 AAV-vector vaccines against influenza A viruses

Xin et al. (2001) wanted to test the hypothesis that AAV-vectors could be used as effective vaccine vehicles for HIV. To additionally evaluate the protective effect of AAV-vector immunization against viral challenge, they used an AAV-vector carrying the HA gene of the influenza A/PR/8/34 strain and subsequently infected the mice with homologous virus. They could show a partial protection of 75% in immunized mice compared to only 5% in non-immunized mice (Xin et al. 2001).

Lin et al. (2009) focused on designing a hybrid AAV from two rhesus macaque isolates, to overcome the limitations of AAV-based vaccines, especially regarding neutralization by pre-existing antibodies and CD8⁺ T-cell responses. They used IAV NP as the vaccine antigen and compared an AAV8 vector with their newly designed AAVrh32.33 vector. To show the impact of neutralizing antibodies from human sera on the efficiency of the AAV-vector vaccines, they additionally transferred human Ig to some groups. They could show that immunization with IAV NP resulted in complete protection against challenge, but neutralization by existing nAbs from human sera reduced protection in the mice immunized with AAV8 NP. Neutralization was avoided in the AAVrh32.33 vector. They explained protection through the NP with a sufficient T-cell response (Lin et al. 2009).

Sipo et al. (2011) used an AAV-vector with the AAV9 capsid and the AAV2 ITR carrying either the HA, NP or M1 genes of influenza A/Mexico/4603/2009 (H1N1). They immunized

mice with each vector individually as well as in a trivalent combination. They could show that all mice immunized with HA and NP were protected against challenge with homologous virus and virus-specific humoral and cellular immune parameters were induced. Partial protection against heterologous virus was also seen in mice immunized with the trivalent vaccine. The strongest T-cell response was developed against NP. Antibody responses were strong against HA and NP, but neutralization was only strain specific (Sipo et al. 2011).

Fiddeke (2016) further examined an AAV9/2 (AAV9 *cap* and AAV2 *rep*) vaccine carrying the NP gene of influenza A H1N1pdm09 and influenza A/PR/8/34. She could show that immunization with these vectors was able to protect mice from homologous challenge and induced a strong T-cell response but could not protect mice from heterologous challenge (Fiddeke 2016).

Demming et al. (2020) used the existing AAV9/2 platform to evaluate broad protection induced by AAV-vectors carrying HA, NP and cHA antigens of influenza A Cal/7/9 (H1N1)pdm virus. AAV-HA, -cHA and -NP, as well as WIV were shown to induce broadly reactive antibodies in mice after intranasal application. The response to HA and cHA was mainly directed against group 1 HAs, while NP and WIV induced antibodies reacting with viruses from both HA groups, with the response to WIV resulting in lower titers than to AAV-NP. Interestingly, the broadly reactive antibodies induced by AAV-vectors showed not to be neutralizing but were rather able to activate Fc γ R responses. Furthermore, AAV-vectorized vaccines were able to protect mice from homologous and heterologous challenge and to reduce disease severity in ferrets (Demming et al. 2020).

The AAV9/2-vector which has been used in the studies of Sipo et al. (2011), Fiddeke (2016) and Demming et al. (2020) has proven to be advantageous for the application to the respiratory tract. AAV9 targets alveolar epithelial cells and has shown a long continuous expression of the transgene (Limberis and Wilson 2006; Bell et al. 2011; Fiddeke 2016). Additionally, it has been shown that AAV9 is less subjected to neutralization by pre-existing immunity and can be re-administered via the respiratory tract without loss of efficiency due to neutralizing antibodies (Gao et al. 2004; Limberis and Wilson 2006; Boutin et al. 2010). The abovementioned findings indicate that AAV-vectors, and more specifically AAV9/2 vectors, have a large potential for the use as broadly protective influenza vaccines. However, the interplay of humoral and cellular responses towards different IAV subtypes, as well as Fc γ R effector functions and the expansion of the immune response over both HA-groups need to be further assessed.

2.5.1.2 AAV-vector vaccines against SARS-CoV and SARS-CoV-2

Du et al. (2006) have described an AAV-vector encoding for the S-RBD of SARS-CoV. They could show, that a single intramuscular injection was able to induce a virus-specific antibody response, significantly higher compared to an inactivated vaccine, which reached their highest level after 1-1.5 months and also showed neutralizing activity (Du et al. 2006). They subsequently conducted a follow-up study evaluating a prime-boost scheme with an RBD-rAAV prime and a boost with specific T-cell peptides. They found that this was able to induce effective, cross- and long-term protective effects against infection (Du et al. 2008b). Additionally, they also studied intranasal application of their RBD-rAAV-vector, which resulted in strong systemic and local mucosal immune response and a stronger T-cell response as intramuscular application, even though the immune response induced by the latter lasted longer (Du et al. 2008c).

Since the beginning of the SARS-CoV-2 pandemic, the AAV-vector platform was also evaluated as a vaccine platform against the virus. So far, one vaccine has reached clinical trials (AAV5-RBD, Biocad, Russia) and one is in pre-clinical evaluation (AAVCOVID, Massachusetts Eye and Ear/Massachusetts General Hospital/AveXis (Zabaleta et al. 2021; Zabaleta et al. 2022)) (WHO 2023a). Other candidate vaccines have also been described. Most of them are based on the S-RBD (Liao et al. 2022; Liu et al. 2022; Qin et al. 2022; Wu et al. 2022; Tong et al. 2023), one on the S1-domain of the spike protein (Zhao et al. 2022) and one on the whole spike protein (Zabaleta et al. 2021; Zabaleta et al. 2022).

The AAVCOVID project uses the abovementioned AAVrh32.33 vector (Lin et al. 2009) carrying the whole, membrane-anchored spike protein of SARS-CoV-2 (Zabaleta et al. 2021). They could demonstrate a durable protection in non-human primates (NHP) after a single intramuscular injection. A strong humoral and cellular immune response was induced. Neutralization titers have shown to be stable in mice for six months and in NHP for eleven months after administration. It also reduces viral load in the upper and lower respiratory tract, suggesting that it can also reduce transmissibility (Zabaleta et al. 2021). They further described that the vaccine can be readily adapted to novel variants (Zabaleta et al. 2022). Another advantage of this platform is that the vaccine can be stored at room temperature for up to one month and at least 12 weeks at 4°C without loss of efficiency (Zabaleta et al. 2021; Zabaleta et al. 2022).

The other AAV-vector vaccines containing the S-RBD or S1 domain in different formulations also described the successful induction of long-lasting immune responses with neutralizing ability.

Overall AAV-vectored vaccines have a potential to be used as a vaccine against SARS-CoV-2. The induction of a strong, protective, and durable immune response already after

one injection seems advantageous. Also, they can be readily adapted to newly emerging variants and other antigens can be incorporated. Whether they can be superior to other vaccine platforms, will have to be proven in the future.

2.6 Mouse models in influenza A virus and vaccine research

Mice are a common and well-established model organism used in IAV research. In this context, there are advantages and disadvantages for their use, which influence the transferability of results to humans.

Technical and organisational advantages of using mice in biomedical research are their small size, low cost, easy husbandry, availability of transgenic strains and availability of analytic reagents, the latter being especially relevant for immunological reagents (Bouvier and Lowen 2010; Margine and Krammer 2014). Furthermore, with the use of inbred strains the results are usually homogenous and reproducible (Roubidoux and Schultz-Cherry 2021).

In IAV vaccine development, typically the first screenings of vaccine efficacy and safety are conducted in the mouse model (Margine and Krammer 2014). The most commonly used mouse strains for this purpose are the inbred strains C57BL/6 and BALB/c, and their use has been well established over time (Bodewes et al. 2010; Bouvier and Lowen 2010; Nguyen et al. 2021).

However, wild mice are not a natural host of influenza viruses (Haller 1981; Margine and Krammer 2014), which is the most relevant drawback of the mouse model for IAV. This natural resistance to seasonal IAV has been linked to the Mx1 protein, which is expressed in wild mice (Staeheli et al. 1986; Grimm et al. 2007). Therefore, in research settings, mouse adapted IAV, like the influenza virus A/Puerto Rico/8/1934 (H1N1) or X31 (H3N2), are used (Bouvier and Lowen 2010; Margine and Krammer 2014), which can differ greatly from the original strains. However, the highly pathogenic IAV strains, i.e. H5N1 or H7 strains, but also the pandemic H1N1 strains of 1918 and 2009, can cause disease in mice without adaptation (Lu et al. 1999; Maines et al. 2009; Medina et al. 2010; Xu et al. 2013). As a reason, differential binding preferences of sialic acid receptors between the different IAV strains and the divergent expression patterns of these receptors in mouse and human respiratory tract cells were described (Ibricevic et al. 2006; Zhao and Pu 2022). The infection with highly pathogenic strains has been found to cause a similar pathology in mice compared to humans (Margine and Krammer 2014). Clinical signs of disease exhibited by mice that can be monitored and act as an indicator for disease severity include loss of bodyweight, ruffled fur, reduced activity or respiratory distress (Margine and Krammer 2014). However, some symptoms that are known from human disease, like nasal discharge,

coughing and fever are not observed (Margine and Krammer 2014). On the contrary, mice develop hypothermia after infection (Yang and Evans 1961; Carey et al. 2010).

As mentioned earlier, the HA-stalk has become an important target for IAV vaccine development. One great advantage of mice in this context is that they have the ability to mount cross-reactive and broadly neutralizing antibodies directed at the HA-stalk, which can be boosted upon viral infection as it is seen in humans (Okuno et al. 1993; Krammer et al. 2012; Tan et al. 2012).

It is known that the BALB/c and C57BL/6 differ in the properties of their immunological reaction, which can influence the outcome of vaccine studies. One difference is that they are known to emphasize different Th1/Th2-cell responses. While the response in BALB/c mice is more skewed towards Th2-cells, Th1-cells dominate in C57BL/6 mice (Heinzel et al. 1989; Hsieh et al. 1995; Mills et al. 2000; Watanabe et al. 2004). Furthermore, inbred mouse strains only carry one haplotype determining which peptides can be presented on their MHC molecules (Zinkernagel and Doherty 1997; Beck et al. 2000). The haplotype of the BALB/c strain is H2^d, while the one of the C57BL/6 strain is H2^b (Charles-River-Laboratories 2023a). This can result in immunodominance of different antigens of the same pathogen in the different mouse strains (Rawle et al. 1991; Busch and Pamer 1998; Geginat et al. 2001). While this narrow haplotype can concentrate the immune response on those specific antigens and make it stronger compared to outbred strains, this can also limit the response, if the available antigen does not suit the present MHC receptors. Such strain-dependent responses could, for example, be detected against an adenoviral vaccine carrying HIV antigens, suggesting that vaccine studies best be carried out in different mouse strains, to get the full picture of the immune response (Herath et al. 2016). Outbred mice, like the NMRI strain, carry different sets of MHC genes and would potentially be able to develop a broader, and more realistic immune response, even though they are still not as genetically heterogenous as wild mice (Tuttle et al. 2018; Charles-River-Laboratories 2023b).

Furthermore, it has been found that the BALB/c and C57BL/6 mouse strains not only differ in the properties of their immune response, but also more generally in their host response to IAV infection, e.g. differences in the time course of their weight loss, due to different gene activation patterns (Ding et al. 2008; Srivastava et al. 2009), which also needs to be taken into account when carrying out vaccine efficacy studies, or comparing studies that utilize different mouse strains.

Overall, the abovementioned benefits make the mouse model a valued initial model organism for IAV vaccine research to evaluate vaccine efficacy and mediators of protection (Margine and Krammer 2014; Roubidou and Schultz-Cherry 2021). Due to the described drawbacks, however, vaccine candidates need to be evaluated in other model organisms,

like ferrets or non-human primates, to gain a more complete picture before entering human clinical trials (Margine and Krammer 2014; Roubidou and Schultz-Cherry 2021).

2.7 Research objectives and aim of study

Influenza A viruses and SARS-CoV-2 are zoonotic pathogens and continue to pose a constant threat to public health. Vaccines are important preventive measures to mitigate disease outcomes.

Current influenza vaccines are only 10-60% effective and require yearly reassessment and updates (Krammer and Palese 2015; Paules et al. 2017; Paules et al. 2018). Novel vaccination strategies explore alternative delivery platforms like viral vector vaccines (Antrobus et al. 2012; Lillie et al. 2012; Altenburg et al. 2014) and new antigen design approaches (Krammer and Palese 2013; Clemens et al. 2018; Eichelberger et al. 2018; Wu and Wilson 2018; Leroux-Roels et al. 2023) with the aim of achieving a universal or broadly protective vaccine (Paules et al. 2018).

This thesis aimed to evaluate a possible synergistic effect of a combined immunization with AAV-vector vaccines delivering the influenza HA (H1) and NP of A/California/7/2009pdm as vaccine antigens. While both antigens had shown promising, but differing effects after individual immunization (Sipo et al. 2011; Fidgeke 2016; Demminger et al. 2020), a synergistic effect on the induction of neutralizing and non-neutralizing, broadly reactive antibodies, e.g. FcγR-activating responses, as well as protection against infection was hypothesized. Additionally, different prime-boost schemes, including vaccination with WIV, were evaluated to assess their influence on the induction of a broadly reactive immune response and the activation of FcγR-mediated effector functions, as immunization with WIV alone had shown not to induce such broad responses (Jegaskanda et al. 2013a). It was hypothesized that the AAV-vector vaccine could act equal to a natural infection in priming such broad responses, while WIV could only act as a booster of these. To broaden the immune response to group 2 HAs, an AAV-vector vaccine carrying the HA of the H3N2 virus A/Aichi/2/68 was evaluated either individually, or in combination with the HA of A/California/7/2009pdm (H1N1). The combination of the group 1 and 2 HAs was hypothesized to induce neutralizing and non-neutralizing immune responses against IAVs of both groups, and thus, broaden the immune response.

Therefore, C57BL/6 mice were immunized with the abovementioned AAV-vectors. Those were generally applied intranasally, because they had shown to be repeatedly administrable via the respiratory tract without a loss due to pre-existing immunity against the vector (Limberis and Wilson 2006), and could induce a strong systemic immune response via this route (Demminger et al. 2020). Furthermore, application of the vaccine

along the route of natural infection and the induction of mucosal immunity, to reduce or prevent infection with respiratory pathogens, is also part of the development of next generation vaccines (Morens et al. 2023). One immunization group received the AAV-HA/NP vaccine via two, the intranasal and subcutaneous, routes simultaneously, to evaluate a possible boosting effect between the two routes with potentially beneficial outcomes. The WIV vaccine was only applied intramuscularly, to mimic the actual route of application for this type of vaccine. In the sera, the humoral responses, such as neutralizing, broadly reactive, and FcγR-activating antibodies were measured, in nasal washes and lung samples the mucosal response was assessed and in the spleens of the mice, the cellular immune responses were evaluated. Furthermore, mice were experimentally infected with homologous, heterologous and heterosubtypic virus, to assess the protective efficiency of the vaccine.

SARS-CoV-2 emerged in December 2019, during the time this thesis was conducted. No vaccines or other pharmaceuticals were available, but research and vaccine development progressed at an unprecedented speed.

In this thesis, an AAV-vector vaccine was designed with the receptor-binding domain of the SARS-CoV-2 spike protein (AAV-S-RBD). It was hypothesized that this vaccine could induce a strong neutralizing immune response, because a similar vaccine had shown promising results, i.e. the induction of a strong systemic immune response after intramuscular injection and of a mucosal immune response after intranasal application, against SARS-CoV (Du et al. 2006; Du et al. 2008b; Du et al. 2008c).

The AAV-S-RBD vaccine was evaluated *in vitro* in mammalian cell culture models to verify correct antigen expression and functionality of the vaccine before its immunological properties were assessed *in vivo*. The *in vivo* analyses were initially performed in different mouse models, to assess differences in the immune response and to identify a suitable model for further analyses. As the pandemic progressed, the vector was adapted to the emerging VOCs. Here, it was hypothesized that there were different levels of cross-reactivity between different VOCs, which was therefore assessed additionally to the immunogenicity of the vaccines. Due to results of the AAV-vector vaccine against IAV, it was hypothesized that also non-neutralizing, broadly reactive responses could be induced by this vaccine, which were additionally evaluated. Outcome measures to be observed for the efficacy of the vaccine were overall antibody titers, neutralizing activity, mucosal antibody development, FcγR-activating ability, and T-cell responses, as described for the IAV experiment. Due to organisational reasons, no challenge study could be conducted.

3 Material and Methods

3.1 Material

3.1.1 Mouse models

Mouse line	Provider
C57BL/6N	Charles River, Sulzfeld, Germany
NMRI	
BALB/c	

3.1.2 Cell lines

Cell line	Origin
HEK293T	Human embryonic kidney cells
MDCKII	Madin-Darby Canine Kidney cells
Vero E6	African green monkey kidney epithelial cells
BW 5147 (& derivates)	Mouse thymus cells
HT1080+ACE2	Human fibrosarcoma cells (kindly provided by Paul Bieniasz, The Rockefeller University, New York, USA)

3.1.3 Viruses

Virus	Subtype	Source	Application
Influenza A viruses			
A/California/7/2009pdm	H1N1	NIBSC (ref. 39570): $10^{7.6}$ TCID ₅₀ /ml, NYMC X-181 (hyH1N1sw); 5:3 reassortant: HA, NA, PB1 of Cal/7/9 (H1N1)pdm in the background of A/PR/8/34 (H1N1) virus grown on embryonated chicken eggs and purified by ultracentrifugation, source: National reference center (NRC) at RKI	mouse infections
A/California/7/2009pdm	H1N1	NIBSC (ref. 39560): $10^{9.1}$ TCID ₅₀ /ml	in vitro assays
A/Puerto Rico/8/1934 (PR8)	H1N1	NIBSC (ref. 39560): $10^{9.1}$ TCID ₅₀ /ml	mouse infections

Virus	Subtype	Source	Application
Influenza A viruses			
A/Puerto Rico/8/1934	H1N1	virus grown on embryonated chicken eggs and purified by ultracentrifugation, source: FG17 (RKI)	in vitro assays
X31	H3N2	6:2 reassortant: HA and NA of A/Aichi/2/1968 (H3N2) in the background of A/PR/8/34 (H1N1); NIBSC (ref. 39600): 10 ^{9.3} TCID ₅₀ /ml	mouse infections
X31	H3N2	virus grown on embryonated chicken eggs and purified by ultracentrifugation, source: FG17 (RKI)	in vitro assays
A/Widgeon/Denmark/66174/G18/2004	H2N3	source: FG17 (RKI)	in vitro assays
A/Turkey/Germany/22/96Amp.3693	H9N2	source: FG17 (RKI)	in vitro assays
A/Turkey/Grub/R43/98Amp3699	H6N5	source: FG17 (RKI)	in vitro assays
A/Gull/Maryland/707/1977	H13N6	source: FG17 (RKI)	in vitro assays
A/Mallard/Nordvorpommern/Wv9417/2004	H10N7	source: FG17 (RKI)	in vitro assays
SARS-CoV-2			
BetaCoV/Munich/ChV984(2020)	wt	kindly provided by C. Drosten, Institute of Virology, Charité Berlin	
B117 21652/2020	Alpha		
NW-RKI-I-0029/2020	Beta		
ENA project PRJEB50616; sequence ID IMSSC2-206-2021-00148	Delta	C. Mache and J. Schulze, FG17, RKI, Berlin	PRNT assays
Germany/BE-RKI-I-353502/2021	BA.1	kindly provided by A. Nitsche, ZBS1,	
Germany/RKI-3066/2021	BA.2	Robert Koch Institute,	
SC2/Norway/20365/2022 BA.5	BA.5	Berlin	

3.1.4 Plasmids

Plasmids (not constructed during this work)	Specification	Source
pHelper	Helper Plasmid expressing Adenovirus E2A, E4 and VA genes	Agilent Technologies (Santa Clara, USA)
p5E18-VD2/9	Helper plasmid expressing AAV2 rep and AAV9 cap genes	
pAAV-HA	pAAV plasmid containing the HA of Cal7/09 (H1N1)pdm, codon optimized for <i>mus musculus</i>	Isaac Sipo (FG18, RKI Berlin)
pAAV-NP	pAAV plasmid containing the NP of Cal7/09 (H1N1)pdm, codon optimized for <i>mus musculus</i>	
pAAV-GFP	pAAV plasmid containing the Green fluorescent protein of Renilla reniformis, humanized	
pAAV.DD-H3	pAAV.DD (pAAV modified by DD) plasmid containing the HA of A/Aichi/2/1968 (H3N2), codon optimized for <i>mus musculus</i>	Daniel Demminger (FG17, RKI Berlin)
pAAV.DD-headless	pAAV plasmid containing a headless construct of the HA of Cal7/09 (H1N1)pdm, codon optimized for <i>mus musculus</i>	
Plasmids (constructed during this work)	Specification	Source
cDNA S-Protein	pUC57-Bsal-Free plasmid with Amp-resistance containing the Wuhan-Hu1 S-Protein sequence	supplied by Biocat (Heidelberg, Germany)
cDNA S-RBD Beta	pUC57-Bsal-Free plasmid with Amp-resistance containing the S-RBD sequence of the SARS-CoV-2 Beta VOC	
cDNA S-RBD Delta	pUC57-Bsal-Free plasmid with Amp-resistance containing the S-RBD sequence of the SARS-CoV-2 Delta VOC	
pAAV.DD-S-RBD (wt)	pAAV.DD plasmid containing the receptor binding domain (aa319-541) of the spike protein of SARS-CoV-2, Wuhan-Hu1	Sandra Stelzer (FG17, RKI)
pAAV.DD-S-Protein	pAAV.DD plasmid containing the Spike protein of SARS-CoV-2, Wuhan-Hu1	
pAAV.DD-S-Protein D614G	pAAV.DD plasmid containing the Spike protein of SARS-CoV-2, Wuhan-Hu1 with the D614G mutation	
pAAV.DD-S-RBD (B.1.1.7)	pAAV.DD plasmid containing the receptor binding domain (aa319-541) of the Spike protein of SARS-CoV-2, B.1.1.7 (N501Y)	
pAAV.DD-S-RBD (B.1.351)	pAAV.DD plasmid containing the receptor binding domain (aa319-541) of the Spike protein of SARS-CoV-2, B.1.351 (K417N, E484K, N501Y)	

Plasmids (constructed during this work)	Specification	Source
pAAV.DD-S-RBD (B.1.617.2)	pAAV.DD plasmid containing the receptor binding domain (aa319-541) of the Spike protein of SARS-CoV-2, B.1.617.2 (L452R, T478K)	Sandra Stelzer (FG17, RKI)
pAAV.DD-S-RBD (Omicron, BA.2)	pAAV.DD plasmid containing the receptor binding domain (aa319-541) of the Spike protein of SARS-CoV-2, B.1.1.529.2 (G339D, S371F, S373P, S375F, T376A, D405N, R408S, K417N, N440K, S477N, T478K, E484A, Q493R, Q498R, N501Y, Y505H)	

3.1.5 Primers

Primers and Probes	Sequence 5'->3'	Source
AAV insert sequencing fw	CCACCAGACATAATAGCG	Sandra Stelzer, supplied by Eurofins Genomics Germany
AAV insert sequencing ref (=Sp6 promoter 3' primer)	ATTTAGGTGACACTATAG	
AAV qPCR (CMV promoter) fw	TGGAGTTCGCGTTACATAACTTAC	
AAV qPCR (CMV promoter) rev	CTATTGGCGTACTATGGGAACATAC	
AAV Probe (CMV promoter)	FAM-CCTGGCTGACCGCCCAACGAC-BBQ	
S-RBD wt fwd	CCCAAGCTTACCATGAGGGTGCAGCCCACA	
S-RBD wt rev	CGCGGATCCGAAGTTCACGCACTTGTTCTT	
S-RBD N501Y QC fwd	ACGGCTTCCAGCCTACATACGGCGTGGGCTACC	
S-RBD N501Y QC rev	GGTAGCCCACGCCGTATGTAGGCTGGAAGCCGT	
D614G QC fwd	GTGGCCGTGCTGTACCAGGGCGTGAAGTGCACCGAGGTGC CT	
D614G QC rev	AGGCACCTCGGTGCAGTTCACGCCCTGGTACAGCACGGC CAC	

Primers and Probes	Sequence 5'→3'	Source
S-RBD BA.2 fwd	CCCAAGCTTACCATGCGGGTGCAGCCCACC	Sandra Stelzer, supplied by Eurofins Genomics Germany
S-RBD BA.2 rev	CGCGGATCCGAAGTTGAAGTTCACGCATT	

3.1.6 Antibodies

Primary antibodies	Origin	Application	Source
ADK9 anti-FluA virion	mouse, monoclonal (IgA)	ELISA: 1:250	Progen (Heidelberg, Germany)
anti-V5-tag	Goat	MNT: 1:1,000	Bio-Rad (Hercules, USA)
anti-mouse-IL2, biotinylated	mouse, monoclonal	WB, IF: 1:250	Bio-Rad (Hercules, USA)
anti-mouse-IL2	rat, monoclonal	ELISA: 1:500	BD Biosciences (Franklin Lakes, USA)
anti-β-actin	rat, monoclonal	ELISA: 1 µg/ml	
anti-ACE2	mouse/monoclonal	WB: 1:10,000	Sigma-Aldrich/Merck (Darmstadt, Germany)
a-SARS-CoV-2 S-protein	rabbit/polyclonal	IF: 1:200	Abcam (Cambridge, UK)
	rabbit/polyclonal	IF, WB: 1:500	Sino Biological (Beijing, China)
Secondary antibodies			
anti-mouse IgG-HRP	rabbit	WB: 1:20,000	Agilent Technologies (Santa Clara, USA)
anti-mouse IgG-AF488	donkey	IF, FC: 1:1,000	
anti-mouse IgG-AF594	Goat	IF: 1:1,000	Thermo Fisher Scientific (Waltham, USA)
anti-mouse IgG-HRP	goat	ELISA: 1:1,000	
anti-mouse-IgA-HRP	goat	ELISA: 1:1,000	
Anti-mouse-CD4 APC-Vio® 770 (REA604)			
Anti-mouse-CD3 PE-Vio® 770 (REA641)			
Anti-mouse-CD8b PerCP-Vio® 700 (REA793)		Flow cytometry	Miltenyi Biotec (Bergisch Gladbach, Germany)
Anti-mouse-CD154 Vio® Bright B515 (REA785)			
Anti-mouse-IFNγ PE (REA638)			
Anti-mouse-TNFα APC (REA636)			

3.1.7 Bacteria

Bacteria	Application	Source
<i>E. coli</i> (DH5a™)	re-transformation	Thermo Fisher Scientific (Waltham, USA)
<i>E. coli</i> C2992H	Cloning	NEB (Ipswich, USA)
<i>E. coli</i> XL1 blue	Site-directed mutagenesis (QuikChange)	Agilent Technologies (Santa Clara, USA)

3.1.8 Enzymes

Enzymes	Source
FastDigest® BamHI	Thermo Fisher Scientific (Waltham, USA)
FastDigest® HindIII	
FastDigest® SmaI	
FastDigest® KflI	
FastDigest® XhoI	
FastDigest® MluI	
FastDigest® MreI	
Pierce® Universal Nuclease for cell lysis (Benzonase) 250 U/μl	
T4 DNA Ligase 5 U/μl	
Phusion Green High-Fidelity DNA Polymerase	
Platinum™ Taq DNA Polymerase, DNA-free	Merck (Darmstadt, Germany)
Trypsin-TPCK	

3.1.9 Kits

Kit	Source
QIAamp MinElute Virus Spin Kit	Qiagen (Hilden, Germany)
QIAfilter Plasmid Maxi Kit	
QIAquick PCR Purification Kit	
Invisorb® Spin DNA Extraction Kit	Stratec Molecular (Berlin, Germany)
Invisorb® Spin Plasmid Mini Two	
SuperSignal™ West Dura Extended Duration Substrate	Thermo Fisher Scientific (Waltham, USA)
Pierce® BCA protein assay kit	
QuikChange mutagenesis Kit II	Agilent Technologies (Santa Clara, USA)
BigDye® Terminator 3.1 Kit	Applied Biosystems (Darmstadt, Germany)
SARS-CoV-2 Surrogate Virus Neutralization Test (sVNT)	GenScript Biotech (New Jersey, USA)

Kit	Source
MACS Inside Stain Kit	Miltenyi Biotec (Bergisch Gladbach, Germany)

3.1.10 Consumables and Equipment

Consumables	Source
Amicon® Ultra-15 centrifugal filter units, 100 kDa	Merck (Darmstadt, Germany)
Quick-Seal® (1 x 3.5 inch) ultracentrifugation tubes	Beckman Coulter (Brea, USA)
Open-Top Thinwall Polypropylene Tube, 25 x 89mm	Beckman Coulter (Brea, USA)
Plastic consumables (reaction tubes, well-plates, cell culture dishes and flasks)	Sarstedt (Nümbrecht, Germany) Carl Roth (Karlsruhe, Germany) GE Healthcare (Chicago, USA) TTP (Trasadingen, Switzerland) Greiner Bio One (Kremsmünster, Austria) Brand (Wertheim, Germany) Thermo Fisher Scientific (Waltham, USA)
Deepwell Plate 96/1,000 µl, Wells klar	Eppendorf (Hamburg, Germany)
ELISA plates Nunc Maxisorb™	Thermo Fisher Scientific (Waltham, USA)
LightCycler® 480 Multiwell Plate 96, white	Roche Life Science (Basel, Switzerland)
ibidi® Chamber slide with a removable 12 well chamber	Ibidi (Gräfelfing, Germany)
40 µm cell strainer	BD Biosciences (NJ, USA)
gentleMACS™ C tubes	Miltenyi Biotec (Bergisch Gladbach, Germany)
gentleMACS™ M tubes	
Syringes	B. Braun (Melsungen, Germany)
Single-use injection cannulas	
Amersham™ Protran® Premium Western blotting nitrocellulose membranes	Whatman (Maidstone, UK)
Filter paper	
Embryonated chicken eggs	Valo Biomedica (Osterholz-Scharmbeck, Germany)
Equipment	Source
Flow cytometer MACSQuant Analyzer 10	Miltenyi Biotec (Bergisch Gladbach, Germany)
Optima™-L 100K ultracentrifuge with 70-Ti or SW32Ti rotors	Beckman Coulter (Brea, USA)
Cell culture incubator	Binder (Tuttlingen, Germany)
Agarose gel system Mini-Sub®	BioRad (Hercules, USA)
Mini-Protean® system	
PowerPac™ 300W HC / Basic	

Equipment	Source
Trans-Blot [®] SD semi-dry Transfer cell	BioRad (Hercules, USA)
FLUOstar [®] Omega Plate Reader	BMG Labtech (Ortenberg, Germany)
Water bath DC10	Thermo Haake (Karlsruhe, Germany)
Sterile work bench Herasafe [™] KS12	Thermo Fisher Scientific (Waltham, USA)
NanoDrop [™] 8000 UV/Vis Spectrophotometer	
Micropipettes Research [®] plus	Eppendorf (Hamburg, Germany)
Thermomixer compact	
5417R cooling centrifuge	Eppendorf (Hamburg, Germany)
Intas UV transilluminator system	Intas (Göttingen, Germany)
Advanced Fluorescence and ECL Imager	
LightCycler [®] 480 II instrument	Roche Life Science (Basel, Switzerland)
Orbital shaker Certomat [®] H	Sartorius Stedim Biotech (Göttingen, Germany)
Shaker Roto-Shake Genie [®]	Scientific Industries (Bohemia, USA)
Shaker Vortex Genie [®] 2	
CKX41 inverse bright field microscope	Olympus (Tokio, Japan)
Leica DM IL	Leica (Wetzlar, Germany)
Confocal laser scan microscope LSM 780	Zeiss (Oberkochen, Germany)
Zeiss Observer.D1	
Centrifuge Sorvall LYNX 4000 superspeed	Sorvall/Thermo Fisher Scientific (Bonn, Germany)
Heraeus [™] Pico [™] 17 microcentrifuge	Heraeus/Thermo Fisher Scientific (Bonn, Germany)
Multifuge 1S-R (rotor: 75002000)	
Microcentrifuge SD	Carl Roth (Karlsruhe, Germany)
gentleMACS [™] Dissociator	Miltenyi Biotec (Bergisch Gladbach, Germany)

3.1.11 Buffers and Media

Buffers	Composition
Cell lysis buffer (RIPA)	10 mM Tris-HCl (pH 8) 150 mM NaCl 0.5 mM EDTA (pH 8) 0.1% SDS 1% Triton X-100 2 mM Na ₃ VO ₄ 1 mM Pefablock [®]
Non-denaturing lysis buffer	20 mM Tris-HCl (pH 8) 137mM NaCl 1% Triton X-100 2mM EDTA 2 mM Na ₃ VO ₄ 1 mM Pefablock [®]

Buffers	Composition
ELISA coating buffer, 50 mM pH 9.6	71.4 mM NaHCO ₃ 28.6 mM Na ₂ CO ₃ in ddH ₂ O
PBS	137 mM NaCl 2.7 mM KCl 80.9 mM Na ₂ HPO ₄ 1.5 mM KH ₂ PO ₄ in ddH ₂ O
D-PBS	1 mM MgCl ₂ 1 mM CaCl ₂ in PBS
PBS-MK	25 mM KCl 5 mM MgCl ₂ in PBS
PBST	0.05% (v/v) Tween-20 in PBS
SDS-PAGE running buffer, 10x	250 mM Tris 1.92 M glycine 34 mM SDS 1.2 ml H ₂ O
SDS-PAGE sample buffer, 6x	9.8 ml 0.5 M Tris-HCl (pH 6.8) 1.7 g SDS 5 ml glycerol 0.5 ml 0.5 mM EDTA (pH 8) 9 g/l Bromphenolblue 5% β-Mercaptoethanol
Semidry blotting buffer	40 mM Tris 30 mM glycine 1.3 mM SDS 20% (v/v) ethanol in ddH ₂ O
TBE buffer, 10x	0.89 M Tris 0.89 M boric acid 10 mM EDTA (pH 8.0) in ddH ₂ O
TBST	100 mM Tris-HCl (pH 8.0) 1.5 M NaCl 0.05% (v/v) Tween-20 in ddH ₂ O
MACS-PBS	0.5% BSA 2mM EDTA in PBS
Media	Composition
2xYT medium, pH 7.2	1.6% (w/v) tryptone 1.0% (w/v) yeast extract 171 mM NaCl 100 mg/l ampicillin in ddH ₂ O
2x YT-agar	1.5% (w/v) bacto-agar 100 mg/l ampicillin in 2xYT medium

Media	Composition
complete DMEM/MEM	10% (v/v) FBS 2 mM L-glutamine 100 mg/l penicillin/streptomycin 1mM Na-Pyruvat (only Vero E6) 1x NEAA (only Vero E6) in DMEM/MEM
infection MEM	0.2% (v/v) BSA 2 mM L-glutamine 100 mg/l penicillin/streptomycin in MEM
R10	10% (v/v) FBS (or mouse serum for flow cytometry) 2 mM L-glutamine 100 mg/l penicillin/streptomycin 1 mM Na-pyruvat 50 µM β-mercaptoethanol in RPMI
Semi viscous overlay medium (Influenza)	0.2% (w/v) BSA 0.05% (w/v) NaHCO ₃ 0.01% (w/v) DEAE-dextran 2 mM L-glutamine 100 mg/l penicillin/streptomycin 1.25% (w/v) Avicel 1-2 µg/ml TPCK-treated trypsin in MEM
Semi viscous overlay medium (SARS-CoV-2)	0.05% (w/v) NaHCO ₃ 0.01% (w/v) DEAE-dextran 2 mM L-glutamine 100 mg/l penicillin/streptomycin 1mM Na-Pyruvat 1x NEAA 1.25% (w/v) Avicel in DMEM
SOC-medium	2.0% (w/v) tryptone 5% (w/v) yeast extract 10 mM NaCl 2.5 mM KCl 20 mM MgCl ₂ in ddH ₂ O
Solutions	Composition
Chicken red blood cells, 1%	(v/v) in PBS
Coomassie de-staining solution	10% (v/v) ethanol 5% (v/v) acetic acid in ddH ₂ O
Coomassie fixation solution	30% (v/v) ethanol 10% (v/v) acetic acid in ddH ₂ O
Coomassie staining solution	20% Roti®-Blue 5x concentrate 20% (v/v) ethanol in ddH ₂ O

Solutions	Composition
Crystal violet solution, 1x	10% (v/v) formaldehyde 10% (v/v) crystal violet stock solution, 10x in ddH ₂ O
Crystal violet stock solution, 10x	20% (v/v) ethanol 1% (w/v) crystal violet in ddH ₂ O
DEAE-dextran, 1%	in ddH ₂ O
L-glutamine, 200 mM	in ddH ₂ O
Glycerol, 1%	(v/v) in PBS
H ₂ O ₂ , 3%	(v/v) in PBS
KIO ₄ , 0.011 M	(w/v) in PBS
Na-deoxycholat, 0.5%	(v/v) in PBS
NaHCO ₃ , 5%	in ddH ₂ O
Polyethylenimine (PEI) solution	2.58 g/l (w/v) in ddH ₂ O
PFA, 4%	in ddH ₂ O
Phenol red, 0.5%	(w/v) in PBS
Sucrose-NTE, 25%	25% sucrose 0.1 M NaCl 0.01 M Tris 1 mM EDTA (pH 8.0) in ddH ₂ O
H ₂ SO ₄ , 1 M	in ddH ₂ O
TPCK-treated trypsin, 1 mg/ml	in ddH ₂ O

3.1.12 Pharmaceuticals

Substance	Source
Isoflurane, 1 ml/ml	CP-Pharma Handels
Xylazin 20 mg/ml ad. us. vet.	WDT
Ketamin 100 mg/ml ad. us. vet. (Ketabel)	Bela-pharm
Isotonic NaCl-solution 0.9%	B. Braun (Melsungen, Germany)

3.1.13 Chemicals

Chemicals & reagents	Source
Influenza antigen A/California/7/09 (H1N1) (NYMC-X181), NIBSC code: 16/106 (WIV)	NIBSC
SARS-CoV-2 (2019-nCoV) Spike S1-His Recombinant Protein	
SARS-CoV-2 (2019-nCoV) Spike S1(K417N, E484K, N501Y, D614G)-His Recombinant Protein	Sino Biological (Beijing, China)

Chemicals & reagents	Source
SARS-CoV-2 Spike S1 (T19R, G142D, E156G, 157-158 deletion, L452R, T478K, D614G, P681R) Protein (His Tag)	Sino Biological (Beijing, China)
SARS-CoV-2 B.1.1.529 (Omicron) Spike S1 Protein (His Tag)	
OptiPrep™ Density Gradient Medium (Iodixanol)	Sigma-Aldrich/Merck (Darmstadt, Germany)
Ionomycin calcium salt from <i>Streptomyces globatus</i>	
Phorbol 12-myristate 13-acetate (PMA)	
Trypan blue	
Brefeldin A	Jackson ImmunoResearch Laboratories (West Grove, USA)
Streptavidin-HRP	
Bacto-agar	
Tryptone	BD Biosciences (Franklin Lakes, USA)
Yeast extract	
Bovine serum albumin (BSA), 30%	BIOZOL Diagnostica (Eching, Germany)
Midori green advanced DNA stain	Nippon Genetics Europe (Düren, Germany)
Polyethylenimine (PEI), molecular weight ca. 25 kDA	Polyscience (Hirschberg, Germany)
Chemicals & reagents	Source
Sodium Dodecyl Sulfate (SDS)	SERVA Electrophoresis (Heidelberg, Germany)
TEMED	
Triton X-100	
Avicel microcrystalline cellulose	FMC (Philadelphia, USA)
Agarose NEEQ Ultra Quality	Carl Roth (Karlsruhe, Germany)
Ammoniumpersulfat (APS)	
Bovine albumin fraction V	
Dithiothreitol (DTT)	
Dimethylsulfoxid (DMSO)	
Ethanol, ≥ 99.9%	
Formaldehyde, 37%	
Glycerole	
Glycine	
H ₂ O ₂ , 30%	
H ₂ SO ₄ , 2.5 M	
Isopropanol	
KIO ₄	
L-Gluatmine	

Chemicals & reagents	Source
Methanol, ≥99.9%	
MgCl ₂	
Na ₂ CO ₃	
NaCl	
Pefabloc® SC-protease-inhibitor	
Paraformaldehyde (PFA)	Carl Roth (Karlsruhe, Germany)
Roti®-Blue 5x concentrate	
Rotiphorese® Gel 30 (37.5:1)	
Skimmed milk powder	
TRIS	
Tween-20	
β-Mercaptoethanol	
MACS® Comp Bead Kit, anti-REA	
PepTivator® SARS-CoV-2 Prot. S1 (6nmol/pep)	
PepTivator® SARS-CoV-2 Prot. S B.1.351 Mutation pool (6nmol/pep)	
PepTivator® SARS-CoV-2 Prot. S B.1.1.7 Mutation pool (6nmol/pep)	
PepTivator® SARS-CoV-2 Prot. S B.1.617.2 Mutation pool (6nmol/pep)	Miltenyi Biotec (Bergisch Gladbach, Germany)
PepTivator® Influenza A (H1N1) HA (6nmol/pep)	
PepTivator® Influenza A (H1N1) NP (6nmol/pep)	
MACS® Tissue Storage Solution	
Viability 405/452 Fixable Dye	
1 Kb Plus DNA Ladder	
6x DNA Loading Dye	
DMEM	
KH ₂ PO ₄	
Lipofectamine™ 2000	
MEM	Thermo Fisher Scientific (Waltham, USA)
Na ₂ HPO ₄	
OptiPro® SFM	
PageRuler™ Prestained Protein Ladder, 10 to 180 kDa	
PBS	
Penicillin/Streptomycin, 10,000 U/ml	
RPMI	
Acetone	
Ampicillin	Merck (Darmstadt, Germany)
CaCl ₂	

Chemicals & reagents	Source
Crystal Violet	
DAPI	
DEAE-dextran	
EDTA	
Fetal bovine serum (FBS)	
KCl	
Na ₃ VO ₄	
Na-deoxycholat	Merck (Darmstadt, Germany)
NaHCO ₃	
Phenol red	
Ponceau S	
Sodiumpyruvate, 100 mM	
Succrose	
TPCK-treated trypsin	
Mouse serum	VWR International (Darmstadt, Germany)

3.1.14 Software

Software	Source
GraphPad Prism 9.1.0	GraphPad Software
Adobe Photoshop CS6 v.13 extended	Adobe Systems
Adobe Illustrator CS6	
Endnote X7.8	Thomson Reuters
Geneious Prime 2021.2.2	Biomatters
Zen 2.6 (blue/black)	Carl Zeiss Microscopy
Microsoft Office 2010/2013	Microsoft
PyMOL 2.5.4	Schrödinger
Chemostar Professional	
Intas GDS	Intas Science Imaging Instruments
FlowJo Software v10.4	Tree Star (Ashland, USA)
Splice Rover	http://bioit2.irc.ugent.be/rover/splicerover
MACSQuantify™ Software	Miltenyi Biotec (Bergisch Gladbach, Germany)
Reader Control Software	
MARS Data Analysis Software	BMG Labtech

3.2 Methods

3.2.1 Cloning of pAAV-vector plasmids

Vector plasmids were designed only for the SARS-CoV-2 vaccine because the respective vector plasmids for the IAV vaccine were already available in the group.

For the evaluation of AAV-vectors carrying SARS-CoV-2 antigens as a possible vaccine vector, the pAAV-vector plasmids carrying the full-length S-protein or the S-RBD (AAV-S-RBD) were cloned. The AAV-vector system has already been available and established in the laboratory. It could thus be utilized immediately to manufacture a vector targeting SARS-CoV-2.

When the sequence of the first described SARS-CoV-2 virus was made available in January 2020 (ref: Wuhan Hu-1), the cDNA of the spike protein was ordered through a commercial supplier including codon optimization for mammalian gene expression. It was equipped with the 5' restriction site HindIII and the 3' restriction site BamHI to enable cloning into the existing AAV-vector plasmid.

From this template, the S-RBD between aa319 and aa541 (Yan et al. 2020) was amplified with the primers "S-RBD wt fwd" and "S-RBD wt rev" (see chapter 3.1.5) which included the same restriction sites mentioned above, as well as a Kozac sequence.

Both cDNAs were then cloned into the pAAV-plasmid already available in the group using the named restriction sites.

In the following sections 3.2.1.1 to 3.2.1.9 the methodology for this part is described.

3.2.1.1 Transformation of plasmids in chemically competent *E. coli* bacteria

To transform plasmid DNA into DH5 α or C2992H *E. coli* bacteria, 50 μ l bacteria aliquots were used per plasmid. The frozen aliquots were thawed carefully on ice and 1-2 μ l of plasmid DNA were added to the cells and mixed carefully. The mixture was incubated on ice for 30 minutes. Following this, a heat shock was performed at 42°C for 45 seconds in a heating block. Cells were then incubated on ice for two minutes. 500 μ l of SOC medium were added to the cells, which were then incubated at 37°C and centrifuged at 200 x *g*. Finally, cells were plated on 2xYT agar plates containing the respective selective antibiotic. After overnight incubation, single clones were picked.

3.2.1.2 Preparation of plasmid DNA from bacteria

For the isolation of plasmid DNA from bacterial cultures commercial kits were used. Large amounts of plasmid DNA were prepared with the QIAfilter Plasmid Maxi Kit (maxi), small amounts with the Invisorb® Spin Plasmid Mini Two Kit (mini). To prepare the bacterial culture, bacteria carrying the desired plasmid were grown overnight on plates with 2xYT

agar containing the specific antibiotic. The next day, individual colonies were picked from the plates and added to 2 ml of 2xYT medium with the antibiotic and grown over the day, if needed for maxi-cultures, or overnight when needed for mini cultures. For the maxi cultures, 200 ml of 2xYT with the respective antibiotic were inoculated with the 2 ml culture and grown overnight. The plasmid DNA was prepared following the manufacturer's instructions. The concentration of the plasmid DNA was measured with a NanoDrop 8000 UV-Vis Spectrophotometer using a volume of 2 μ l and set to a final concentration of 1 μ g/ μ l.

3.2.1.3 PCR

PCR was performed with the Phusion High Fidelity polymerase following the manufacturer's instructions. Annealing temperature and number of cycles can vary depending on primer and template.

Component	Volume	PCR conditions		
Template DNA	10 ng	Initial denaturing	98°C	30 sec
5x Phusion HF buffer	10 μ l	Denaturing	98°C	10 sec
10 mM dNTPs	1 μ l	Annealing	62°C	20 sec
10 μ M forward primer	2.5 μ l	Elongation	72°C	15 sec
10 μ M reverse primer	2.5 μ l	Final Elongation	72°C	5 min
DMSO	1.5 μ l			
Phusion High Fidelity Polymerase	0.5 μ l			35 cycles
ddH ₂ O	Ad 50 μ l			

3.2.1.4 QuikChange PCR

To insert point mutations into plasmids, the QuikChange site-directed mutagenesis kit according to the manufacturer's instructions.

3.2.1.5 Enzymatic restriction of plasmids

For enzymatic restriction of plasmid DNA with FastDigest (Fermentas) enzymes, 2 μ g of plasmid DNA were used. 1 U of restriction endonuclease per μ g of DNA was added, following the manufacturer's instructions. The respective buffer was added at a 1:10 dilution and nuclease-free water was added to a final volume of 20 μ l. The mixture was incubated at 37°C for 15 minutes. The final product was obtained by agarose gel electrophoresis.

3.2.1.6 Agarose gel electrophoresis

Agarose gels of concentrations between 0.5 – 2% were prepared by dissolving agarose in 1xTBE buffer. Before solidification of the gel, Midori Green was added at 6 μ l per 100 ml to label the DNA. The gel was covered with 1x TBE buffer in the gel chamber. To load the

DNA, it was mixed with 6x loading buffer. In addition to the samples, a DNA ladder was added. A constant voltage of 100 V was applied for at least 30 minutes, until the DNA fragments were separated. DNA was visualized with UV-light.

3.2.1.7 Gel extraction

Extraction of DNA fragments from agarose gels was performed by using the QIAEX II Gel Extraction Kit following the manufacturer's instructions. DNA was eluted with nuclease-free water and concentration was measured by using a NanoDrop 8000 UV-Vis Spectrophotometer using a volume of 2 μ l.

3.2.1.8 Ligation

Ligation was performed with the T4-Ligase following the manufacturer's instructions, usually leaving the ligation reaction overnight at 16°C. For cloning of the S-RBD a vector:insert ratio of 1:3 was applied and for cloning of the full S-protein a 1:1 ratio was needed.

3.2.1.9 Sequencing

Sequencing was performed at the RKI's in-house sequencing laboratory. The sequencing conditions are displayed below. The resulting sequences were analyzed using the Geneious software.

Component	Volume	PCR conditions			
Template DNA	50-100 ng	Initial denaturing	96°C	2 min	25 cycles
5x ABI reaction buffer	2 μ l	Denaturing	96°C	10 sec	
Sequencing Primer (10 μ M)	0.5 μ l	Annealing	45°C	5 sec	
BigDye 3.1 Mix	0.5 μ l	Elongation	60°C	4 sec	
ddH ₂ O	ad 10 μ l				

3.2.2 Verification of the pAAV-plasmids

Following the verification of the correct molecular composition of the pAAV-vectors, their functionality was assessed *in vitro* by transfection into mammalian cells to verify that the correct transgene is expressed in sufficient amounts with the following methods (sections 3.2.2.1 to 3.2.2.13).

3.2.2.1 General cell culture conditions

All cell culture work was carried out under sterile working conditions. Cells were maintained in incubators at 5% CO₂, 37°C and 95% (+/- 5%) humidity.

3.2.2.2 Maintenance of permanent cell lines

Adherent cell lines were grown in their respective medium in cell culture flasks. When the cells reached 90-95% confluency they were passaged to maintain their healthy growth behaviour. All solutions were warmed up to 37°C before use. The old growth medium was removed from the flask and cells were washed once with PBS carefully, without detaching them from the surface. The PBS was removed and Trypsin-Versene solution was added to the flask. After a cell line specific incubation time at 37°C, the trypsin was deactivated by adding serum-containing fresh medium and the desired amount of cell-solution was transferred to a new flask.

3.2.2.3 Transfection of cells

For the transfection of HEK293T-cells, Lipofectamin 2000® was used following the manufacturer's instructions with 2.5 µg DNA/ 1 x 10⁶ cells. Cells were usually seeded the day before the transfection on the desired surface, e.g., glass coverslips or ibidi® 12-well slides. To prepare the surface for a strong attachment of the cells, it was coated with poly-D-lysine. After transfection, cells were further incubated for 48 hours and further processed for either immunofluorescence staining (3.2.2.4) or cell lysates (3.2.2.6).

3.2.2.4 Immunofluorescence staining

Cells were grown on glass coverslips or ibidi® 12-well slides and treated as desired. When they were ready to be prepared, cell culture medium was removed, and cells were fixed with 4% PFA for ten minutes. Afterwards they were washed three times with PBS and subsequently permeabilized with 0.2% Triton-X-100 for 10 minutes. Again, cells were carefully washed three times with PBS before unspecific binding sites were blocked with 10% FBS solution for one hour at 37°C. Following the blocking step, the primary antibody or serum in 10% FBS was added in the respective dilution in a wet chamber, where the coverslip is placed upside down on the antibody solution, and incubated for 90 minutes at 37°C. The coverslips were then washed three times with PBS and the corresponding secondary dye-conjugated antibody was added in a dilution of 1:1,000 for one hour at 37°C. Cells were washed again and incubated for a maximum of 10 minutes with DAPI solution before being mounted on to microscope slides with Mowiol.

3.2.2.5 Microscopy

Pictures of immunofluorescence stainings were taken either with a Zeiss Axio Observer D1 inverted epifluorescence microscope or a Zeiss LSM 780 confocal laser scanning microscope.

3.2.2.6 Preparation of cell lysates

For the preparation of cell lysates, transfected or transduced cells were washed with ice cold PBS and transferred to a tube. They were then centrifuged at 2,500 rcf for 2 minutes at 4°C. The supernatant was removed, and lysis buffer was added and cells were incubated on ice for 20 minutes. To remove cell debris, the lysates were centrifuged at 10,000 rcf at 4°C for 10 minutes. The supernatant was collected and used for SDS-PAGE (3.2.2.8), Western Blot (3.2.2.9), or ELISA (3.2.2.11).

3.2.2.7 BCA Assay

Protein concentrations were determined in the 96-well plate format using the Pierce BCA protein assay kit following the manufacturer's instructions. Absorption was measured in a plate reader at 562 nm.

3.2.2.8 SDS-PAGE

SDS-PAGE was used to separate proteins in the electric field within a porous polyacrylamide-matrix by their molecular weight. Suitable gels were prepared with the in-house system. Gels were cast between two glass plates, either spaced 0.75 mm (for Coomassie staining, 3.2.2.10) or 1.5 mm (for Western Blots, 3.2.2.9) according to the table. The stacking gel was layered on top of the separation gel and a comb was inserted. Gels were run in a suitable gel chamber with running buffer. Before samples were added, they were mixed with 6x sample buffer containing β -mercaptoethanol and boiled at 95°C for 5 minutes. A constant current of 25 mA/gel was applied to separate proteins.

Table 3: Composition of SDS-PAGE gels

Component (amounts for 2x 0.75 mm gels)	Separation Gel		Stacking Gel
	10%	12.5%	5%
30% acrylamide/0.8% bisacrylamide (37.5:1)	3.3 ml	4.1 ml	0.83 ml
ddH ₂ O	4.0 ml	3.2 ml	2.8 ml
1.5 M Tris-HCl pH 8.8	2.5 ml	2.5 ml	-
0.5 M Tris-HCl pH 6.8	-	-	1.25 ml
10% SDS	100 μ l	100 μ l	50 μ l
10% APS	100 μ l	100 μ l	50 μ l
TEMED	6 μ l	6 μ l	6 μ l

3.2.2.9 Western Blot

Western Blots were performed in a semi-dry system. Proteins were transferred from an SDS-PAGE to a nitrocellulose membrane. The membrane was washed in water and added onto the gel. On both sides, 3 layers of Whatman paper soaked in blotting buffer were added. Blotting was performed at a constant current of 80 mA/gel for 60 to 90 minutes, depending on the size of the main fragment. Correct transfer was verified with a Ponceau S staining. The membranes were then blocked with 5% skimmed milk in TBST buffer for 1 hour at room temperature. The primary antibody was added in a suitable dilution in blocking buffer overnight at 4°C. Subsequently, the membrane was washed three times for five minutes with TBST before the HRP-conjugated secondary antibody was added in blocking buffer. The membrane was now washed again, and SuperSignal™ West Dura Extended Duration Substrate was added according to the manufacturer's instructions. The resulting chemiluminescence was detected with a ChemiDoc™ imager.

3.2.2.10 Coomassie staining of SDS-PAGE gels

The SDS-PAGE acrylamide gels were incubated in Coomassie fixation solution for 30 minutes. This was followed by incubation step in Coomassie staining solution at room temperature overnight. The next day, the staining solution was removed, and de-staining solution was added at room temperature. Incubation was continued, until the clear parts of the gel were unstained. The gel was washed in water and scanned or dried to conserve the results.

3.2.2.11 ELISA

96-well ELISA plates were coated with the respective antigen (4-8 µg/ml of purified influenza virus, 1:500 dilution of empty AAV9 capsids, 1 µg/ml S1-protein) diluted in coating buffer overnight at 4°C. The plates were washed three times with PBST and blocked with 5% BSA (S1-protein and IgA-ELISA) or with 5% skimmed milk (influenza, AAV). Blocking buffer was removed and the primary antibody (e.g. serum) was added in serial dilution in blocking buffer (50 µl/well) and incubated for 2 hours at 37°C. Plates were then washed three times with PBST and a suitable HRP-conjugated secondary antibody was added in a 1:1,000 dilution in blocking buffer (50 µl/well). Plates were incubated for 1 hour at 37°C. Finally, plates were washed again three times with PBST before 50 µl of ELISA substrate solution were added per well. The reaction was stopped after colour development with 50 µl H₂SO₄ per well and the absorption was measured at 450 nm.

3.2.2.12 Flow Cytometry

For the quantification of signal in transfected or transduced cells, flow cytometry measurement was performed. All centrifugation steps were carried out at 300 x *g* for 5 minutes. Cells were either transfected with the respective plasmid or transduced with AAV-vectors and incubated for 48 – 72 hours. Cells were then harvested and a live/dead-staining was performed following the manufacturer's instructions. Here, the live/dead fixable dye was added to the cells and incubated for 30 minutes in the dark. Cells were centrifuged and resuspended in 4% PFA for fixation and incubated for 15 minutes. Cells were washed again, followed by a permeabilization step with 0.2% Triton-X for 15 minutes. Subsequently, cells were washed again and then blocked with 10% FBS for 1 hour at 37°C. Following the blocking step, cells were incubated with the primary antibody for 2 hours at 37°C, followed by another washing step and then staining with the secondary antibody for 1 hour at 37°C. Before measurement, cells were washed again and resuspended in FACS-PBS. Cells were gated for single cells, live cells, and finally, signal-positive cells.

3.2.2.13 ACE2-binding assay (flow cytometry)

Cell lysates were prepared of cells transfected with the pAAV-S-RBD plasmids of the different VOCs. Cell lysis was performed with non-denaturing lysis buffer. Lysates were cleaned with ultra-centrifugal filter units (MW 100,000 kDa) to remove the lysis buffer. HT1080+ACE2 were used to bind to the proteins in the lysates. They were stained for dead cells and fixed, blocked with 10% FBS for 1 hour and 1×10^6 cells/well were separated into a 96-well U-bottom plate. Fixed HT1080+ACE2 cells and lysates were mixed and incubated overnight at 4°C. The mixture was then stained for the V5-tag (mouse-anti-V5, 1:250) for two hours at 37°C. They were washed three times and the secondary antibody with a fluorophore was added at a 1:1,000 dilution. Cells were washed again and subsequently measured with the MACSQuant flow cytometer.

3.2.3 Production of recombinant AAV-vectors

After the verification of the pAAV-vector plasmids, AAV-vectors were produced and their quality was assessed (sections 3.2.3.1 to 3.2.3.3).

3.2.3.1 Production of recombinant AAV-Vectors

AAV-vector preparations were produced in HEK293T-cells. The protocol used here is based on the Iodixanol-based protocol by Strobel et al. (2015), as it had been implemented in the group (Strobel et al. 2015). For a sufficient number of AAV-vector particles, usually 20 15-cm cell culture dishes of HEK293T-cells were seeded the day before transfection to be confluent the next day. The three vector plasmids, p5E18, pHelper and pAAV, were

prepared for transfection in an equimolar ratio with PEI reagent. The plasmids were mixed in 1 ml of serum-free DMEM per dish. PEI was added, the solution was mixed and incubated for 15 minutes at room temperature. The transfection-solution was then added to the dishes, 1 ml per dish in slow drops. The transfected cells were incubated for 72 hours before cells were harvested. The cell culture medium was removed, and 10 ml PBS-MK were added to each dish. Cells were detached and centrifuged for 10 minutes at 2,000 x g. The supernatant was removed, and cells were resuspended in 5 ml PBS-MK. Cells were lysed using 0.5% Sodium-Deoxycholat. 0.5 µl/ml Benzonase was added, and cells were incubated at 37°C for 1 hour. The cell suspension was then centrifuged at 10,000 x g for 15 minutes to remove cell debris. The supernatant was transferred to a new tube and filled up to 12 ml with PBS-MK. The lysate was then underlaid with a discontinuous Iodixanol gradient and ultracentrifuged at 300,000 rcf at 18°C for 2.5 hours. To obtain the 40%-phase with the AAV-vectors, the tube was punctured with a needle and the phase was aspirated. Finally, 25 ml of PBS-MK were added to the solution and the AAV-vector preparation was concentrated using ultra-centrifugal filter units (MW 100,000 kDa) at 3,000 rcf down to 1-2 ml. The AAV-vector stocks were stored at -80°C.

3.2.3.2 Titration of AAV-vectors via qPCR

The number of encapsidated viral genomes in intact AAV-vector particles was measured via qPCR. To eliminate viral genomes that are not resistant to DNase treatment, and thus, are not inside of intact particles, initially 10 µl of the AAV-vector preparation was treated with 0.5 µl/ml Benzonase at 37°C for 1 hour. Viral DNA was then purified with the QIAamp MinElute Virus Spin Kit according to the manufacturer's instructions and eluted in 100 µl of H₂O. This results in a 10⁻¹ dilution of the original preparation. For the qPCR, serial 10-fold dilutions were prepared, and the 10⁻³ to 10⁻⁶ dilutions were analyzed. As a standard, the dsDNA cassette containing the CMV-promoter, intron, and transgene, was prepared from the corresponding pAAV plasmid DNA by digestion with the SmaI restriction enzyme. After cleanup, the concentration was set to 1 µg/ml and ten-fold dilutions were prepared as well and the 10⁻³ to 10⁻⁶ dilutions were used in the qPCR.

The qPCR was carried out in white 96-well plates in a LightCycler®480 instrument. Fluorescence was measured at the start of each annealing cycle and analyzed with the setting "Abs Quant/2nd Derivative Max" using the integrated software.

For the calculation of viral genomes, the absolute number of ssDNA molecules in the standard stock preparation (N_{DNA}) was calculated with the formula $N_{\text{DNA}} = N_A * \left(\frac{1 * 10^{-9}}{MW} \right)$. N_A is the Avogadro constant and MW is the molecular weight of the DNA fragment, which was calculated by multiplication of the number of the individual DNA bases with their specific molecular weights $MW = (A_n * 313.2) + (T_n * 304.2) + (C_n * 289.2) + (G_n * 329.2)$.

Component	Volume	PCR conditions			
10x PCR buffer	2 μ l	Initial denaturing	95°C	10 min	40 cycles
50 mM MgCl ₂	2 μ l	Denaturing	95°C	15 sec	
10 mM dNTPs	1.6 μ l	Annealing	60°C	20 sec	
10 μ M forward primer	0.6 μ l	Elongation	72°C	10 sec	
10 μ M reverse primer	0.6 μ l				
10 μ M Taqman-probe	0.2 μ l				
5U/ μ l Platinum®-Taq DNA polymerase	0.16 μ l				
H ₂ O	10.84 μ l				
Sample	2 μ l				

3.2.3.3 Quality control of AAV-vector preparations

Purity assessment via SDS-PAGE

10 μ l of AAV-vector preparation were analyzed by separation in an SDS-PAGE (3.2.2.8) and staining with Coomassie (3.2.2.10). Here, the three capsid proteins VP1, VP2 and VP3 can be visualized.

ADK9 ELISA

To assess the integrity of the AAV9-capsid, an ELISA was performed with the ADK9-antibody, which only recognized intact capsids. 96-well ELISA plates were coated with 50 μ l/well of twofold dilutions in coating buffer of the AAV-vector preparation at 4°C overnight. The general procedure for ELISAs is described in 3.2.2.11. The ADK9-antibody was diluted 1:250 in blocking buffer. As a secondary antibody HRP-conjugated anti-mouse-IgA was added in a 1:1,000 dilution.

Electron micrographs

Electron micrographs were performed at the RKI by Lars Möller of the the *Centre for Biological Threats and Special Pathogens 4 (ZBS4): Advanced Light and Electron Microscopy*.

Transduction efficiency and transgene expression

Transgene expression was assessed in HEK293T-cells by adding 20-40 μ l of AAV-vector preparation to the cell culture medium in 24-well plates and incubating the cells for 72 hours. Cell culture medium was exchanged after 24 hours. The cells were then further processed for different analyses. Either, the cells were used for immunofluorescence

staining (3.2.2.4), or flow cytometry (3.2.2.12, 3.2.2.13), or cell lysates were prepared (3.2.2.6) for SDS-PAGE (3.2.2.8), Western Blot (3.2.2.9), or ELISA (3.2.2.11).

3.2.4 Laboratory animal work

After the successful *in vitro* evaluation und quality control of the AAV-vector stocks, they were further evaluated *in vivo* in the mouse model. For IAV, the immunizations phase was followed by a viral challenge, while for SARS-CoV-2 only the immunogenicity of the AAV-vectors was evaluated, without a subsequent infection. In the following, the setup of those mouse experiments is described. If the conditions differ between the IAV and SARS-CoV-2 experiments, this is indicated, otherwise the conditions are equal for both.

3.2.4.1 General conditions for the mouse experiments

All described experiments have been approved by the *Landesamt für Gesundheit und Soziales* (LAGeSo) Berlin (reference numbers H 0129/18, G 0195/20, G 0167/21).

All mice were female, 6-8 weeks old and were purchased from Charles River Germany. For the IAV experiments, C57BL/6N mice were used and for the SARS-CoV-2 experiments NMRI, BALB/c and C57BL/6J, were used as indicated for the individual experiments.

Mice were kept in standardized type III IVC cages under BSL-2 conditions. The housing facilities of the RKI were previously approved by the LAGeSo. Before the start of the experiments, animals had an adaptation phase of at least seven days and up to 14 days to their new surroundings.

3.2.4.2 Immunizations

Immunizations with AAV-vectors were conducted either intranasally or subcutaneously. Mice received a volume of 50 µl intranasally, applied through both nostrils. For subcutaneous injection, 100 µl were injected into the skin at the flank. WIV was applied intramuscularly, with 30 µl applied to the hind limb. For i.n. and i.m. immunizations, mice were anesthetized with isoflurane. For animals receiving two subsequent i.m. or s.c. injections, the respective opposite limb or side was used for the second injection. The animals received an immunization dose of 10^{11} viral genomes (vg) of AAV-vectors at each time point, or 20 µg of WIV.

3.2.4.3 IAV challenge

Mice were infected intranasally with 50 μ l virus solution per mouse, applied via both nostrils under isoflurane anaesthesia. They were monitored for clinical symptoms and weight loss and were euthanized when they reached the defined humane end point (scoring in 3.2.4.4). When the clinical scores started to rise, they were provided with glucose-containing water and soft feed. Half of the mice were sacrificed on day 3 after infection for viral lung titers and the animals that did not reach the humane end point were sacrificed at the end of the experiment at day 14 after infection. Those timepoints are well established in influenza research (Heaton et al. 2013; Demminger et al. 2020; Bliss et al. 2022).

Challenge virus	TCID ₅₀ /mouse
A/California/7/09 (H1N1)pdm	7.94x10 ³
A/Puerto Rico/8/34 (H1N1)	5.01x10 ⁴
X31 (H3N2)	1.00x10 ⁵

Table 4: Lethal doses of IAV used for mouse infections

3.2.4.4 Scoring

During the experimental phase, mice were monitored daily according to the score sheets for the experiment. For scoring, different score sheets were used for the immunization and infection phases.

During the immunization phase a minimal burden was expected for the animals, while a medium burden was expected for the immunized animals during the infection phase, and a high burden for the control groups, requiring more intense monitoring. If animals reached the defined end point, they were euthanized.

During the immunization phase, the scoring parameters were: 1) behavior after isoflurane anesthesia, 2) anomalies around the site of application (i.n., s.c., i.m.), 3) anomalies around the site of blood sampling (retrobulbar plexus or tail vein).

During the IAV challenge, the scoring parameters were: 1) body weight, 2) general condition (fur coat, eyes, body openings, neurological symptoms), 3) spontaneous behavior, 4) breathing, 5) anomalies at the site of infection (i.n.).

3.2.4.5 Finalization

Uninfected mice were sacrificed through final bleeding via the *vena cava* after deep ketamine/xylazine anesthesia (160 mg/kg ketamine and 16 mg/kg xylazine), to sample spleens for T-cell analysis, nasal washes and lungs.

Infected mice were sacrificed by cervical dislocation and lungs were collected.

3.2.4.6 Sampling and sample processing

Serum

Blood was collected from either the retrobulbar plexus or from the tail vein at all indicated time points and at finalization. During the immunization period, small amounts of blood (<10% of the total blood volume of the animal, according to the GV-SOLAS) were collected. The blood was left at room temperature for at least 30 minutes to coagulate. The blood samples were then centrifuged at 2500 rcf for 30 minutes to separate the serum, which was then stored at -80°C until further processing.

Nasal washes

Nasal washes were collected from dead mice immediately after the final bleeding. The nose was rinsed with 100 µl of PBS buffer from the tracheal side by inserting a long, thin pipet tip into the trachea until it was in the correct position and collecting the PBS in a plastic tube.

Lungs

Lungs of mice were collected in PBS, kept on ice and immediately processed to determine viral titers of infected mice or IgA antibodies after immunization. First, lungs were weighed and then transferred to gentleMACS™ M-tubes and diluted 1:10 according to their individual weight. They were then processed with the gentleMACS™ Dissociator program „Protein_01“. The tubes were centrifuged for 10 minutes at 4,000 x *g* and 4°C before the supernatant was collected and centrifuged again at 10,000 x *g* and 4°C. The supernatants were then used to assess viral lung titers via plaque assay (3.2.5.1) or IgA-antibodies via ELISA (3.2.2.11, only from uninfected mice).

Spleens

Spleens were collected only from uninfected mice to measure T-cells. For this purpose, it is crucial, that the cells remain viable after collection of the organ from the mouse. Spleens were directly stored in MACS-PBS and processed as soon as possible or in MACS® Tissue storage solution and processed within 24 hours.

3.2.5 Methods for the immunological and virological evaluation of samples

3.2.5.1 Plaque Assay (Titration)

The plaque assay was carried out to assess the virus titer of a certain virus preparation or viral lung titers of the infected animals.

For IAV, MDCK cells were used and for SARS-CoV-2, Vero E6 cells were used (for cell culture conditions see 3.2.2.1 and 3.2.2.2). Cells needed to be confluent on the day of infection.

The virus solution was prepared in a series of subsequent 1:10 dilutions. Pipet tips were changed between each well. For IAV, the virus dilutions were prepared in D-PBS + 0.2% BA and for SARS-CoV-2 OptiPro medium was used. Growth medium was aspirated from the cells, and they were washed carefully two times with PBS. Virus dilutions were then added to the cells. In 6-well plates 250 μ l and in 12-well plates 100 μ l of virus dilution were added. Cells were incubated for 45 minutes at room temperature for IAV and for one hour at 37°C for SARS-CoV-2. During that time, they were gently rocked every 10-15 minutes. Subsequently, the virus suspension was taken off the cells and they were washed one to two times with PBS, before the overlay-medium was added and incubated at 37°C for 48 hours for IAV. For SARS-CoV-2, optimal incubation times varied between strains (72 h for SARS-CoV-2 wt, Alpha, Beta; 96 h for SARS-CoV-2 Delta, Omicron).

After the incubation period, cells were stained with crystal violet solution for one hour at room temperature. Plates were air-dried and viral plaques were counted. Viral titers in

PFU/ml were calculated: $PFU/ml = \frac{\text{number of plaques} * 1 \text{ ml}}{\text{dilution factor} * \text{volume used for infection [ml]}}$

3.2.5.2 Fc γ R reporter cell assay

BW 5147 reporter cells, which stably express the extracellular domains of the murine Fc γ RI, -IIb, -III or -IV and the intracellular signaling module of the murine CD3- ζ chain, were thawed approximately two weeks before the assay and expanded to the amount needed. 96-well plates were coated with the test antigen (4-8 μ g/ml of purified influenza virus, 1 μ g/ml S1-protein) and incubated overnight at 4°C. The plates were then washed three times with PBS and blocked with 10% FBS for 1h at 37°C. Twofold dilutions of inactivated serum were prepared in 10% FBS and added to the 96-well plated for 1h at 37°C. Fc γ R-cells were then harvested, counted and set to a concentration of 1x10⁶ cells/ml in R10 medium. The antigen-coated plates were then washed with D-PBS, the wash solution was completely removed and 200 μ l of cell suspension was added to each well. The plates were incubated overnight in the regular cell culture incubator. ELISA-plates were coated with 1 μ g/ml anti-IL2 antibody in 50 μ l of coating buffer/well overnight at 4°C.

The following day, the ELISA plates were washed three times with PBST and blocked with 10% FBS. During that time, 100 μ l of PFT were added to each well of the Fc γ R-cell-plates and resuspended five times to lyse the cells. 150 μ l of the lysed Fc γ R-cell-supernatant were then added to the blocked ELISA plates and incubated for two hours at room temperature. Subsequently, the plates were washed three times with PBST and 50 μ l of secondary anti-mouse-IL2-Biotin antibody in a 1:500 dilution in PFT were added for 1.5 hours at room temperature. The plates were then washed again three times with PBST before Streptavidin-HRP was added in a concentration of 1:1,000 in PFT for 30 minutes at room temperature. Finally, plates were washed again three times with PBST before 50 μ l of ELISA substrate solution were added per well. The reaction was stopped after color development with 50 μ l H₂SO₄ per well and the absorption was measured at 450 nm. Fc γ R-activation was calculated by subtracting the background signal obtained from mock wells and BW-cells without an Fc γ R from the reactive wells.

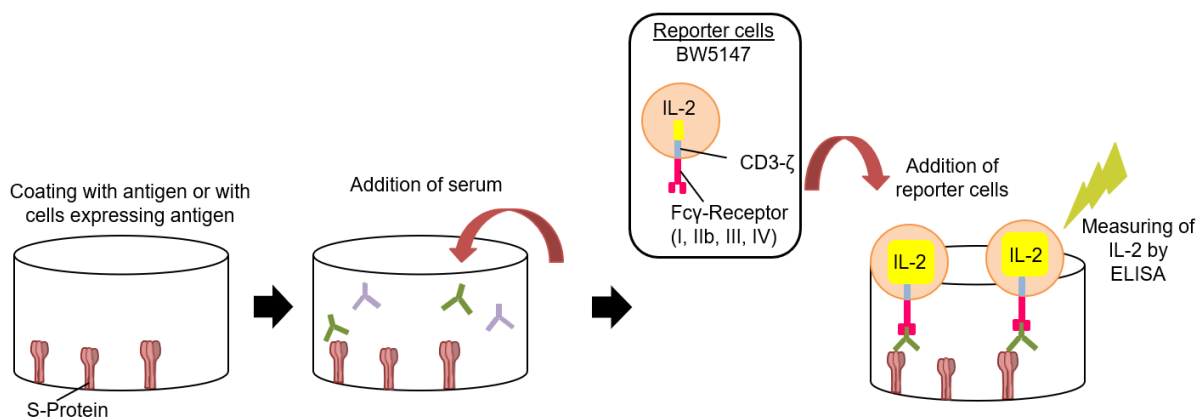


Figure 16: Fc γ R reporter cell assay

Displayed here is a schematic representation of the protocol of the Fc γ R-assay as described in section 3.2.5.2. Own illustration.

3.2.5.3 Intracellular cytokine staining of antigen-specific T-cells

They were transferred to gentleMACS™ C-tubes containing 3 ml of MACS-PBS and then processed in the gentleMACS™ Dissociator with the programm „m_spleen_01“.

Cell suspensions were then filtered through 40 μ m nylon filters on 50 ml tubes. The filters were washed with 5 ml MACS-PBS and cell suspensions were centrifuged at 300 x g for 10 minutes at room temperature. Supernatant was removed and cells were resuspended in 500 μ l of MACS-PBS. To count the cells 1:100 dilutions of each spleen were prepared in a U-bottom 96-well plate. DAPI stain was added to an end concentration of 0.3 μ M. The

cells were counted with the MACSQuant flow cytometer. Cells were split to 1.5×10^6 cells/well into a 96-well plate.

Next, cells were stimulated with the respective peptide pools. First, cells were washed with MACS-PBS and centrifuged at $300 \times g$ for 10 minutes at room temperature. They were then resuspended in 150 μ l/well of R10 medium (with mouse serum) containing the peptivator mix corresponding to the manufacturer's instructions. As a positive control, cells were stimulated with PMA and Ionomycin. Cells were incubated at 37°C for 2 hours before 1 μ g/ml of brefeldin A was added to each well and they were further incubated for another 4 hours. Further on, they were stained. Initially, a live/dead staining was performed. Cells were washed, then resuspended in 100 μ l of Dye-solution (viability fixable dye) in PBS and incubated for 15 minutes in the dark at room temperature. Cells were washed again and were then stained for surface antigens (CD3, CD4, CD8b, CD154) with 250 μ l of antibody solution per well and incubated for 10 minutes at 4°C. After another washing step, cells were fixed with 250 μ l of „Inside Fix“-solution for 20 minutes at room temperature. Cells were washed again and finally stained for intracellular cytokines. First, they were permeabilized with 250 μ l of „InsidePerm“-solution, and then resuspended in 100 μ l of antibody-mix (TNF α , IFN γ) and incubated for 10 minutes at room temperature. Cells were washed again, resuspended in 200 μ l MACS-PBS and measured on the MACSQuant flow cytometer. The gating strategy is displayed in Figure 43.

Before measurement, compensation controls were prepared for each antibody. All antibodies used here were REA-coupled. 100 μ l of MACSQuant running buffer were added into a tube and 4 μ l of each antibody, only one per tube, were added to it. One drop of MACS Comp beads (anti-REA and blank) was added to each tube and incubated for 10 minutes in the dark. 1 ml of running buffer was added and the instrument was calibrated.

3.2.6 IAV-specific immunological and virological methods

3.2.6.1 Production of Influenza A viruses from embryonated chicken eggs

7- or 10-day old embryonated chicken eggs were provided externally. Eggs were placed in racks with the tip facing downwards and the position of the embryos were labeled on the eggshell. The eggshell was disinfected and perforated at the indicated spot. Eggs were inoculated with 50 μ l (7d) or 100 μ l (10d) of virus stock (1,000 pfu/egg) and incubated for 48h at 37°C. They were then cooled at 4°C overnight. To continue, eggs were disinfected from the outside and opened at the top without perforating the eggshell membrane. The allantoic fluid was recovered and centrifuged at $3500 \times g$ for 10 minutes at 4°C. Subsequently, an HA-assay was performed, and allantois was either directly aliquoted or further cleaned up via ultracentrifugation. For this purpose, 5 ml of 25% sucrose solution

in NTE buffer was added to appropriate tubes and 33 ml of allantoic fluid was added on top. Tubes were centrifuged at 24,000 x *g* for 90 minutes at 4°C. The supernatant was discarded, and pellets were dried as much as possible and were then recovered in 0.5 – 3 ml of PBS buffer. They were left overnight at 4°C and subsequently aliquoted.

3.2.6.2 HAI-Assay

To measure the extend of hemagglutination inhibition by the antibodies in the mouse sera, the sera were inactivated by adding 0.5 volumes of 0.8 µg/ml TPCK-treated trypsin to 1 volume of serum followed by incubation at 56°C for 30 minutes. After samples were cooled down to room temperature, 3 volumes of 0.011 M KIO₄ were added, and samples were incubated for 15 minutes at room temperature. Subsequently, 3 volumes of 1% glycerol were added, and samples were incubated as before again. To prepare the starting dilution of 1:20, 12.5 volumes of PBS were added. Samples were diluted twofold in V-bottom 96-well plates with a final volume of 25 µl/well. 25 µl containing 4 HA-units of virus were added to each well. As controls, two wells without added virus and two wells without serum were prepared, where the missing part was replaced with PBS. The serum-virus mixture was incubated at 37°C for 1 hour in order for the antibodies to react with the virus. Finally, 50 µl of 1% chicken red blood cells were added to each well and the plate was further incubated for 20 minutes at 4°C for the hemagglutination to take place. When tilting the plate, the hemagglutination could be read and the final concentration at which it occurred could be determined. The HAI titer was then calculated as the reciprocate of that dilution at which hemagglutination was still inhibited.

3.2.6.3 Virus microneutralization assay for IAV (MN)

The assay was performed as previously established in the group on the basis of the protocol described by He et al. (2015). By this assay, anti-HA neutralization effects in the late replication cycle can be measured (He et al. 2015). For the assay, MDCK cells were prepared in 96-well plates the day before. Sera were inactivated at 56°C for 30 minutes. 1:20 serum dilutions were prepared in MEM medium containing 0.2% BSA and 1 µg/ml TPCK-treated trypsin. All further steps use the same medium. The diluted sera were subsequently further diluted twofold. As controls, a cell-only control and virus-only control were prepared. Initially, the serum was incubated with virus. To 25 µl of each serum-dilution and the virus-only controls, 3.5 x 10⁴ pfu of the respective IAV were added (starting serum dilution = 1:40). To the cell-only control, plain medium was added. The mixture was incubated at 37°C for one hour. Before 50 µl of the serum/virus-mixture was added to the MDCK cells, those were washed once with D-PBS. They were incubated at 37°C for one hour for the cells to be inoculated, then washed with D-PBS. Subsequently, another 50 µl

of the identical serum dilution was added to the wells. Plates were incubated for 24 hours at 37°C. The medium was then removed, and cells were fixed with 80% ice-cold acetone for ten minutes, air-dried and blocked with 5% skimmed milk in PBST for 45 minutes at 37°C. To quench the endogenous peroxidase, 100 µl 3% H₂O₂ were added per well and incubated for 30 minutes at room temperature. Cells were then washed with PBST and incubated with 50 µl/well of primary antibody (goat anti-FluA virion) in a 1:1,000 dilution in blocking buffer for one to two hours at 37°C. The plates were washed three times with PBST before HRP-conjugated secondary antibody was added in a 1:1,000 dilution in blocking buffer for one hour at 37°C. Finally, plates were washed again three times with PBST before 50 µl of ELISA substrate solution were added per well. The reaction was stopped after colour development with 50 µl H₂SO₄ per well and the absorption was measured at 450 nm.

To calculate neutralization values, the following formula was used:

$$MN (fold) = 1 - \frac{OD(well) - meanOD(cell\ ctrl\ wells)}{meanOD (all\ wells\ of\ resp.\ dilution)}$$

Resulting values above 1 were set to 1 and values below 0 were set to 0.

3.2.7 SARS-CoV-2-specific immunological and virological methods

3.2.7.1 Production of SARS-CoV-2 virus stocks

Vero E6 cells were seeded in T75-cell culture flasks. The next day they were infected with an MOI of 0.01 and incubated at 37°C for 48 hours. The cell culture medium was then collected and residual cell debris was removed by centrifugation. The medium was finally divided into aliquots and stored at -80°C for further applications. The titer of the stocks was measured after one freeze-thaw cycle.

3.2.7.2 Neutralization Assay with the “SARS-CoV-2 Surrogate Virus Neutralization Test (sVNT)” Kit

The assay was carried out following the manufacturer’s (GenScript) instructions in an ELISA format. The assay utilizes an HRP-conjugated recombinant SARS-CoV-2 RBD (HRP-RBD). ELISA plates were pre-coated with hACE2. The samples and controls were incubated with the HRP-RBD and then added to the plate. Only those HRP-RBD molecules can bind to the hACE2 that have not been complexed by antibodies in the sera. The absorbance of the sample was inversely dependent on the titer of the neutralizing antibodies.

3.2.7.3 Plaque-Reduction Neutralization Test (PRNT)

The PRNT was used for SARS-CoV-2 samples. Vero E6 cells were prepared in 24-well plates to be confluent on the day of infection. Serum samples were inactivated for 30

minutes at 56°C and diluted twofold, starting with 1:20 in OptiPro-medium. The virus stock was set to 50 pfu/100 µl in OptiPro-medium. Virus and serum were mixed 1:1 and incubated for 1 hour at 37°C. Culture medium was aspirated from the Vero E6 cells and 200 µl/well of the virus/serum-mixture was added to the cells. As a control, virus was mixed with OptiPro-medium and added to the cells. A control without virus was also prepared. The cells were incubated for 1 hour at 37°C. During that time, they were gently rocked every 10-15 minutes. The virus/serum-mix was then aspirated from the cells and 500 µl of overlay-medium was added to each well and cells were incubated for the suitable amount of time. Finally, cells were stained with crystal violet solution for one hour at room temperature. Plates were air-dried and viral plaques were counted. Plaque-reduction was calculated in relation to the number of plaques in the virus control and the titer at which 50% reduction was achieved was assessed.

3.2.8 Statistics

All statistical analyses were conducted using the GraphPad Prism software.

For comparison of two unmatched groups, a non-paired, non-parametric Mann-Whitney-U test was performed. Three or more unmatched groups were compared using a non-paired, non-parametric Kruskal-Wallis test. When matched data were analysed, a paired, non-parametric Friedman-test was conducted. Comparisons were performed as indicated. ELISA data are presented as the area under the curve (AUC) of the measured OD_{450nm} of the serum dilution curve. Survival data was analyzed with a log rank Mantel-Cox test. Correlations were calculated with a linear regression analysis.

4 Results

4.1 Influenza

In the following sections, the results regarding the immunological evaluation of the bivalent AAV-HA/NP vaccine, evaluating possible synergistic effects of the vaccine antigens HA and NP of A/California/7/2009pdm in mice are described (Figure 17, groups 1-6). Different prime – boost schemes were assessed. Those included WIV immunizations to assess its influence on the development of broadly reactive immune responses and the activation of FcγR-mediated effector functions (Figure 17, groups 1-3). Furthermore, a single-shot (prime-only) AAV-HA/NP immunization was conducted, to evaluate a possible self-boosting effect of AAV-vectors. Additionally, another group of mice was simultaneously immunized via two different routes (Figure 17, group 6), to assess possible effects.

To determine the effects of a group 2 HA from A/Aichi/2/68 on a broadly reactive immune response, mice were immunized either with HA (H1) or H3 alone (Figure 17, groups 8 and 9), or in combination (Figure 17, group 7).

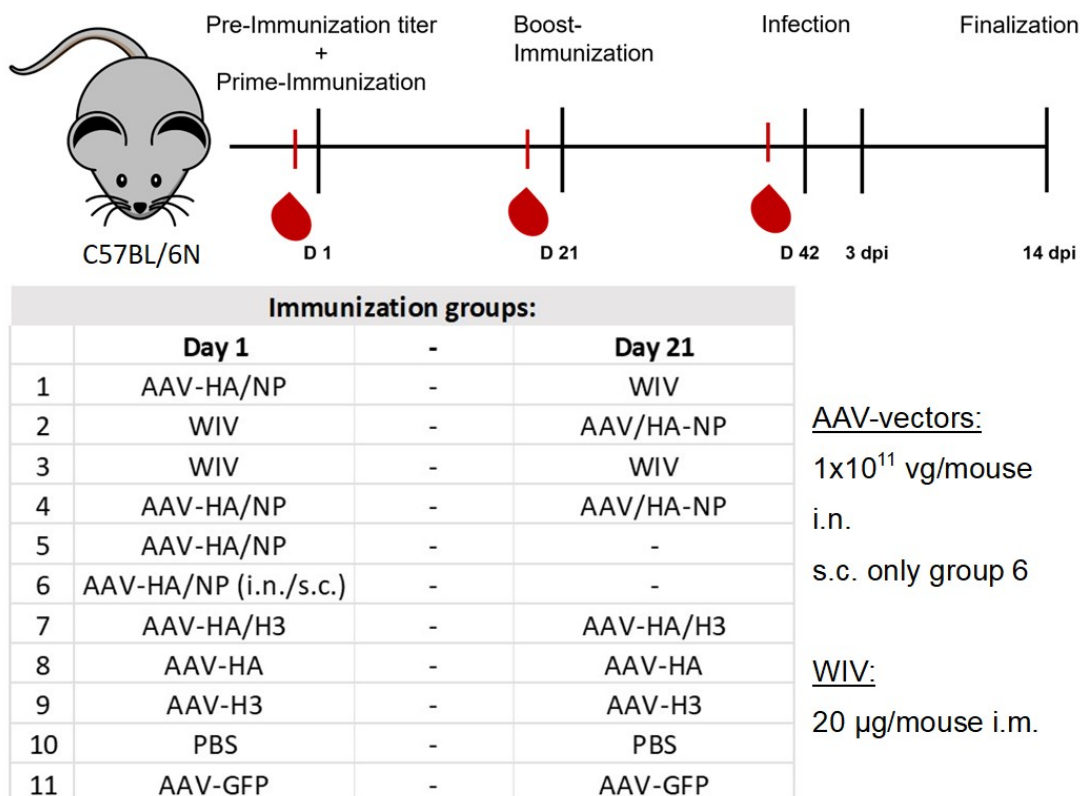


Figure 17: Immunization schedule for the evaluation of AAV-vector vaccines against influenza A viruses

Ten C57BL/6N mice per group were immunized as outlined in the table. Blood was taken at the indicated time points. 21 Days after the second immunization, mice were challenged with either homologous, heterologous or heterosubtypic virus. Survival and weight loss were monitored. At day three post infection, five mice per group were sacrificed for lung viral titers. All surviving animals were sacrificed at day 14 post infection.

For the evaluation of the immune response, serological parameters, i.e., IgG antibody titers, FcγR-activating responses, HAI titers, MN titers, antibodies against the HA-stalk, as well as IgA mucosal antibodies, protection against infection and T-cell responses were assessed. In the following sections 4.1.1 - 4.1.4 and 4.1.10 - 4.1.11, the results for the immunization groups 1-6 will be displayed and described separately from the results for the groups 7-9 for clarity reasons, but the experiments were conducted at the same time.

4.1.1 AAV-HA/NP immunization results in a more broadly reactive antibody response than can be achieved with WIV immunization alone

AAV-vectors were produced, and their quality was assessed following the established protocols (Figure 18): full AAV-vector particles were counted via electron microscopy (EM, carried out by Lars Möller, ZBS4 unit of the RKI, Figure 18 A); an ADK9-ELISA was performed to evaluate the integrity of the AAV-vector capsid (Figure 18 B); transgene expression was assessed after transduction of HEK293T cells with AAV-vectors by Western Blot analysis of cell lysates (Figure 18 C), and immunofluorescence staining of

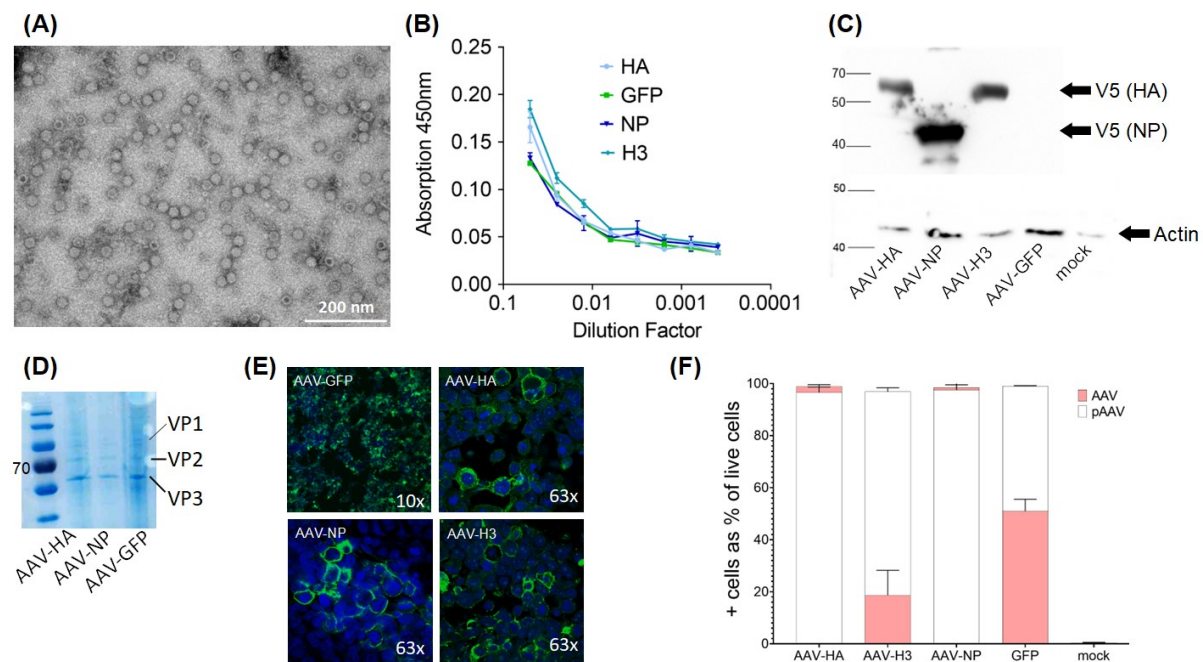


Figure 18: Quality control of AAV-vectors for influenza A virus antigens

(A) Electron micrographs of the AAV-HA preparation used to assess the proportion of full particles and impurities. **(B)** ADK9-ELISA of the AAV-HA, AAV-NP, AAV-H3 and AAV-GFP preparations (mean ± SD of technical duplicates) **(C)** Western Blot analysis of HEK293T-cell lysates transduced with the indicated AAV-vector preparations after 48h incubation **(D)** Coomassie staining of AAV-preparations separated by SDS-PAGE; VP1, VP2 and VP3 proteins (AAV cap gene proteins) are labelled **(E)** IF staining of HEK293T-cells transduced with AAV-vector preparations after 48h of incubation, V5-Tag was detected, no staining in the AAV-GFP cells because of endogenous signal, blue=DAPI, magnification as indicated **(F)** Quantification of V5-positive cells via flow cytometry (mean ± SD of technical duplicates)

transduced cells (Figure 18 E); the amount of successfully transduced cells was quantified via flow cytometric analysis (Figure 18 F); purity of AAV-vector preparations was checked via SDS-PAGE and subsequent Coomassie staining, where the VP1, VP2 and VP3 proteins (AAV cap gene proteins) could be visualized (Figure 18 D).

Mice were immunized either intranasally or subcutaneously (group 6) for AAV-vectors or intramuscularly for WIV. The immunization schedule is outlined in Figure 17. Mice immunized with AAV-GFP and PBS served as negative control groups. AAV-GFP immunized mice were used to monitor the anti-AAV-vector immunity.

Blood was taken from the animals at the indicated time points before each immunization and before the challenge. Total antibody titers in the serum were assessed via ELISA against a panel of group 1 and 2 IAV (Figure 20).

Over time, the WIV-primed immunization groups mounted the strain-specific antibody response the fastest, reaching levels close to the peak final titers already after the prime-immunization, while the AAV-primed groups reached the same level of titers only after six weeks (Figure 20 A). Here, it is notable that for the peak antibody level, a boost immunization is not necessary, as also the prime-only AAV-group reached the same antibody level after six weeks, showing an equal titer increase as the prime-boost AAV-groups. Peak anti-AAV9 antibody titers were mounted in all AAV-immunized mice within three weeks (Figure 20 B). The immunization groups primed with AAV-HA/NP had similarly high titers against all included virus strains, namely Cal/7/09pdm, PR8 (H1N1), X31 (H3N2),

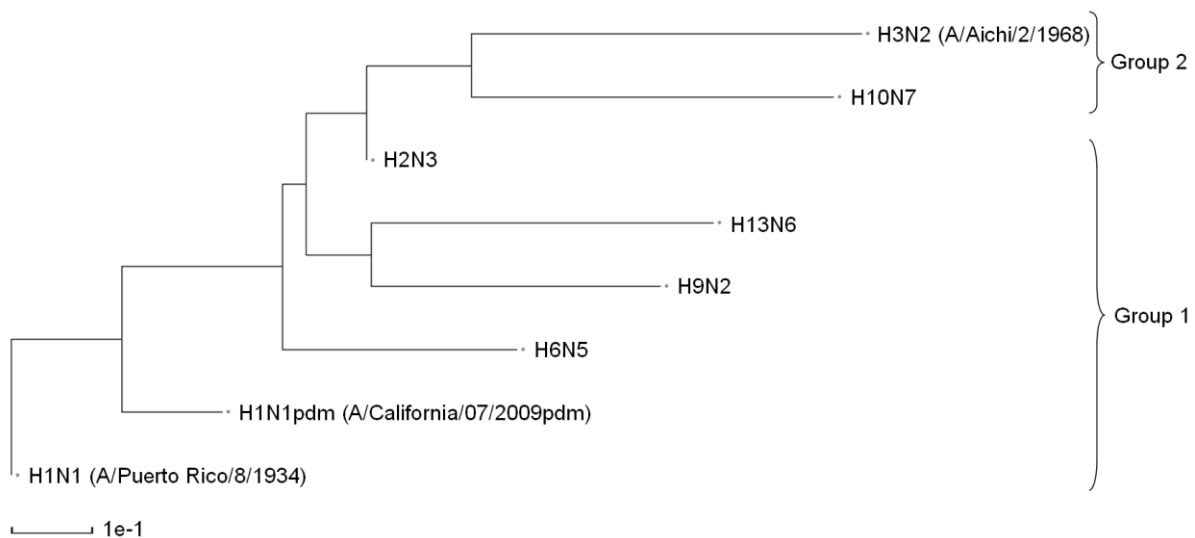


Figure 19: Phylogenetic tree of influenza A viruses used for serological analysis

The phylogenetic tree of the indicated influenza A subtypes was created using the influenza virus database of NCBI (by Neighbor-Joining method, F84 distance). The analysis was based on the full-length sequences of the hemagglutinin (HA) protein. Allocation of the subtypes to the HA-groups 1 or 2 is indicated. A comparison of the HA amino acid sequences of A/Cal/7/09pdm, PR8 and X31 is in the Appendix, Figure 45 and of the nucleoprotein (NP) in Figure 46 (Bao et al. 2008; NCBI 2023)

H2N3, H6N4, H9N2, H13N6, and H10N7 (Figure 19, Figure 20 C, F, G, H). The group primed with WIV and boosted with AAV had lower titers compared to the AAV-primed groups for most strains, but still mounted a broadly reactive response against all virus strains (Figure 20 D). The response of the WIV-only group showed only a strain specific reaction and low titers against all other strains (Figure 20 E).

More specifically, against homologous virus, all groups had similarly high titers. Against the heterologous PR8 virus, the difference between the groups was more pronounced. The 2x WIV group had the lowest titers (Figure 20 E), followed by the WIV-AAV-HA/NP group (Figure 20 D). The AAV-HA/NP-prime/WIV-boost group had similar titers to the other AAV-primed groups (Figure 20 C). A similar pattern could be observed for the heterosubtypic X31 virus and for the other viruses analyzed. Overall, the 2x AAV-HA/NP group mounted the highest titers against all tested viruses (Figure 20 F).

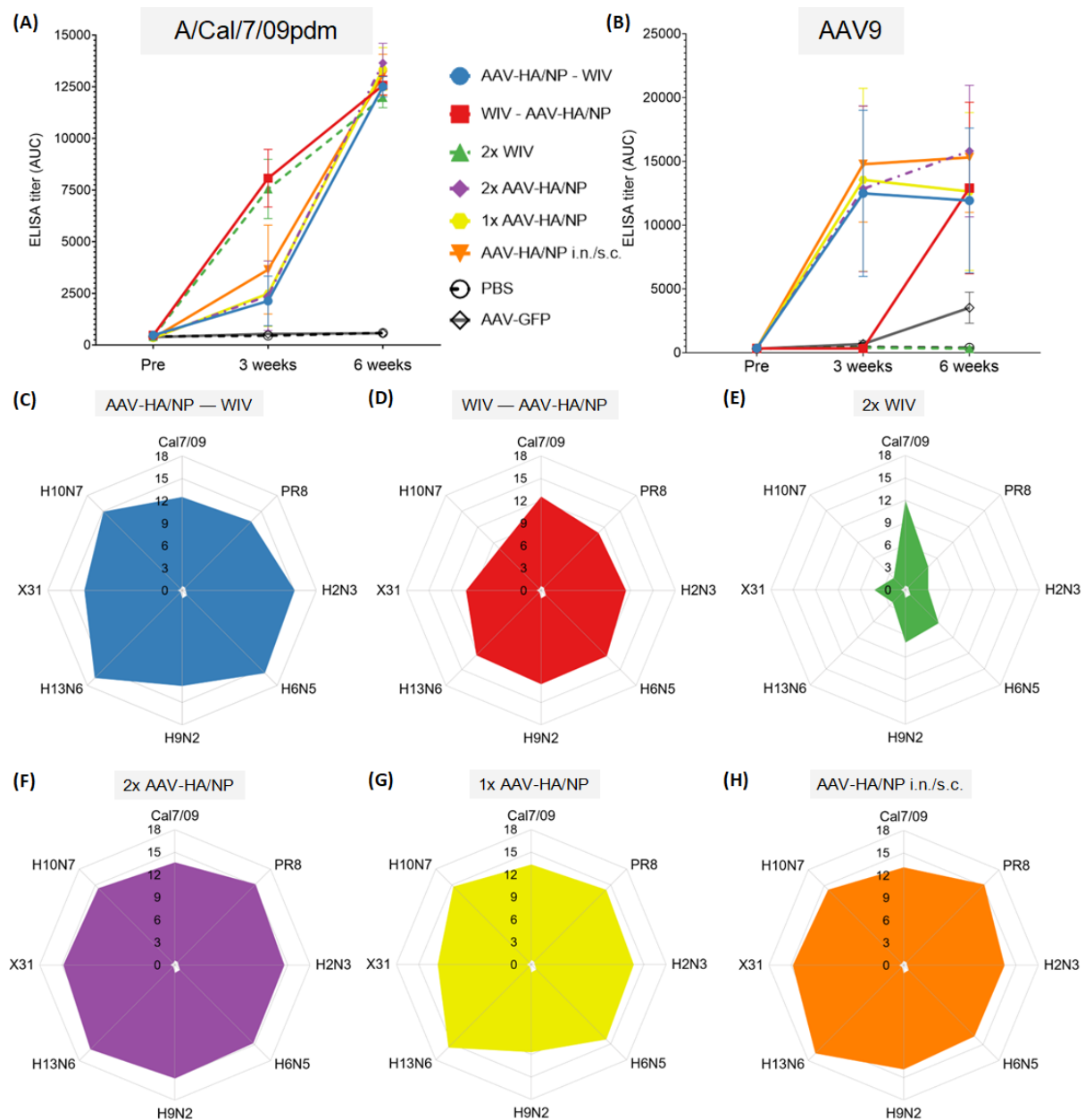


Figure 20: Immunization with AAV-HA/NP, but not WIV results in a broadly reactive antibody response

Displayed here are the immunization groups 1-6 for the evaluation of different prime-boost schemes and the combination of AAV-HA/NP with WIV. **(A)** ELISA titers of IgG antibodies in pooled sera of the indicated immunization groups against the A/Cal/7/09pdm virus at the indicated time points (antigen: purified virus; mean \pm SEM, $n=5$ groups of pooled sera analyzed in technical duplicates). **(B)** ELISA titers of AAV9-specific IgG antibodies in pooled sera at the indicated time points (antigen: empty AAV9 capsids; mean \pm SD, $n=5$ in technical duplicates). **(C) - (H)** ELISA titers of IgG antibodies in pooled pre-challenge sera of the immunization groups indicated above each panel against the stated group 1 and 2 IAVs (antigen: purified virus; ELISA titers expressed as AUC (axis value displayed as 1/1,000); coloured area: specific IgG response; white area in the middle: background reactivity of control groups). $p < 0.0001$ for all immunization groups against all antigens compared to control groups.

In summary these results indicate that AAV-priming is more efficient in inducing a broadly reactive immune response than WIV-priming. AAV-boosting after WIV-priming can broaden the reactive antibody response compared to WIV-boosting. AAV-vectors seem to display a self-boosting effect, as titers are equally high in the prime-only group compared to the prime-boost groups. The boosting effect seems not to be inhibited by existing anti-AAV-vector antibodies.

4.1.2 AAV-H3 is immunogenic in mice after intranasal application and induces virus strain-specific antibodies

To enhance the repertoire of AAV-vectors against IAV antigens, the AAV-H3 vector with a group 2 HA, for which the pAAV-vector-plasmid had been constructed in the group previously, was analyzed regarding immunogenicity and breadth of antibody response.

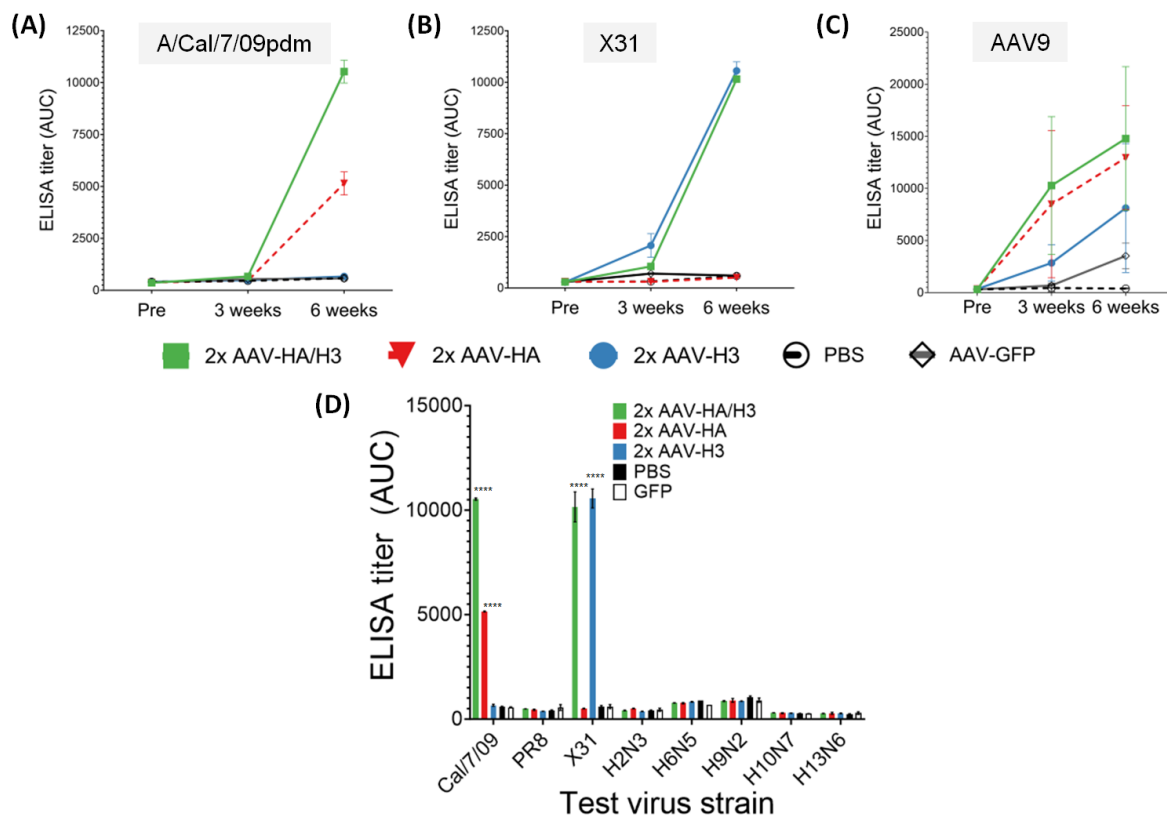


Figure 21: Immunization with AAV-HA and AAV-H3 results in a strain-specific antibody response

(A) ELISA titers of IgG antibodies in pooled sera of the indicated immunization groups against the A/Cal/7/09pdm virus at the indicated time points (mean \pm SEM, n=5 groups of pooled sera). **(B)** ELISA titers of IgG antibodies in pooled sera of the indicated immunization groups against the X31 virus at the indicated time points (mean \pm SEM, n=5 groups of pooled sera, analyzed in technical duplicates). **(C)** ELISA titers of AAV9-specific antibodies in pooled sera at the indicated time points (mean \pm SD, n=5 in technical duplicates). **(D)** ELISA titers in pooled pre-challenge sera of the indicated immunization groups against the stated group 1 and 2 IAVs (mean \pm SD of technical replicates, n=2, compared to control groups). **** p<0.0001

This was evaluated with the immunization groups 7-9 (Figure 17). Mice were immunized intranasally, and a prime-boost scheme was applied in all groups. One group was immunized with H1 of Cal/7/09pdm, one with H3 of X31 and one with a combination of H1 and H3.

AAV-H3 immunization resulted in strain specific antibody responses against the parental virus strain (). Antibody levels only rose slowly against the Cal/7/09pdm (Figure 21 A) and X31 (Figure 21 B) viruses after the prime immunization, but continued to rise more steeply after the booster dose, while anti-AAV9 also increased continuously (Figure 21 C), indicating that there was no inhibition by those. No broadly reactive, but only strain specific antibodies could be detected (Figure 21 D).

4.1.3 AAV-HA/NP immunization results in a different pattern of Fc γ -receptor activation compared to WIV-immunization

It had been shown that WIV-immunization could enhance existing, broadly reactive Fc γ -receptor-activating antibody titers, which were induced either by natural influenza infection or vaccination with a live-attenuated vaccine, but was not able to induce such antibodies *de novo* (Jegaskanda et al. 2013a). Demminger et al. (2020) showed that non-neutralizing antibodies induced by AAV-immunization were able to induce Fc γ -receptor activating responses. To assess the Fc γ R-effector function and to compare the antibody responses after AAV- or WIV-immunization, pooled pre-challenge sera were analyzed with the abovementioned reporter assay. For this assay, antigens in the form of purified influenza viruses were coated on ELISA plates and incubated with the pooled mouse sera of the different immunization groups, before the reporter cells, which stably express the extracellular domains of the murine Fc γ RI, -IIB, -III or -IV and the intracellular signaling module of the murine CD3- ζ chain, were added. Upon activation, which is initiated by the binding of the Fc γ R to an activating antibody, IL-2 is produced by the reporter cells, which could then be quantified in an ELISA assay.

All immunization groups showed some level of Fc γ R-activation compared to the control groups, but levels and patterns differed between the groups (Figure 22).

Against the homologous virus, activation of Fc γ RI was strongest in the group primed via two different application routes (in/sc AAV-HA/NP), but also strong in all other groups immunized with AAV-HA/NP only (Figure 22 A). Interestingly, the groups that have only been primed with the AAV vaccine displayed the highest activating response for Fc γ RI. In the AAV-HA/NP-prime and WIV-boost group, activation was lower than in the AAV-only groups, but higher than in the WIV-primed groups. In both WIV-primed groups, the activation was lowest. There was no difference between the WIV- or AAV-HA/NP-boost (Figure 22 A, Fc γ RI).

FcγR-responses activating FcγRIIb and FcγRIII did not display the marked inter-group differences detected for FcγRI. They were overall lower than the FcγRI response in the AAV-primed groups and higher in the WIV-primed groups, so overall they were more equal. Still, the prime-only AAV groups showed the largest level of activation.

For homologous virus, total IgG titers strongly correlated with the FcγRIIb ($r^2=0.8785$, $p<0.0001$) and FcγRIII ($r^2=0.8477$, $p<0.0001$) responses, but only moderately with FcγRI ($r^2=0.4870$, $p=0.0026$) (Figure 22 D). This is due to the fact, that the total peak IgG titers

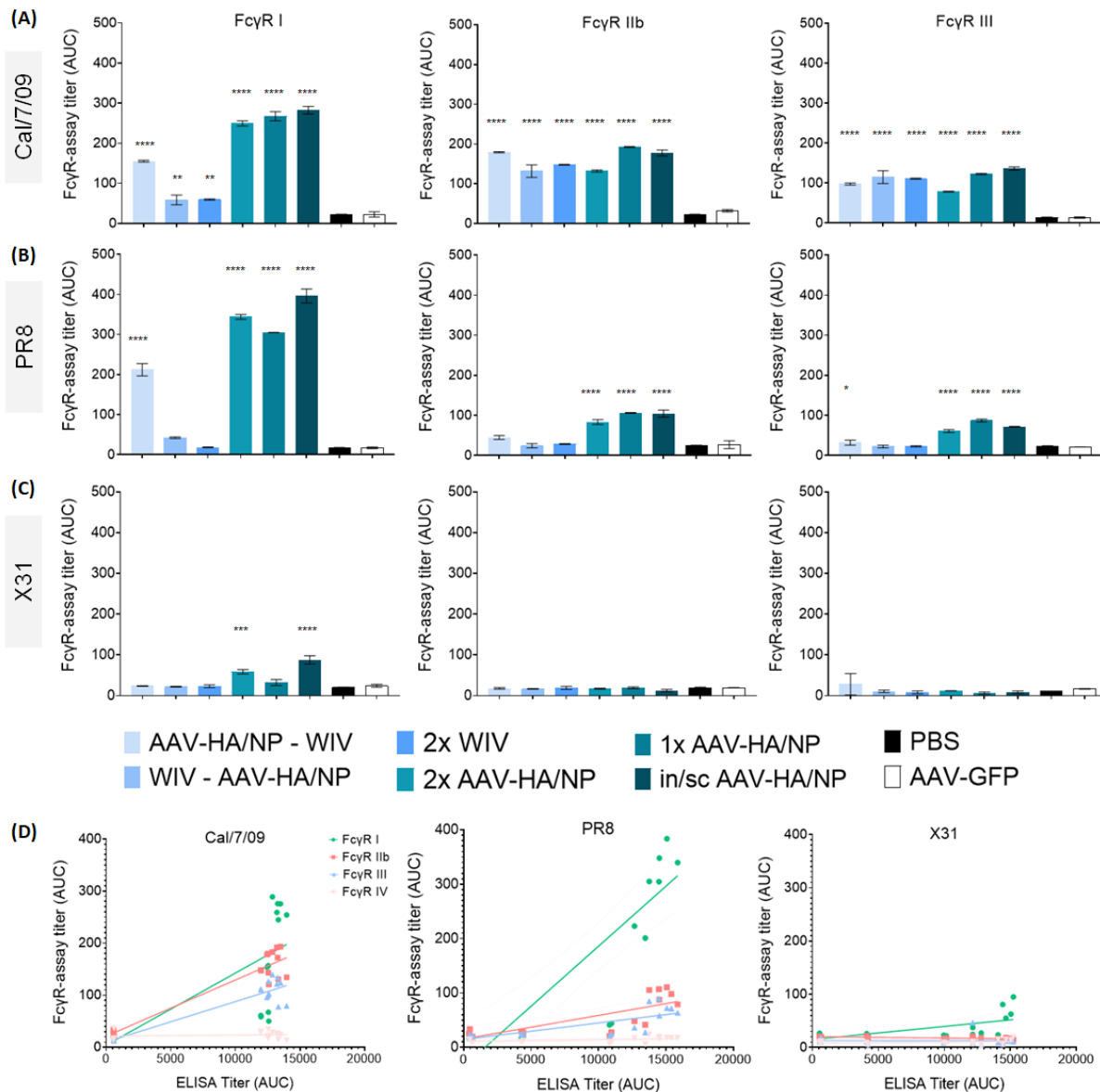


Figure 22: Immunization with AAV-HA/NP results in a different FcγR-activation profile than WIV immunization

(A) – (C) Activation of murine FcγRI, -IIb and -III by IgG antibodies specific for A/Cal/7/09pdm, PR8 or X31 in pooled pre-challenge sera of the indicated immunization groups (mean ± SD of technical replicates, n=2; * $p<0.05$, ** $p<0.01$, *** $p<0.001$, **** $p<0.0001$, compared to control groups)

(D) Linear regression between total IgG ELISA titers and FcγR-assay titers for the indicated virus strain.

of the WIV-immunized groups were just as high as in the AAV-immunized groups but differ from those significantly in the FcγRI response.

Against PR8, the response was highest for the FcγRI (Figure 22 B). Again, the activation was stronger in the AAV-primed groups compared to the WIV-primed groups, which didn't display a significantly upregulated response. Out of the AAV-primed groups, activation was lowest in the WIV-boosted group, similar to the response for homologous virus.

For FcγRIIb and FcγRIII, there was significant activation in all groups primed and/or boosted with AAV-only, but not in the groups primed and/or boosted with WIV. The level of activation was significantly lower than the activation level for FcγRI.

A strong correlation with total IgG titers could only be observed for responses against FcγRI ($r^2=0.7547$, $p<0.0001$), while only medium correlation levels could be observed for FcγRIIb ($r^2=0.5795$, $p=0.0006$) and FcγRIII ($r^2=0.5426$, $p=0.0011$) (Figure 22 D).

For X31, the FcγR response was very low for all receptor-subtypes. Most groups didn't show any activation (Figure 22 C). There was a low, but significant level of FcγRI activation in the AAV prime/boost and AAV in/sc groups.

None of the groups showed activation of FcγRIV responses.

These results indicate that prime-immunization with AAV results in higher activation of FcγRI for homologous and heterologous virus compared to WIV-priming. Furthermore, the results display the limited capability of the WIV-vaccine to either prime or boost a FcγR-activating response compared to the AAV-vectors. For heterosubtypic virus, activation is not very prominent in all groups.

4.1.4 AAV-H3 induces virus strain-specific FcγR-responses

Immunization with AAV-HA and AAV-H3 overall resulted in strain-specific activation of FcγR-activating responses (Figure 23). All FcγR-responses against X31 were elevated in the groups immunized with AAV-HA/H3 and AAV-H3, while the response in the group immunized with AAV-H3 was always stronger than in the AAV-HA/H3 group (Figure 23 A). A strong correlation could be detected between total IgG titers against X31 and FcγRI ($r^2=0.9075$, $p<0.0001$), FcγRIIb ($r^2=0.9354$, $p<0.0001$) and FcγRIII ($r^2=0.9482$, $p<0.0001$) titers (Figure 23 B). Of interest here is the result that after immunization with AAV-HA or AAV-H3 alone, the FcγR-activating responses were stronger for FcγRIIb and -III and not -I, as it was seen after immunization with AAV-HA/NP (Figure 22).

The FcγRIIb and FcγRIII responses were highly elevated against Cal/7/09pdm in the group immunized with AAV-HA/H3 (Figure 23 A). Here, the FcγR-assay titers strongly correlated with the total IgG antibody titers (FcγRIIb: $r^2=0.8527$, $p=0.0001$; FcγRIII: $r^2=0.8456$, $p=0.0002$) (Figure 23 B).

Against PR8, there were no above background FcγR-activating responses.

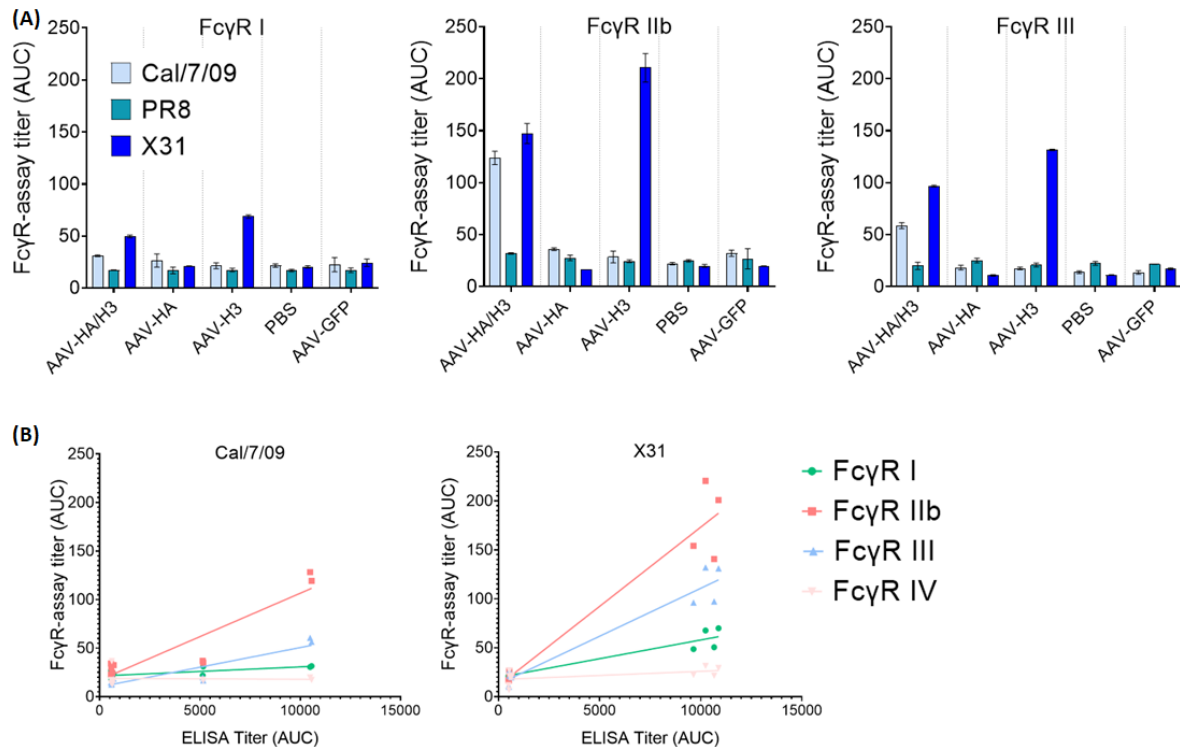


Figure 23: Immunization with AAV-HA and AAV-H3 results in strain-specific FcγR-responses

(A) Activation of murine FcγRI, -IIb and -III by IgG antibodies specific for A/Cal/7/09pdm, PR8 or X31 in pooled pre-challenge sera of the indicated immunization groups (mean \pm SD of technical replicates, n=2) (B) Linear regression between total IgG ELISA titers and FcγR-assay titers for the indicated virus strain.

4.1.5 Neutralizing and hemagglutination inhibition titers display virus-strain specificity after immunization with AAV-HA/NP and WIV

Hemagglutination inhibition (HAI) and neutralizing antibody titers (MN₅₀) of the sera were determined.

Test virus	Assay	AAV-HA/NP - WIV	WIV - AAV-HA/NP	2x WIV	2x AAV- HA/NP	1x AAV- HA/NP	in+sc AAV-HA/NP	PBS	2x AAV-GFP
Cal/7/09	MNT50	3490	2952	2381	2215	2715	2909	<40	<40
	HAI	320	320	320	160	640	640	<40	<40
PR8	MNT50	<40	<40	<40	<40	<40	<40	<40	<40
	HAI	<40	<40	<40	<40	<40	<40	<40	<40
X31	MNT50	<40	<40	<40	<40	<40	<40	<40	<40
	HAI	<40	<40	<40	<40	<40	<40	<40	<40

Table 5: Hemagglutination inhibition and neutralizing titers are virus strain-specific Displayed are mean HAI and MN₅₀ titers in pooled pre-challenge sera of the specified immunization groups against the indicated virus strains (n=2 in technical duplicates).

HAI and MN₅₀ titers against the homologous Cal/7/09pdm virus could be detected in the sera of all mice immunized with AAV-HA/NP and/or WIV (Table 5). HAI titers were highest in the sera of the mice immunized once with AAV-HA/NP and AAV-HA/NP i.n./s.c., while they were lowest in the group primed and boosted with AAV-HA/NP. MN₅₀ titers are high

in all groups immunized with AAV-HA/NP and/or WIV. Inhibition in the group primed and boosted with WIV was lower than in the groups immunized with AAV-HA/NP-WIV and WIV-AAV-HA/NP. No HAI or MN₅₀ titers could be detected against PR8 or X31.

4.1.6 Neutralizing and hemagglutination inhibition titers display virus-strain specificity after immunization with AAV-HA and AAV-H3

In the sera of the mice immunized with AAV-HA and AAV-HA/H3, HAI and MN₅₀ titers against Cal/7/09pdm could be detected (Table 6). In the AAV-HA/H3 group, hemagglutination inhibiting and neutralizing antibodies were also present against X31. In the group immunized with AAV-H3 alone, such titers could be determined only against X31, which were higher than in the group immunized with AAV-HA/H3 (Table 6).

Overall, HAI and neutralizing antibodies appear to be strain specific against the HA head. The broadly reactive antibodies detected (see above) seem not to display hemagglutination inhibiting and neutralizing properties.

Test virus	Assay	2x AAV-HA/H3	2x AAV-HA	2x AAV-H3	PBS	2x AAV-GFP
Cal/7/09	MNT50	1840	2120	<40	<40	<40
	HAI	320	80	<40	<40	<40
PR8	MNT50	<40	<40	<40	<40	<40
	HAI	<40	<40	<40	<40	<40
X31	MNT50	1675	<40	2176	<40	<40
	HAI	160	<40	640	<40	<40

Table 6: Hemagglutination inhibition and neutralizing titers are virus strain-specific after AAV-HA and AAV-H3 immunization

Displayed are mean HAI and MN₅₀ titers in pooled pre-challenge sera of the specified immunization groups against the indicated virus strains (n=2 in technical duplicates).

4.1.7 Induction of antibodies against the hemagglutinin stalk

To analyze if the broadly reactive antibodies were directed against the HA-stalk, those were analyzed via flow cytometry.

Stalk antibodies were present in most groups against Cal/7/09pdm headless HA, but no significance could be detected (Figure 24). Only the group immunized with AAV-HA/NP vial the i.n. and s.c. route simultaneously did not seem to induce antibodies against the HA-stalk (Figure 24).

4.1.8 Mucosal antibodies were induced in the respiratory tract after immunization with AAV-HA/NP and AAV-H3 immunization

Another desirable property of the AAV-vector vaccines is the induction of a strong local mucosal immune response because of the intranasal administration. To evaluate the mucosal antibody response after immunization, nasal washes were performed, and lung

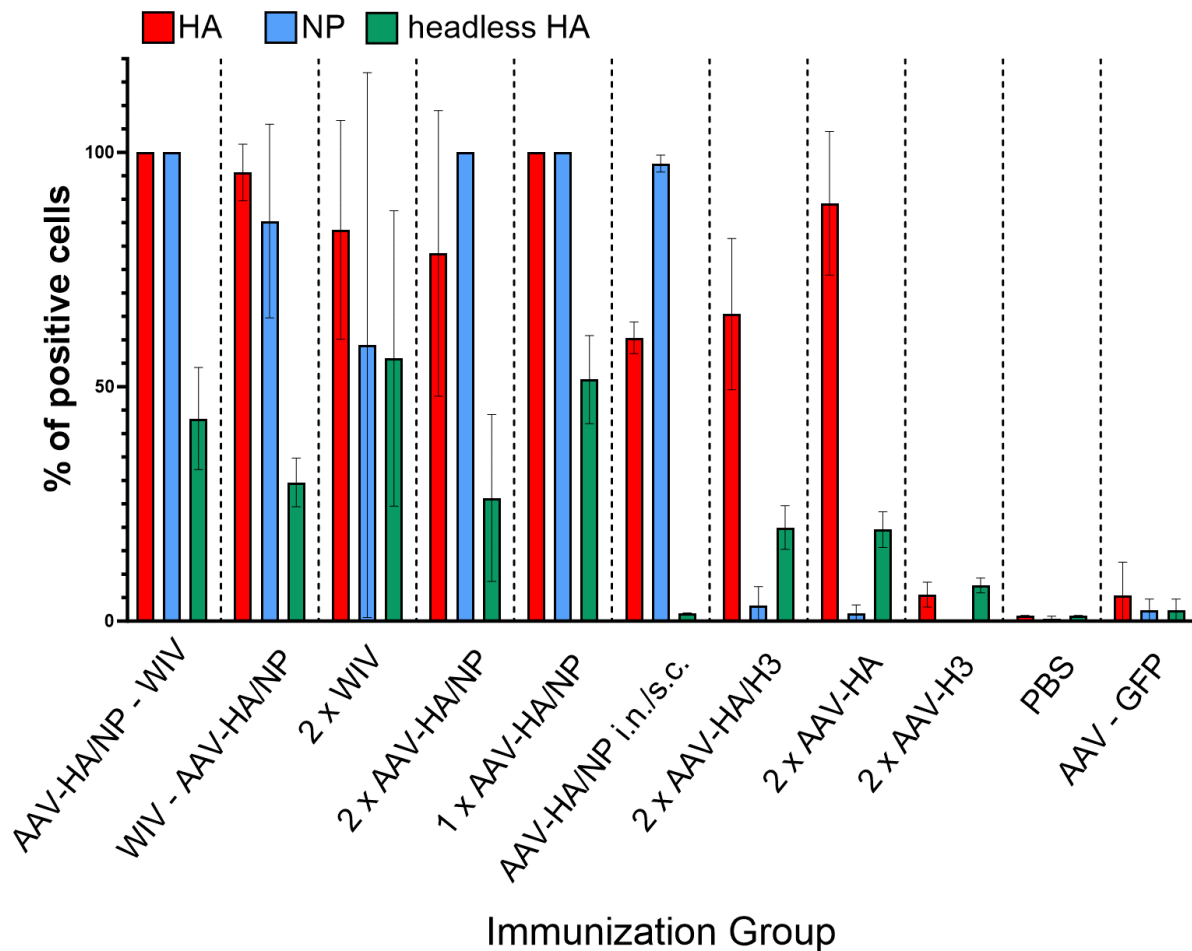


Figure 24: Induction of antibodies towards the hemagglutinin stalk

Antibodies against the hemagglutinin (HA) stalk were measured via flow cytometry. For that purpose, HEK293T-cells were transfected with either HA, NP or headless-HA of Cal/7/09pdm and incubated with the pooled final sera of the immunization groups after 48h. The signal is displayed as the proportion of the signal towards full-HA in the respective group (mean \pm SD, n=2 in technical duplicates)

homogenates prepared from uninfected mice at the end point of the immunization schedule at six weeks. IgA titers were measured by ELISA.

The IgA titers in the lung homogenates and the nasal washes showed a high variance between the individual mice, while the signal in the nasal washes was around 10x lower in than in the lung homogenates.

Against homologous virus, IgA titers in the lung homogenates from the AAV-prime/WIV-boost, the prime-boost AAV-HA/NP and the prime-only AAV-HA/NP vaccination-groups were significantly elevated compared to the control groups (Figure 25 A). In the nasal washes, those two groups were elevated as well, but they didn't show significance. Only in the i.n./s.c.-AAV-HA/NP group elevated titers could be detected (Figure 25 D).

Against PR8, the lung homogenates of the same immunization groups as for homologous virus showed significantly elevated IgA levels (Figure 25 B), but there were no significant IgA levels in the nasal washes (Figure 25 E).

Interestingly, against X31, IgA levels in the lung homogenates of the AAV-HA/NP-prime/WIV-boost, 2x AAV-HA/NP and 1x AAV-HA/NP groups were elevated, as they were for the other virus strains, but additionally also in the AAV-H3 group (Figure 25 C). In the nasal washes of the 2x AAV-HA/NP, 1x AAV-HA/NP and AAV-H3 groups, elevated titers could be detected as well (Figure 25 F).

These results indicate that mucosal IgA antibodies are induced along the administration route by intranasal application of the AAV-vector vaccines, and those have the potential to be broadly reactive. Overall, because significant IgA levels were only found in the groups primed with AAV, the boost seems to be less relevant.

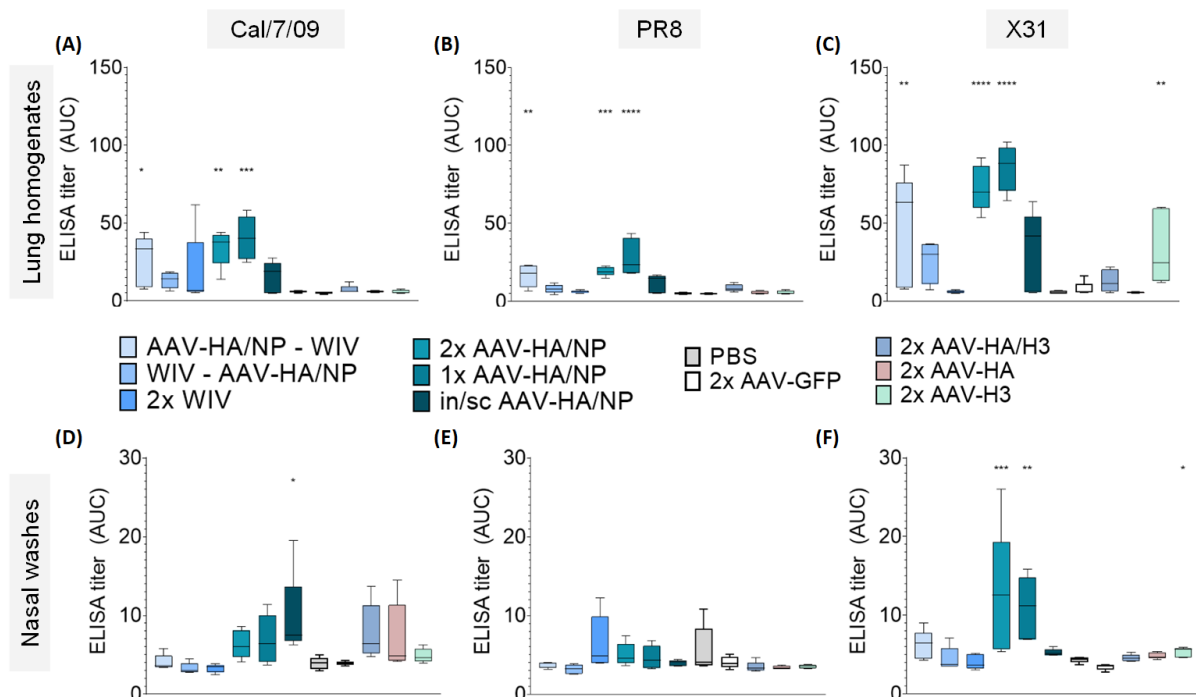


Figure 25: IgA antibodies were induced against homologous, heterologous and heterosubtypic virus in the respiratory tract after AAV-HA/NP immunization, and against X31 after AAV-H3 immunization

(A) – (C) ELISA titers of IgA antibodies in lung homogenates of the indicated immunization groups against the specified virus-strain at the indicated time points (Box and whiskers with 5.95 percentile, n=5). **(D) – (F)** ELISA titers of IgA antibodies in nasal washes of the indicated immunization groups against the specified virus-strain at the indicated time points (Box and whiskers with 5.95 percentile, n=5).

* p<0.05, ** p<0.01, *** p<0.001, **** p<0.0001

4.1.9 Induction of T-cell responses

Antigen-specific CD4⁺ and CD8⁺ T-cells were measured with intracellular cytokine staining. The cells were isolated from the spleens of the immunized mice at day 42, three weeks after the boost immunization.

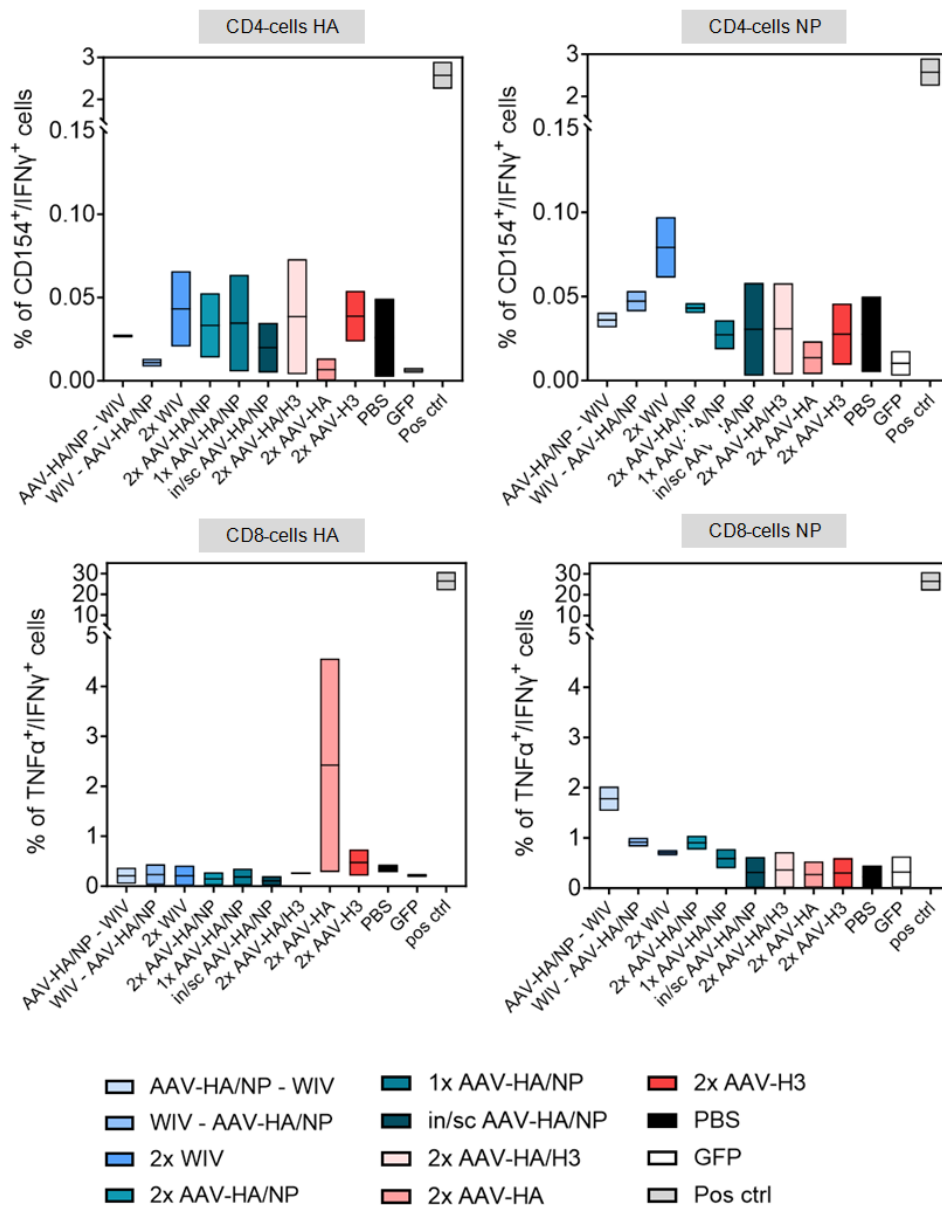


Figure 26: No CD4 and CD8 T-cell responses against influenza A antigens were detected

Antigen-specific T-cells were measured with intracellular cytokine staining. Isolated spleen cells were stimulated with peptide pools of Cal/7/09pdm (H1N1) HA or NP, stained and measured with flow cytometry. Through the staining, CD4 and CD8 T-cells were separated. For CD4 T-cells double positive cells for CD154 and IFN γ were counted as positive cells and for CD8 T-cells double positive cells for TNF α and IFN γ . Single mouse spleens were analysed (n=5) in technical duplicates. Bars show minimum to maximum with line at median. Gating strategy in the Appendix, Figure 43

In this analysis, the background signal of the control groups was rather strong and the number of potential antigen-specific T-cells was low. No significantly elevated T-cell responses could be detected here (Figure 26).

4.1.10 AAV-HA/NP prime-boost immunization protected mice against homologous, heterologous and heterosubtypic challenge

To evaluate, to which extent the described humoral properties of the immune response confer protection against infection, the immunized mice were infected three weeks after the final immunization and monitored over the following 14 days. At three days post infection, the peak of viral replication would usually be reached, so one half of the animals were finalized at this time point to assess viral lung titers, while all surviving animals will be finalized at day 14 post infection, when they are in the convalescent phase and no virus should be left (Heaton et al. 2013).

TCID₅₀ of the challenge virus stock for Cal/7/09pdm (NIBSC, ref. 39570) was given as 10^{7.6} TCID₅₀/ml and the lethal dose was given as 7.94 x 10³ TCID₅₀/mouse. The final titer of the virus dilution used for infection was assessed after infection by plaque assay, which resulted in 1.75 x 10⁴ pfu/ml.

After infection with the lethal dose of Cal/7/09pdm, 100% of the mice in the immunized groups – AAV-HA/NP – WIV, WIV – AAV-HA/NP, 2x WIV, 2x AAV-HA/NP, AAV-HA/NP i.n./s.c. – survived, except for the group only immunized once with AAV-HA/NP intranasally (Figure 27 A). In this group, 60% (3/5) survived. All animals in the PBS control group and 80% (4/5) of the AAV-GFP control group reached the humane end point at day seven (two animals) or eight after infection. The one remaining animal of the AAV-GFP group survived until the end of the infection period.

The mean maximum weight loss of all immunization groups did not differ significantly from each other, however it is noteworthy that in the group immunized 2x with AAV-HA/NP, three animals did not lose weight at all, while in the group immunized 2x with WIV, all animals lost some weight initially (Figure 28 A). All immunized groups had a significantly reduced mean maximum weight loss when compared to the control groups. The maximum weight loss correlated with the total serum IgG titers measured via ELISA ($r^2=0.6038$, $p<0.0001$).

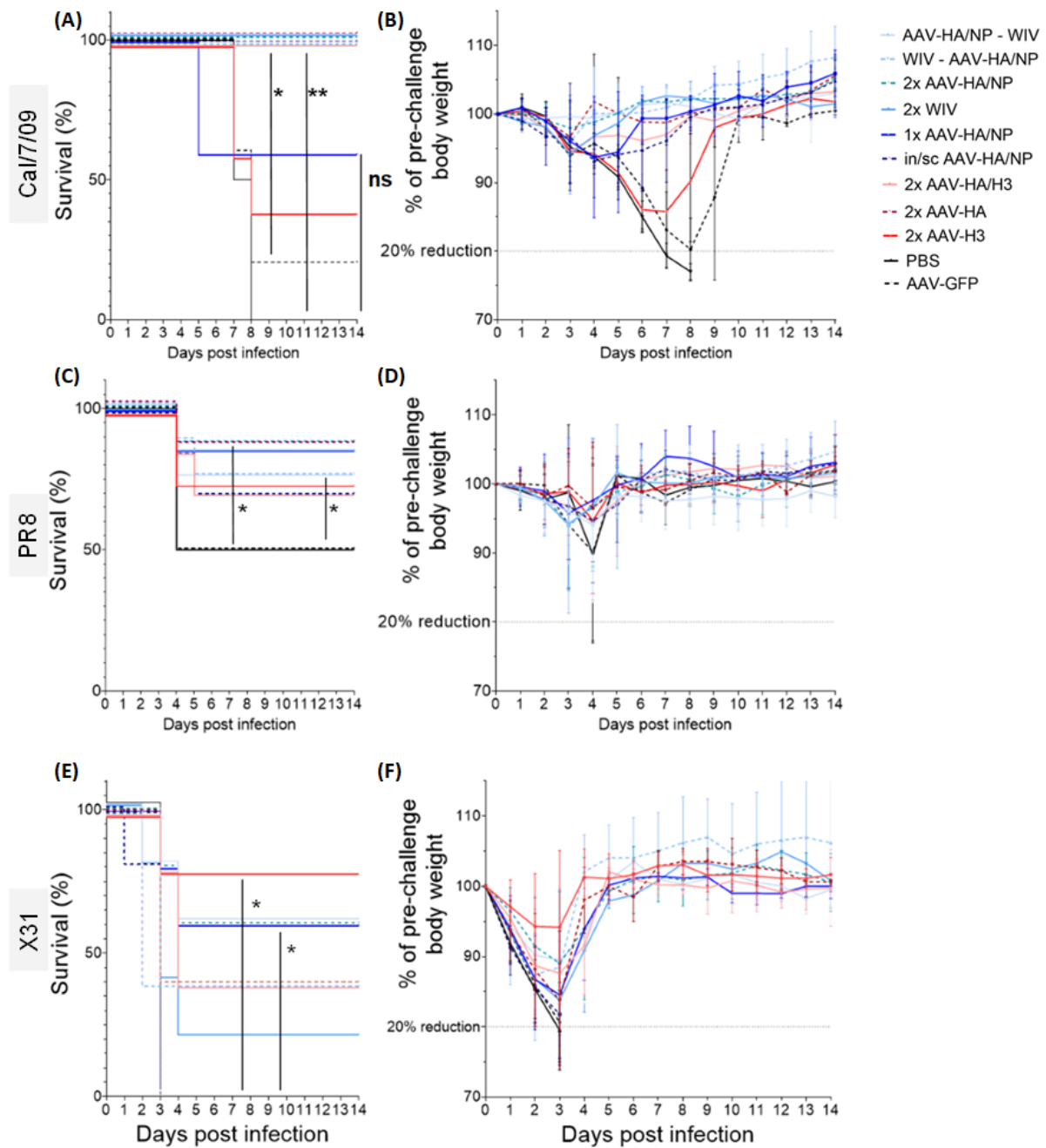


Figure 27: AAV-HA/NP prime-boost immunization protected mice from homologous, heterologous and heterosubtypic challenge

(A) – (B) Challenge with homologous Cal/7/09pdm ($7,94 \times 10^3$ TCID₅₀/mouse): **(A)** Kaplan-Meier plot of survival rate **(B)** relative weight loss **(C) – (D)** Challenge with heterologous PR8 (5.01×10^4 TCID₅₀/mouse): **(C)** Kaplan-Meier plot survival rate **(D)** relative weight loss **(E) – (F)** Challenge with heterosubtypic X31 (1.00×10^5 TCID₅₀/mouse): **(E)** Kaplan-Meier plot survival rate **(F)** relative weight loss

(A), (C), (E): Mantel-Cox test analysis, groups compared to control groups (B), (D), (F): mean body weight of individual animals in one group relative to the pre-challenge body weight \pm SD; * $p < 0.05$, ** $p < 0.01$, *** $p < 0.001$, **** $p < 0.0001$

The clinical scores – body weight, general condition, spontaneous behavior, breathing, and anomalies at the site of infection – rose until day three in most groups and then fell and remained close to zero (Figure 29 A). The lowest score level was monitored in the group immunized with 2x AAV-HA/NP. In the group immunized with i.n./s.c.-AAV, the mean score remained high up until day eight before starting to fall. The score of the control groups rose equally to the immunized groups until day four, but then continued to rise until the humane endpoint was reached. The surviving animal from the AAV-GFP group did develop a score until day eight, indicating that the infection started as it did in the other animals, but was then cleared.

Lung viral titers three days post infection were significantly lower in all immunized groups than in the control groups (Figure 28 B). In the groups immunized with AAV-HA/NP-prime/WIV-boost and i.n./s.c.-AAV-HA/NP, the virus was already cleared in all animals. By day 14, all surviving mice had cleared the virus. For the animals in the control groups which reached the humane endpoint, the virus titer was one log-level lower than at day three.

To assess the influence of the broadly reactive antibodies on survival, the groups of immunized mice were also challenged with a heterologous (PR8-H1N1) and a heterosubtypic (X31-H3N2) virus.

The first infection with the heterologous PR8 did not cause symptomatic infection in the mice (separate data in Appendix, Figure 47). Also, the control groups did not show symptoms and all animals survived. Three days after infection, lung viral titers could be detected in some animals, but those were on a very low level. There was no difference in weight loss or clinical scores of the animals. This was most likely due to a faulty virus stock aliquot. TCID₅₀ of the stock (NIBSC, ref. 39560) was given as 10^{9.1} TCID₅₀/ml and the lethal dose was given as 5.01 x 10⁴ TCID₅₀/mouse. The final titer of the virus dilution used for infection was assessed after infection by plaque assay, which resulted in 8 x 10¹ pfu/ml.

Thus, additional animals were used, which were taken from the amount of reserve animals, as had been specified in the animal trial application. For the groups of immunized animals, 10% of all animals (21 animals) and for the control groups 20% of all animals (14 animals) were available.

In the second experiment, mice developed severe symptoms very early on in the course of infection (separate data in Appendix, Figure 48). The titer level of the virus solution used for infection was now at 5 x 10² pfu/ml. 100% of the control animals succumbed to infection by day four, so total survival was 50% (5/10) (Figure 27 C). In the groups immunized with 2x AAV-HA/NP survival was 87.5% (7/8) and in the groups immunized with 2x WIV and 1x AAV-HA/NP 85.7% of the animals survived (6/7). In the groups WIV-prime/AAV-HA/NP-boost and AAV-HA/NP-prime/WIV-boost there was 75% survival (6/8). In the group i.n./s.c.-AAV the infection was 100% lethal in the additional animals, so the total survival was 71.4%

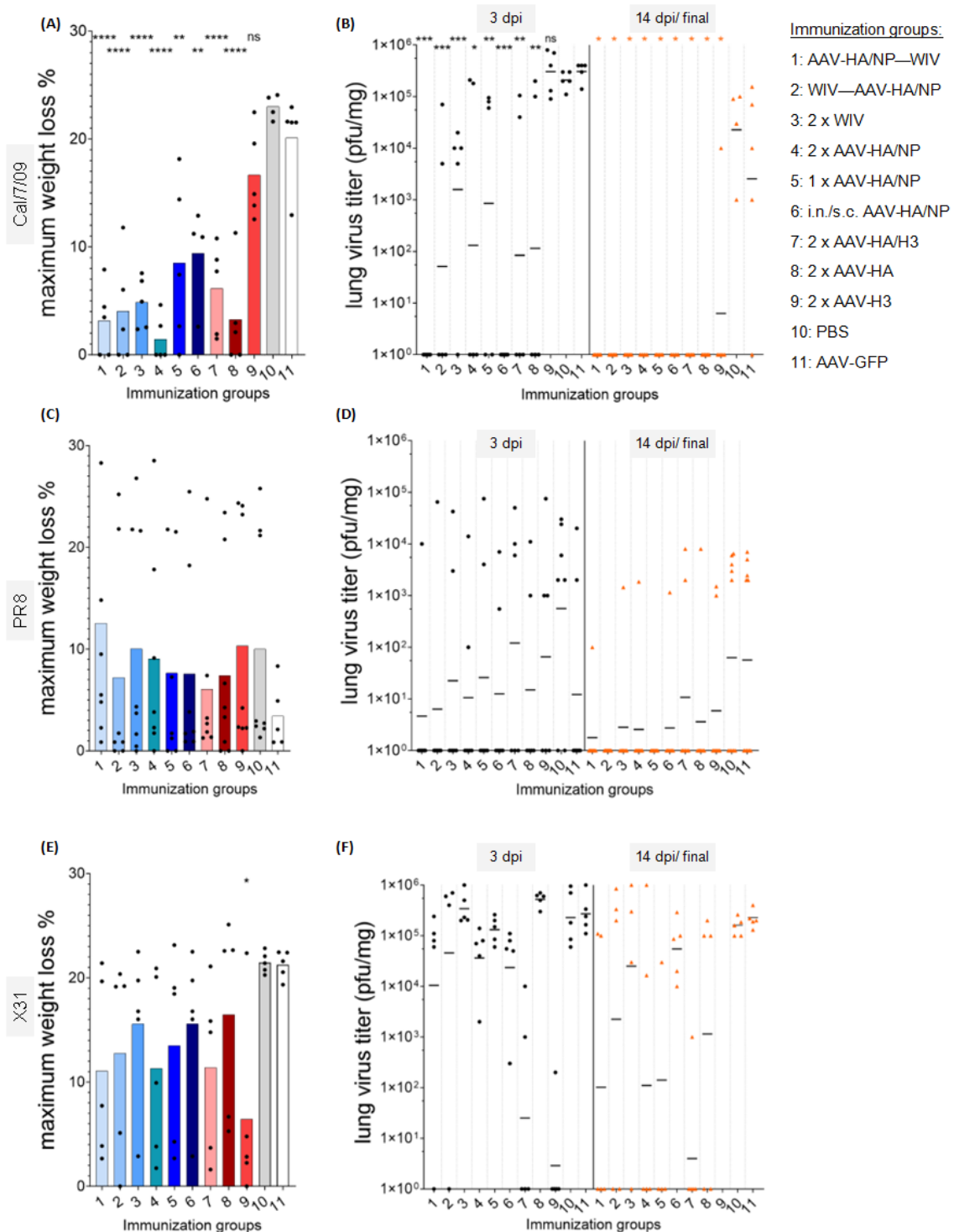


Figure 28: Viral challenge: Weight loss and lung virus titers

Challenge with homologous Cal/7/09pdm (A) maximum weight loss, (B) lung viral titers at 3 days post infection (black) or the respective end point of the animal (orange); Challenge with heterologous PR8 (C) maximum weight loss, (D) lung viral titers at 3 days post infection (black) or the respective end point of the animal (orange); Challenge with heterosubtypic X31 (E) maximum weight loss, (F) lung viral titers at 3 days post infection (black) or the respective end point of the animal (orange)

(A), (C), (E): symbols represent individual animals, bars: mean; (B), (D), (F): geometric mean, symbols represent individual animals, black: 3 days post infection, orange: individual end point or 14 days post infection; * p<0.05, ** p<0.01, *** p<0.001, **** p<0.0001

(5/7). The survival rates in the groups immunized with 2x AAV-HA/NP ($p=0.0486$) and WIV-AAV-HA/NP ($p=0.0486$) were significant compared to the control groups.

The mean maximum weight loss did not show differences between the groups (Figure 28 C). The clinical scores of the additional animals in the group immunized with 2xWIV were significantly reduced compared to the control groups (Figure 29 B).

Lung virus titers at day three after infection did not differ between the groups (Figure 28 D). By the end of the infection period, all surviving animals had cleared the virus (Figure 28 D).

A heterosubtypic infection with X31 was also performed. TCID₅₀ of the challenge virus stock (NIBSC, ref. 39600) was given as $10^{9.3}$ TCID₅₀/ml and the lethal dose was given as 1.00×10^5 TCID₅₀/mouse. The final titer of the virus dilution used for infection was assessed after infection by plaque assay, which resulted in 1.2×10^3 pfu/ml.

The challenge resulted in very harsh effects on the animals, leading to 100% lethality in the control groups by day three after infection (Figure 27 E). The immunization groups AAV-HA/NP-prime/WIV-boost, 2x AAV-HA/NP and 1x AAV-HA/NP achieved 60% survival (3/5), the group WIV-AAV-HA/NP 40% survival (2/5) and the group 2x WIV 20% survival (1/5). Lethality was also 100% in the i.n./s.c.-AAV-HA/NP group. The survival rates of the

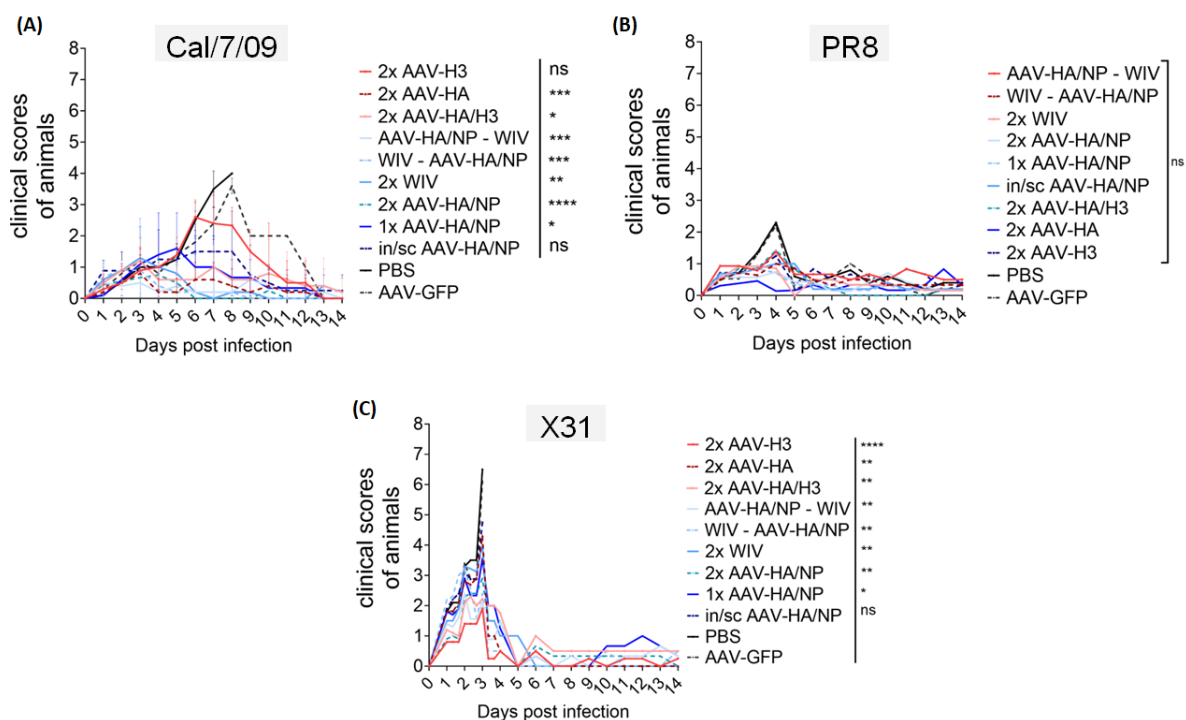


Figure 29: Clinical scores differed from control groups after Cal/7/09pdm and X31, but not after PR8 challenge in immunized mice

(A) Challenge with homologous Cal/7/09pdm: clinical score development; **(B)** Challenge with heterologous PR8: clinical score development; **(C)** Challenge with heterosubtypic X31: clinical score development

(A) – (C): mean of daily clinical scores of individual animals in the groups.

* $p < 0.05$, ** $p < 0.01$, *** $p < 0.001$, **** $p < 0.0001$

groups immunized with 2x AAV-HA/NP ($p=0.0143$) and 1x AAV-HA/NP ($p=0.0143$) were significant compared to the control groups.

The mean maximum weight loss was high in all groups and didn't differ significantly between the immunized and control groups (Figure 28 E). The lowest mean maximum weight loss was found in the groups immunized with AAV-HA/NP-WIV ($11.06\% \pm 8.87\%$) and 2x AAV-HA/NP ($11.29\% \pm 8.93\%$), but due to the high inter-animal variance, there was no significance.

The clinical scores were significantly reduced in all immunization groups compared to the control groups, except in the i.n./s.c.-AAV group, which also showed 100% lethality (Figure 29 C).

The lung viral titers three days after infection were about one log-level lower in the AAV-HA/NP-prime/WIV-boost, 2x AAV-HA/NP and i.n./s.c.-AAV-HA/NP groups than in the other immunization and control groups (Figure 28 F). The lung viral titers of the animals that reached the humane end point were still at the same level as on day three, because most animals reached their humane end point latest on day four after infection. All surviving animals had cleared the virus by day 14.

4.1.11 AAV-H3 immunization protected mice from challenge with X31

As expected, after infection with Cal/7/09pdm, all animals of the groups immunized with AAV-HA/H3 and AAV-HA survived (Figure 27 A). In the group immunized with AAV-H3 still 40% of the animals (2/5) survived, but this was not significant compared to the control groups. The mean maximum weight loss of the AAV-HA and AAV-HA/H3 groups was significantly lower than for the control groups, but also for the AAV-H3 group, which is at a similar level as the control groups (Figure 28 A).

The same effect could be observed for the lung viral titers three days after infection (Figure 28 B). All surviving animals cleared the virus until the end of the infection period. Only one of the animals in the AAV-H3 group still had an elevated viral lung titer at the humane end point.

As mentioned above, in these groups additional animals also had been used for the PR8 infection, 10% of all animals in this part of the experiment (10 animals).

The total survival on the PR8 challenged group immunized with 2x AAV-HA was 85.7% (6/7), 75% in the 2x AAV-H3 group (6/8) and in the group 2x AAV-HA/H3 71.4% (5/7) (Figure 27 C), but all groups were not significant compared to the control groups.

The mean maximum weight loss did not show differences between the groups (Figure 28 C). The clinical scores did not differ significantly (Figure 29 B).

Lung virus titers at day three after infection did not differ between the groups (Figure 28 D). At the humane end point, animals of the immunization groups had significantly lower

lung virus titers than the control groups. By the end of the infection period, all surviving animals had cleared the virus.

After the X31 challenge (1.00×10^5 TCID₅₀/mouse), still 80% (4/5) protection was achieved in the group immunized with AAV-H3 (Figure 27 E), which was significant compared to the control groups ($p=0.0143$). The total antibody titer of the deceased animal of this group was at the same level as the mean titer of this group, not specifically low, so that other factors must have been involved which led to its high clinical score. The AAV-HA and AAV-HA/H3 groups had a 40% (2/5) survival rate.

The mean maximum weight loss was lower in the immunized groups and significantly reduced in the AAV-H3 group compared to the control groups (Figure 28 E). One animal did not lose weight. The mean maximum weight loss correlated with the total IgG titer in the serum ($r^2=0.5372$, $p<0.0001$). Clinical scores were significantly lower in all groups compared to the control groups (Figure 29 C).

The viral lung titers three days after infection in the AAV-HA/H3 and AAV-H3 groups were significantly reduced compared to the control groups, while the AAV-HA group had an equal titer level to the control groups (Figure 28 F). The one animal of the AAV-H3 group which reached the humane end point, had already cleared the virus from the lungs. In the AAV-HA/H3 group, only one animal still had a viral lung titer at the humane end point, while in the AAV-HA group three animals still had measurable virus titers in the lungs. All surviving animals cleared the virus from the lungs by day 14 after infection.

In summary, a high protective efficacy was achieved by AAV-HA/NP, AAV-HA, as well as WIV immunization against infection with homologous virus (Cal/7/09pdm). Only the animals immunized only once i.n. with AAV-HA/NP and the animals immunized only with AAV-H3 did not show significant protection after Cal/7/09pdm challenge, but only one mouse of the latter group still had detectable virus in the lungs at finalization. Clinical scores and mean maximum weight loss were lowest in the group primed and boosted with AAV-HA/NP.

In the groups challenged with heterologous PR8 virus after immunization, the group primed and boosted with AAV-HA/NP and the one immunized with WIV – AAV-HA/NP had a significantly higher survival rate compared to the control groups. No significant differences could be detected for the other parameters, i.e. weight loss, clinical scores and lung virus titers.

For the heterosubtypic challenge with the X31 virus, the groups primed and boosted with AAV-HA/NP, only primed with AAV-HA/NP and immunized twice with AAV-H3 had significantly elevated survival rates, with the highest rate of the three in the latter group. Clinical scores were reduced in all groups, except for the AAV-HA/NP i.n./s.c. immunized

group. However, there was no significance in viral lung titers or weight loss between all groups.

The only immunization group that demonstrated significant survival rates throughout all three challenges was the one primed and boosted with AAV-HA/NP.

4.2 SARS-CoV-2

In the following sections the results of the design process and immunogenicity evaluation of an AAV-vector vaccine carrying the S-RBD of SARS-CoV-2 are described. For this purpose, pAAV plasmids were constructed with the full-length S-protein and the S-RBD. The antigens were analyzed *in vitro* before conducting an initial immunogenicity evaluation in different mouse strains. Along the progression of the SARS-CoV-2 pandemic, AAV-S-RBD vectors were further constructed containing the S-RBDs of VOCs. Sera of immunized mice were analyzed regarding cross-reactivity between VOCs. Furthermore, neutralizing activity and FcγR-activating responses, as well as T-cell induction were analyzed.

4.2.1 Design and *in vitro* evaluation of AAV-S-RBD of SARS-CoV-2 wildtype and VOCs

This project started when SARS-CoV-2 was first described and no vaccine against COVID-19 was on the horizon.

Due to the successful results of AAV-vectors used as an influenza A virus vaccine, the assumption was made that this vector system could also be successfully utilized as a vaccine against SARS-CoV-2.

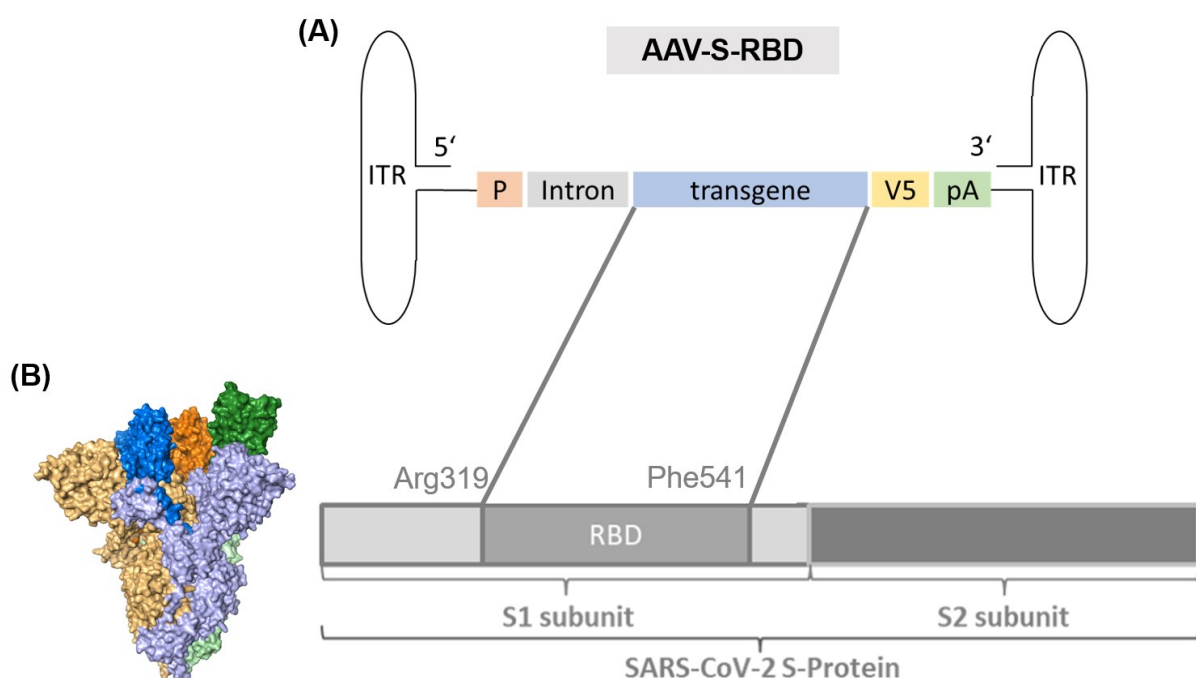


Figure 30: Design of the AAV-S-RBD vector

(A) Schematic representation of the AAV-S-RBD vector. The SARS-CoV-2 S-RBD between the amino acids 319 to 541 is inserted as the transgene (own illustration). **(B)** surface representation of the SARS-CoV-2 S-protein trimer, S-RBDs in brighter colors (PDB: 7DK3, own illustration generated in PyMOL).

The initial part of this project focuses on the design of a suitable AAV-vector. The main immunogen of SARS-CoV-2 is the spike protein containing the receptor-binding domain (S-RBD), which facilitates binding to the ACE2 receptor, making it the prime target of the antiviral immune response. Neutralizing antibodies directed against the S-RBD are able to inhibit binding of the virus to the target cells and thus, suppress infection. The majority of the vaccines manufactured against SARS-CoV-2 in response to the pandemic carry the gene of the whole S-protein.

In a study conducted following the SARS-CoV outbreak in 2002-2004, it was shown that an AAV-vector containing the S-RBD of SARS-CoV induced a potent neutralizing antibody response in BALB/c mice after i.m. application. The initial response could be boosted to a 5-fold higher level with two subsequent immunizations. Also, the antibody level increased until the end of the experiment after 5.5 months.

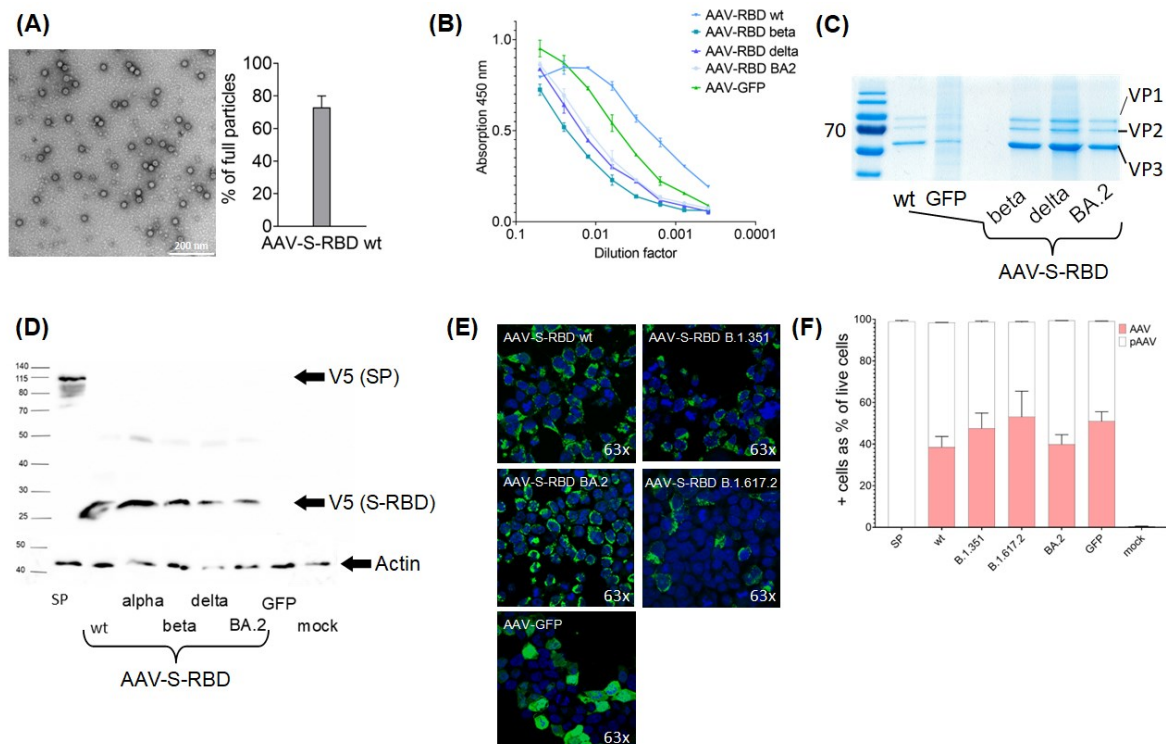


Figure 31: Quality control of the AAV-S-RBD vectors

(A) Electron micrographs of the AAV-S-RBD wt preparation were used to assess the proportion of full particles and impurities, displayed here for the AAV-S-RBD wt vector. **(B)** ADK9-ELISA of the AAV-S-RBD variant preparations (mean \pm SD of technical duplicates) **(C)** Coomassie staining of AAV-preparations separated by SDS-PAGE **(D)** Western Blot analysis of HEK293T-cell lysates transduced with AAV-vector preparations after 48h incubation **(E)** IF staining of HEK293T-cells transduced with AAV-vector preparations after 48h of incubation, V5-Tag was detected, no staining in the AAV-GFP cells, blue=DAPI, magnification as indicated **(F)** Quantification of V5-positive cells via flow cytometry (mean \pm SD of technical duplicates)

Here, the whole S-Protein of SARS-CoV-2 Wuhan-Hu1, as well as just the S-RBD (Arg319-Phe541) were initially cloned into AAV-vector plasmids (pAAV) to assess their functionality (Figure 30).

For both antigens, high transgene expression levels could be shown after transfection into HEK293T-cells. To further assess the functionality of the expressed proteins, an ACE2-binding assay was performed.

After successful verification of transgene expression, AAV-vectors were produced following the established protocol. Quality assessment of the AAV-vector stocks was performed, assessing the morphology, integrity, and purity via electron microscopy, an ADK9 ELISA and SDS-PAGE (Figure 31). The genome counts were titrated by qPCR and the transgene expression was verified by immunofluorescence staining and western blot analysis. The AAV-S-RBD preparations were found to have a high transduction efficiency *in vivo*, showing strong transgene expression in transduced cells. The plasmid containing the complete S-protein could not be successfully packaged into the AAV-vector particle (data not shown).

To overcome the limitation of the packaging size of AAV vectors at about 4.7 kb, the Dual-AAV approach was applied to be able to transduce the whole S-Protein (Ghosh et al. 2011; Trapani et al. 2014; Tornabene and Trapani 2020). In this approach, the expression cassette containing the Coding Sequence (CDS) is being split between two AAV-vector particles, with the promoter integrated in the vector with the 5'-sequence and the V5-tag and the pA-signal in the vector containing the 3'-sequence (Tornabene and Trapani 2020). Via the process of concatemerization both sequences are re-combined when both AAV-

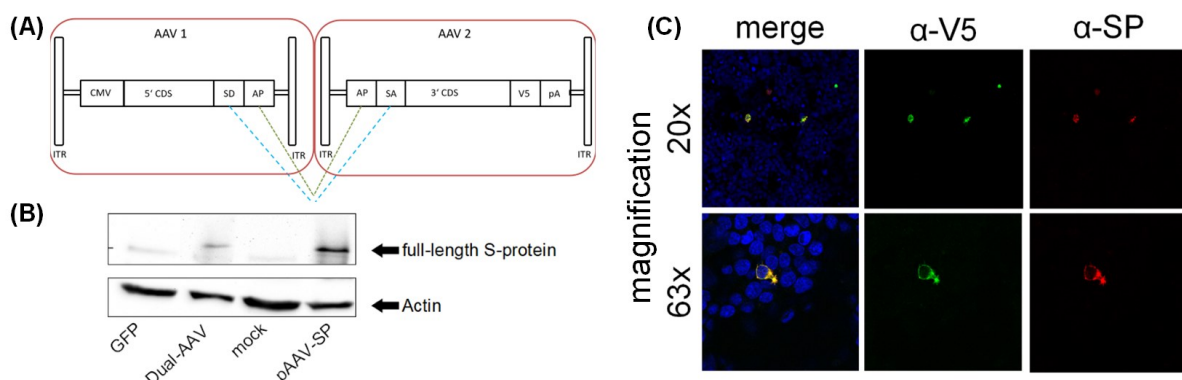


Figure 32: The Dual-AAV-vector system for the SARS-CoV-2 S-Protein

(A) Two separate AAV-vectors are generated, AAV1 containing the 5' and AAV2 the 3' end of the full sequence. The sequence is artificially split at the S1-S2-cleavage site and the AP gene, as well as an SD and SA sequence are added. Via the process of concatemerization, the complete protein will be expressed by the transduced cells. **(B)** Western Blot analysis with lysates of cells either transduced with the Dual-AAV-vectors at an MOI of 5 or transfected with the pAAV-SP plasmid or AAV-GFP as controls after 48h of incubation. **(C)** IF of cells transduced with the Dual-AAV-vectors at an MOI of 5 after 48h of incubation.

vectors transduce the same cell, and the complete gene is acquired through splicing (Tornabene and Trapani 2020). To optimize the recombination process, a highly recombinant region of the human placental alkaline phosphatase (AP) gene was inserted as a bridging sequence (Ghosh et al. 2011). For the splicing process, a Splicing Donor (SD) and Splicing Acceptor (SA) sequence are required (Tornabene and Trapani 2020). Here, the S-protein gene was artificially split at the cleavage site between the S1 and S2 subunits and cloned into the AAV-vector backbone, resulting in AAV-SP-1 (CMV-5'CDS (S1)-SD-AP) and AAV-SP-2 (AP-SA-3'CDS (S2)-V5-pA). A successful double-transduction should then result in a co-localization of S1-signal and V5 signal. However, after transduction, only few cells with the V5-signal could be detected after transduction with both vectors in the highest concentrations. Due to the low success rate the approach was not followed further and the project continued focusing on the development of the S-RBD constructs, for which production of AAV-vectors was successful, with a plasmid size of 5.5 kb.

Over the duration of the project, as the pandemic progressed, new variants of SARS-CoV-2 started to emerge. Along this process, the cDNA coding for the S-protein of the D614G variant, as well as for the S-RBDs of the Alpha-, Beta-, Delta- and BA.2-variants were also cloned into the AAV-vector plasmid.

After transfection of HEK293T-cells with the pAAV-S-RBD variant plasmids, equally high expression of the transgene could be observed. The functionality of the expressed transgenes was also assessed, by measuring the binding capacity to the ACE2-receptor compared to full length S-protein (Figure 33). For the full-length S-protein, the wildtype- and the D614G-variant were used. The D614G-variant has been found to have higher affinity for ACE2 (Hou et al. 2020; Korber et al. 2020; Volz et al. 2021). Here, the full-length D614G-variant S-protein showed the overall highest binding capacity to ACE2 (Figure 33 A). Binding is significantly enhanced compared to the wildtype S-protein. For the expressed S-RBD variants, binding was verified, but was much lower than for the full-length S-protein. There were no large differences in binding capacity between the different S-RBDs. The reduced binding capacity in comparison to full-length constructs is most likely due to the fact, that the S-RBD molecules do not trimerize when they are expressed individually.

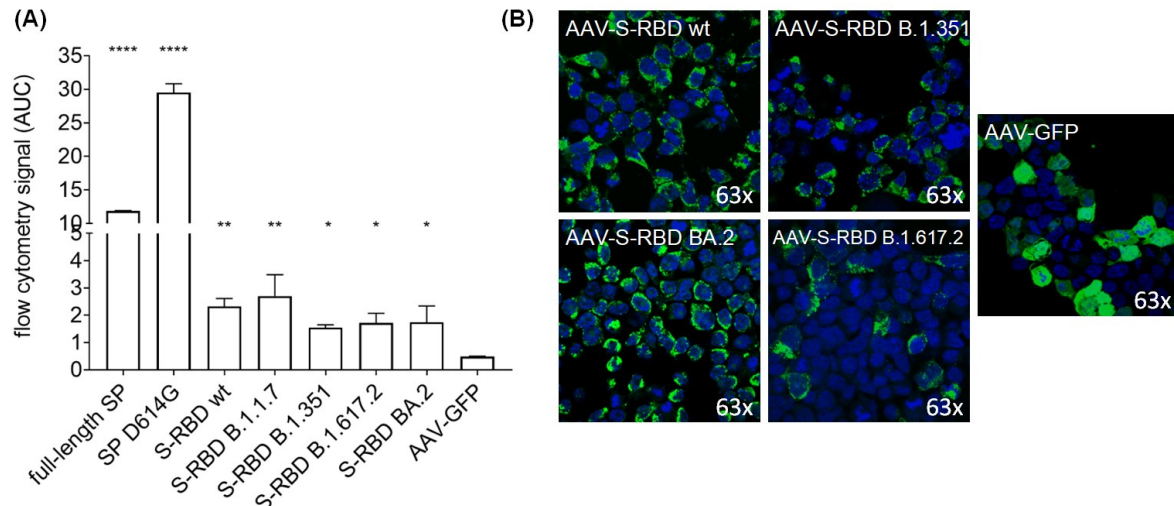


Figure 33: Receptor-binding domain variant proteins demonstrated binding to ACE2 *in vitro*

(A) ACE2 binding assay results: cell lysates were prepared of HEK293T cells transfected with 2.5 μg DNA/ 1×10^6 cells of the pAAV plasmids coding for the indicated full-length S-protein, full-length S-protein with the D614G mutation, or the S-RBD variant constructs. Those lysates were incubated with HT1080+ACE2 cells for the S-protein or S-RBDs to bind. The V5-tag was labelled, and the signal was measured via flow cytometry; the signal was gated as the proportion of positive cells within live cells, bars: mean \pm SD, $n=2$ in technical duplicates (* $p < 0.05$, ** $p < 0.01$, *** $p < 0.001$, **** $p < 0.0001$, compared to AAV-GFP). **(B)** IF staining of HEK293T-cells transduced with indicated AAV-vectors after 48h, staining for V5-Tag, AAV-GFP transduced cells were not stained (blue=DAPI).

4.2.2 AAV-S-RBD immunization results in different patterns of titer development in different mouse strains

After the promising *in vitro* evaluation of the AAV-S-RBD vectors, the *in vivo* immunogenicity was explored as well in a pilot experiment.

Initially, immunogenicity was compared in three different mouse strains – NMRI, BALB/c and C57BL/6J, to assess differences in the immune response, as the strains differ in their immunological properties (Figure 34).

For this initial evaluation, two mice were used per strain and per application route. They were immunized six times, over a period of 6.5 months, with 10^{11} viral genomes per dose. Interestingly, the titer development differed greatly between the mouse strains.

Antibody titers were measured with the multiplex serological assay against the SARS-CoV-2 S1-domain of the spike protein (carried out by the ZBS 3 unit of the RKI). The NMRI mice developed the highest titers against the S1-domain of SARS-CoV-2 spike protein (Figure 34 A) But they also showed a high difference between the two animals receiving the vaccine via the same application route. One animal of each pair had the highest titer, while the other animal only developed a titer 1.8x (i.n.) or 2.8x (s.c.) lower. This trend was consistent over the entire immunization period.

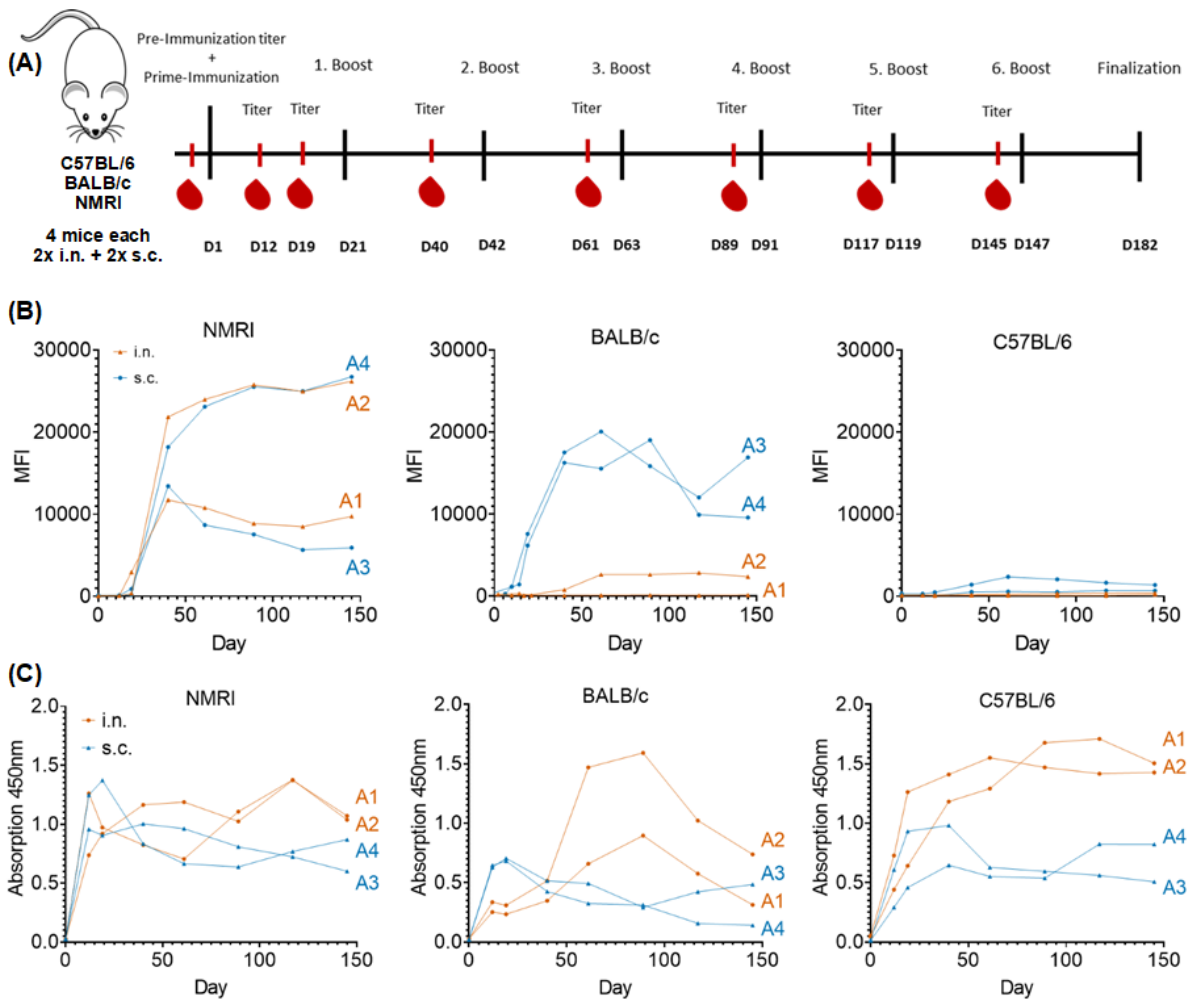


Figure 34: Immunogenicity of the AAV-S-RBD vector varied in different mouse strains

(A) Immunization schedule: Two mice of each specified strain were immunized repeatedly with the AAV-S-RBD vector (10^{11} vg/dose), and blood was taken at the indicated time points. **(B)** Serum signals from immunized mice as results of the multiplex serological assay from the 3 different mouse strains against SARS-CoV-2 S1 (assay carried out by the ZBS3 unit of the RKI). Displayed here are raw data from the analysis. Serum dilutions: **NMRI**:1:1,000, **BALB/c**: 1:1,000, **C57BL/6**: 1:100, A1-A4 = animals 1-4 **(C)** ELISA titers of AAV9-specific antibodies; serum dilutions 1:100,000

In contrast, the two BALB/c mice immunized subcutaneously both developed high titers, while those were still 1.5x lower than the highest titers in the NMRI mice (Figure 34 A). One of the intranasally immunized BALB/c mice developed titers 7x lower than the titers of the BALB/c mice that were immunized subcutaneously, while the other one developed titers only slightly above the pre-immunization titers.

The C57BL/6 developed the lowest titers (Figure 34 A). They only went slightly above the pre-immunization titers, with the titers of the subcutaneously immunized animals being 5x higher than the ones of the intranasally immunized animals.

Anti-AAV9-vector antibody titers developed in all mouse strains (Figure 34 B). While those developed equally in all NMRI mice, the i.n. immunized BALB/c and C57BL/6 mice

developed higher levels than the s.c. immunized animals. This result implies that in BALB/c and C57BL/6 mice, neutralization of AAV-vectors occurs after s.c. application, but not after i.n. application, as it was previously shown (Gao et al. 2004; Limberis and Wilson 2006; Boutin et al. 2010; Demminger et al. 2020).

Neutralizing activity of the antibodies was measured 1) via SARS-CoV-2 Surrogate Virus Neutralization Test (sVNT, by GenScript) and 2) via PRNT assay using live virus. The sVNT assay was an ELISA assay based on the interaction of an HRP-conjugated recombinant wildtype SARS-CoV-2 RBD (HRP-RBD) with hACE2. Sera were incubated with the HRP-RBD and added to an ELISA plate coated with hACE2. The signal was determined by the

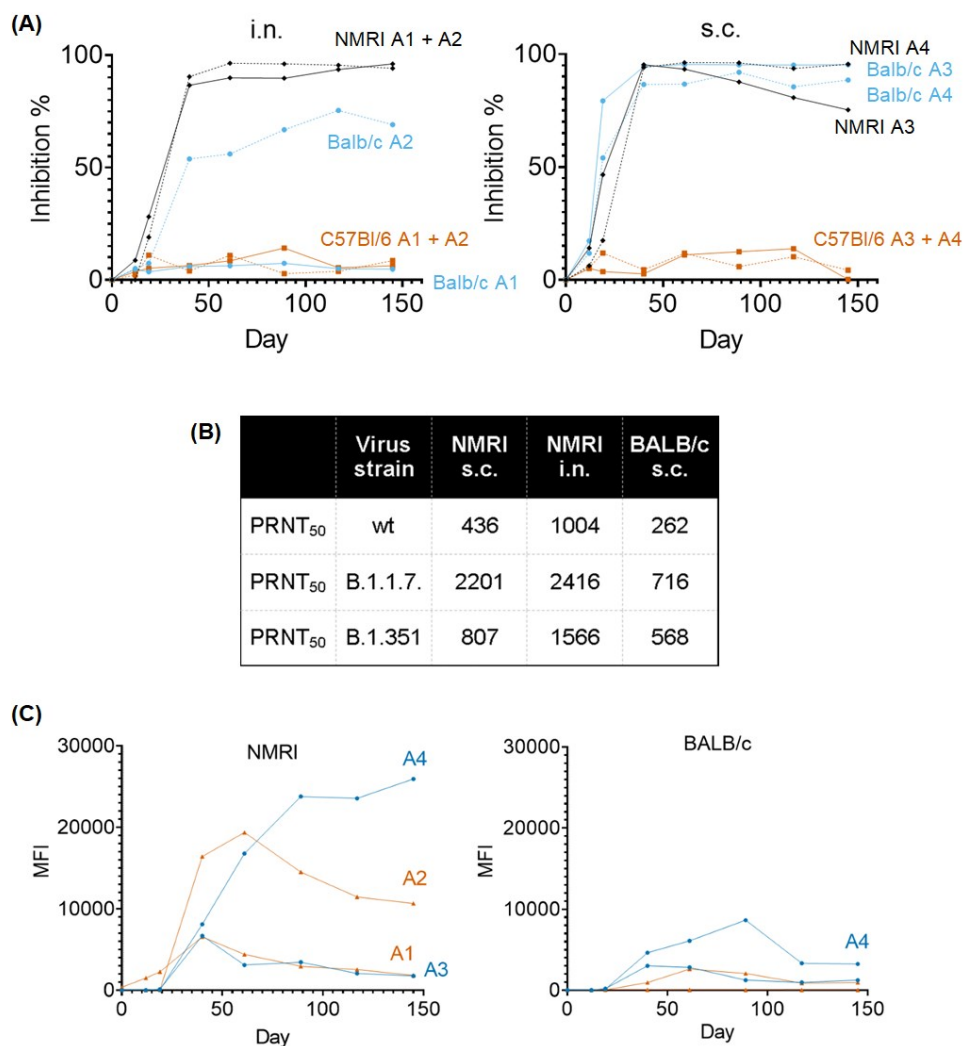


Figure 35: Antibodies induced after immunization with the AAV-S-RBD wt vector showed neutralizing activity against SARS-CoV-2

(A) Results of the SARS-CoV-2 Surrogate Virus Neutralization Test (sVNT) Kit (GenScript); NMRI: all positive from day 12, BALB/c: s.c.: positive from day 12; i.n.: A2 positive from day 19; A1 negative, C57BL/6: all negative. (B) PRNT-results; Pooled final sera were added to the virus in 2-fold dilutions in technical duplicates (mean \pm SD). PRNT₅₀ values were calculated via non-linear regression analysis. (C) Serum signals from immunized mice as results of the multiplex serological assay from the 3 different mouse strains against SARS-CoV S1. Displayed here are raw data from the analysis. Serum dilutions: 1:100.

amount of HRP-RBD molecules bound to the hACE2 compared to a no-antibody control, resulting in the neutralizing capacity of the sera. Here, sera of NMRI mice and s.c. immunized BALB/c mice showed neutralizing activity from day 12 of the immunization schedule onwards, while the sera of only one i.n. immunized BALB/c mouse demonstrated neutralizing activity from day 19 onwards, and the sera of the other animal did not (Figure 35 A). In the PRNT assay, where live virus was incubated with the sera followed by a plaque titration, the sera demonstrated neutralizing activity not only against the wildtype strain, but also against the B.1.1.7 and B.1.351 variants (Figure 35 B).

NMRI and BALB/c mice also showed reactivity against the S1-domain of SARS-CoV in the multiplex serological assay (carried out by the ZBS 3 unit of the RKI), but reactivity of the NMRI mice was higher than of the BALB/c mice (Figure 35 C). This leads to the conclusion that the domains leading to cross-reactivity between SARS-CoV-2 and SARS-CoV in the S-RBD-domain of the spike protein are not immunodominant in the immune response mounted in BALB/c mice, but they are in NMRI mice, which can react to a broader set of antigens.

From these initial results it can be concluded, that the AAV-S-RBD vector possesses the ability to induce a humoral immune response against the S-RBD of SARS-CoV-2. However, C57BL/6 mice appear not to be a suitable model strain to analyse the immunization properties of the vaccine. Furthermore, the presentation of titer development indicates that not every individual animal reacts equally strong to the vaccine. In BALB/c mice, subcutaneous application of the vaccine seems to be more promising than intranasal application.

Overall, these results strongly suggest including different mouse strains in the evaluation of the immune response towards a novel vaccine candidate, as well as utilize different immunization routes in those strains, as the responses differ between strains and immunization routes, so that results could potentially be skewed if these parameters are not assessed.

To further explore the immunization properties of the vaccine, the immunogenicity evaluation was continued in a representative group size of BALB/c mice, as this mouse strain seemed to develop the most consistent antibody response and was also capable of developing antibodies with neutralizing activity (Figure 36). The immunization schedule was adjusted to a prime-boost-boost scheme, to represent a more realistic schedule. Also, in the previous experiment the development of total IgG titers and neutralizing titers did not show substantial changes after the second booster dose.

Here, the titers of the individual groups did not differ from each other (Figure 36 A). There was also no neutralizing activity detected (data not shown). When compared in an ELISA measurement to the sera of the previous experiment, the titers compared to the level of the C57BL/6 mice and the one BALB/c mouse which developed the lowest titer (data not shown). Anti-AAV-vector antibodies developed quickly and resulted in high titers in all groups (Figure 36 B). These results were unexpected, because the same AAV-S-RBD

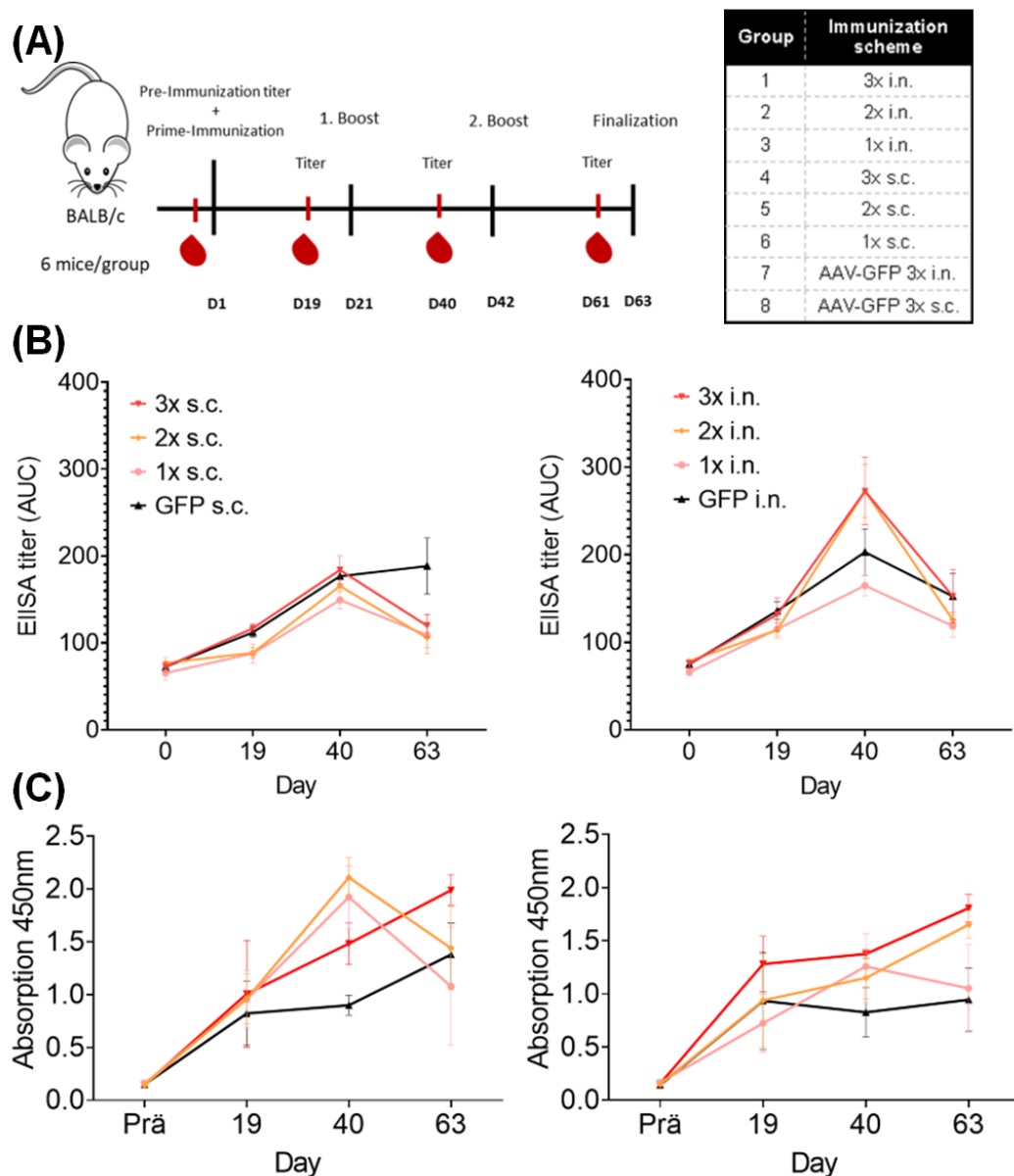


Figure 36: *In vivo* immunogenicity evaluation of varying immunization schemes with the AAV-S-RBD wt vector in BALB/c mice did not result in antibody induction

(A) Immunization schedule: Groups of six mice were immunized following the schedule outlined in the table. Blood was taken at the indicated time points. Mice immunized with AAV-GFP served as control groups. **(B)** ELISA titers displayed as AUC against the SARS-CoV-2 S1-domain, left: i.n. immunizations, right: s.c. immunizations (mean \pm SEM of individual mice, $n=6$ in technical duplicates). **(C)** ELISA titers of AAV9-specific antibodies; serum dilutions 1:10,000 (mean \pm SD of individual animals, $n=6$ in technical duplicates)

preparation was used as in the previous experiment, which displayed a good *in vitro* quality and efficiency, and the same methods were used to immunize the mice.

4.2.3 Immunogenicity of AAV-S-RBD with variant receptor-binding domains

As the NMRI mice previously developed the overall highest titers, the immunogenicity of the variant AAV-S-RBD vectors was evaluated in this mouse strain. AAV-vectors expressing the S-RBDs of the SARS-CoV-2 wt, Beta, Delta and BA.2 variants were used (Figure 37). Mice were immunized twice, first subcutaneously and three weeks later boosted intranasally with the same antigen. One group received a mix of all variant AAV-S-RBD vectors. As controls, one group received AAV-GFP and another group PBS.

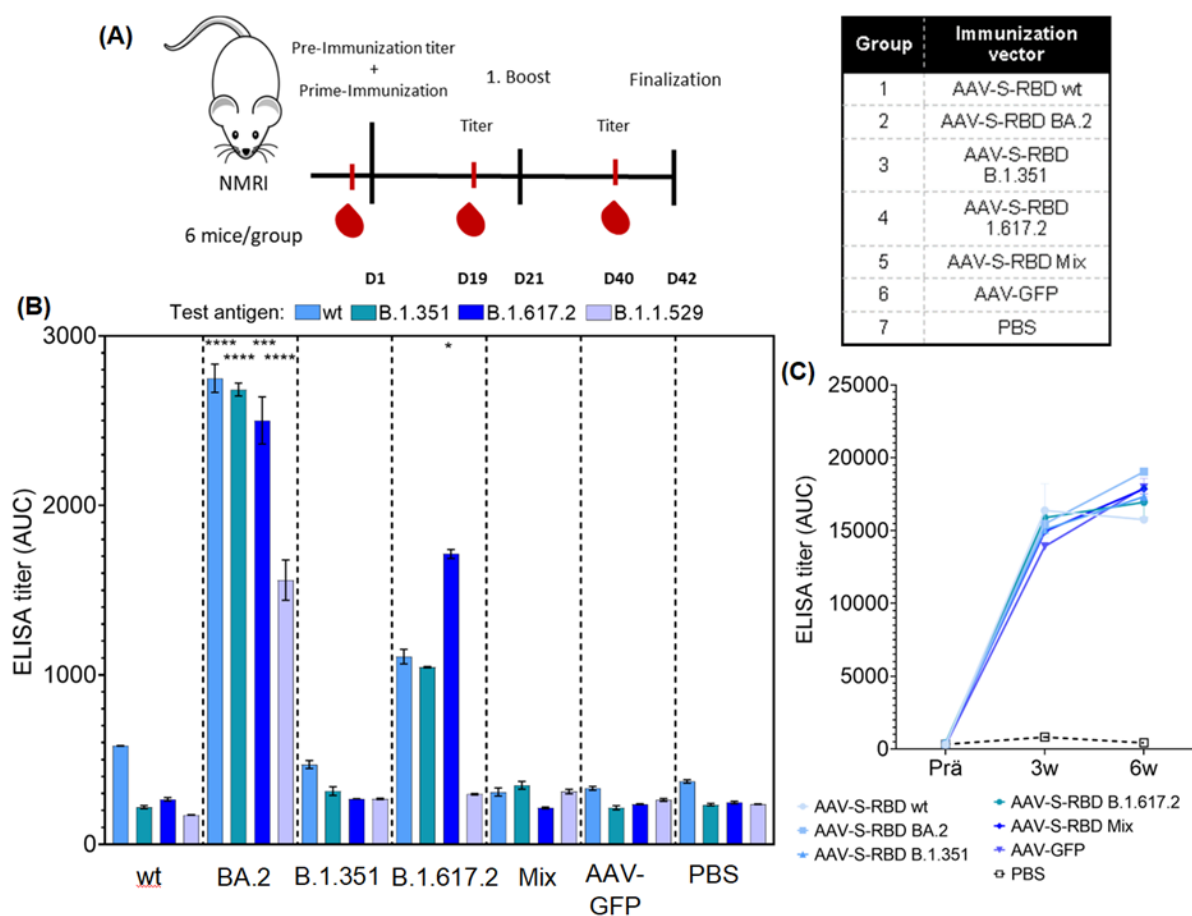


Figure 37: Immunization with the AAV-S-RBD BA.2 vector resulted in strong antibody titers against SARS-CoV-2 wt, Beta, Delta and BA.1 variants

(A) Immunization schedule: Groups of six NMRI mice were immunized according to the table. Mice were primed s.c. and boosted i.n. Blood was taken at the indicated time points.

(B) ELISA titers of IgG antibodies as AUC of the immunization groups as indicated below the columns against the specified test antigens (on top of the graph) (bars: mean of n=6 individual animals \pm SD of technical duplicates) (C) ELISA titers as AUC of AAV9-specific antibodies in pooled sera (mean \pm SD of technical duplicates)

(* $p < 0.05$, ** $p < 0.01$, *** $p < 0.001$, **** $p < 0.0001$, compared to control groups)

The sera were tested in ELISA analyses against the S1-domains of the wt, Beta, Delta and B.1.1.529 (BA.1) strains. At the time the experiment was conducted, an appropriate test antigen representing the BA.2 strain was not yet accessible, which is why the BA.1 test antigen was used in the following evaluations, as they are evolutionary close. This antigen contained the following shared mutations in the S-RBD: G339D, S373P, S375F, K417N, N440K, S477N, T478K, E484A, Q493R, Q498R, N501Y. Furthermore, it contained the following unique BA.1 mutations: S371L, G446S, G496S, Y505H.

The AAV-S-RBD of BA.2 showed the overall highest immunogenicity (Figure 37 A). The antibody titers were significantly elevated against all antigens compared to the other immunization groups. Only the group immunized with the Delta S-RBD showed equally high levels to BA.2 immunization against the Delta S1-antigen. In that group, antibody titers against the Delta-antigen were also significantly elevated compared to all other immunization groups. Within all immunization groups, titers against the different antigens did not differ significantly. Unexpectedly, the group immunized with the mix of all AAV-S-RBD variant vectors did not develop antibody titers against any of the antigens. Anti-AAV9 vector antibody rose steeply within the first three weeks and remained on that high level until the end of the experiment (Figure 37 B).

4.2.4 Mucosal antibody response to the AAV-S-RBD vaccine in lung homogenates and nasal washes

The mucosal response of the NMRI mice against the variant AAV-S-RBD vectors was measured via an ELISA assay in lung homogenates and nasal washes at day 42 of the experiment when the experiment was finalized. The plates were coated with test antigen and the material obtained after the nasal washes and the lung homogenates of the individual mice were applied in twofold dilutions and detected with an HRP-coupled IgA antibody. This did not result in strong signals. There was a strong background signal from the control groups, which also differed between the two control groups (Figure 38). Only the Beta-immunized group showed a significantly elevated signal compared to all other groups in the nasal washes against the wildtype antigen (Figure 38 A).

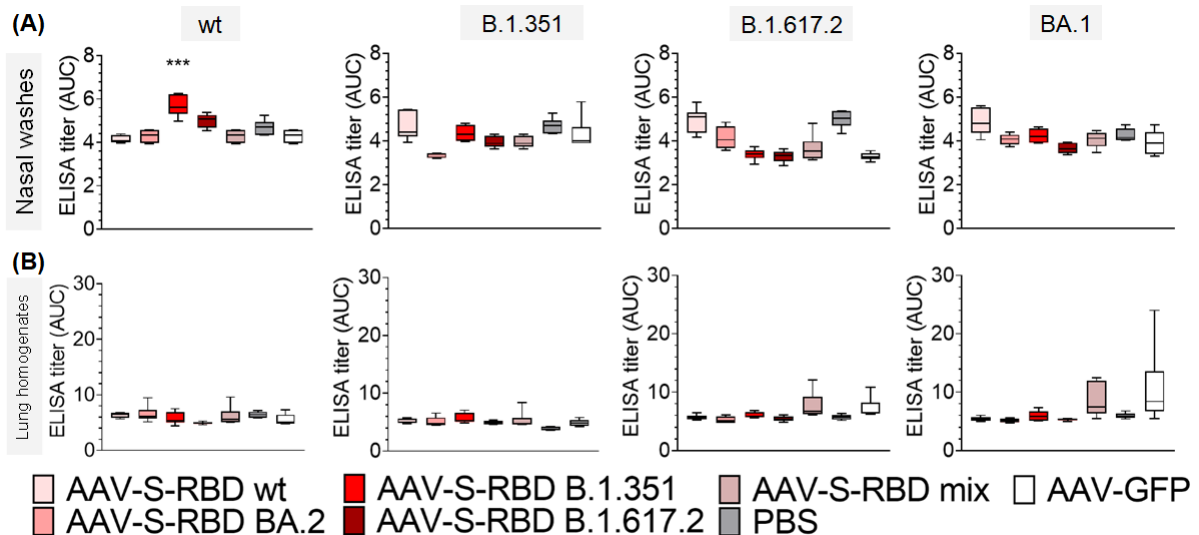


Figure 38: No mucosal antibody responses to immunization with the AAV-S-RBD variant vaccines could be detected

(A) IgA ELISA titers displayed as AUC in the nasal washes of immunized mice at the end of the immunization period, ELISA test-antigens were the S1-domains of the specified virus strains (box plots with 5-95 percentile of $n=6$ individual mice in technical duplicates). (B) IgA ELISA titers displayed as AUC in the lung homogenates of immunized mice at the end of the immunization period, ELISA test-antigens were the S1-domains of the specified virus strains (box plots with 5-95 percentile of $n=6$ individual mice in technical duplicates). (* $p<0.05$, ** $p<0.01$, *** $p<0.001$, **** $p<0.0001$, compared to control groups)

4.2.5 Immunization with AAV-S-RBD BA.2 results in broadly reactive FcγRI-activating responses

An FcγR-assay was performed with the pooled final sera of the immunized NMRI mice against the same antigens as the antibody ELISAs: the S1-domains of wt, Beta, Delta and BA.1. Against IAV, AAV-vector immunization has shown to induce non-neutralizing antibodies capable of activating broadly-reactive FcγR effector functions in previous studies (Demming et al. 2020). Such broadly reactive FcγR-activation after AAV-immunization against IAV could also be shown in this thesis (Figure 22). Thus, the FcγR-activation was also evaluated for the sera of the mice immunized with AAV-S-RBD variant vectors in the NMRI mice to assess possible effector functions against the immunization antigens and cross-variant effects.

For this purpose, ELISA plates were coated with the test antigens, which then were incubated with the pooled final sera of the mice in the different immunization groups, followed by incubation with the FcγR reporter cells, which produced IL-2 after activation. The IL-2 signal was then measured in a subsequent ELISA.

The sera of the AAV-BA.2 group induced the strongest FcγR-activating response (Figure 39 B). Interestingly, this group did not develop FcγR-titers against the BA.1 S1-antigen. However, FcγRI levels against the other antigens were significantly elevated, while the

titers against wt and Delta were equally high and against Beta was still significant, but lower than the former two. Also, FcγRIIb levels against the Delta variant and FcγRIII levels against the wt variant were slightly but significantly elevated in this group.

The group which had been immunized with AAV-S-RBD of Delta, even though there were elevated IgG titers, did not induce an FcγR-response (Figure 39 D).

In the AAV-S-RBD Beta group, the FcγRIV against the wildtype antigen was elevated.

Overall, there was a strong correlation between total ELISA titers and FcγRI ($r^2=0.8779$, $p<0.0001$) and FcγRIII ($r^2=0.6963$, $p=0.0002$) for the response against the wildtype virus.

The FcγRI responses also strongly correlated with the total IgG titers against the Beta ($r^2=0.8261$, $p<0.0001$), Delta ($r^2=0.7144$, $p=0.0001$) antigen.

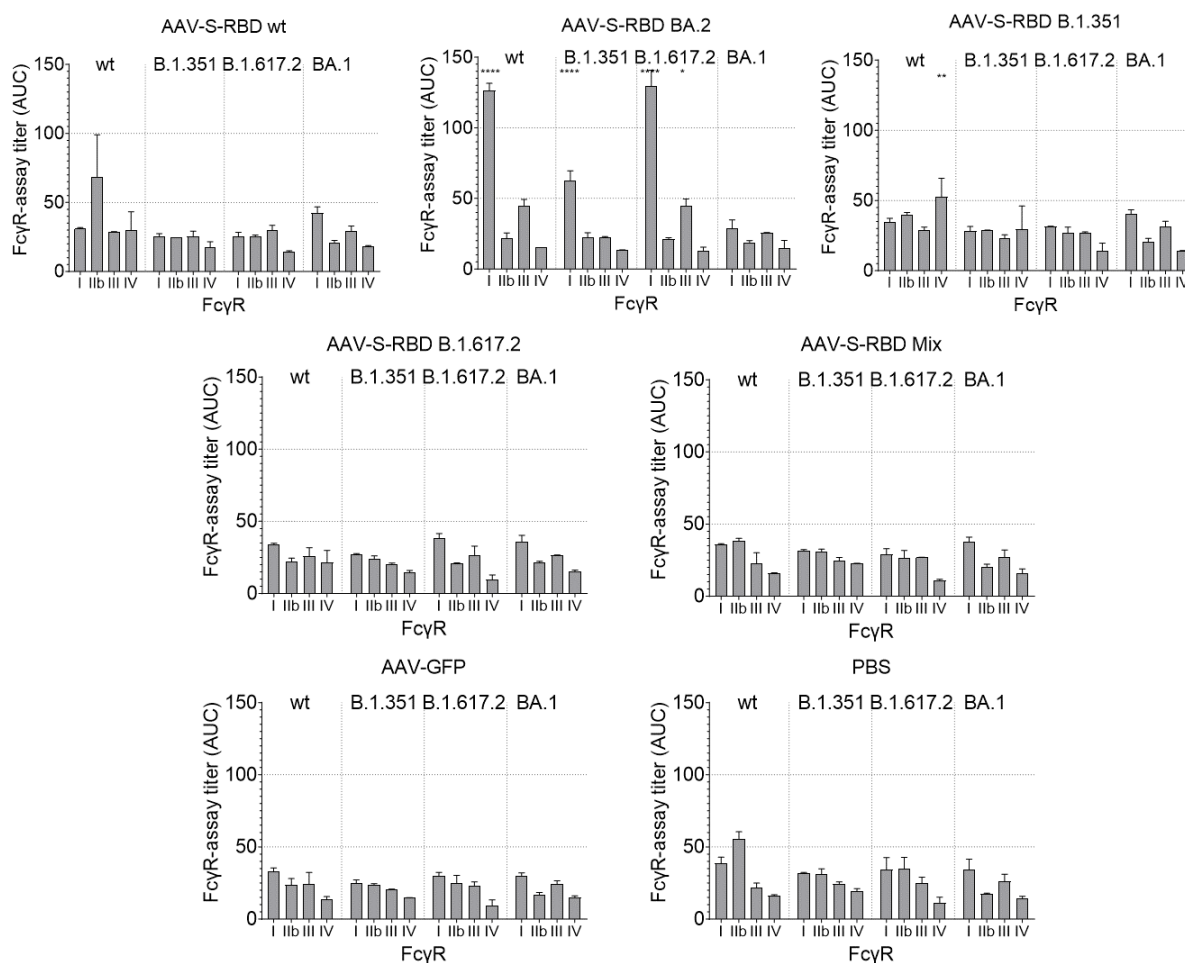


Figure 39: Immunization with the AAV-S-RBD BA.2 vector resulted in strong FcγRI-activating responses against wt, Beta and Delta S1-domain, but not against BA.1

Activation of murine FcγRI, -IIb, -III and -IV by IgG antibodies specific for the indicated test antigens (within panels) in pooled pre-challenge sera of the indicated immunization groups (above panels); mean \pm SD of technical replicates, $n=2$; * $p<0.05$, ** $p<0.01$, *** $p<0.001$, **** $p<0.0001$, compared to control groups

4.2.6 Neutralizing titers of variant AAV-S-RBDs

To assess neutralizing titers of the sera for immunized NMRI mice, a plaque reduction neutralization test (PRNT) was performed. Only the group immunized with BA.2 showed neutralizing activity (Figure 40). Interestingly, neutralization was only detectable against BA.1, BA.2 and BA.5 strains. None of the other variant strains that were tested (wt, Alpha, Beta, Delta) was neutralized.

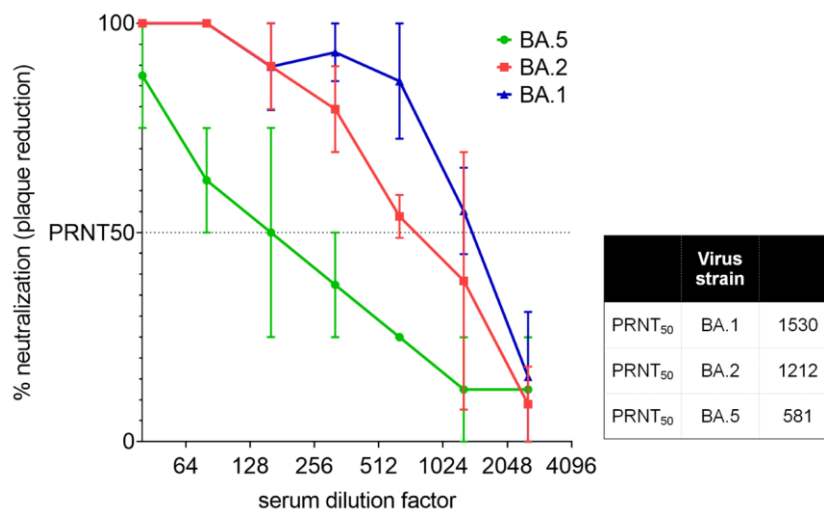


Figure 40: Immunization with AAV-S-RBD BA.2 resulted in neutralizing titers against SARS-CoV-2 Omicron BA.1, BA.2 and BA.5 variants, but not against others

Pooled sera were analyzed in technical duplicates against the indicated virus strains; results are displayed as % of plaque reduction compared to the virus control (mean \pm SEM). PRNT₅₀ values were calculated via linear regression analysis.

4.2.7 T-cell responses against SARS-CoV-2 wildtype and different variant receptor-binding domains

Antigen-specific CD4⁺ and CD8⁺ T-cells were measured with intracellular cytokine staining in the BALB/c mice immunized with the wt AAV-S-RBD vector (described in Figure 36) and the NMRI mice immunized with the wt and variant AAV-S-RBD vectors (described in Figure 37).

Overall, the background signal of the control groups was rather strong in this analysis, and the number of potential antigen-specific T-cells was low.

In the BALB/c experiment, no significant results could be obtained, but a tendency could be observed for higher T-cell induction in the s.c. immunized groups (Figure 41 I + J).

In the NMRI experiment, which also evaluated the VOC S-RBDs, also no significant results could be obtained, as the number of detected T-cells was very low (Figure 41 A-H).

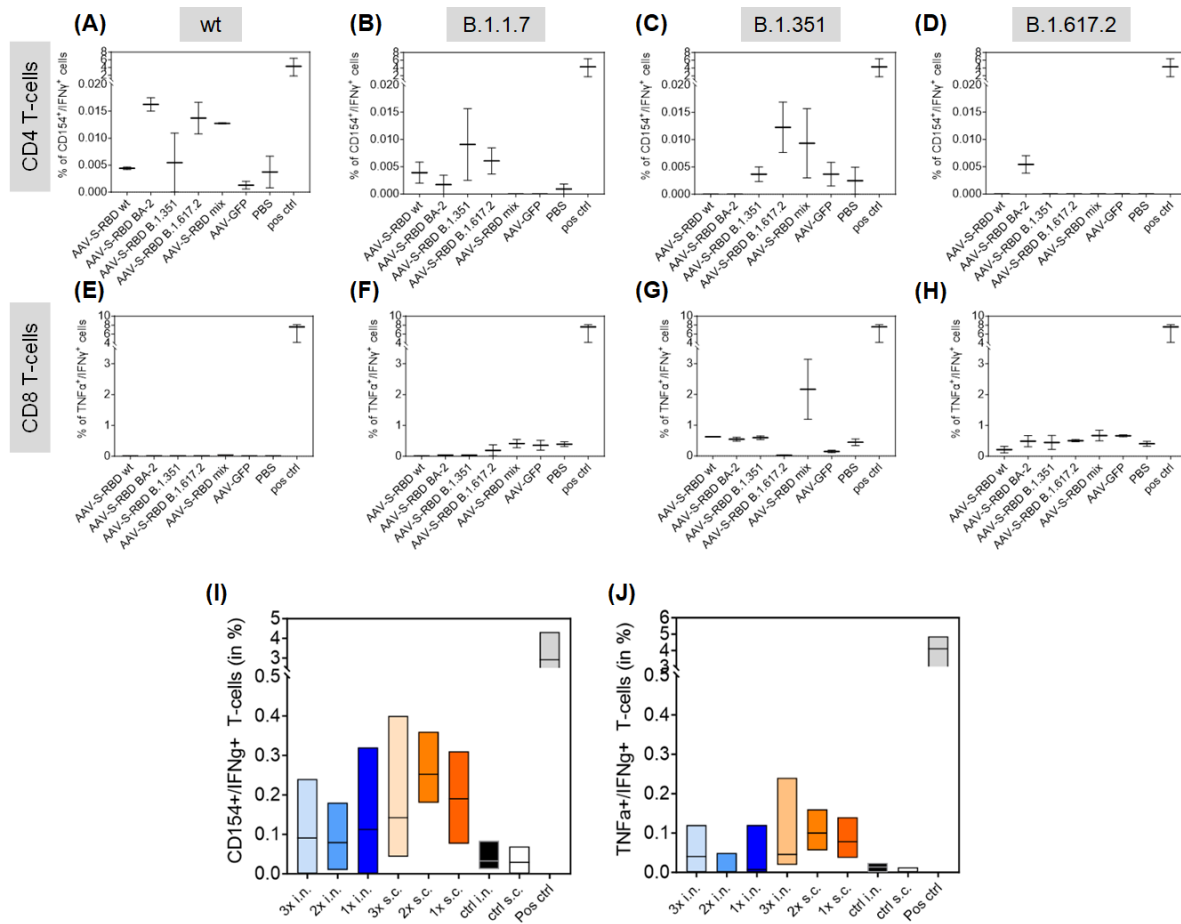


Figure 41: No antigen-specific T-cells were detected after immunization with the AAV-S-RBD wt and variant vectors

Antigen-specific T-cells were measured with intracellular cytokine staining. Isolated spleen cells were stimulated with peptide pools of SARS-CoV-2 S1 of the indicated VOCs, stained and measured with flow cytometry. By staining, CD4 and CD8 T-cells were separated. For CD4 T-cells double positive cells for CD154 and IFN γ were counted as positive cells and for CD8 T-cells double positive cells for TNF α and IFN γ . Single mouse spleens were analysed (n=6) in technical duplicates. Gating strategy in Figure 43.

(A) – (D): CD4⁺ T-cells and (E) – (H) CD8⁺ T-cells of NMRI mice immunized with AAV-S-RBD VOCs, immunization groups are indicated below each panel and test antigens are indicated above each panel. Box and whiskers are displayed with the 5-95 percentile.

(I) CD4⁺ T-cells and (J) CD8⁺ T-cells of BALB/c mice immunized with AAV-S-RBD wt. Immunization groups are indicated below each panel. The test antigen was the SARS-CoV-2 S1 domain of the wt virus. Bars show minimum to maximum with line at median.

5 Discussion

Influenza A viruses and SARS-CoV-2 both continue to be a severe threat to public health. Even though the Public Health Emergency of International Concern (PHEIC) has been terminated for SARS-CoV-2 in May 2023, the virus continues to circulate worldwide in the human population. The pandemic has led to a loss in life expectancy around the world (Scholey et al. 2022) and continues to cause prolonged symptoms and new-onset disabilities following recovery from acute infection (Kroonstrom et al. 2022; Lau et al. 2022; Davis et al. 2023; WHO 2023d).

Both viruses pose a threat for the emergence of new pandemics as they are continuously present and evolving at the human-animal interface.

Non-pharmaceutical interventions can help to mitigate the danger of infection throughout the population, but in order to be effective, they need to be applied correctly and strictly reinforced. This is challenging, especially over a long period of time. Therefore, pharmaceutical interventions are needed, preferably focusing on the prophylaxis of infection.

Currently, vaccination is one of the major tools to lower the impact of both viral infections. For IAV, there has been a long history and experience with vaccines, but still there is no universal vaccine. The current vaccines need to be reformulated and repeatedly administered seasonally, due to the variable viral surface glycoprotein HA. Due to this variability, there is always the chance of mismatch between the vaccine strain and the circulating strain.

For SARS-CoV-2, a lot of research has been conducted since the start of the pandemic and vaccines have been designed and produced in record time. The virus also continues to evolve, and the emerging variants continue to evade immunity. A 4.93-fold lower mutation rate has been estimated for SARS-CoV-2 compared to IAV in the human population, while it has been found to be much lower in cell culture (23.9-fold), which could be due to its wide spread, longer infection period, higher replication numbers and immune pressure (Kawasaki et al. 2023). Vaccines were a valuable tool to decrease severe disease and death, especially in the elderly, but they cannot fully prevent the long-term effects infection can induce.

For both viruses, the goal for the development of vaccines is the reduction of severe disease and long-term effects, protection against viral variants, durable protection over a long time span, suitability for different age groups and reasonable production, storage and handling conditions. Current analyses of SARS-CoV-2 vaccines mostly focus on the induction of neutralizing antibodies and how well they hold up against disease triggered by newly emerging variants.

Both pathogens enter the body via the respiratory tract. Seasonal IAV mostly causes respiratory disease, which can progress to severe courses including symptoms like myocarditis or encephalitis and resulting in death, especially in the vulnerable members of the population (WHO 2023b). SARS-CoV-2 is by now known to cause severe vascular (Xie et al. 2022) and immunological pathology (Merad et al. 2022), resulting in an increased risk for thrombosis, heart attacks and strokes, neurodegenerative diseases, and autoimmune disorders like new-onset type-I diabetes (Chourasia et al. 2023).

The development of mucosal vaccines has been discussed and pushed forward for both viruses, taking into account the infection route. With a potent mucosal immunity, consisting of secretory IgA and tissue-resident T-cells, the infection could be stopped before it establishes in the respiratory tract (Lavelle and Ward 2022).

Additionally, for both viruses FcγR-effector functions have been identified as an important factor in the context of vaccine design for a broadly reactive immune response (Jegaskanda 2018; Zhang et al. 2022).

To achieve the abovementioned goals for the development of vaccines, different delivery platforms and immunogenic antigens are evaluated.

One of those alternative delivery platforms are viral vectors. Viral vectors mimic natural infection and use the host cell machinery to produce the vaccine antigens. In this way, viral vectors have an advantage over inactivated vaccines because they can trigger strong T- and B-cell responses. Downsides are the difficult production process and pre-existing immunity towards the viral vector.

The here utilized AAV-vectors have shown to be a safe and efficacious vector system to be used as a vaccine against IAV, as well as SARS-CoV-2, while, due to organizational reasons, only for IAV a challenge experiment could be conducted.

5.1 Influenza A

Against IAV, AAV-vectors have shown to be a promising vaccine vehicle to induce broadly reactive immune responses by delivering certain viral antigens (Sipo et al. 2011; Fiddeke 2016; Demminger et al. 2020). The HA of A/California/7/2009pdm has been shown to induce strain-specific neutralizing antibodies in the mouse model, but also non-neutralizing antibodies against group 1 HAs that showed activation of FcγR-functions (Demminger et al. 2020). The NP induced broadly reactive responses, covering group 1 and 2 IAVs (Demminger et al. 2020). Those antibodies also induced FcγR-activation (Demminger et al. 2020). The responses towards AAV-HA and AAV-NP were able to protect mice from homologous and heterologous challenge (Demminger et al. 2020).

In this thesis, the combination of these antigens was thus evaluated for potential synergetic effects. Also, different prime-boost schemes were evaluated including immunization with

and comparison to a WIV-vaccine, to assess if the AAV-vector vaccine could induce a more potent and broader immunity after the prime-immunization than WIV, and if, in this way, it could have a similar priming-effect as a natural influenza infection. A single-shot immunization scheme was also included in the analysis, as AAV-vectors have shown to display a self-boosting effect and to circumvent the anti-vector immunity, this could be beneficial for future applications. Furthermore, for the first time, the immunogenicity parameters of an AAV-vector vaccine carrying the HA of the group 2 H3N2 virus A/Aichi/2/68 were evaluated, and, in combination with the H1 HA, the potential expansion of the immune response to also include groups 2 HAs was assessed.

5.1.1 Antigenes, vectors, mouse model and application routes

The HA and NP antigens, as well as the WIV preparation used in this thesis are based on the A/California/07/2009pdm (H1N1) (Cal/7/09pdm) virus, which caused the IAV pandemic in 2009. It was included in the vaccine formulations up until the 2016/17 season (PEI 2023). As the representative of the group 2 HAs, the H3 of the A/Aichi/2/68 (H3N2) virus was used, which had been isolated during the 1968 IAV pandemic.

The H1N1-vectors had been constructed during work leading up to this thesis and had also been evaluated in previous studies at the RKI (Sipo et al. 2011; Fiddeke 2016; Demminger et al. 2020), however, the AAV-H3 vector had only been evaluated *in vitro* so far.

As described above, Demminger et al. (2020) demonstrated in C57BL/6 mice that immunization with AAV-HA resulted in a group-specific antibody response, while AAV-NP and WIV i.n. immunization induced antibodies directed against viruses of both HA-groups. Immunization with WIV, however, resulted in lower titers than immunization with AAV-NP. This effect of i.n. WIV immunization is consistent with previous findings (Dong et al. 2018; Bhide et al. 2019). Comparison to the i.m. route showed that the latter resulted in strongly elevated antibody titers against homologous virus, which, in contrast to i.n. immunization, also recognized HA1 and NP and showed HAI⁺ and MN⁺ activity (Demminger et al. 2020). These differences strongly indicate that the immunization route is crucial for the outcome of vaccination.

Thus, in this thesis WIV was applied intramuscularly, as this is the way in which inactivated vaccines are usually applied and the differences in immunization outcomes between the AAV-vector based vaccines and WIV can be demonstrated more realistically.

The AAV-vectored vaccines, on the other hand, showed a preferable outcome after i.n. vaccination (Demminger 2019). Opposed to WIV immunization, mice vaccinated intranasally with AAV-HA were protected against infection with heterologous virus, which was thought to be due to the FcγR-activating antibodies, which the animals immunized with WIV did not have. AAV-NP immunization was also able to protect mice against homologous

and heterologous challenge, despite the lack of neutralizing antibodies. Those antibodies also displayed the ability to activate FcγR-responses. Furthermore, NP has shown to induce strong T-cell responses after i.m. immunization with AAV-vectors (Sipo et al. 2011; Fidgeke 2016).

The intranasal route of administration resembles the way of natural infection by IAV, which is also utilized for live-attenuated influenza vaccines. In this thesis, it was hypothesized that vaccination with a vector vaccine could possibly mimic immunization with a LAIV, which had shown to result in a priming effect for a broadly-reactive, FcγR-activating immune response (Jegaskanda et al. 2013a; Sobhanie et al. 2016) and additionally could induce mucosal immunity at the site of infection. Additionally, heterologous prime-boost schemes with combinations of AAV and WIV immunizations were evaluated, as it has been shown before that WIV was able to boost existing broadly-reactive FcγR-activating responses after natural infection, but was not able to induce those (Jegaskanda et al. 2013a).

Furthermore, as has already been mentioned, the intranasal route is favourable as it has been shown that AAV-vectors can be repeatedly administered via the respiratory tract without loss of potency due to a pre-existing immune response to the AAV-vector capsid (Limberis and Wilson 2006). Based on these findings, the intranasal route was chosen for the administration of the AAV-vector based vaccines.

AAV-HA and AAV-NP both displayed a promising protective effect as monovalent vaccines. In a trivalent formulation with AAV-HA, -NP and -M1, full protection was conferred after homologous challenge, and partial protection against heterologous challenge after i.m. administration, which had mostly been attributed to the HA and NP antigens (Sipo et al. 2011). Thus, the combination of the AAV-HA and -NP vaccines after intranasal administration should be further evaluated for its immunogenic profile in this thesis.

Furthermore, as it has been shown that the immune response even to the conserved stem of the HA is restricted to HAs of the same group (Krammer et al. 2013; Margine et al. 2013), a group 2 HA could enhance the breadth of the immune response. For this purpose, the immunization properties of the AAV-H3 vector have been evaluated here.

AAV-vectors are known to express the transgene over a long period of time, which could lead to a continuous boosting effect after a single administration (Limberis and Wilson 2006; Bell et al. 2011; Fidgeke 2016). Therefore, it has also been assessed, if a single administration is sufficient to induce a potent and protective immune response compared to a prime-boost vaccination scheme.

The AAV-vector preparations used here were produced following the established protocol and subsequently assessed for the described quality parameters (Figure 18). Expression of the transgenes was evaluated *in vitro* before using them in the mouse studies.

The *in vivo* analyses for the AAV-vector vaccine against IAV described in this thesis were carried out in C57BL/6 mice, as the same mouse model was used in the analyses of Demminger et al. (2020). As described in chapter 2.6, C57BL/6 mice are a well-established mouse model in IAV vaccine research, and results obtained in this thesis would furthermore be comparable to earlier studies with this vector system, which used the same mouse strain (Sipo et al. 2011; Demminger et al. 2020). This mouse strain had already been successfully immunized with the used AAV-vectors carrying the respective IAV antigens and displayed a favourable vaccine efficacy and protection from infection after vaccination. However, for future progression of the vaccine towards clinical use, evaluation of the vaccine in other model organisms, e.g. ferrets, as outlined in chapter 2.6, would still be necessary to assess, if the promising effects of vaccination would be replicable there. Demminger et al. (2020) already initially evaluated the intranasal AAV-HA vaccine in ferrets and could show a protective effect against viral challenge.

5.1.2 Immunogenic properties of AAV and WIV vaccination

5.1.2.1 Breadth of the immune response

In the here conducted mouse study on influenza vaccination, all AAV-HA/NP-primed groups displayed a broadly reactive antibody response spanning over IAVs of both HA groups. In this study it could be reproduced that priming with WIV was not able to achieve that, only displaying high titers against the homologous virus. Interestingly, an AAV-HA/NP boost after WIV priming was able to broaden the response compared to the WIV-only prime-boost regimen. However, titers did not reach the same levels of broadly reactive antibodies compared to AAV priming. Animals receiving an AAV-HA/NP prime immunization followed by a WIV boost showed comparable titers of broadly reactive antibodies to the other AAV-prime groups, and thus, leaving it unclear, if the WIV boost further contributes to immunity. Because of the narrow response of the WIV-only group, WIV boosting most likely does not enhance the breadth of the response, but it also does not hinder it.

The breadth of the response in the groups immunized with AAV-HA/NP seems to be mostly attributed to the NP antigen, because immunization with AAV-HA alone, regardless of the group, only led to antibody responses against the homologous virus (AAV-HA/NP in Figure 20 and AAV-HA in Figure 21). A broad response to different group 1 HAs after AAV-HA or to different group 2 HAs after AAV-H3 immunization could not be observed in this study. This leads to the conclusion that the HA-head is the main target of the immune response, and there is no relevant induction of responses against conserved epitopes. Demminger et al. (2020), however, had shown, that AAV-HA was able to induce a broadly reactive

antibody response at least against some other viruses from the HA-group 1. The circumstances under which the immune response could be directed to more conserved areas of the HA-protein to ensure a broader immune response remains to be investigated.

5.1.2.2 Prime-Boost regimens

Different prime-boost regimens were applied to determine if a booster dose supports sufficient immunization with AAV-vectors.

The AAV-vector vaccine here showed a self-boosting effect, as antibody titers continued to steadily rise after only a prime immunization, finally reaching similar titer levels as the AAV prime-boost groups after 6 weeks. The combination of different immunization routes for the prime immunization also reached similar levels.

These results also confirm that anti-AAV-vector antibodies do not inhibit the boosting effect, as anti-AAV antibody titers reached their peak already after three weeks, while anti-influenza A antibodies continued to rise.

The group primed with WIV and boosted with AAV did not reach the same level of broadly reactive antibodies as the other AAV-primed groups. However, all immunization groups were finalized at the same timepoint, thus only three weeks after AAV immunization for this group. As antibody levels in the other AAV groups only reached their peak levels after six, not after three weeks, it would be interesting to investigate, if titer levels would reach the same peak at six weeks after AAV immunization in this group as well.

Even though the i.m. WIV immunization reached high titer levels already after the prime immunization, it became apparent that the characteristics of the induced antibodies, regarding breadth and the ability to induce effector functions, were inferior to the antibodies induced by AAV-HA/NP immunization, indicating that high titer levels alone are not a good indicator for the overall strength of antibody properties.

5.1.2.3 AAV immunization has an increased capability to induce or boost FcγR-activating responses compared to WIV immunization

The induction of Fc-receptor functions, such as ADCC, has long been neglected when evaluating immunity to IAV. However, this has changed in recent years and ADCC has been described as an important mediator of immunity and protection, especially for broadly reactive antibodies (DiLillo et al. 2014; DiLillo et al. 2016; Jegaskanda 2018; Thulin and Wang 2018).

FcγR-activating responses were analyzed in the final sera after the six-week immunization period. Activating responses were detected against the murine FcγRI, -IIb and -III, but not against -IV.

Most strikingly, the response towards the activating FcγRI displayed significant differences between the AAV-HA/NP-primed and WIV-primed immunization groups with homologous and heterologous virus. The WIV-primed groups both showed very low levels of activation, while the AAV-HA/NP-only groups had high activation levels, not depending on the number of immunizations. An AAV-HA/NP boost after WIV priming, unlike in the evaluation of the breadth of the immune response, did not lead to an enhanced response compared to a WIV boost. In the AAV-HA/NP-WIV group, the titers reached medium levels between the WIV-only and AAV-HA/NP-only groups. It seems as if WIV immunization as either prime or boost, hinders maturation of FcγRI responses. Interestingly, this effect was not seen in the FcγRIIb and -III responses, where medium activation was seen in all groups against homologous virus. Against heterologous virus, however, only the groups not involving WIV immunization displayed low activation of FcγRIIb and -III responses. In the AAV-HA/NP prime/boost and AAV-HA/NP i.n./s.c. groups levels low FcγRI-activation levels against heterosubtypic virus were detected, but not in any other groups.

Overall, these results indicate that the AAV-HA and -NP vectors have the capability to induce strong and broadly reactive FcγR-activating responses, even after only a single dose. In comparison, WIV immunization does not have the capability to induce or boost these responses. On the contrary, it seems that it even hinders the maturation of such responses, when comparing the AAV-prime-only and the AAV-prime/WIV-boost groups, as the AAV-prime-only group reaches higher activation levels for FcγRI. The possible reasons for this effect remain to be investigated.

Thus, the report that WIV immunization was able to boost broadly reactive FcγR-activating responses but could not induce them *de novo* (Jegaskanda et al. 2013a) could not be reproduced in this study using the AAV-HA/NP vaccine.

In this study, the broadly reactive FcγR I-activating responses were most likely due to AAV-NP immunization, which can be concluded from the lack of such responses in the AAV-HA-only group.

Demminger et al., who focused on humoral responses towards subtype H1N1 viruses, described broadly reactive FcγR-activating responses after AAV-HA (H1) immunization. This was not observed in this study. There are no such responses in the groups immunized with AAV-HA, AAV-H3 or the combination of the two against the PR8 virus. AAV-HA/H3 induced activation of FcγRIIb and -III against Cal/7/09pdm, but none of the monovalent AAV-HA or AAV-H3 did. This could result from antibodies directed more against conserved epitopes when immunizing with the two different HAs in combination. Interestingly, when compared to the HA of Cal/7/09pdm, the H3 of A/Aichi/2/68 induced strong activation of FcγRI, -IIb and -III against homologous virus when immunized in a monovalent formulation as well as in the bivalent form. Those strain-specific responses reflect the results described

above, indicating that no broadly reactive antibodies were induced by immunization with AAV-HA or AAV-H3. The investigation of the epitopes involved and the mechanisms by which the two HA-antigens act in the course of the immune response, to explain the discrepancies between the responses against H1 and H3 would be an interesting asset for the future of the vaccine.

The effect of immunization with an inactivated influenza vaccine on the induction and expansion of antibodies inducing ADCC in humans has been assessed in several studies, which found that there was a strong increase in ADCC antibodies after vaccination in all age groups (Jegaskanda et al. 2016; Kristensen et al. 2016; de Vries et al. 2017; Vanderven et al. 2017). This was not observed in the present study in mice. However, in those studies the participants had all been naturally infected with IAV at least once in their lifetime, most adults several times, which could have an influence on the generation of such antibodies. One study mentioned that increased ADCC titers were already present as soon as three days after vaccination, pointing towards a recruitment of memory B-cells (Jegaskanda et al. 2016).

AAV immunization in naïve individuals seems to be able to induce broadly reactive Fc effector functions. However, the results differ from LAIV immunization regarding the effect of a following immunization with an inactivated vaccine, as there is no expansion of Fc effector functions, but rather the opposite.

5.1.2.4 CD4 and CD8 T-cell immunity

T-cells have been discussed as an important factor in protection against disease. To assess the level of antigen-specific T-cells after vaccination, spleen cells of uninfected mice were stimulated and analyzed via intracellular cytokine staining, which is a widely used technique to detect cytokine producing cells via flow cytometry (Lovelace and Maecker 2011; Gong et al. 2022). A commercial preparation kit and antibody panel were used to distinguish activated CD4⁺ and CD8⁺ T-cells. Spleen cells were stimulated with commercial peptide pools of HA (H1) and NP of Cal/7/09pdm. Due to availability reasons, no H3 could be used. This, unfortunately, did not result in high number of positive spleen cells or significant results. The background of the two control groups was quite high, which also hindered the analysis.

As antibody levels were high in all immunization groups immunized with homologous antigen (H1, Cal/7/09pdm: AAV-HA/NP-WIV, WIV-AAV-HA/NP, 2x AAV-HA/NP, 2x WIV, 1x AAV-HA/NP, AAV-HA/NP i.n./s.c., 2x AAV-HA and 2x AAV-HA/H3), CD4⁺ T-cells should have been detected, as they stimulate B-cells to produce antibodies. Immunization with NP is known to result in strong T-cell responses (Zheng et al. 2014; Clemens et al. 2018;

Leroux-Roels et al. 2023), so it was expected to see elevated levels of T-cells in all groups, where NP was incorporated in the vaccine.

For detection of antigen-specific T-cells, the here used method should be further refined to be more sensitive. Also, additional methods could also be employed, like ELISpot assay, ELISA or qPCR, to quantify cytokine production in immune cells.

5.1.2.5 Protection against infection

Overall, protection against lethal infection with homologous virus was equally strong in most immunization groups – all mice in the groups immunized with AAV-HA/NP-WIV, WIV-AAV-HA/NP, 2x AAV-HA/NP, 2x WIV, AAV-HA/NP i.n./s.c., 2x AAV-HA and 2x AAV-HA/H3 were protected, while 90% of the animals in the control groups (PBS and AAV-GFP) succumbed to infection by day 8 dpi. These results demonstrate that the indicated immunization schemes are able to induce a potent protective immune response against homologous virus. All groups had a significantly lower mean maximum weight loss (not group 9, 2x AAV-H3), lower clinical scores (not groups 6 and 9, AAV-HA/NP i.n./s.c. or 2x AAV-H3) and lower lung viral titer at 3dpi (not group 9, 2x AAV-H3).

Unexpectedly, the group immunized once with AAV-HA/NP intranasally only showed 60% survival, which was not significant compared to the control groups, even though total IgG, neutralizing antibody titers and HAI titers reached equally high levels compared to the other immunization groups, and mucosal and anti-HA-stalk antibodies could be detected. Also, the harmful effect of infection was more pronounced in the animals only receiving the vaccine at a single time point via two different immunization routes, which showed in the elevated clinical scores, while here 100% protection could still be reached.

Even though ADCC is recognized as a desired feature of broadly reactive, non-neutralizing antibodies induced by next-generation IAV vaccines (Jegaskanda 2018; Von Holle and Moody 2019), it has also been described before that antibodies against specific epitopes in the IAV HA which induce strong ADCC effects, led to a higher mortality level after viral challenge in mice (Ye et al. 2017; Wang et al. 2018).

Such effects could have played a role in the here described study. After a single application of the vaccine, mainly epitopes could have been targeted that induce FcγR-mediated ADCC, indicated by the high levels of FcγR-activating antibodies shown above (Figure 22). It can be hypothesized that a booster-vaccination introduces additional epitopes, while without a booster, the response matures towards the epitopes targeted originally. When applying the vaccine via different immunization routes at the same time, the number of APCs picking up the antigen and presenting epitopes is larger as well than after application via one route only, so this could also lead to a larger pool of different epitopes, leading to a higher survival rate than in the intranasal-only 1x AAV-HA/NP group. These processes

could finally have resulted in a less beneficial balance between the humoral and cellular immune responses in the 1x AAV-HA/NP group and might have led to the higher mortality and clinical score. The properties of FcγR-activating antibodies could further be evaluated with *in vitro* ADCC assays, while the influence of such antibodies on protection and mortality could be assessed in FcγR-knockout mice (Van den Hoecke et al. 2017; Fransen et al. 2018).

In the group immunized with AAV-H3, survival after challenge with the Cal/7/09pdm strain was only 40%. It was expected that immunization with a group 2 HA would not confer complete protection against challenge with the H1N1-strain. Interestingly, two mice survived, indicating that they must have mounted antibodies against more conserved epitopes, which the other mice have not. In this group, however, no humoral or cellular components of the immune response could be detected that would indicate the specific parameters via which protection was conferred.

The second heterologous (PR8) and heterosubtypic (X31) infections both were quite harsh, as lethal doses were aspired. The virus stocks used for infection were checked before set to the desired amount, to achieve the lethal dose for each virus as outlined in Table 4 (3.2.4). Also, after infection, the titer of the inoculation stock was measured, and the titers showed to be at the anticipated level. Only for the first infection with PR8, which didn't induce any pathology in the mice, the titer was too low, which could have been due to a faulty aliquot of the viral stock used to prepare the inoculation solution. Still, it was unexpected that even the control groups didn't show any signs of disease, because mice usually react quite strongly to PR8 infection, even with low titers – Gowda et al. describe a significant decline in body weight of mice infected with 50 pfu (4% at 3 dpi to 17% at 6 dpi) or 500 pfu (13% at 3 dpi to 25% at 6 dpi) and Fukushi et al. (2011) observed 50% mortality at day six, and 100% mortality at day 9 after infection with a dose of 5 x MLD₅₀ (Fukushi et al. 2011; Gowda et al. 2021). On the contrary, X31 usually only causes mild to moderate disease even at higher infectious titers, so the early rise of clinical scores and the early decline of body weight seen here was also unexpected – Askovich et al. (2013) infected mice with 10⁵ pfu of X31 and all mice survived at 16 dpi, with a mean maximum weight loss of less than 20% at 7 dpi and Rutigliano infected mice with 10⁴ EID₅₀ and observed 100% survival and clearance of the virus by day 8 post infection (Askovich et al. 2013; Rutigliano et al. 2014).

In both, the heterologous and heterosubtypic infections, the group immunized with 2x AAV-HA/NP showed significantly elevated survival rates compared to the control groups. Sera from these animals also displayed high neutralizing and HAI titers, as well as high FcγR-activating responses and anti-HA-stalk antibodies. Significantly elevated mucosal IgA could also be detected in these animals. The groups immunized with 2x WIV did not

achieve this. These results point to an advantage of AAV-HA/NP immunization in the context of broad protection compared to repeated WIV immunization.

As expected, the highest survival rate in the X31 challenge was seen in the group immunized with 2x AAV-H3, and also the group immunized with 2x AAV-HA/H3 showed a significant increase in the survival rate compared to the control groups. Even though in these groups only strain-specific antibodies were induced, those antibodies displayed strong neutralizing and HAI titers as well as FcγR-activating responses. Also, mucosal IgA was detected in the 2x AAV-H3 group. The combination of these responses most likely resulted in the increased survival rate after this harsh challenge. Possible reasons for the lethality in some animals of these two groups might be that individual animals failed to induce a protective immune response after vaccination, even though antibody titers in the deceased animal were equally high as in the surviving animals of the group (data not shown). The animal could also have mounted an overshooting immune response, which could have caused the high clinical scores. Such effects in individual animals can never be completely ruled out. In the group immunized with the combination of HA and H3, some animals might have had a more H1-focused immune response, leading to a lowered protective efficacy.

Overall, the only group that was able to protect mice against challenge with all three viruses at a significant level was the 2x AAV-HA/NP group.

5.1.2.6 Conclusion

The study conducted in this thesis demonstrates that AAV-HA/NP immunization is superior to WIV immunization regarding the induction and expansion of a broadly reactive immune response. WIV-immunization was not able to induce or boost broadly reactive responses. On the contrary, it even seemed to hinder the maturation of FcγR-activating responses after an AAV-HA/NP-boost.

The group immunized with 2x AAV-HA/NP demonstrated the best results in all assessed parameters, most importantly protection against infection, where it was the only immunization group which demonstrated elevated survival rates against all three challenge viruses. The broad reactivity here seems to be mostly attributed to the NP, while the strain-specific neutralization and HAI titers are due to the HA, which emphasizes the positive synergic effects of these two antigens in this bivalent formulation.

A boost immunization would still be of importance, as it was found here that a single shot could still reach equal antibody titers, but the quality of the response is inferior to the prime-boost group.

It would be interesting to evaluate the effects of AAV-HA/-NP immunization in non-naïve individuals. This would represent real-world circumstances. The assessment of the effects

of immunization after a longer period of time after vaccination and in different age groups would also be of importance to further assess the potential for this vaccine as a next-generation vaccine for influenza A viruses.

A more sensitive assessment of T-cells would also be of further importance for future vaccine evaluations.

Overall, the AAV-HA/NP vaccine proves to be a promising candidate for further development as a next-generation influenza vaccine.

5.2 SARS-CoV-2

After the emergence of SARS-CoV in 2003, an AAV-vector vaccine was described carrying the S-RBD of the virus, which demonstrated a strong systemic immune response after intramuscular injection, which could be expanded by a local mucosal immune response after intranasal application.

As the pandemic started during this thesis, there were no available vaccines, but there was an urgent need for preventive measures. Thus, the AAV-vector system that had just been successfully used for the immunization against IAV was evaluated for the use as a vaccine against SARS-CoV-2.

Outcome measures to be observed for the efficiency of the vaccine were overall antibody titers, neutralizing activity, mucosal antibody development, FcγR-activating ability, and T-cell responses. Due to organisational reasons, challenge experiments with SARS-CoV-2 were not possible at the RKI.

5.2.1 Design and *in vitro* evaluation of an AAV-S-RBD vaccine

Initially, the full-length S-protein seemed to be the most favourable target for a vaccine against SARS-CoV-2, as it facilitates receptor binding (Hofmann and Pohlmann 2004; Jackson et al. 2022) and has been described as a promising vaccine target for SARS-CoV (Xiao and Dimitrov 2004; Du et al. 2008a; Du et al. 2009). However, also the S-RBD of SARS-CoV alone was shown to induce a protective neutralizing antibody response, while having a more desirable safety profile, as harmful immune or inflammatory responses induced by full-length S-protein could be avoided (He and Jiang 2005; Jiang et al. 2005; Jiang et al. 2012). Thus, AAV-vector plasmids were constructed containing either the SARS-CoV-2 full-length S-protein or the S-RBD alone.

The functionality of the proteins expressed by the AAV-vector vaccine is essential for the induction of the immune response towards the viral proteins. For that reason, protein expression and their functionality were assessed *in vitro*.

It could be shown in this work that the constructed AAV-vector plasmids are successful in reaching high levels of transgene expression in transfected cells and that the encoded proteins show ACE2 binding properties, proving their correct functionality. The S-RBD showed a reduced binding capacity compared to the full-length S-protein, probably resulting from the stronger binding strength of the trimeric S-protein compared to monomeric S-RBD (Basavarajappa et al. 2022).

During the subsequent production process of the AAV-vector particles, the plasmid carrying the full-length S-protein could not be efficiently packaged into functional vector particles. This was most likely due to the limited packaging capacity of the here used AAV-

vectors. Their usual genome size is around 4.7 kb (Naso et al. 2017). The packaging capabilities of AAV-vectors seem to be dependent on the serotype of the capsid used (Allocca et al. 2008). AAV-vector capsids of the subtypes 2, 5 and 8 have shown to not package anything above 5.2 kb, truncating all larger genomes at the 5' end (Wu et al. 2010). Additionally, with larger genomes, not only the packaging, but also the transgene expression efficiency decreases (Dong et al. 1996; Wu et al. 2010). The combination of the AAV2 ITR with the AAV9 vector capsid used here seems to be efficient in packaging and delivering genomes of at least ~7 kb, as this is the size of the vector plasmids containing the IAV constructs, for which it works nicely, as could be demonstrated by the successful *in vitro* evaluation of AAV-vectors containing the HA or NP of IAV, e.g. high numbers of full vector particles and high transgene expression after transduction (Figure 18), which was followed by the induction of a strong immune response after *in vivo* application. The genome containing the full-length S-protein of SARS-CoV-2, however, has a size of 8.7 kb (S-protein cDNA 3.8 kb), which apparently could not be packaged. To circumvent the known size problem existing for AAV-vectors, an approach had been described: the dual AAV-vector method (Ghosh et al. 2011; Trapani et al. 2014; Tornabene and Trapani 2020). This approach, where the expression cassette containing the Coding Sequence (CDS) is being split between two AAV-vector particles, was applied to find a way to deliver the full-length S-protein (4.2.1). In this thesis, the S-protein was artificially split at the S1-S2 cleavage site and the two segments were integrated into separate AAV-vector plasmids. However, co-transduction of the two AAV-vectors only resulted in a very low transgene expression efficiency *in vitro* with very high amounts of AAV-vectors needed, so this approach was not followed further, as it would not have been practical for delivering a vaccine.

The results presented here allow the conclusion that the constructed vector plasmids can be used to efficiently express the transgenes, but only the pAAV-S-RBD, which is 5.5 kb in size, can be used to produce effective AAV-vectors to be used as vaccines against SARS-CoV-2.

As the pandemic progressed, the AAV-S-RBD was adapted to the different VOC S-RBDs. For the full-length S-protein, the pAAV-vector plasmid was altered to express the D614G mutation. For the pAAV-S-RBD plasmids, the Alpha, Beta, Delta and BA.2 VOC were constructed. As it had been described before, the D614G mutation increases the number of open-state conformations and thus, leads to enhanced binding to ACE2 (Yurkovetskiy et al. 2020).

Enhanced binding compared to the wt spike protein could be observed in the here conducted ACE2 binding evaluation (Figure 33 A) as well. The different S-RBD proteins demonstrated binding compared to the GFP control, but the binding capacity was

significantly lower than the binding capacity of the full-length S-protein. The S-RBD constructs used here have not been modified and are expressed as monomers. Trimerization and the optimization of the glycosylation profile of the S-RBD were found to substantially enhance binding and improve immunization properties of the S-RBD compared to the monomeric protein (Bouwman et al. 2021; Routhu et al. 2021; Basavarajappa et al. 2022), so this could be an approach for optimization.

Different expression patterns and binding characteristics could also be due to the splicing effects. Those had been studied, after people who received the AstraZeneca vaccine were hospitalized with cerebral venous sinus thromboses (CVST) or, less frequent, with Splanchnic Vein Thrombosis (SVT) (2.4.2.2).

When analyzing the splicing donor sites of the DNA constructs that were used in this thesis with the Splice Rover online tool (Zuallaert et al. 2018; Kowarz et al. 2022), there are two additional sites in the wt S-RBD after codon-optimization compared to the original sequence (Table 7). The site that both sequences share also has a higher score in the codon-optimized version. The splicing donor sites are also present in the Alpha and Beta S-RBD constructs. In the Delta construct, the same sites are included with an additional fourth site. In the BA.2 construct used here, those splicing sites were not included. There is only one site with a low score. If the delivered DNA of this short construct is spliced multiple times, also within the RBM, the function of the protein would be impaired, and the immune response would not be able to recognize the correct antigen. Depending on the splicing acceptor sites, the resulting product, in addition to lacking important regions, can be in frame or out of frame. Such effects should not be disregarded when working with DNA-vectors delivering the genome of RNA-viruses. Such splicing sites could have resulted in a lower vaccine efficiency with the AAV-vaccines used in this thesis.

		Splicing sites (position)			
		230	264	378	401
S-RBD construct	S-RBD wt (non-codon-optimized)			X	
	S-RBD wt	X	X	X	
	S-RBD Alpha	X	X	X	
	S-RBD Beta	X	X	X	
	S-RBD Delta	X	X	X	X
	S-RBD BA.2	X			

Table 7: Splicing donor sites of the S-RBD constructs used in this thesis
Splicing sites of the given receptor-binding domain (S-RBD) constructs were analyzed with the Splice Rover online tool (Zuallaert et al. 2018).

5.2.2 Immunogenicity of the AAV-S-RBD vector vaccine

5.2.2.1 Comparison of different mouse strains

Initially, the immunogenicity of the AAV-S-RBD vaccine was assessed in three different laboratory mouse strains. This was done, because the different strains are known to mount different immune responses and recognize different immunogenic regions of the antigen, depending on their haplotype, as described in chapter 2.6.

In the immunogenicity studies presented here, a strong strain-dependent effect could be observed. Surprisingly, C57BL/6J mice developed the weakest overall antibody titers, which only went slightly above the pre-immunization levels. As this mouse strain had usually been successfully used in the previous studies for IAV vaccines based on AAV-vectors, this result had not been expected. Those antibodies did also not display any neutralizing activity. Thus, the C57BL/6 mouse strain was excluded from the further analyses conducted to evaluate the AAV-S-RBD vaccine.

In the studies evaluating AAV-vectors as a vaccine against SARS-CoV by using the S-RBD, BALB/c mice had been used (Du et al. 2006; Du et al. 2008b; Du et al. 2008c). In this initial evaluation conducted here, BALB/c mice showed mixed results, dependent on the application route of the vaccine. After s.c. immunization, both mice developed similarly high antibody titers, also showing a potent neutralizing activity. However, after i.n. immunization, only one animal developed medium antibody titers with a reduced, but still potent neutralizing activity. One possible reason for the low titers in the one i.n. immunized animal could be, that during the application, the animal swallowed more of the vaccine than reached the respiratory tract.

The NMRI mice displayed the strongest neutralizing activity, which was equal in all animals and was retained from day 12 onwards until the end of the experiment. The overall antibody titer levels, however, displayed strong inter-animal differences. One animal of each pair immunized either via the s.c. or the i.n. route, developed very high overall antibody titers, while the respective other animal only developed medium titers.

When analyzing IgA levels in the lungs, surprisingly, in the NMRI mice the total systemic IgG titers inversely correlated with those on an individual animal basis, hinting towards the conclusion that the higher the systemic antibody response, the lower the mucosal IgA response. In the BALB/c mice, this observation could not be made, as all animals had elevated IgA levels comparable to the higher titers of the NMRI mice. Even though the C57BL/6 mice did not develop a systemic IgG response, elevated IgA levels of equal intensity could be detected in the two intranasally immunized mice, indicating that this mouse strain is capable of reacting to the antigen, but only locally in the airway mucosa without mounting a strong systemic response.

The NMRI mice also developed FcγR-activating responses, mainly towards FcγRI, while this did not develop in BALB/c mice. Again surprisingly, the sera of the C57BL/6 mice did also show FcγR-activation for FcγRI, which was higher in the subcutaneously immunized mice than for the intranasally immunized mice. This could imply that antibodies generated by the C57BL/6 strain, even only present at low levels and non-neutralizing, could still mobilize effector functions like FcγR-activating responses. Important to note is that NMRI and BALB/c mice also developed antibodies that cross-reacted with the SARS-CoV S-RBD, which is not surprising, as the S-RBDs of both viruses have shown to be 73% conserved and indicate convergent evolution for improved ACE2 binding (Gralinski and Menachery 2020; Lan et al. 2020). The titer towards the SARS-CoV S1-domain in NMRI mice was higher than in BALB/c mice and were one log-level lower than against the SARS-CoV-2 S-RBD.

For all mouse strains, antibodies against the AAV9 vector-capsid were determined as well as a control. In all strains, the i.n. application resulted in higher anti-AAV9 antibodies than the s.c. immunization. However, it had been shown before that despite high levels of anti-AAV antibodies, the vaccine can still be re-applied intranasally without a loss due to neutralization of the vector (Gao et al. 2004; Limberis and Wilson 2006; Boutin et al. 2010). As this was an initial pilot experiment, the sample size was kept low. There are only two mice per group, so that no general conclusions could be drawn from this. Also, the immunization pattern of one prime immunization and six boost immunizations over a time span of 182 days is not realistic for the use as a vaccine but was only applied here for the initial evaluation of the vector. Nonetheless, this experiment was necessary to determine whether the AAV-S-RBD vector vaccine has the potential to induce an antigen-specific and functional, i.e. neutralizing immune response.

It could be concluded that the inbred BALB/c strain and the outbred NMRI strain, but not the C57BL/6 strain, were suitable models to further evaluate the immunogenicity of the AAV-S-RBD vaccine. However, also with these strains, inter-animal differences and differences depending on the route of administration still need to be taken into consideration.

5.2.2.2 Immunogenicity of AAV-S-RBD with wt and variant S-RBDs

Overall, the immunogenicity evaluation of the here described AAV-vectors gave very mixed results. To guarantee a good quality of the AAV-vector preparations, their quality was always assessed by the parameters described in 4.2.1 and Figure 31, and they always showed a high transduction efficiency *in vitro*. Additionally, the respective AAV-vector preparation used for immunization was assessed *in vitro* for transduction efficiency in HEK293T cells directly after application, which was always satisfactory.

The first immunogenicity study was carried out in BALB/c mice solely with the wt AAV-S-RBD vector. BALB/c mice were chosen because they had been successfully used in previous studies evaluating an AAV-S-RBD vaccine for SARS-CoV, and they had shown to develop an antigen-specific immune response in the initial experiment described above. The goal of this study was to evaluate the differences in response depending on the immunization route and to assess, if one or more booster immunization were necessary, or if a single shot could be sufficient to induce a protective immune response.

This study, however, did not reveal an effective immune response. Low ELISA-based titers toward the viral spike protein developed, but they were not significantly higher than the titers of the AAV-GFP control groups. No neutralizing activity could be detected in the sera of immunized mice. Consistently, the mice also did not develop FcγR-activating responses. Interestingly, however, the animals vaccinated three times intranasally had significantly elevated IgA levels in the lungs at the final timepoint compared to all other groups. This could've been due to the fact, that three immunizations were necessary to develop a strong mucosal immune response, or that the time span from the last immunization to the endpoint of the experiment was shortest for this group, and IgA was still detectable, when in the other groups, the local response to the vaccine had already faded. For the anti-AAV9 titers, the same trend could be observed as in the initial study. The i.n. immunized mice developed higher peak titers than the s.c. immunized mice. Antigen-specific T-cells were also evaluated. They displayed a trend towards a stronger response in the s.c. immunized animals, but the results were not significant. Reactive CD4⁺ T-cells should be present when antigen-specific antibodies are produced, so these two factors would be related to each other.

The subsequent immunogenicity study included the variant AAV-S-RBD vectors and was carried out in NMRI mice, as they were identified as the second mouse strain that mounted an antigen-specific immune response towards the here used vaccine and overall displayed the most effective response in terms of neutralization and FcγR-activating responses. A combination of a s.c. prime and an i.n. boost immunization was applied, to initially avoid the anti-AAV antibody response induced by i.n. immunization and to mount a strong T-cell response.

The AAV-S-RBD variants investigated were the wt, Beta, Delta and BA.2 variants. The Alpha variant was excluded, as the N501Y mutation is also present in the Beta and Omicron variants. For availability reasons, the test antigens used in the ELISA assays were the S1-domains of the wt, Beta, Delta and BA.1 variants, which is not ideal, as the BA.1 and BA.2 Omicron-variants do differ from each other in six amino acid positions in the S-RBD (Figure 42), but they are still evolutionary close. Another goal of this evaluation was to specify if

immunization with these AAV-vectors was able to induce a cross-reactive antibody response towards the other SARS-CoV-2 variants.

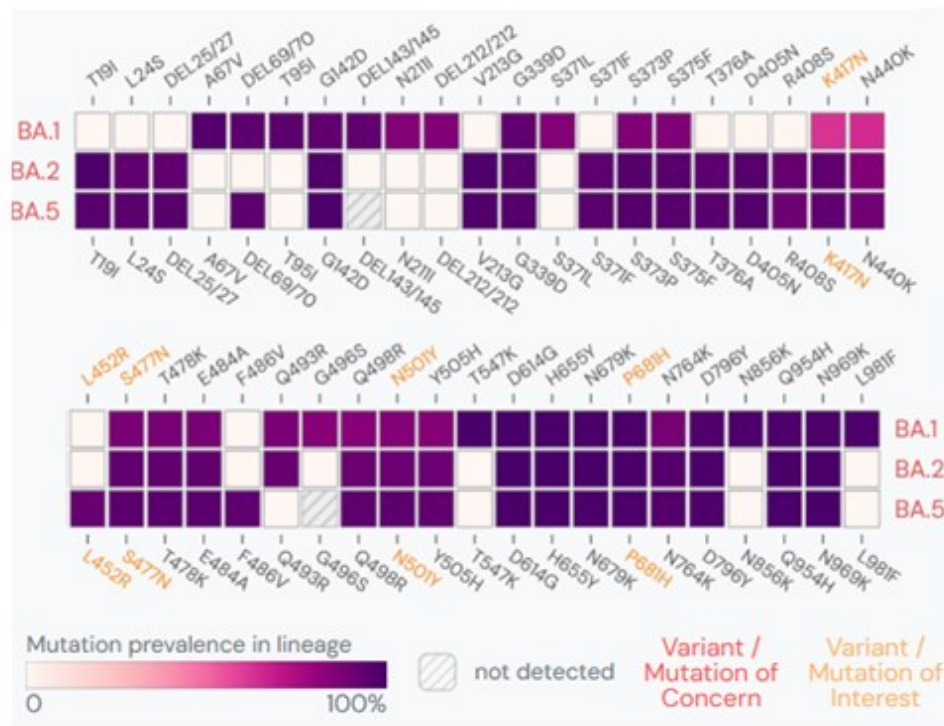


Figure 42: Differences in the spike protein of the SARS-CoV-2 Omicron variants BA.1, BA.2 and BA.5

Displayed are amino acid mutations in the SARS-CoV-2 spike protein of Omicron BA.1, BA.2 and BA.5 variants. Source: Outbreak.info (Khare et al. 2021; Gangavarapu et al. 2023), image rights in chapter 14

Regarding cross-reactivity of the respective VOCs, it has been described that the Omicron subvariants can escape immunity induced by earlier variants, because of the high number of mutations in the S-protein (Iketani et al. 2022; McLean et al. 2022; Rossler et al. 2022). Even though the different Omicron subvariants BA.1, BA.2 and BA.5 share many mutations in their S-protein (Figure 42), they also exhibit different mutations, especially in the S-RBD or NTD, resulting in subvariant-specific neutralization profiles (Bruehl et al. 2022; Rossler et al. 2022). It has been described that immunization with an BA.1-only mRNA vaccine resulted in reduced neutralization against all previous variants, while neutralization against BA.2 and BA.4/5 was slightly reduced, but still robust (Muik et al. 2022a). When using an BA.4/5-only mRNA vaccine, neutralization activity was sharply reduced against earlier VOCs and also reduced against BA.1, while it was similarly robust against BA.2 as the BA.1-only immunization (Muik et al. 2022a).

In the here described evaluation, the AAV-vectors carrying the S-RBD of the Delta and the BA.2 variant displayed a potent immunogenicity. The sera of the BA.2 immunized mice

showed a strong reactivity against all tested S1-domains, while the mice immunized with the S-RBD of the Delta variant developed antibodies against the wt, Beta and Delta variants, but not against the BA.1 variant, which displays the evolutionary distance of Delta to Omicron and is an indicator for immune escape. The other AAV-vectors failed to induce a specific immune response, which is surprising, as all vectors demonstrated potent *in vitro* transduction. Surprisingly, also the mice immunized with a mix of all variant AAV-vectors did not develop any antibody titers, even though the mix also contained the BA.2 and Delta S-RBDs, which alone induced strong immune responses.

The neutralizing activity in the BA.2 immunized group was strong against all Omicron variants, but no neutralization could be detected against the earlier variants, even though there were antibodies present, indicating that cross-reactive antibodies might be non-neutralizing. The sera of the groups immunized with the Delta antigen did not have neutralizing titers.

Interestingly, of those two groups that had developed a strong antibody response, only the BA.2 immunized animals also developed FcγR-activating responses, while the group immunized with Delta did not.

These results indicate that immunization with the BA.2 S-RBD could induce cross-reactive antibodies. Those antibodies show neutralizing activity only against the other Omicron

Test antigen	wt			BA.1		Beta			Delta			BA.2	BA.5
	IgG titer (AUC)	FcγR	FcγR-assay titer (AUC)	IgG titer (AUC)	PRNT ₅₀	IgG titer (AUC)	FcγR	FcγR-assay titer (AUC)	IgG titer (AUC)	FcγR	FcγR-assay titer (AUC)	PRNT ₅₀	PRNT ₅₀
BA.2	2750 ****	I	126.21 ****	1560 ****	1530	2684 ***	I	62.76 ****	2501 ****	I	129.61 ****	1212	581
		IIb	21.6				IIb	22.135		IIb	21.25		
		III	44.7				III	22.55		III	44.4 *		
		IV	15.065				IV	13.385		IV	12.56		
Beta	471.2	I	34.64	268.3	<40	314.2	I	28.12	269.4	I	31.465	<40	<40
		IIb	39.455				IIb	28.66		IIb	26.7		
		III	28.73				III	23.31		III	26.95		
		IV	52.565 **				IV	29.585		IV	13.775		
Delta	1108	I	33.64	295.9	<40	1046	I	27.35	1714 *	I	38.49	<40	<40
		IIb	21.815				IIb	23.695		IIb	20.925		
		III	25.94				III	20.435		III	26.15		
		IV	21.38				IV	14.46		IV	9.54		

Table 8: IgG antibody titers, FcγR-activating titers, and PRNT₅₀ titers of the AAV-S-RBD immunizations

Displayed is an overview of significant immunization results in NMRI mice with wt and variant AAV-S-RBD vectors against the different SARS-CoV-2 antigens. Mice were immunized with AAV-S-RBD vectors with the wt, BA.2, Beta and Delta S-RBD, as well as a mix of all variant S-RBDs. For each test antigen (S1-domain of wt, BA.1, Beta and Delta variants), total IgG titers (AUC), FcγR-assay titers (AUC) and PRNT₅₀ are shown. For BA.2 and BA.5, only PRNT₅₀ results are available. Significant results are highlighted in green.

* p<0.05, ** p<0.01, *** p<0.001, **** p<0.0001

lineages, but not against the other variants. However, against the other variants, an FcγR-activating response is induced, which cannot be observed against the Omicron BA.1 antigen. An important aspect of further investigation would be to analyze, if these cross-reactive, non-neutralizing antibodies could also exhibit a protective effect after infection and if that effect would also hold up against upcoming variants.

However, in this last evaluation, no mucosal antibodies could be detected in either the lungs or the nasal washes. Considering the previous experiments, more than one intranasal booster dose might be necessary to induce a strong IgA response in the respiratory tract.

5.2.2.3 Conclusion

The AAV-S-RBD vaccine designed and evaluated in this thesis initially demonstrated a promising potential as a vaccine candidate against SARS-CoV-2. The further evaluations resulted in rather mixed outcomes, indicating that optimization of the vaccine design might be necessary to obtain more robust results. An interesting finding was the cross-reactivity of the antibodies induced by the AAV-S-RBD BA.2 vaccine, and the induction of FcγR-activating responses of non-neutralizing, cross-reactive antibodies, which could be important for future vaccine design, especially against newly emerging variants.

For future evaluations, protection from infection after viral challenge should also be assessed. For this purpose, more suitable animal models should be used, which could mimic the clinical signs of human disease, like the Roborovski dwarf hamster (*P. roborovskii*) (Trimpert et al. 2020; Gruber et al. 2022).

5.3 Perspective and Outlook

In this thesis the bivalent AAV-HA/NP vaccine against influenza A viruses has shown to be a promising vaccine candidate, proving to be superior to vaccination with an inactivated vaccine in all of the assessed parameters. Especially the induction of mucosal IgA and FcγR-functions add important aspects as additional layers of protection, which is not achieved by WIV immunization.

For the here evaluated AAV-S-RBD vaccine, results were not as intriguing, but an interesting aspect observed here was the induction of cross-variant FcγR-activating responses by antibodies that did not show neutralizing activity.

So far, the focus of vaccination mostly lies on the induction of neutralizing antibodies, but effector functions with broadly reactive characteristics have come more into focus (Keeler and Fox 2021; Richardson and Moore 2021; Zhang et al. 2022). For SARS-CoV-2, the two most used mRNA vaccines have shown to result in distinct epitope recognition and effector

functions, so antigen-design and epitope analysis should be a crucial aspect for future vaccines.

AAV-vectors have shown to be able to induce such effector functions with the here evaluated antigens. They seem to be able to deliver the antigens in such a way, that different epitopes can be assessed, resulting in an immune response with a wide array of humoral and cellular effector functions, which makes them a promising delivery tool for vaccines.

However, also the downsides of cellular effector functions need to be assessed very carefully to avoid severe side effects of vaccination. Thus, in addition to epitope mapping, also the balance between beneficial and detrimental immune responses needs to be evaluated.

For the two viruses that have been the subject of this thesis, new vaccination strategies and vaccine technologies are intensely studied. For IAV, universal vaccine candidates are being investigated and pushed forward to clinical trials, e.g. an nucleoprotein-based universal IAV vaccine candidate, which has started a Phase 2a clinical trial just in June 2023 (Leroux-Roels et al. 2023). For SARS-CoV-2, many vaccine candidates are in pre-clinical (199) or clinical development (183), registered in the WHO COVID-19 vaccine tracker (WHO 2023a). One AAV-based vaccine of the Russian company Biocad is in Phase 1/2 clinical trial, while the other AAV-based vaccine (AAVCOVID), which had emerged early on in the pandemic, has not progressed to clinical trials yet, despite very promising results in pre-clinical NHP studies (Zabaleta et al. 2021; Zabaleta et al. 2022; WHO 2023a). Of all registered vaccine candidates, 16 (9%) are intended for intranasal application. One of those, for example, is the live-attenuated virus vaccine candidate sCPD9 by the Swiss company RocketVax in cooperation with the Institute of Virology of the Freie Universität Berlin, which showed promising results in the hamster model (Adler et al. 2023).

Overall, it is crucial that future vaccines can be protective against the continuously emerging variants without the need to constantly re-design and re-apply those. Both viruses pose the threat of the emergence of future pandemic variants at the human-animal-interface. Hence, vaccines should ideally also be able to protect the population from death, severe disease, and long-term effects in the case such a new divergent pandemic virus arises.

6 Summary

AAV-vector based vaccines for pandemic viruses: Evaluation of broadly reactive responses against influenza A viruses and SARS-CoV-2

Sandra Stelzer

Influenza A viruses and SARS-CoV-2 continue to pose a severe threat to public health. Both are zoonotic pathogens, having arisen from the close human-animal interface.

For both viruses vaccines are available, however their continuous evolution leads to immune escape so that the vaccines need to be continuously evaluated, updated and re-administered.

For influenza viruses, immunity is mainly directed against the head of the viral surface protein HA, which is continuously changing due to drift processes, resulting in strain-specific responses.

For SARS-CoV-2, the spike glycoprotein on the surface, which facilitates receptor-binding is the target of current vaccines.

For both viruses, the interest lies in the development of broadly reactive vaccines which can protect against current and future variants.

A concept that has gained interest in the development of vaccines is the induction of non-neutralizing antibodies that can activate cellular effector-functions, like ADCC. Another important aspect is the induction of mucosal antibodies, in regard to the infection route of both viruses. New delivery platforms have also been evaluated and gained momentum during the SARS-CoV-2 pandemic, for example vector vaccines (e.g. Vakzevria[®]), or mRNA-based vaccines (e.g. Comirnaty[®]). New vaccine candidates are also continuously developed and evaluated, for example the nucleoprotein-based vaccine by Leroux-Roels et al. (2023), which is currently in clinical trials.

The AAV-vectors used in this thesis have shown to be safe for the use in humans and have already been successfully evaluated for the use as vaccine vectors. Intriguingly, they can be repeatedly administered via the respiratory tract, following the natural infection route.

For IAV, this thesis aimed to assess a possible synergistic effect of an AAV-vector vaccine combining the HA and NP antigens of the influenza virus A/California/7/2009pdm. Furthermore, it was hypothesized that, opposed to WIV vaccination, the AAV-vaccine could induce broadly reactive responses. Additionally, an AAV-vector vaccine carrying the HA of the group 2 virus A/Aichi/2/68 (H3N2) was assessed regarding the hypothesis of the induction of a broadened immune response in combination with the group 1 HA of

A/California/7/2009pdm. Furthermore, the induction of a mucosal immune response along the route of application in the respiratory tract was evaluated. To measure these responses, humoral, i.e. neutralizing, broadly reactive, and FcγR-activating responses were evaluated in the sera of immunized C57BL/6 mice, mucosal responses were assessed in nasal washes and lung samples, and T-cells were measured in spleens. The protective efficiency was assessed by an experimental challenge of mice with homologous, heterologous and heterosubtypic virus.

Here, it was shown that a bivalent AAV-HA/NP vaccine was superior to WIV immunization. In the serum of mice immunized with AAV-HA/NP, broadly reactive antibodies and FcγR-activating responses could be detected, while in nasal washes and lung samples mucosal antibodies were present. After a prime-boost i.n. application the vaccine was also capable of protecting mice from viral challenge of homologous, heterologous and heterosubtypic virus, which WIV did not. An AAV-vector vaccine containing a group 2 HA (H3) was evaluated for the first time *in vivo* and proved to be successful in inducing strain-specific antibodies and protecting against homologous challenge but did not induce broadly reactive antibodies.

Another aim of this thesis was the design and evaluation of an AAV-vector vaccine against SARS-CoV-2, because earlier studies evaluating a similar AAV-vector vaccine against SARS-CoV showed promising results. In the course of this thesis, the vaccine was further adapted to the emerging VOCs. In addition to the overall immunogenicity, the hypothesized cross-reactivity and broadly reactive responses induced by the AAV-vaccines against the wildtype virus and the different VOCs were evaluated. The AAV-S-RBD vaccine was initially evaluated in mammalian cell culture models before the *in vivo* analyses were conducted. Initially, different mouse strains were evaluated, and for subsequent analyses BALB/c and NMRI mice were used. Sera, nasal washes, lung samples and spleens were analysed as mentioned for the mice in the IAV experiment. No viral challenge was conducted.

For this part, an induction of variant-specific antibodies by the designed AAV-S-RBD vector could be shown, but it wasn't robust. Interestingly, non-neutralizing antibodies induced by the AAV-S-RBD BA.2 vector could be shown to induce FcγR-activating responses.

Overall, in this thesis AAV-vectors have been demonstrated to be promising vaccine candidates for the induction of broadly reactive immune responses against influenza viruses and SARS-CoV-2.

7 Zusammenfassung

AAV-Vektor basierte Impfstoffe gegen pandemische Viren: Untersuchung von breit-reaktiven Immunantworten gegen Influenza A Viren und SARS-CoV-2

Sandra Stelzer

Influenza-A-Viren und SARS-CoV-2 stellen weiterhin eine ernsthafte Bedrohung für die öffentliche Gesundheit dar. Beides sind zoonotische Erreger, die durch enge Kontakte zwischen Mensch und Tier entstanden sind. Für beide Viren sind Impfstoffe verfügbar, jedoch führt ihre ständige evolutive Weiterentwicklung zu Immunevasion, weshalb die Impfstoffe kontinuierlich überprüft und ggf. aktualisiert und erneut verabreicht werden müssen. Bei Influenza-Viren richtet sich die Immunität hauptsächlich gegen den Kopfbereich des viralen Oberflächenproteins HA, das aufgrund von Drift-Prozessen kontinuierlich verändert wird, was zu stamm-spezifischen Reaktionen führt. Bei SARS-CoV-2 ist das Spike-Glykoprotein auf der Virion-Oberfläche, welches die Rezeptorbindung ermöglicht, das Ziel der aktuellen Impfstoffe.

Für beide Viren besteht das Interesse an der Entwicklung von breit reaktiven Impfstoffen, die vor aktuellen und zukünftigen Varianten schützen können. Ein Konzept, das in der Entwicklung von Impfstoffen Interesse gewonnen hat, ist die Induktion von nicht-neutralisierenden Antikörpern, die zelluläre Effektorfunktionen wie ADCC aktivieren können. Ein weiterer wichtiger Aspekt ist die Induktion von Schleimhautantikörpern in Bezug auf den Infektionsweg beider Viren. Während der SARS-CoV-2-Pandemie wurden auch neue Impfstoffplattformen evaluiert und gewonnen an Bedeutung, wie z.B. Vektorimpfstoffe (z.B. Vakzevria®) oder mRNA-basierte Impfstoffe (z.B. Comirnaty®). Auch für Influenzaviren werden kontinuierlich neue Impfstoffkandidaten entwickelt und untersucht, wie z.B. der Nukleoprotein-basierte Impfstoff von Leroux-Roels et al. (2023), welcher mittlerweile in der klinischen Entwicklung ist.

Die hier verwendeten AAV-Vektoren haben sich als sicher für den Einsatz beim Menschen erwiesen und wurden bereits erfolgreich als Impfstoffvektoren evaluiert. Interessanterweise können sie über den Atemweg wiederholt verabreicht werden und folgen so dem natürlichen Infektionsweg.

Für IAV zielte diese Arbeit darauf ab, einen möglichen synergistischen Effekt eines AAV-Vektor-Impfstoffs zu untersuchen, der die HA- und NP-Antigene des Influenza-Virus A/California/7/2009pdm kombiniert. Darüber hinaus wurde die Hypothese aufgestellt, dass im Gegensatz zur WIV-Impfung der AAV-Impfstoff breit-reaktive Reaktionen hervorrufen könnte. Zusätzlich wurde ein AAV-Vektor-Impfstoffs, der das HA des Gruppe-2 Virus

A/Aichi/2/68 (H3N2) trägt, im Hinblick auf die Hypothese der Induktion einer verbreiterten Immunantwort in Kombination mit dem Gruppe-1-HA von A/California/7/2009pdm untersucht. Auch wurde die Induktion von mukosaler Immunität entlang der Applikationsroute im Respirationstrakt untersucht. Zur Messung der Immunparameter wurden humorale, d.h. neutralisierende, breit-reaktive und FcγR-aktivierende Antikörper im Serum immunisierter C57BL/6 Mäuse bestimmt, mukosale Reaktionen wurden in Proben von nasaler Lavage und Lungen beurteilt, und T-Zellen wurden in Milzen gemessen. Die schützende Wirkung der Impfung wurde durch eine experimentelle Infektion der Mäuse mit homologen, heterologen und heterosubtypischen Viren evaluiert.

Hier konnte gezeigt werden, dass ein bivalenter AAV-HA/NP-Impfstoff der WIV-Impfung überlegen war. Er konnte breit reaktive Antikörper, Schleimhautantikörper und FcγR-aktivierende Reaktionen induzieren. Nach einer i.n.-Anwendung im Prime-Boost-Schema war er auch in der Lage, Mäuse vor viralen Infektionen durch homologe, heterologe und heterosubtypische Viren zu schützen, was mit WIV nicht der Fall war. Ein

AAV-Vektor-Impfstoff mit einem Gruppe-2-HA (H3) wurde erstmals in vivo evaluiert und erwies sich als erfolgreich bei der Induktion von stamm-spezifischen Antikörpern und dem Schutz vor homologer Infektion, induzierte jedoch keine breit reaktiven Antikörper.

Ein weiteres Ziel dieser Arbeit war das Design und die immunologische Untersuchung eines AAV-Vektor-Impfstoffes gegen SARS-CoV-2, da frühere Studien, die einen ähnlichen AAV-Vektor-Impfstoff gegen SARS-CoV untersuchten, vielversprechende Ergebnisse zeigten. Im Verlauf dieser Arbeit wurde der Impfstoff weiter an die aufkommenden VOCs angepasst. Neben der Immunogenität wurden auch die hypothetische Kreuzreaktivität und die breit-reaktiven Reaktionen, die durch die AAV-Impfstoffe gegen das Wildtyp-Virus und die verschiedenen VOCs hervorgerufen wurden, analysiert. Der AAV-S-RBD-Impfstoff wurde zunächst in Zellkulturmodellen an Säugetierzellen evaluiert, bevor die in vivo-Analysen durchgeführt wurden. Zunächst wurden verschiedene Mausstämme evaluiert, und für anschließende Analysen wurden BALB/c- und NMRI-Mäuse verwendet. Seren, Proben von nasaler Lavage und Lungen, sowie Milzen der Mäuse wurden wie im IAV-Experiment analysiert. Es wurde keine experimentellen Infektionen durchgeführt.

In diesem Teil konnte gezeigt werden, dass der entwickelte AAV-S-RBD Impfstoff stamm-spezifische Antikörper induziert. Interessanterweise konnte auch nachgewiesen werden, dass nicht-neutralisierende Antikörper, die durch den AAV-S-RBD-BA.2-Vektor induziert wurden, FcγR-aktivierende Reaktionen hervorrufen. Insgesamt haben sich AAV-Vektoren in dieser Arbeit als vielversprechende Impfstoffkandidaten für die Induktion breit reaktiver Immunantworten gegen Influenza-Viren und SARS-CoV-2 erwiesen.

8 Bibliography

Adler, J. M., R. Martin Vidal, A. Voss, S. Kunder, M. Nascimento, A. Abdelgawad, C. Langner, D. Vladimirova, N. Osterrieder, A. D. Gruber, D. Kunec and J. Trimpert (2023): A non-transmissible live attenuated SARS-CoV-2 vaccine. *Mol Ther* 31: 2391-2407. DOI: 10.1016/j.ymthe.2023.05.004.

Al-Fattah Yahaya, A. A., K. Khalid, H. X. Lim and C. L. Poh (2023): Development of Next Generation Vaccines against SARS-CoV-2 and Variants of Concern. *Viruses* 15. DOI: 10.3390/v15030624.

al-Mazrou, A., D. W. Scheifele, T. Soong and G. Bjornson (1991): Comparison of adverse reactions to whole-virion and split-virion influenza vaccines in hospital personnel. *CMAJ* 145: 213-218.

Allocca, M., M. Doria, M. Petrillo, P. Colella, M. Garcia-Hoyos, D. Gibbs, S. R. Kim, A. Maguire, T. S. Rex, U. Di Vicino, L. Cutillo, J. R. Sparrow, D. S. Williams, J. Bennett and A. Auricchio (2008): Serotype-dependent packaging of large genes in adeno-associated viral vectors results in effective gene delivery in mice. *J Clin Invest* 118: 1955-1964. DOI: 10.1172/JCI34316.

Altenburg, A. F., J. H. Kreijtz, R. D. de Vries, F. Song, R. Fux, G. F. Rimmelzwaan, G. Sutter and A. Volz (2014): Modified vaccinia virus ankara (MVA) as production platform for vaccines against influenza and other viral respiratory diseases. *Viruses* 6: 2735-2761. DOI: 10.3390/v6072735.

Amanat, F., J. Clark, J. M. Carreno, S. Strohmeier, T. Yellin, P. S. Meade, D. Bhavsar, H. Muramatsu, W. Sun, L. Coughlan, N. Pardi and F. Krammer (2023): Immunity to Seasonal Coronavirus Spike Proteins Does Not Protect from SARS-CoV-2 Challenge in a Mouse Model but Has No Detrimental Effect on Protection Mediated by COVID-19 mRNA Vaccination. *J Virol* 97: e0166422. DOI: 10.1128/jvi.01664-22.

Amorim, M. J., E. A. Bruce, E. K. Read, A. Foeglein, R. Mahen, A. D. Stuart and P. Digard (2011): A Rab11- and microtubule-dependent mechanism for cytoplasmic transport of influenza A virus viral RNA. *J Virol* 85: 4143-4156. DOI: 10.1128/JVI.02606-10.

Andrade, F. (2010): Non-cytotoxic antiviral activities of granzymes in the context of the immune antiviral state. *Immunol Rev* 235: 128-146. DOI: 10.1111/j.0105-2896.2010.00909.x.

Andrews, N., J. Stowe, F. Kirsebom, S. Toffa, T. Rickeard, E. Gallagher, C. Gower, M. Kall, N. Groves, A. M. O'Connell, D. Simons, P. B. Blomquist, A. Zaidi, S. Nash, N. Iwani Binti Abdul Aziz, S. Thelwall, G. Dabrera, R. Myers, G. Amirthalingam, S. Gharbia, J. C. Barrett, R. Elson, S. N. Ladhani, N. Ferguson, M. Zambon, C. N. J. Campbell, K. Brown, S. Hopkins, M. Chand, M. Ramsay and J. Lopez Bernal (2022): Covid-19 Vaccine Effectiveness against the Omicron (B.1.1.529) Variant. *N Engl J Med* 386: 1532-1546. DOI: 10.1056/NEJMoa2119451.

Antrobus, R. D., L. Coughlan, T. K. Berthoud, M. D. Dicks, A. V. Hill, T. Lambe and S. C. Gilbert (2014):

Clinical assessment of a novel recombinant simian adenovirus ChAdOx1 as a vectored vaccine expressing conserved Influenza A antigens.
Mol Ther 22: 668-674. DOI: 10.1038/mt.2013.284.

Antrobus, R. D., P. J. Lillie, T. K. Berthoud, A. J. Spencer, J. E. McLaren, K. Ladell, T. Lambe, A. Milicic, D. A. Price, A. V. Hill and S. C. Gilbert (2012):

A T cell-inducing influenza vaccine for the elderly: safety and immunogenicity of MVA-NP+M1 in adults aged over 50 years.
PLoS One 7: e48322. DOI: 10.1371/journal.pone.0048322.

Arevalo, C. P., M. J. Bolton, V. Le Sage, N. Ye, C. Furey, H. Muramatsu, M. G. Alameh, N. Pardi, E. M. Drapeau, K. Parkhouse, T. Garretson, J. S. Morris, L. H. Moncla, Y. K. Tam, S. H. Y. Fan, S. S. Lakdawala, D. Weissman and S. E. Hensley (2022):

A multivalent nucleoside-modified mRNA vaccine against all known influenza virus subtypes.
Science 378: 899-904. DOI: 10.1126/science.abm0271.

Arunachalam, P. S., F. Wimmers, C. K. P. Mok, R. Perera, M. Scott, T. Hagan, N. Sigal, Y. Feng, L. Bristow, O. Tak-Yin Tsang, D. Wagh, J. Coller, K. L. Pellegrini, D. Kazmin, G. Alaaeddine, W. S. Leung, J. M. C. Chan, T. S. H. Chik, C. Y. C. Choi, C. Huerta, M. Paine McCullough, H. Lv, E. Anderson, S. Edupuganti, A. A. Upadhyay, S. E. Bosinger, H. T. Maecker, P. Khatri, N. Rouphael, M. Peiris and B. Pulendran (2020):

Systems biological assessment of immunity to mild versus severe COVID-19 infection in humans.
Science 369: 1210-1220. DOI: 10.1126/science.abc6261.

Askovich, P. S., C. J. Sanders, C. M. Rosenberger, A. H. Diercks, P. Dash, G. Navarro, P. Vogel, P. C. Doherty, P. G. Thomas and A. Aderem (2013):

Differential host response, rather than early viral replication efficiency, correlates with pathogenicity caused by influenza viruses.
PLoS One 8: e74863. DOI: 10.1371/journal.pone.0074863.

Atchison, R. W., B. C. Casto and W. M. Hammon (1965):

Adenovirus-Associated Defective Virus Particles.
Science 149: 754-756. DOI: 10.1126/science.149.3685.754.

Auladell, M., H. V. M. Phuong, L. T. Q. Mai, Y. Y. Tseng, L. Carolan, S. Wilks, P. Q. Thai, D. Price, N. T. Duong, N. L. K. Hang, L. T. Thanh, N. T. H. Thuong, T. T. K. Huong, N. T. N. Diep, V. T. N. Bich, A. Khvorov, L. Hensen, T. N. Duong, K. Kedzierska, D. D. Anh, H. Wertheim, S. D. Boyd, K. L. Good-Jacobson, D. Smith, I. Barr, S. Sullivan, H. R. van Doorn and A. Fox (2022):

Influenza virus infection history shapes antibody responses to influenza vaccination.
Nat Med 28: 363-372. DOI: 10.1038/s41591-022-01690-w.

Balsitis, S. J., K. L. Williams, R. Lachica, D. Flores, J. L. Kyle, E. Mehlhop, S. Johnson, M. S. Diamond, P. R. Beatty and E. Harris (2010):

Lethal antibody enhancement of dengue disease in mice is prevented by Fc modification.
PLoS Pathog 6: e1000790. DOI: 10.1371/journal.ppat.1000790.

Bannert, N. and L. Möller.

Influenza A virus, Berlin/H1N1 (Orthomyxoviruses). Negative staining, transmission electron microscopy (TEM). Bar = 100 nm.

Retrieved 25.08., 2023, from https://www.rki.de/EN/Content/infections/Diagnostics/NatRefCentresConsultantLab/CONSULAB/EM-images/EM_Tab_Influenza_en.html.

Bao, Y., P. Bolotov, D. Dernovoy, B. Kiryutin, L. Zaslavsky, T. Tatusova, J. Ostell and D. Lipman (2008):

The influenza virus resource at the National Center for Biotechnology Information. *J Virol* 82: 596-601. DOI: 10.1128/JVI.02005-07.

Barberis, I., P. Myles, S. K. Ault, N. L. Bragazzi and M. Martini (2016):

History and evolution of influenza control through vaccination: from the first monovalent vaccine to universal vaccines.

J Prev Med Hyg 57: E115-E120.

Barnes, C., O. Scheideler and D. Schaffer (2019):

Engineering the AAV capsid to evade immune responses.

Curr Opin Biotechnol 60: 99-103. DOI: 10.1016/j.copbio.2019.01.002.

Bartlett, J. S., R. Wilcher and R. J. Samulski (2000):

Infectious entry pathway of adeno-associated virus and adeno-associated virus vectors.

J Virol 74: 2777-2785. DOI: 10.1128/jvi.74.6.2777-2785.2000.

Basavarajappa, S. C., A. R. Liu, A. Bruchez, Z. Li, V. G. Suzart, Z. Liu, Y. Chen, T. S. Xiao, M. Buck and P. Ramakrishnan (2022):

Trimeric receptor-binding domain of SARS-CoV-2 acts as a potent inhibitor of ACE2 receptor-mediated viral entry.

iScience 25: 104716. DOI: 10.1016/j.isci.2022.104716.

Bastard, P., L. B. Rosen, Q. Zhang, E. Michailidis, H. H. Hoffmann, Y. Zhang, K. Dorgham, Q. Philippot, J. Rosain, V. Beziat, J. Manry, E. Shaw, L. Haljasmagi, P. Peterson, L. Lorenzo, L. Bizien, S. Trouillet-Assant, K. Dobbs, A. A. de Jesus, A. Belot, A. Kallaste, E. Catherinot, Y. Tandjaoui-Lambiotte, J. Le Pen, G. Kerner, B. Bigio, Y. Seeleuthner, R. Yang, A. Bolze, A. N. Spaan, O. M. Delmonte, M. S. Abers, A. Aiuti, G. Casari, V. Lampasona, L. Piemonti, F. Ciceri, K. Bilguvar, R. P. Lifton, M. Vasse, D. M. Smadja, M. Migaud, J. Hadjadj, B. Terrier, D. Duffy, L. Quintana-Murci, D. van de Beek, L. Roussel, D. C. Vinh, S. G. Tangye, F. Haerynck, D. Dalmau, J. Martinez-Picado, P. Brodin, M. C. Nussenzweig, S. Boisson-Dupuis, C. Rodriguez-Gallego, G. Vogt, T. H. Mogensen, A. J. Oler, J. Gu, P. D. Burbelo, J. I. Cohen, A. Biondi, L. R. Bettini, M. D'Angio, P. Bonfanti, P. Rossignol, J. Mayaux, F. Rieux-Laucat, E. S. Husebye, F. Fusco, M. V. Ursini, L. Imberti, A. Sottini, S. Paghera, E. Quiros-Roldan, C. Rossi, R. Castagnoli, D. Montagna, A. Licari, G. L. Marseglia, X. Duval, J. Ghosn, H. Lab, N.-U. I. R. t. C. Group, C. Clinicians, C.-S. Clinicians, C. G. Imagine, C. C. S. G. French, C. Milieu Interieur, V. C. C. Co, U. M. C. C. - B. Amsterdam, C. H. G. Effort, J. S. Tsang, R. Goldbach-Mansky, K. Kisand, M. S. Lionakis, A. Puel, S. Y. Zhang, S. M. Holland, G. Gorochov, E. Jouanguy, C. M. Rice, A. Cobat, L. D. Notarangelo, L. Abel, H. C. Su and J. L. Casanova (2020):

Autoantibodies against type I IFNs in patients with life-threatening COVID-19.

Science 370. DOI: 10.1126/science.abd4585.

Becerra, S. P., F. Koczot, P. Fabisch and J. A. Rose (1988):

Synthesis of adeno-associated virus structural proteins requires both alternative mRNA splicing and alternative initiations from a single transcript.

J Virol 62: 2745-2754. DOI: 10.1128/JVI.62.8.2745-2754.1988.

Beck, J. A., S. Lloyd, M. Hafezparast, M. Lennon-Pierce, J. T. Eppig, M. F. Festing and E. M. Fisher (2000):

Genealogies of mouse inbred strains.
Nat Genet 24: 23-25. DOI: 10.1038/71641.

Bell, C. L., L. H. Vandenberghe, P. Bell, M. P. Limberis, G. P. Gao, K. Van Vliet, M. Agbandje-McKenna and J. M. Wilson (2011):
The AAV9 receptor and its modification to improve in vivo lung gene transfer in mice.
J Clin Invest 121: 2427-2435. DOI: 10.1172/JCI57367.

Belshe, R. B., K. M. Edwards, T. Vesikari, S. V. Black, R. E. Walker, M. Hultquist, G. Kemble, E. M. Connor and C.-T. C. E. S. Group (2007):
Live attenuated versus inactivated influenza vaccine in infants and young children.
N Engl J Med 356: 685-696. DOI: 10.1056/NEJMoa065368.

Bennett, J., J. Wellman, K. A. Marshall, S. McCague, M. Ashtari, J. DiStefano-Pappas, O. U. Elci, D. C. Chung, J. Sun, J. F. Wright, D. R. Cross, P. Aravand, L. L. Cyckowski, J. L. Bennicelli, F. Mingozzi, A. Auricchio, E. A. Pierce, J. Ruggiero, B. P. Leroy, F. Simonelli, K. A. High and A. M. Maguire (2016):
Safety and durability of effect of contralateral-eye administration of AAV2 gene therapy in patients with childhood-onset blindness caused by RPE65 mutations: a follow-on phase 1 trial.
Lancet 388: 661-672. DOI: 10.1016/S0140-6736(16)30371-3.

Berger, I. and C. Schaffitzel (2020):
The SARS-CoV-2 spike protein: balancing stability and infectivity.
Cell Res 30: 1059-1060. DOI: 10.1038/s41422-020-00430-4.

Berns, K. I. and R. M. Linden (1995):
The cryptic life style of adeno-associated virus.
Bioessays 17: 237-245. DOI: 10.1002/bies.950170310.

Beyer, W. E., J. J. Nauta, A. M. Palache, K. M. Giezenman and A. D. Osterhaus (2011):
Immunogenicity and safety of inactivated influenza vaccines in primed populations: a systematic literature review and meta-analysis.
Vaccine 29: 5785-5792. DOI: 10.1016/j.vaccine.2011.05.040.

Beyer, W. E., A. M. Palache and A. D. Osterhaus (1998):
Comparison of Serology and Reactogenicity between Influenza Subunit Vaccines and Whole Virus or Split Vaccines: A Review and Meta-Analysis of the Literature.
Clin Drug Investig 15: 1-12. DOI: 10.2165/00044011-199815010-00001.

Bhide, Y., W. Dong, I. Gribonika, D. Voshart, T. Meijerhof, J. de Vries-Idema, S. Norley, K. Guilfoyle, S. Skeldon, O. G. Engelhardt, L. Boon, D. Christensen, N. Lycke and A. Huckriede (2019):
Cross-Protective Potential and Protection-Relevant Immune Mechanisms of Whole Inactivated Influenza Virus Vaccines Are Determined by Adjuvants and Route of Immunization.
Front Immunol 10: 646. DOI: 10.3389/fimmu.2019.00646.

Blanco-Melo, D., B. E. Nilsson-Payant, W. C. Liu, S. Uhl, D. Hoagland, R. Moller, T. X. Jordan, K. Oishi, M. Panis, D. Sachs, T. T. Wang, R. E. Schwartz, J. K. Lim, R. A. Albrecht and B. R. tenOever (2020):
Imbalanced Host Response to SARS-CoV-2 Drives Development of COVID-19.
Cell 181: 1036-1045 e1039. DOI: 10.1016/j.cell.2020.04.026.

Bliss, C. M., A. W. Freyn, T. G. Caniels, V. H. Leyva-Grado, R. Nachbagauer, W. Sun, G. S. Tan, V. L. Gillespie, M. McMahon, F. Krammer, A. V. S. Hill, P. Palese and L. Coughlan (2022):

A single-shot adenoviral vaccine provides hemagglutinin stalk-mediated protection against heterosubtypic influenza challenge in mice.

Mol Ther 30: 2024-2047. DOI: 10.1016/j.ymthe.2022.01.011.

Bobay, L. M., A. C. O'Donnell and H. Ochman (2020):

Recombination events are concentrated in the spike protein region of Betacoronaviruses.

PLoS Genet 16: e1009272. DOI: 10.1371/journal.pgen.1009272.

Bodewes, R., G. F. Rimmelzwaan and A. D. Osterhaus (2010):

Animal models for the preclinical evaluation of candidate influenza vaccines.

Expert Rev Vaccines 9: 59-72. DOI: 10.1586/erv.09.148.

Boruchov, A. M., G. Heller, M. C. Veri, E. Bonvini, J. V. Ravetch and J. W. Young (2005):

Activating and inhibitory IgG Fc receptors on human DCs mediate opposing functions.

J Clin Invest 115: 2914-2923. DOI: 10.1172/JCI24772.

Bournazos, S., J. M. Woof, S. P. Hart and I. Dransfield (2009):

Functional and clinical consequences of Fc receptor polymorphic and copy number variants.

Clin Exp Immunol 157: 244-254. DOI: 10.1111/j.1365-2249.2009.03980.x.

Boutin, S., V. Monteilhet, P. Veron, C. Leborgne, O. Benveniste, M. F. Montus and C. Masurier (2010):

Prevalence of serum IgG and neutralizing factors against adeno-associated virus (AAV) types 1, 2, 5, 6, 8, and 9 in the healthy population: implications for gene therapy using AAV vectors.

Hum Gene Ther 21: 704-712. DOI: 10.1089/hum.2009.182.

Bouvier, N. M. and A. C. Lowen (2010):

Animal Models for Influenza Virus Pathogenesis and Transmission.

Viruses 2: 1530-1563. DOI: 10.3390/v20801530.

Bouvier, N. M. and P. Palese (2008):

The biology of influenza viruses.

Vaccine 26 Suppl 4: D49-53. DOI: 10.1016/j.vaccine.2008.07.039.

Bouwman, K. M., I. Tomris, H. L. Turner, R. van der Woude, T. M. Shamorkina, G. P. Bosman, B. Rockx, S. Herfst, J. Snijder, B. L. Haagmans, A. B. Ward, G. J. Boons and R. P. de Vries (2021):

Multimerization- and glycosylation-dependent receptor binding of SARS-CoV-2 spike proteins.

PLoS Pathog 17: e1009282. DOI: 10.1371/journal.ppat.1009282.

Brandolini, M., G. Gatti, L. Grumiro, S. Zannoli, V. Arfilli, M. Cricca, G. Dirani, A. Denicolo, M. M. Marino, M. Manera, A. Mancini, F. Taddei, S. Semprini and V. Sambri (2023):

Omicron Sub-Lineage BA.5 and Recombinant XBB Evasion from Antibody Neutralisation in BNT162b2 Vaccine Recipients.

Microorganisms 11. DOI: 10.3390/microorganisms11010191.

Bröker, B., C. Schütt and B. Fleischer (2019):

Grundwissen Immunologie, 4. Auflage.

Heidelberg, Springer Spektrum Berlin.

- Bruel, T., J. Hadjadj, P. Maes, D. Planas, A. Seve, I. Staropoli, F. Guivel-Benhassine, F. Porrot, W. H. Bolland, Y. Nguyen, M. Casadevall, C. Charre, H. Pere, D. Veyer, M. Prot, A. Baidaliuk, L. Cuypers, C. Planchais, H. Mouquet, G. Baele, L. Mouthon, L. Hocqueloux, E. Simon-Loriere, E. Andre, B. Terrier, T. Prazuck and O. Schwartz (2022):
Serum neutralization of SARS-CoV-2 Omicron sublineages BA.1 and BA.2 in patients receiving monoclonal antibodies.
Nat Med 28: 1297-1302. DOI: 10.1038/s41591-022-01792-5.
- Bruhns, P. (2012):
Properties of mouse and human IgG receptors and their contribution to disease models.
Blood 119: 5640-5649. DOI: 10.1182/blood-2012-01-380121.
- Brunotte, L., J. Flies, H. Bolte, P. Reuther, F. Vreede and M. Schwemmler (2014):
The nuclear export protein of H5N1 influenza A viruses recruits Matrix 1 (M1) protein to the viral ribonucleoprotein to mediate nuclear export.
J Biol Chem 289: 20067-20077. DOI: 10.1074/jbc.M114.569178.
- Burkholz, S., M. Rubsamen, L. Blankenberg, R. T. Carback, 3rd, D. Mochly-Rosen and P. E. Harris (2023):
Analysis of well-annotated next-generation sequencing data reveals increasing cases of SARS-CoV-2 reinfection with Omicron.
Commun Biol 6: 288. DOI: 10.1038/s42003-023-04687-4.
- Busch, D. H. and E. G. Pamer (1998):
MHC class I/peptide stability: implications for immunodominance, in vitro proliferation, and diversity of responding CTL.
J Immunol 160: 4441-4448.
- Calcedo, R., L. H. Vandenberghe, G. Gao, J. Lin and J. M. Wilson (2009):
Worldwide epidemiology of neutralizing antibodies to adeno-associated viruses.
J Infect Dis 199: 381-390. DOI: 10.1086/595830.
- Callaway, E. (2023):
The next generation of coronavirus vaccines: a graphical guide.
Nature 614: 22-25. DOI: 10.1038/d41586-023-00220-z.
- Cao, X. (2016):
Self-regulation and cross-regulation of pattern-recognition receptor signalling in health and disease.
Nat Rev Immunol 16: 35-50. DOI: 10.1038/nri.2015.8.
- Carey, M. A., J. A. Bradbury, Y. D. Reboloso, J. P. Graves, D. C. Zeldin and D. R. Germolec (2010):
Pharmacologic inhibition of COX-1 and COX-2 in influenza A viral infection in mice.
PLoS One 5: e11610. DOI: 10.1371/journal.pone.0011610.
- Carter, B. J. (2004):
Adeno-associated virus and the development of adeno-associated virus vectors: a historical perspective.
Mol Ther 10: 981-989. DOI: 10.1016/j.ymthe.2004.09.011.
- Carvalho, T., F. Krammer and A. Iwasaki (2021):
The first 12 months of COVID-19: a timeline of immunological insights.
Nat Rev Immunol 21: 245-256. DOI: 10.1038/s41577-021-00522-1.

Cassinotti, P., M. Weitz and J. D. Tratschin (1988):
Organization of the adeno-associated virus (AAV) capsid gene: mapping of a minor spliced mRNA coding for virus capsid protein 1.
Virology 167: 176-184.

Charles-River-Laboratories. (2023a, 2023).
C57BL/6 Mice or BALB/c Mice.
Retrieved 25.08., 2023, from <https://www.criver.com/products-services/find-model/c57bl6-mouse?region=23>,
<https://www.criver.com/products-services/find-model/balbc-mouse?region=23>.

Charles-River-Laboratories. (2023b, 2023).
NMRI mice.
Retrieved 25.08., 2023, from <https://www.criver.com/products-services/find-model/nmri-mouse?region=23>.

Chatila, T. A. (2005):
Role of regulatory T cells in human diseases.
J Allergy Clin Immunol 116: 949-959; quiz 960. DOI: 10.1016/j.jaci.2005.08.047.

Chen, J., K. H. Lee, D. A. Steinhauer, D. J. Stevens, J. J. Skehel and D. C. Wiley (1998):
Structure of the hemagglutinin precursor cleavage site, a determinant of influenza pathogenicity and the origin of the labile conformation.
Cell 95: 409-417. DOI: 10.1016/s0092-8674(00)81771-7.

Chourasia, P., L. Goyal, D. Kansal, S. Roy, R. Singh, I. Mahata, A. B. Sheikh and R. Shekhar (2023):
Risk of New-Onset Diabetes Mellitus as a Post-COVID-19 Condition and Possible Mechanisms: A Scoping Review.
J Clin Med 12. DOI: 10.3390/jcm12031159.

Clemens, E. B., C. van de Sandt, S. S. Wong, L. M. Wakim and S. A. Valkenburg (2018):
Harnessing the Power of T Cells: The Promising Hope for a Universal Influenza Vaccine.
Vaccines (Basel) 6. DOI: 10.3390/vaccines6020018.

Copeland, C. S., R. W. Doms, E. M. Bolzau, R. G. Webster and A. Helenius (1986):
Assembly of influenza hemagglutinin trimers and its role in intracellular transport.
J Cell Biol 103: 1179-1191. DOI: 10.1083/jcb.103.4.1179.

Corman, V. M., D. Muth, D. Niemeyer and C. Drosten (2018):
Hosts and Sources of Endemic Human Coronaviruses.
Adv Virus Res 100: 163-188. DOI: 10.1016/bs.aivir.2018.01.001.

Coronaviridae Study Group of the International Committee on Taxonomy of, V. (2020):
The species Severe acute respiratory syndrome-related coronavirus: classifying 2019-nCoV and naming it SARS-CoV-2.
Nat Microbiol 5: 536-544. DOI: 10.1038/s41564-020-0695-z.

Cottard, V., C. Valvason, G. Falgarone, D. Lutomski, M. C. Boissier and N. Bessis (2004):
Immune response against gene therapy vectors: influence of synovial fluid on adeno-associated virus mediated gene transfer to chondrocytes.
J Clin Immunol 24: 162-169. DOI: 10.1023/B:JOCI.0000019781.64421.5c.

- Couch, R. B., R. L. Atmar, L. M. Franco, J. M. Quarles, J. Wells, N. Arden, D. Nino and J. W. Belmont (2013):
Antibody correlates and predictors of immunity to naturally occurring influenza in humans and the importance of antibody to the neuraminidase.
J Infect Dis 207: 974-981. DOI: 10.1093/infdis/jis935.
- CoVariants. (2022, 14.09.2022).
CoVariants.
Retrieved 25.08., 2023, from <https://covariants.org/>.
- Cromer, D., J. A. Juno, D. Khoury, A. Reynaldi, A. K. Wheatley, S. J. Kent and M. P. Davenport (2021):
Prospects for durable immune control of SARS-CoV-2 and prevention of reinfection.
Nat Rev Immunol 21: 395-404. DOI: 10.1038/s41577-021-00550-x.
- Cuppen, E. (2005):
Haplotype-based genetics in mice and rats.
Trends Genet 21: 318-322. DOI: 10.1016/j.tig.2005.03.010.
- Dalmaso, A. P., C. Martinez, K. Sjodin and R. A. Good (1963):
Studies on the Role of the Thymus in Immunobiology; Reconstitution of Immunologic Capacity in Mice Thymectomized at Birth.
J Exp Med 118: 1089-1109. DOI: 10.1084/jem.118.6.1089.
- Davis, H. E., L. McCorkell, J. M. Vogel and E. J. Topol (2023):
Long COVID: major findings, mechanisms and recommendations.
Nat Rev Microbiol 21: 133-146. DOI: 10.1038/s41579-022-00846-2.
- Daya, S. and K. I. Berns (2008):
Gene therapy using adeno-associated virus vectors.
Clin Microbiol Rev 21: 583-593. DOI: 10.1128/CMR.00008-08.
- de Vries, E., D. M. Tscherne, M. J. Wienholts, V. Cobos-Jimenez, F. Scholte, A. Garcia-Sastre, P. J. Rottier and C. A. de Haan (2011):
Dissection of the influenza A virus endocytic routes reveals macropinocytosis as an alternative entry pathway.
PLoS Pathog 7: e1001329. DOI: 10.1371/journal.ppat.1001329.
- de Vries, R. D., N. J. Nieuwkoop, M. Pronk, E. de Bruin, G. Leroux-Roels, E. G. W. Huijskens, R. S. van Binnendijk, F. Krammer, M. P. G. Koopmans and G. F. Rimmelzwaan (2017):
Influenza virus-specific antibody dependent cellular cytotoxicity induced by vaccination or natural infection.
Vaccine 35: 238-247. DOI: 10.1016/j.vaccine.2016.11.082.
- Dekkers, G., A. E. H. Bentlage, T. C. Stegmann, H. L. Howie, S. Lissenberg-Thunnissen, J. Zimring, T. Rispens and G. Vidarsson (2017):
Affinity of human IgG subclasses to mouse Fc gamma receptors.
MAbs 9: 767-773. DOI: 10.1080/19420862.2017.1323159.
- Demminger, D. E. (2019):
Evaluation of an Adeno-associated virus-vector based broadly reactive influenza vaccine.
Doctoral Dissertation (Dr. rer. nat.) Monograph, Humboldt-Universität zu Berlin.

Demminger, D. E., L. Walz, K. Dietert, H. Hoffmann, O. Planz, A. D. Gruber, V. von Messling and T. Wolff (2020):

Adeno-associated virus-vectored influenza vaccine elicits neutralizing and Fcγ receptor-activating antibodies.

EMBO Mol Med 12: e10938. DOI: 10.15252/emmm.201910938.

Deng, J., Y. Ma, Q. Liu, M. Du, M. Liu and J. Liu (2023a):

Severity and Outcomes of SARS-CoV-2 Reinfection Compared with Primary Infection: A Systematic Review and Meta-Analysis.

Int J Environ Res Public Health 20. DOI: 10.3390/ijerph20043335.

Deng, S., Y. Liu, R. C. Tam, P. Chen, A. J. Zhang, B. W. Mok, T. Long, A. Kukic, R. Zhou, H. Xu, W. Song, J. F. Chan, K. K. To, Z. Chen, K. Y. Yuen, P. Wang and H. Chen (2023b): An intranasal influenza virus-vectored vaccine prevents SARS-CoV-2 replication in respiratory tissues of mice and hamsters.

Nat Commun 14: 2081. DOI: 10.1038/s41467-023-37697-1.

Denison, M. R., R. L. Graham, E. F. Donaldson, L. D. Eckerle and R. S. Baric (2011):

Coronaviruses: an RNA proofreading machine regulates replication fidelity and diversity.

RNA Biol 8: 270-279. DOI: 10.4161/rna.8.2.15013.

DeWitt, W. S., R. O. Emerson, P. Lindau, M. Vignali, T. M. Snyder, C. Desmarais, C. Sanders, H. Utsugi, E. H. Warren, J. McElrath, K. W. Makar, A. Wald and H. S. Robins (2015):

Dynamics of the cytotoxic T cell response to a model of acute viral infection.

J Virol 89: 4517-4526. DOI: 10.1128/JVI.03474-14.

Deyle, D. R. and D. W. Russell (2009):

Adeno-associated virus vector integration.

Curr Opin Mol Ther 11: 442-447.

Dias, A., D. Bouvier, T. Crepin, A. A. McCarthy, D. J. Hart, F. Baudin, S. Cusack and R. W. Ruigrok (2009):

The cap-snatching endonuclease of influenza virus polymerase resides in the PA subunit.

Nature 458: 914-918. DOI: 10.1038/nature07745.

DiLillo, D. J., P. Palese, P. C. Wilson and J. V. Ravetch (2016):

Broadly neutralizing anti-influenza antibodies require Fc receptor engagement for in vivo protection.

J Clin Invest 126: 605-610. DOI: 10.1172/JCI84428.

DiLillo, D. J., G. S. Tan, P. Palese and J. V. Ravetch (2014):

Broadly neutralizing hemagglutinin stalk-specific antibodies require FcγR interactions for protection against influenza virus in vivo.

Nat Med 20: 143-151. DOI: 10.1038/nm.3443.

Dinarello, C. A. (2009):

Immunological and inflammatory functions of the interleukin-1 family.

Annu Rev Immunol 27: 519-550. DOI: 10.1146/annurev.immunol.021908.132612.

Ding, M., L. Lu and L. A. Toth (2008):

Gene expression in lung and basal forebrain during influenza infection in mice.

Genes Brain Behav 7: 173-183. DOI: 10.1111/j.1601-183X.2007.00335.x.

Dong, J. Y., P. D. Fan and R. A. Frizzell (1996):

Quantitative analysis of the packaging capacity of recombinant adeno-associated virus. *Hum Gene Ther* 7: 2101-2112. DOI: 10.1089/hum.1996.7.17-2101.

Dong, W., Y. Bhide, F. Sicca, T. Meijerhof, K. Guilfoyle, O. G. Engelhardt, L. Boon, C. A. M. de Haan, G. Carnell, N. Temperton, J. de Vries-Idema, D. Kelvin and A. Huckriede (2018):

Cross-Protective Immune Responses Induced by Sequential Influenza Virus Infection and by Sequential Vaccination With Inactivated Influenza Vaccines. *Front Immunol* 9: 2312. DOI: 10.3389/fimmu.2018.02312.

Dou, D., R. Revol, H. Ostbye, H. Wang and R. Daniels (2018):

Influenza A Virus Cell Entry, Replication, Virion Assembly and Movement. *Front Immunol* 9: 1581. DOI: 10.3389/fimmu.2018.01581.

Drosten, C., S. Gunther, W. Preiser, S. van der Werf, H. R. Brodt, S. Becker, H. Rabenau, M. Panning, L. Kolesnikova, R. A. Fouchier, A. Berger, A. M. Burguiere, J. Cinatl, M. Eickmann, N. Escriou, K. Grywna, S. Kramme, J. C. Manuguerra, S. Muller, V. Rickerts, M. Sturmer, S. Vieth, H. D. Klenk, A. D. Osterhaus, H. Schmitz and H. W. Doerr (2003): Identification of a novel coronavirus in patients with severe acute respiratory syndrome. *N Engl J Med* 348: 1967-1976. DOI: 10.1056/NEJMoa030747.

Du, L., Y. He, S. Jiang and B. J. Zheng (2008a):

Development of subunit vaccines against severe acute respiratory syndrome. *Drugs Today (Barc)* 44: 63-73. DOI: 10.1358/dot.2008.44.1.1131830.

Du, L., Y. He, Y. Wang, H. Zhang, S. Ma, C. K. Wong, S. H. Wu, F. Ng, J. D. Huang, K. Y. Yuen, S. Jiang, Y. Zhou and B. J. Zheng (2006):

Recombinant adeno-associated virus expressing the receptor-binding domain of severe acute respiratory syndrome coronavirus S protein elicits neutralizing antibodies: Implication for developing SARS vaccines.

Virology 353: 6-16. DOI: 10.1016/j.virol.2006.03.049.

Du, L., Y. He, Y. Zhou, S. Liu, B. J. Zheng and S. Jiang (2009):

The spike protein of SARS-CoV--a target for vaccine and therapeutic development. *Nat Rev Microbiol* 7: 226-236. DOI: 10.1038/nrmicro2090.

Du, L., G. Zhao, Y. Lin, C. Chan, Y. He, S. Jiang, C. Wu, D. Y. Jin, K. Y. Yuen, Y. Zhou and B. J. Zheng (2008b):

Priming with rAAV encoding RBD of SARS-CoV S protein and boosting with RBD-specific peptides for T cell epitopes elevated humoral and cellular immune responses against SARS-CoV infection.

Vaccine 26: 1644-1651. DOI: 10.1016/j.vaccine.2008.01.025.

Du, L., G. Zhao, Y. Lin, H. Sui, C. Chan, S. Ma, Y. He, S. Jiang, C. Wu, K. Y. Yuen, D. Y. Jin, Y. Zhou and B. J. Zheng (2008c):

Intranasal vaccination of recombinant adeno-associated virus encoding receptor-binding domain of severe acute respiratory syndrome coronavirus (SARS-CoV) spike protein induces strong mucosal immune responses and provides long-term protection against SARS-CoV infection.

J Immunol 180: 948-956. DOI: 10.4049/jimmunol.180.2.948.

ECDC. (2023, 01.03.2023).

Cluster of avian influenza in Cambodia.

Retrieved 25.08., 2023, from <https://www.ecdc.europa.eu/en/news-events/cluster-avian-influenza-cambodia>.

Echaide, M., L. Chocarro de Erauso, A. Bocanegra, E. Blanco, G. Kochan and D. Escors (2023):

mRNA Vaccines against SARS-CoV-2: Advantages and Caveats.

Int J Mol Sci 24. DOI: 10.3390/ijms24065944.

Echaide, M., I. Labiano, M. Delgado, A. Fernandez de Lascoiti, P. Ochoa, M. Garnica, P. Ramos, L. Chocarro, L. Fernandez, H. Arasanz, A. Bocanegra, E. Blanco, S. Pineiro-Hermida, P. Morente, R. Vera, M. Alsina, D. Escors and G. Kochan (2022):

Immune Profiling Uncovers Memory T-Cell Responses with a Th17 Signature in Cancer Patients with Previous SARS-CoV-2 Infection Followed by mRNA Vaccination.

Cancers (Basel) 14. DOI: 10.3390/cancers14184464.

Edridge, A. W. D., J. Kaczorowska, A. C. R. Hoste, M. Bakker, M. Klein, K. Loens, M. F. Jebbink, A. Matser, C. M. Kinsella, P. Rueda, M. Ieven, H. Goossens, M. Prins, P. Sastre, M. Deijis and L. van der Hoek (2020):

Seasonal coronavirus protective immunity is short-lasting.

Nat Med 26: 1691-1693. DOI: 10.1038/s41591-020-1083-1.

Eichelberger, M. C., D. M. Morens and J. K. Taubenberger (2018):

Neuraminidase as an influenza vaccine antigen: a low hanging fruit, ready for picking to improve vaccine effectiveness.

Curr Opin Immunol 53: 38-44. DOI: 10.1016/j.coi.2018.03.025.

Eisfeld, A. J., E. Kawakami, T. Watanabe, G. Neumann and Y. Kawaoka (2011):

RAB11A is essential for transport of the influenza virus genome to the plasma membrane.

J Virol 85: 6117-6126. DOI: 10.1128/JVI.00378-11.

Erles, K., P. Sebkova and J. R. Schlehofer (1999):

Update on the prevalence of serum antibodies (IgG and IgM) to adeno-associated virus (AAV).

J Med Virol 59: 406-411. DOI: 10.1002/(sici)1096-9071(199911)59:3<406::aid-jmv22>3.0.co;2-n.

Everard, M., P. Johnston, D. Santillo and C. Staddon (2020):

The role of ecosystems in mitigation and management of Covid-19 and other zoonoses.

Environ Sci Policy 111: 7-17. DOI: 10.1016/j.envsci.2020.05.017.

Faria, N. R., I. M. Claro, D. Candido, L. A. Moyses Franco, P. S. Andrade, T. M. Coletti, C. A. M. Silva, F. C. Sales, E. R. Manuli, R. S. Aguiar, N. Gaburo, C. da C. Camilo, N. A. Fraiji, M. A. Esashika Crispim, M. do Perpétuo S. S. Carvalho, A. Rambaut, N. Loman, O. G. Pybus and E. C. Sabino. (2021, 12.01.2021).

Genomic characterisation of an emergent SARS-CoV-2 lineage in Manaus: preliminary findings.

on behalf of CADDE Genomic Network Retrieved 25.08., 2022, from <https://virological.org/t/genomic-characterisation-of-an-emergent-sars-cov-2-lineage-in-manaus-preliminary-findings/586>.

Fehr, A. R. and S. Perlman (2015):

Coronaviruses: an overview of their replication and pathogenesis.

Methods Mol Biol 1282: 1-23. DOI: 10.1007/978-1-4939-2438-7_1.

Ferrari, F. K., T. Samulski, T. Shenk and R. J. Samulski (1996):

Second-strand synthesis is a rate-limiting step for efficient transduction by recombinant adeno-associated virus vectors.

J Virol 70: 3227-3234. DOI: 10.1128/JVI.70.5.3227-3234.1996.

Fiddeke, K. (2016):

Evaluierung von Nukleoprotein-kodierenden AAV-Vektoren als breitenwirksame Influenza-Impfstoffe.

Doctoral Dissertation (Dr. rer. nat.) Monograph, Freie Universität Berlin.

Finkel, Y., O. Mizrahi, A. Nachshon, S. Weingarten-Gabbay, D. Morgenstern, Y. Yahalom-Ronen, H. Tamir, H. Achdout, D. Stein, O. Israeli, A. Beth-Din, S. Melamed, S. Weiss, T. Israely, N. Paran, M. Schwartz and N. Stern-Ginossar (2021):

The coding capacity of SARS-CoV-2.

Nature 589: 125-130. DOI: 10.1038/s41586-020-2739-1.

Fisher, K. J., K. Jooss, J. Alston, Y. Yang, S. E. Haecker, K. High, R. Pathak, S. E. Raper and J. M. Wilson (1997):

Recombinant adeno-associated virus for muscle directed gene therapy.

Nat Med 3: 306-312. DOI: 10.1038/nm0397-306.

Fodor, E. (2013):

The RNA polymerase of influenza A virus: mechanisms of viral transcription and replication.

Acta Virol 57: 113-122. DOI: 10.4149/av_2013_02_113.

Fonseca, M. H. G., G. P. Furtado, M. R. L. Bezerra, L. Q. Pontes and C. F. C. Fernandes (2018):

Boosting half-life and effector functions of therapeutic antibodies by Fc-engineering: An interaction-function review.

Int J Biol Macromol 119: 306-311. DOI: 10.1016/j.ijbiomac.2018.07.141.

Francis, T. (1960):

On the Doctrine of Original Antigenic Sin.

Proceedings of the American Philosophical Society 104: 572-578.

Fransen, M. F., H. Benonisson, W. W. van Maren, H. S. Sow, C. Breukel, M. M. Linssen, J. W. C. Claassens, C. Brouwers, J. van der Kaa, M. Camps, J. W. Kleinovink, K. K. Vonk, S. van Heiningen, N. Klar, L. van Beek, V. van Harmelen, L. Daxinger, K. S. Nandakumar, R. Holmdahl, C. Coward, Q. Lin, S. Hirose, D. Salvatori, T. van Hall, C. van Kooten, P. Mastroeni, F. Ossendorp and J. S. Verbeek (2018):

A Restricted Role for FcγR3 in the Regulation of Adaptive Immunity.

J Immunol 200: 2615-2626. DOI: 10.4049/jimmunol.1700429.

Friedrich-Loeffler-Institut, B. f. T. (2023):

Risikoeinschätzung zur Hochpathogenen Aviären Influenza H5 (HPAI H5) Klade 2.3.4.4B, Aktualisierung für den Zeitraum 01.02.bis 06.03.2023.

Fukushi, M., T. Ito, T. Oka, T. Kitazawa, T. Miyoshi-Akiyama, T. Kirikae, M. Yamashita and K. Kudo (2011):

Serial histopathological examination of the lungs of mice infected with influenza A virus PR8 strain.

PLoS One 6: e21207. DOI: 10.1371/journal.pone.0021207.

Fung, T. S. and D. X. Liu (2019):

Human Coronavirus: Host-Pathogen Interaction.

Annu Rev Microbiol 73: 529-557. DOI: 10.1146/annurev-micro-020518-115759.

Galani, I. E., N. Rovina, V. Lampropoulou, V. Triantafyllia, M. Manioudaki, E. Pavlos, E. Koukaki, P. C. Fragkou, V. Panou, V. Rapti, O. Koltsida, A. Mentis, N. Koulouris, S. Tsiodras, A. Koutsoukou and E. Andreakos (2021):
Untuned antiviral immunity in COVID-19 revealed by temporal type I/III interferon patterns and flu comparison.
Nat Immunol 22: 32-40. DOI: 10.1038/s41590-020-00840-x.

Gangavarapu, K., A. A. Latif, J. L. Mullen, M. Alkuzweny, E. Hufbauer, G. Tsueng, E. Haag, M. Zeller, C. M. Aceves, K. Zaiets, M. Cano, X. Zhou, Z. Qian, R. Sattler, N. L. Matteson, J. I. Levy, R. T. C. Lee, L. Freitas, S. Maurer-Stroh, G. Core, T. Curation, M. A. Suchard, C. Wu, A. I. Su, K. G. Andersen and L. D. Hughes (2023):
Outbreak.info genomic reports: scalable and dynamic surveillance of SARS-CoV-2 variants and mutations.
Nat Methods 20: 512-522. DOI: 10.1038/s41592-023-01769-3.

Gao, G., L. H. Vandenberghe, M. R. Alvira, Y. Lu, R. Calcedo, X. Zhou and J. M. Wilson (2004):
Clades of Adeno-associated viruses are widely disseminated in human tissues.
J Virol 78: 6381-6388. DOI: 10.1128/JVI.78.12.6381-6388.2004.

Gao, G. P., M. R. Alvira, L. Wang, R. Calcedo, J. Johnston and J. M. Wilson (2002):
Novel adeno-associated viruses from rhesus monkeys as vectors for human gene therapy.
Proc Natl Acad Sci U S A 99: 11854-11859. DOI: 10.1073/pnas.182412299.

Geginat, G., S. Schenk, M. Skoberne, W. Goebel and H. Hof (2001):
A novel approach of direct ex vivo epitope mapping identifies dominant and subdominant CD4 and CD8 T cell epitopes from *Listeria monocytogenes*.
J Immunol 166: 1877-1884. DOI: 10.4049/jimmunol.166.3.1877.

Ghosh, A., Y. Yue and D. Duan (2011):
Efficient transgene reconstitution with hybrid dual AAV vectors carrying the minimized bridging sequences.
Hum Gene Ther 22: 77-83. DOI: 10.1089/hum.2010.122.

Ghosn, E. E., R. Yamamoto, S. Hamanaka, Y. Yang, L. A. Herzenberg, H. Nakauchi and L. A. Herzenberg (2012):
Distinct B-cell lineage commitment distinguishes adult bone marrow hematopoietic stem cells.
Proc Natl Acad Sci U S A 109: 5394-5398. DOI: 10.1073/pnas.1121632109.

GISAID. (2021, 02.03.2021).
Clade and lineage nomenclature.
Retrieved 25.08., 2022, from <https://gisaid.org/resources/statements-clarifications/clade-and-lineage-nomenclature-aids-in-genomic-epidemiology-of-active-hcov-19-viruses/>.

Gong, Z., Q. Li, J. Shi and G. Ren (2022):
An Artifact in Intracellular Cytokine Staining for Studying T Cell Responses and Its Alleviation.
Front Immunol 13: 759188. DOI: 10.3389/fimmu.2022.759188.

Goto, H., Y. Muramoto, T. Noda and Y. Kawaoka (2013):
The genome-packaging signal of the influenza A virus genome comprises a genome incorporation signal and a genome-bundling signal.
J Virol 87: 11316-11322. DOI: 10.1128/JVI.01301-13.

- Gowda, D., M. Ohno, B. G. SG, H. Chiba, M. Shingai, H. Kida and S. P. Hui (2021):
Defining the kinetic effects of infection with influenza virus A/PR8/34 (H1N1) on sphingosine-1-phosphate signaling in mice by targeted LC/MS.
Sci Rep 11: 20161. DOI: 10.1038/s41598-021-99765-0.
- Gralinski, L. E. and V. D. Menachery (2020):
Return of the Coronavirus: 2019-nCoV.
Viruses 12. DOI: 10.3390/v12020135.
- Grana, C., L. Ghosn, T. Evrenoglou, A. Jarde, S. Minozzi, H. Bergman, B. S. Buckley, K. Probyn, G. Villanueva, N. Henschke, H. Bonnet, R. Assi, S. Menon, M. Marti, D. Devane, P. Mallon, J. D. Lelievre, L. M. Askie, T. Kredo, G. Ferrand, M. Davidson, C. Riveros, D. Tovey, J. J. Meerpohl, G. Grasselli, G. Rada, A. Hrobjartsson, P. Ravaud, A. Chaimani and I. Boutron (2022):
Efficacy and safety of COVID-19 vaccines.
Cochrane Database Syst Rev 12: CD015477. DOI: 10.1002/14651858.CD015477.
- Grant, E. J., S. M. Quinones-Parra, E. B. Clemens and K. Kedzierska (2016):
Human influenza viruses and CD8(+) T cell responses.
Curr Opin Virol 16: 132-142. DOI: 10.1016/j.coviro.2016.01.016.
- Gray, S. J., S. Nagabhushan Kalburgi, T. J. McCown and R. Jude Samulski (2013):
Global CNS gene delivery and evasion of anti-AAV-neutralizing antibodies by intrathecal AAV administration in non-human primates.
Gene Ther 20: 450-459. DOI: 10.1038/gt.2012.101.
- Greinacher, A., K. Selleng, J. Mayerle, R. Palankar, J. Wesche, S. Reiche, A. Aebischer, T. E. Warkentin, M. Muenchhoff, J. C. Hellmuth, O. T. Keppler, D. Duerschmied, A. Lotter, S. Rieg, M. P. Gawaz, K. A. L. Mueller, C. S. Scheer, M. Napp, K. Hahnenkamp, G. Lucchese, A. Vogelgesang, A. Floel, P. Lovreglio, A. Stufano, R. Marschalek, T. Thiele and C.-V. S. G. Immune-Response in (2021a):
Anti-platelet factor 4 antibodies causing VITT do not cross-react with SARS-CoV-2 spike protein.
Blood 138: 1269-1277. DOI: 10.1182/blood.2021012938.
- Greinacher, A., T. Thiele, T. E. Warkentin, K. Weisser, P. A. Kyrle and S. Eichinger (2021b):
Thrombotic Thrombocytopenia after ChAdOx1 nCov-19 Vaccination.
N Engl J Med 384: 2092-2101. DOI: 10.1056/NEJMoa2104840.
- Grimm, D., P. Staeheli, M. Hufbauer, I. Koerner, L. Martinez-Sobrido, A. Solorzano, A. Garcia-Sastre, O. Haller and G. Kochs (2007):
Replication fitness determines high virulence of influenza A virus in mice carrying functional Mx1 resistance gene.
Proc Natl Acad Sci U S A 104: 6806-6811. DOI: 10.1073/pnas.0701849104.
- Gruber, A. D., T. C. Firsching, J. Trimpert and K. Dietert (2022):
Hamster models of COVID-19 pneumonia reviewed: How human can they be?
Vet Pathol 59: 528-545. DOI: 10.1177/03009858211057197.
- Gur, M., E. Taka, S. Z. Yilmaz, C. Kilinc, U. Aktas and M. Golcuk (2020):
Conformational transition of SARS-CoV-2 spike glycoprotein between its closed and open states.
J Chem Phys 153: 075101. DOI: 10.1063/5.0011141.

Gurwith, M., M. Lock, E. M. Taylor, G. Ishioka, J. Alexander, T. Mayall, J. E. Ervin, R. N. Greenberg, C. Strout, J. J. Treanor, R. Webby and P. F. Wright (2013):
Safety and immunogenicity of an oral, replicating adenovirus serotype 4 vector vaccine for H5N1 influenza: a randomised, double-blind, placebo-controlled, phase 1 study.
Lancet Infect Dis 13: 238-250. DOI: 10.1016/S1473-3099(12)70345-6.

Hadfield, J., C. Megill, S. M. Bell, J. Huddleston, B. Potter, C. Callender, P. Sagulenko, T. Bedford and R. A. Neher (2018):
Nextstrain: real-time tracking of pathogen evolution.
Bioinformatics 34: 4121-4123. DOI: 10.1093/bioinformatics/bty407.

Hadjadj, J., N. Yatim, L. Barnabei, A. Corneau, J. Boussier, N. Smith, H. Pere, B. Charbit, V. Bondet, C. Chenevier-Gobeaux, P. Breillat, N. Carlier, R. Gauzit, C. Morbieu, F. Pene, N. Marin, N. Roche, T. A. Szwebel, S. H. Merklings, J. M. Treluyer, D. Veyer, L. Mouthon, C. Blanc, P. L. Tharoux, F. Rozenberg, A. Fischer, D. Duffy, F. Rieux-Laucat, S. Kerneis and B. Terrier (2020):
Impaired type I interferon activity and inflammatory responses in severe COVID-19 patients.
Science 369: 718-724. DOI: 10.1126/science.abc6027.

Haller, O. (1981):
Inborn resistance of mice to orthomyxoviruses.
Curr Top Microbiol Immunol 92: 25-52. DOI: 10.1007/978-3-642-68069-4_3.

Halstead, S. B., S. Mahalingam, M. A. Marovich, S. Ubol and D. M. Mosser (2010):
Intrinsic antibody-dependent enhancement of microbial infection in macrophages: disease regulation by immune complexes.
Lancet Infect Dis 10: 712-722. DOI: 10.1016/S1473-3099(10)70166-3.

Hampton, H. R. and T. Chtanova (2019):
Lymphatic Migration of Immune Cells.
Front Immunol 10: 1168. DOI: 10.3389/fimmu.2019.01168.

Hamre, D. and J. J. Procknow (1966):
A new virus isolated from the human respiratory tract.
Proc Soc Exp Biol Med 121: 190-193. DOI: 10.3181/00379727-121-30734.

Harris, A., G. Cardone, D. C. Winkler, J. B. Heymann, M. Brecher, J. M. White and A. C. Steven (2006):
Influenza virus pleiomorphy characterized by cryoelectron tomography.
Proc Natl Acad Sci U S A 103: 19123-19127. DOI: 10.1073/pnas.0607614103.

Hartenian, E., D. Nandakumar, A. Lari, M. Ly, J. M. Tucker and B. A. Glaunsinger (2020):
The molecular virology of coronaviruses.
J Biol Chem 295: 12910-12934. DOI: 10.1074/jbc.REV120.013930.

Harvey, W. T., A. M. Carabelli, B. Jackson, R. K. Gupta, E. C. Thomson, E. M. Harrison, C. Ludden, R. Reeve, A. Rambaut, C.-G. U. Consortium, S. J. Peacock and D. L. Robertson (2021):
SARS-CoV-2 variants, spike mutations and immune escape.
Nat Rev Microbiol 19: 409-424. DOI: 10.1038/s41579-021-00573-0.

Hause, B. M., E. A. Collin, R. Liu, B. Huang, Z. Sheng, W. Lu, D. Wang, E. A. Nelson and F. Li (2014):
Characterization of a novel influenza virus in cattle and Swine: proposal for a new genus in the Orthomyxoviridae family.

mBio 5: e00031-00014. DOI: 10.1128/mBio.00031-14.

Hauswirth, W. W. and K. I. Berns (1977):
Origin and termination of adeno-associated virus DNA replication.
Virology 78: 488-499. DOI: 10.1016/0042-6822(77)90125-8.

He, W., C. E. Mullarkey and M. S. Miller (2015):
Measuring the neutralization potency of influenza A virus hemagglutinin stalk/stem-binding antibodies in polyclonal preparations by microneutralization assay.
Methods 90: 95-100. DOI: 10.1016/j.ymeth.2015.04.037.

He, W. T., R. Musharrafieh, G. Song, K. Dueker, L. V. Tse, D. R. Martinez, A. Schafer, S. Callaghan, P. Yong, N. Beutler, J. L. Torres, R. M. Volk, P. Zhou, M. Yuan, H. Liu, F. Anzanello, T. Capozzola, M. Parren, E. Garcia, S. A. Rawlings, D. M. Smith, I. A. Wilson, Y. Safonova, A. B. Ward, T. F. Rogers, R. S. Baric, L. E. Gralinski, D. R. Burton and R. Andrabi (2022):
Targeted isolation of diverse human protective broadly neutralizing antibodies against SARS-like viruses.
Nat Immunol 23: 960-970. DOI: 10.1038/s41590-022-01222-1.

He, Y. and S. Jiang (2005):
Vaccine design for severe acute respiratory syndrome coronavirus.
Viral Immunol 18: 327-332. DOI: 10.1089/vim.2005.18.327.

He, Y. W., B. Adkins, R. K. Furse and T. R. Malek (1995):
Expression and function of the gamma c subunit of the IL-2, IL-4, and IL-7 receptors. Distinct interaction of gamma c in the IL-4 receptor.
J Immunol 154: 1596-1605.

Heaton, N. S., V. H. Leyva-Grado, G. S. Tan, D. Eggink, R. Hai and P. Palese (2013):
In vivo bioluminescent imaging of influenza A virus infection and characterization of novel cross-protective monoclonal antibodies.
J Virol 87: 8272-8281. DOI: 10.1128/JVI.00969-13.

Hebert, D. N., B. Foellmer and A. Helenius (1995):
Glucose trimming and reglucosylation determine glycoprotein association with calnexin in the endoplasmic reticulum.
Cell 81: 425-433. DOI: 10.1016/0092-8674(95)90395-x.

Heinzel, F. P., M. D. Sadick, B. J. Holaday, R. L. Coffman and R. M. Locksley (1989):
Reciprocal expression of interferon gamma or interleukin 4 during the resolution or progression of murine leishmaniasis. Evidence for expansion of distinct helper T cell subsets.
J Exp Med 169: 59-72. DOI: 10.1084/jem.169.1.59.

Helenius, A. (1992):
Unpacking the incoming influenza virus.
Cell 69: 577-578. DOI: 10.1016/0092-8674(92)90219-3.

Herath, S., A. Le Heron, S. Colloca, S. Patterson, R. Tatoud, J. Weber and G. Dickson (2016):
Strain-dependent and distinctive T-cell responses to HIV antigens following immunisation of mice with differing chimpanzee adenovirus vaccine vectors.
Vaccine 34: 4378-4385. DOI: 10.1016/j.vaccine.2016.07.028.

Hintzen, G., L. Ohi, M. L. del Rio, J. I. Rodriguez-Barbosa, O. Pabst, J. R. Kocks, J. Krege, S. Hardtke and R. Forster (2006):

Induction of tolerance to innocuous inhaled antigen relies on a CCR7-dependent dendritic cell-mediated antigen transport to the bronchial lymph node.

J Immunol 177: 7346-7354. DOI: 10.4049/jimmunol.177.10.7346.

Hobson, D., R. L. Curry, A. S. Beare and A. Ward-Gardner (1972):

The role of serum haemagglutination-inhibiting antibody in protection against challenge infection with influenza A2 and B viruses.

J Hyg (Lond) 70: 767-777. DOI: 10.1017/s0022172400022610.

Hoffmann, M., H. Kleine-Weber, S. Schroeder, N. Kruger, T. Herrler, S. Erichsen, T. S. Schiergens, G. Herrler, N. H. Wu, A. Nitsche, M. A. Muller, C. Drosten and S. Pohlmann (2020):

SARS-CoV-2 Cell Entry Depends on ACE2 and TMPRSS2 and Is Blocked by a Clinically Proven Protease Inhibitor.

Cell 181: 271-280 e278. DOI: 10.1016/j.cell.2020.02.052.

Hofmann, H. and S. Pohlmann (2004):

Cellular entry of the SARS coronavirus.

Trends Microbiol 12: 466-472. DOI: 10.1016/j.tim.2004.08.008.

Hoggan, M. D., N. R. Blacklow and W. P. Rowe (1966):

Studies of small DNA viruses found in various adenovirus preparations: physical, biological, and immunological characteristics.

Proc Natl Acad Sci U S A 55: 1467-1474. DOI: 10.1073/pnas.55.6.1467.

Holland, G. and N. Bannert.

Influenza A virus A/California/7/2009 (H1N1), colouring, negative staining, Transmission electron microscopy (TEM). Initial magnification x 85000.

Retrieved 25.08., 2023, from https://www.rki.de/EN/Content/infections/Diagnostics/NatRefCentresConsultantLab/CONSULAB/EM-images/EM_Tab_Influenza_en.html.

Hosel, M., J. Lucifora, T. Michler, G. Holz, M. Gruffaz, S. Stahnke, F. Zoulim, D. Durantel, M. Heikenwalder, D. Nierhoff, R. Millet, A. Salvetti, U. Protzer and H. Buning (2014):

Hepatitis B virus infection enhances susceptibility toward adeno-associated viral vector transduction in vitro and in vivo.

Hepatology 59: 2110-2120. DOI: 10.1002/hep.26990.

Hou, Y. J., S. Chiba, P. Halfmann, C. Ehre, M. Kuroda, K. H. Dinno, 3rd, S. R. Leist, A. Schafer, N. Nakajima, K. Takahashi, R. E. Lee, T. M. Mascenik, R. Graham, C. E. Edwards, L. V. Tse, K. Okuda, A. J. Markmann, L. Bartelt, A. de Silva, D. M. Margolis, R. C. Boucher, S. H. Randell, T. Suzuki, L. E. Gralinski, Y. Kawaoka and R. S. Baric (2020):

SARS-CoV-2 D614G variant exhibits efficient replication ex vivo and transmission in vivo. Science 370: 1464-1468. DOI: 10.1126/science.abe8499.

Hsieh, C. S., S. E. Macatonia, A. O'Garra and K. M. Murphy (1995):

T cell genetic background determines default T helper phenotype development in vitro.

J Exp Med 181: 713-721. DOI: 10.1084/jem.181.2.713.

Hudry, E., C. Martin, S. Gandhi, B. Gyorgy, D. I. Scheffer, D. Mu, S. F. Merkel, F. Mingozi, Z. Fitzpatrick, H. Dimant, M. Masek, T. Ragan, S. Tan, A. R. Brisson, S. H. Ramirez, B. T. Hyman and C. A. Maguire (2016):

Exosome-associated AAV vector as a robust and convenient neuroscience tool.

Gene Ther 23: 380-392. DOI: 10.1038/gt.2016.11.

Hutchinson, E. C. (2018):
Influenza Virus.

Trends Microbiol 26: 809-810. DOI: 10.1016/j.tim.2018.05.013.

Hutchinson, E. C., P. D. Charles, S. S. Hester, B. Thomas, D. Trudgian, M. Martinez-Alonso and E. Fodor (2014):

Conserved and host-specific features of influenza virion architecture.

Nat Commun 5: 4816. DOI: 10.1038/ncomms5816.

Ibricevic, A., A. Pekosz, M. J. Walter, C. Newby, J. T. Battaile, E. G. Brown, M. J. Holtzman and S. L. Brody (2006):

Influenza virus receptor specificity and cell tropism in mouse and human airway epithelial cells.

J Virol 80: 7469-7480. DOI: 10.1128/JVI.02677-05.

Iketani, S., L. Liu, Y. Guo, L. Liu, J. F. Chan, Y. Huang, M. Wang, Y. Luo, J. Yu, H. Chu, K. K. Chik, T. T. Yuen, M. T. Yin, M. E. Sobieszczyk, Y. Huang, K. Y. Yuen, H. H. Wang, Z. Sheng and D. D. Ho (2022):

Antibody evasion properties of SARS-CoV-2 Omicron sublineages.

Nature 604: 553-556. DOI: 10.1038/s41586-022-04594-4.

Iwasaki, A. and P. S. Pillai (2014):

Innate immunity to influenza virus infection.

Nat Rev Immunol 14: 315-328. DOI: 10.1038/nri3665.

Jackson, C. B., M. Farzan, B. Chen and H. Choe (2022):

Mechanisms of SARS-CoV-2 entry into cells.

Nat Rev Mol Cell Biol 23: 3-20. DOI: 10.1038/s41580-021-00418-x.

Jackson, L. A., E. J. Anderson, N. G. Rouphael, P. C. Roberts, M. Makhene, R. N. Coler, M. P. McCullough, J. D. Chappell, M. R. Denison, L. J. Stevens, A. J. Pruijssers, A. McDermott, B. Flach, N. A. Doria-Rose, K. S. Corbett, K. M. Morabito, S. O'Dell, S. D. Schmidt, P. A. Swanson, 2nd, M. Padilla, J. R. Mascola, K. M. Neuzil, H. Bennett, W. Sun, E. Peters, M. Makowski, J. Albert, K. Cross, W. Buchanan, R. Pikaart-Tautges, J. E. Ledgerwood, B. S. Graham, J. H. Beigel and R. N. A. S. G. m (2020):

An mRNA Vaccine against SARS-CoV-2 - Preliminary Report.

N Engl J Med 383: 1920-1931. DOI: 10.1056/NEJMoa2022483.

Jamison, D. A., Jr., S. Anand Narayanan, N. S. Trovao, J. W. Guarnieri, M. J. Topper, P. M. Moraes-Vieira, V. Zaksas, K. K. Singh, E. S. Wurtele and A. Beheshti (2022):

A comprehensive SARS-CoV-2 and COVID-19 review, Part 1: Intracellular overdrive for SARS-CoV-2 infection.

Eur J Hum Genet 30: 889-898. DOI: 10.1038/s41431-022-01108-8.

Jegaskanda, S. (2018):

The Potential Role of Fc-Receptor Functions in the Development of a Universal Influenza Vaccine.

Vaccines (Basel) 6. DOI: 10.3390/vaccines6020027.

Jegaskanda, S., T. H. Amarasena, K. L. Laurie, H. X. Tan, J. Butler, M. S. Parsons, S. Alcantara, J. Petravac, M. P. Davenport, A. C. Hurt, P. C. Reading and S. J. Kent (2013a):

Standard trivalent influenza virus protein vaccination does not prime antibody-dependent cellular cytotoxicity in macaques.

J Virol 87: 13706-13718. DOI: 10.1128/JVI.01666-13.

Jegaskanda, S., E. R. Job, M. Kramski, K. Laurie, G. Isitman, R. de Rose, W. R. Winnall, I. Stratov, A. G. Brooks, P. C. Reading and S. J. Kent (2013b):
Cross-reactive influenza-specific antibody-dependent cellular cytotoxicity antibodies in the absence of neutralizing antibodies.

J Immunol 190: 1837-1848. DOI: 10.4049/jimmunol.1201574.

Jegaskanda, S., C. Luke, H. D. Hickman, M. Y. Sangster, W. F. Wieland-Alter, J. M. McBride, J. W. Yewdell, P. F. Wright, J. Treanor, C. M. Rosenberger and K. Subbarao (2016):

Generation and Protective Ability of Influenza Virus-Specific Antibody-Dependent Cellular Cytotoxicity in Humans Elicited by Vaccination, Natural Infection, and Experimental Challenge.

J Infect Dis 214: 945-952. DOI: 10.1093/infdis/jiw262.

Jegaskanda, S., P. C. Reading and S. J. Kent (2014):

Influenza-specific antibody-dependent cellular cytotoxicity: toward a universal influenza vaccine.

J Immunol 193: 469-475. DOI: 10.4049/jimmunol.1400432.

Jegaskanda, S., J. T. Weinfurter, T. C. Friedrich and S. J. Kent (2013c):

Antibody-dependent cellular cytotoxicity is associated with control of pandemic H1N1 influenza virus infection of macaques.

J Virol 87: 5512-5522. DOI: 10.1128/JVI.03030-12.

Jiang, S., Y. He and S. Liu (2005):

SARS vaccine development.

Emerg Infect Dis 11: 1016-1020. DOI: 10.3201/1107.050219.

Jiang, S., L. Lu, Q. Liu, W. Xu and L. Du (2012):

Receptor-binding domains of spike proteins of emerging or re-emerging viruses as targets for development of antiviral vaccines.

Emerg Microbes Infect 1: e13. DOI: 10.1038/emi.2012.1.

Jones, B. A., D. Grace, R. Kock, S. Alonso, J. Rushton, M. Y. Said, D. McKeever, F. Mutua, J. Young, J. McDermott and D. U. Pfeiffer (2013):

Zoonosis emergence linked to agricultural intensification and environmental change.

Proc Natl Acad Sci U S A 110: 8399-8404. DOI: 10.1073/pnas.1208059110.

Jones, K. E., N. G. Patel, M. A. Levy, A. Storeygard, D. Balk, J. L. Gittleman and P. Daszak (2008):

Global trends in emerging infectious diseases.

Nature 451: 990-993. DOI: 10.1038/nature06536.

Jonges, M., M. R. Welkers, R. E. Jeeninga, A. Meijer, P. Schneeberger, R. A. Fouchier, M. D. de Jong and M. Koopmans (2014):

Emergence of the virulence-associated PB2 E627K substitution in a fatal human case of highly pathogenic avian influenza virus A(H7N7) infection as determined by Illumina ultra-deep sequencing.

J Virol 88: 1694-1702. DOI: 10.1128/JVI.02044-13.

Kalimuddin, S., C. Y. L. Tham, M. Qui, R. de Alwis, J. X. Y. Sim, J. M. E. Lim, H. C. Tan, A. Syenina, S. L. Zhang, N. Le Bert, A. T. Tan, Y. S. Leong, J. X. Yee, E. Z. Ong, E. E. Ooi, A. Bertolotti and J. G. Low (2021):

Early T cell and binding antibody responses are associated with COVID-19 RNA vaccine efficacy onset.

Med 2: 682-688 e684. DOI: 10.1016/j.medj.2021.04.003.

Kasuga, Y., B. Zhu, K. J. Jang and J. S. Yoo (2021):

Innate immune sensing of coronavirus and viral evasion strategies.

Exp Mol Med 53: 723-736. DOI: 10.1038/s12276-021-00602-1.

Kawasaki, Y., H. Abe and J. Yasuda (2023):

Comparison of genome replication fidelity between SARS-CoV-2 and influenza A virus in cell culture.

Sci Rep 13: 13105. DOI: 10.1038/s41598-023-40463-4.

Keeler, S. P. and J. M. Fox (2021):

Requirement of Fc-Fc Gamma Receptor Interaction for Antibody-Based Protection against Emerging Virus Infections.

Viruses 13. DOI: 10.3390/v13061037.

Kenyon, C. (2020):

Emergence of zoonoses such as COVID-19 reveals the need for health sciences to embrace an explicit eco-social conceptual framework of health and disease.

Epidemics 33: 100410. DOI: 10.1016/j.epidem.2020.100410.

Khare, S., C. Gurry, L. Freitas, M. B. Schultz, G. Bach, A. Diallo, N. Akite, J. Ho, R. T. Lee, W. Yeo, G. C. Curation Team and S. Maurer-Stroh (2021):

GISAID's Role in Pandemic Response.

China CDC Wkly 3: 1049-1051. DOI: 10.46234/ccdcw2021.255.

Korber, B., W. M. Fischer, S. Gnanakaran, H. Yoon, J. Theiler, W. Abfalterer, N. Hengartner, E. E. Giorgi, T. Bhattacharya, B. Foley, K. M. Hastie, M. D. Parker, D. G. Partridge, C. M. Evans, T. M. Freeman, T. I. de Silva, C.-G. G. Sheffield, C. McDanal, L. G. Perez, H. Tang, A. Moon-Walker, S. P. Whelan, C. C. LaBranche, E. O. Saphire and D. C. Montefiori (2020): Tracking Changes in SARS-CoV-2 Spike: Evidence that D614G Increases Infectivity of the COVID-19 Virus.

Cell 182: 812-827 e819. DOI: 10.1016/j.cell.2020.06.043.

Kowarz, E., L. Krutzke, M. Kulp, P. Streb, P. Larghero, J. Reis, S. Bracharz, T. Engler, S. Kochanek and R. Marschalek (2022):

Vaccine-induced COVID-19 mimicry syndrome.

Elife 11. DOI: 10.7554/eLife.74974.

Krammer, F. (2019):

The human antibody response to influenza A virus infection and vaccination.

Nat Rev Immunol 19: 383-397. DOI: 10.1038/s41577-019-0143-6.

Krammer, F. and P. Palese (2013):

Influenza virus hemagglutinin stalk-based antibodies and vaccines.

Curr Opin Virol 3: 521-530. DOI: 10.1016/j.coviro.2013.07.007.

Krammer, F. and P. Palese (2015):

Advances in the development of influenza virus vaccines.

Nat Rev Drug Discov 14: 167-182. DOI: 10.1038/nrd4529.

Krammer, F., N. Pica, R. Hai, I. Margine and P. Palese (2013):

Chimeric hemagglutinin influenza virus vaccine constructs elicit broadly protective stalk-specific antibodies.

J Virol 87: 6542-6550. DOI: 10.1128/JVI.00641-13.

Krammer, F., N. Pica, R. Hai, G. S. Tan and P. Palese (2012):

Hemagglutinin Stalk-Reactive Antibodies Are Boosted following Sequential Infection with Seasonal and Pandemic H1N1 Influenza Virus in Mice.

J Virol 86: 10302-10307. DOI: 10.1128/JVI.01336-12.

Krammer, F., G. J. D. Smith, R. A. M. Fouchier, M. Peiris, K. Kedzierska, P. C. Doherty, P. Palese, M. L. Shaw, J. Treanor, R. G. Webster and A. Garcia-Sastre (2018):
Influenza.

Nat Rev Dis Primers 4: 3. DOI: 10.1038/s41572-018-0002-y.

Kristensen, A. B., W. N. Lay, F. Ana-Sosa-Batiz, H. A. Vanderven, V. Madhavi, K. L. Laurie, L. Carolan, B. D. Wines, M. Hogarth, A. K. Wheatley and S. J. Kent (2016):

Antibody Responses with Fc-Mediated Functions after Vaccination of HIV-Infected Subjects with Trivalent Influenza Vaccine.

J Virol 90: 5724-5734. DOI: 10.1128/JVI.00285-16.

Kroonstrom, L. A., J. Krause, S. B. Larsson, R. Sigstrom and K. S. Sunnerhagen (2022):

Long-term self-reported health and disability after COVID-19 in public employees.

BMC Public Health 22: 2400. DOI: 10.1186/s12889-022-14820-3.

Kuhn, J. H., S. Adkins, B. R. Agwanda, R. Al Kubrusli, S. V. Alkhovsky, G. K. Amarasinghe, T. Avsic-Zupanc, M. A. Ayllon, J. Bahl, A. Balkema-Buschmann, M. J. Ballinger, C. F. Basler, S. Bavari, M. Beer, N. Bejerman, A. J. Bennett, D. A. Bente, E. Bergeron, B. H. Bird, C. D. Blair, K. R. Blasdell, D. R. Blystad, J. Bojko, W. B. Borth, S. Bradfute, R. Breyta, T. Briese, P. A. Brown, J. K. Brown, U. J. Buchholz, M. J. Buchmeier, A. Bukreyev, F. Burt, C. Buttner, C. H. Calisher, M. Cao, I. Casas, K. Chandran, R. N. Charrel, Q. Cheng, Y. Chiaki, M. Chiapello, I. R. Choi, M. Ciuffo, J. C. S. Clegg, I. Crozier, E. Dal Bo, J. C. de la Torre, X. de Lamballerie, R. L. de Swart, H. Debat, N. M. Dheilly, E. Di Cicco, N. Di Paola, F. Di Serio, R. G. Dietzgen, M. Digiaro, O. Dolnik, M. A. Drebot, J. F. Drexler, W. G. Dundon, W. P. Duprex, R. Durrwald, J. M. Dye, A. J. Easton, H. Ebihara, T. Elbeaino, K. Ergunay, H. W. Ferguson, A. R. Fooks, M. Forgia, P. B. H. Formenty, J. Franova, J. Freitas-Astua, J. Fu, S. Furl, S. Gago-Zachert, G. F. Gao, M. L. Garcia, A. Garcia-Sastre, A. R. Garrison, T. Gaskin, J. J. Gonzalez, A. Griffiths, T. L. Goldberg, M. H. Groschup, S. Gunther, R. A. Hall, J. Hammond, T. Han, J. Hepojoki, R. Hewson, J. Hong, N. Hong, S. Hongo, M. Horie, J. S. Hu, T. Hu, H. R. Hughes, F. Huttner, T. H. Hyndman, M. Ilyas, R. Jalkanen, D. Jiang, G. B. Jonson, S. Junglen, F. Kadono, K. H. Kaukinen, M. Kawate, B. Klempa, J. Klingstrom, G. Kobinger, I. Koloniuk, H. Kondo, E. V. Koonin, M. Krupovic, K. Kubota, G. Kurath, L. Laenen, A. J. Lambert, S. L. Langevin, B. Lee, E. J. Lefkowitz, E. M. Leroy, S. Li, L. Li, J. Li, H. Liu, I. S. Lukashevich, P. Maes, W. M. de Souza, M. Marklewitz, S. H. Marshall, S. L. Marzano, S. Massart, J. W. McCauley, M. Melzer, N. Mielke-Ehret, K. M. Miller, T. J. Ming, A. Mirazimi, G. J. Mordecai, H. P. Muhlbach, E. Muhlberger, R. Naidu, T. Natsuaki, J. A. Navarro, S. V. Netesov, G. Neumann, N. Nowotny, M. R. T. Nunes, A. Olmedo-Velarde, G. Palacios, V. Pallas, B. Palyi, A. Papa, S. Paraskevopoulou, A. C. Park, C. R. Parrish, D. A. Patterson, A. Pauvolid-Correa, J. T. Paweska, S. Payne, C. Peracchio, D. R. Perez, T. S. Postler, L. Qi, S. R. Radoshitzky, R. O. Resende, C. A. Reyes, B. K. Rima, G. R. Luna, V. Romanowski, P. Rota, D. Rubbenstroth, L. Rubino, J. A. Runstadler, S. Sabanadzovic, A. A. Sall, M. S. Salvato, R. Sang, T. Sasaya, A. D. Schulze, M. Schwemmler, M. Shi, X. Shi, Z. Shi, Y. Shimamoto, Y. Shirako, S. G. Siddell, P. Simmonds, M. Sironi, G. Smagghe, S. Smither, J. W. Song, K. Spann, J. R. Spengler, M. D. Stenglein, D. M. Stone, J. Sugano, C. A. Suttle, A. Tabata, A. Takada, S. Takeuchi, D. P. Tchouassi, A. Teffer, R. B. Tesh, N. J. Thornburg, Y. Tomitaka, K. Tomonaga, N. Tordo, B. Torto, J. S. Towner, S.

- Tsuda, C. Tu, M. Turina, I. E. Tzanetakis, J. Uchida, T. Usugi, A. M. Vaira, M. Vallino, B. van den Hoogen, A. Varsani, N. Vasilakis, M. Verbeek, S. von Bargen, J. Wada, V. Wahl, P. J. Walker, L. F. Wang, G. Wang, Y. Wang, Y. Wang, M. Waqas, T. Wei, S. Wen, A. E. Whitfield, J. V. Williams, Y. I. Wolf, J. Wu, L. Xu, H. Yanagisawa, C. Yang, Z. Yang, F. M. Zerbini, L. Zhai, Y. Z. Zhang, S. Zhang, J. Zhang, Z. Zhang and X. Zhou (2021):
2021 Taxonomic update of phylum Negarnaviricota (Riboviria: Orthornavirae), including the large orders Bunyavirales and Mononegavirales.
Arch Virol 166: 3513-3566. DOI: 10.1007/s00705-021-05143-6.
- Kumar, B. V., T. J. Connors and D. L. Farber (2018):
Human T Cell Development, Localization, and Function throughout Life.
Immunity 48: 202-213. DOI: 10.1016/j.immuni.2018.01.007.
- Kwon, I. and D. V. Schaffer (2008):
Designer gene delivery vectors: molecular engineering and evolution of adeno-associated viral vectors for enhanced gene transfer.
Pharm Res 25: 489-499. DOI: 10.1007/s11095-007-9431-0.
- La Gruta, N. L. and S. J. Turner (2014):
T cell mediated immunity to influenza: mechanisms of viral control.
Trends Immunol 35: 396-402. DOI: 10.1016/j.it.2014.06.004.
- Lai, M. M. C. and D. Cavanagh (1997):
The Molecular Biology of Coronaviruses.
Advances in Virus Research. K. Maramorosch, F. A. Murphy and A. J. Shatkin, Academic Press. 48: 1-100.
- Laing, A. G., A. Lorenc, I. Del Molino Del Barrio, A. Das, M. Fish, L. Monin, M. Munoz-Ruiz, D. R. McKenzie, T. S. Hayday, I. Francos-Quijorna, S. Kamdar, M. Joseph, D. Davies, R. Davis, A. Jennings, I. Zlatareva, P. Vantourout, Y. Wu, V. Sofra, F. Cano, M. Greco, E. Theodoridis, J. D. Freedman, S. Gee, J. N. E. Chan, S. Ryan, E. Bugallo-Blanco, P. Peterson, K. Kisand, L. Haljasmagi, L. Chadli, P. Moingeon, L. Martinez, B. Merrick, K. Bisnauthsing, K. Brooks, M. A. A. Ibrahim, J. Mason, F. Lopez Gomez, K. Babalola, S. Abdul-Jawad, J. Cason, C. Mant, J. Seow, C. Graham, K. J. Doores, F. Di Rosa, J. Edgeworth, M. Shankar-Hari and A. C. Hayday (2020):
A dynamic COVID-19 immune signature includes associations with poor prognosis.
Nat Med 26: 1623-1635. DOI: 10.1038/s41591-020-1038-6.
- Lakdawala, S. S., E. Fodor and K. Subbarao (2016):
Moving On Out: Transport and Packaging of Influenza Viral RNA into Virions.
Annu Rev Virol 3: 411-427. DOI: 10.1146/annurev-virology-110615-042345.
- Lan, J., J. Ge, J. Yu, S. Shan, H. Zhou, S. Fan, Q. Zhang, X. Shi, Q. Wang, L. Zhang and X. Wang (2020):
Structure of the SARS-CoV-2 spike receptor-binding domain bound to the ACE2 receptor.
Nature 581: 215-220. DOI: 10.1038/s41586-020-2180-5.
- Lau, B., E. Wentz, Z. Ni, K. Yenokyan, C. Coggiano, S. H. Mehta and P. Duggal (2022):
Physical and mental health disability associated with long-COVID: Baseline results from a US nationwide cohort.
medRxiv. DOI: 10.1101/2022.12.07.22283203.
- Lavelle, E. C. and R. W. Ward (2022):
Mucosal vaccines - fortifying the frontiers.
Nat Rev Immunol 22: 236-250. DOI: 10.1038/s41577-021-00583-2.

- Lee, G. K., N. Maheshri, B. Kaspar and D. V. Schaffer (2005):
PEG conjugation moderately protects adeno-associated viral vectors against antibody neutralization.
Biotechnol Bioeng 92: 24-34. DOI: 10.1002/bit.20562.
- Lee, M., M. Major and H. Hong (2023):
Distinct Conformations of SARS-CoV-2 Omicron Spike Protein and Its Interaction with ACE2 and Antibody.
Int J Mol Sci 24. DOI: 10.3390/ijms24043774.
- Leroux-Roels, I., P. Willems, G. Waerlop, Y. Janssens, J. Tourneur, F. De Boever, J. Bruhwyler, A. Alhatemi, B. Jacobs, F. Nicolas, G. Leroux-Roels and A. Le Vert (2023):
Immunogenicity, safety, and preliminary efficacy evaluation of OVX836, a nucleoprotein-based universal influenza A vaccine candidate: a randomised, double-blind, placebo-controlled, phase 2a trial.
Lancet Infect Dis. DOI: 10.1016/S1473-3099(23)00351-1.
- Leser, G. P. and R. A. Lamb (2005):
Influenza virus assembly and budding in raft-derived microdomains: a quantitative analysis of the surface distribution of HA, NA and M2 proteins.
Virology 342: 215-227. DOI: 10.1016/j.virol.2005.09.049.
- Lewis, S. M., A. Williams and S. C. Eisenbarth (2019):
Structure and function of the immune system in the spleen.
Sci Immunol 4. DOI: 10.1126/sciimmunol.aau6085.
- Li, Q., J. Wu, J. Nie, L. Zhang, H. Hao, S. Liu, C. Zhao, Q. Zhang, H. Liu, L. Nie, H. Qin, M. Wang, Q. Lu, X. Li, Q. Sun, J. Liu, L. Zhang, X. Li, W. Huang and Y. Wang (2020):
The Impact of Mutations in SARS-CoV-2 Spike on Viral Infectivity and Antigenicity.
Cell 182: 1284-1294 e1289. DOI: 10.1016/j.cell.2020.07.012.
- Li, Q., L. Zhou, M. Zhou, Z. Chen, F. Li, H. Wu, N. Xiang, E. Chen, F. Tang, D. Wang, L. Meng, Z. Hong, W. Tu, Y. Cao, L. Li, F. Ding, B. Liu, M. Wang, R. Xie, R. Gao, X. Li, T. Bai, S. Zou, J. He, J. Hu, Y. Xu, C. Chai, S. Wang, Y. Gao, L. Jin, Y. Zhang, H. Luo, H. Yu, J. He, Q. Li, X. Wang, L. Gao, X. Pang, G. Liu, Y. Yan, H. Yuan, Y. Shu, W. Yang, Y. Wang, F. Wu, T. M. Uyeki and Z. Feng (2014):
Epidemiology of human infections with avian influenza A(H7N9) virus in China.
N Engl J Med 370: 520-532. DOI: 10.1056/NEJMoa1304617.
- Liao, G., H. Lau, Z. Liu, C. Li, Z. Xu, X. Qi, Y. Zhang, Q. Feng, R. Li, X. Deng, Y. Li, Q. Zhu, S. Zhu, H. Zhou, H. Pan, X. Fan, Y. Li, D. Li, L. Chen, B. Ke, Z. Cong, Q. Lv, J. Liu, D. Liang, A. Li, W. Hong, L. Bao, F. Zhou, H. Gao, S. Liang, B. Huang, M. Wu, C. Qin, C. Ke and L. Liu (2022):
Single-dose rAAV5-based vaccine provides long-term protective immunity against SARS-CoV-2 and its variants.
Virology 19: 212. DOI: 10.1186/s12985-022-01940-w.
- Liao, M., Y. Liu, J. Yuan, Y. Wen, G. Xu, J. Zhao, L. Cheng, J. Li, X. Wang, F. Wang, L. Liu, I. Amit, S. Zhang and Z. Zhang (2020):
Single-cell landscape of bronchoalveolar immune cells in patients with COVID-19.
Nat Med 26: 842-844. DOI: 10.1038/s41591-020-0901-9.

- Lillie, P. J., T. K. Berthoud, T. J. Powell, T. Lambe, C. Mullarkey, A. J. Spencer, M. Hamill, Y. Peng, M. E. Blais, C. J. Duncan, S. H. Sheehy, T. Havelock, S. N. Faust, R. L. Williams, A. Gilbert, J. Oxford, T. Dong, A. V. Hill and S. C. Gilbert (2012): Preliminary assessment of the efficacy of a T-cell-based influenza vaccine, MVA-NP+M1, in humans. *Clin Infect Dis* 55: 19-25. DOI: 10.1093/cid/cis327.
- Limberis, M. P. and J. M. Wilson (2006): Adeno-associated virus serotype 9 vectors transduce murine alveolar and nasal epithelia and can be readministered. *Proc Natl Acad Sci U S A* 103: 12993-12998. DOI: 10.1073/pnas.0601433103.
- Lin, D. Y., Y. Xu, Y. Gu, D. Zeng, S. K. Sunny and Z. Moore (2023): Durability of Bivalent Boosters against Omicron Subvariants. *N Engl J Med*. DOI: 10.1056/NEJMc2302462.
- Lin, J., R. Calcedo, L. H. Vandenberghe, P. Bell, S. Somanathan and J. M. Wilson (2009): A new genetic vaccine platform based on an adeno-associated virus isolated from a rhesus macaque. *J Virol* 83: 12738-12750. DOI: 10.1128/JVI.01441-09.
- Link-Gelles, R., M. E. Levy, K. Natarajan, S. E. Reese, A. L. Naleway, S. J. Grannis, N. P. Klein, M. B. DeSilva, T. C. Ong, M. Gaglani, E. Hartmann, M. Dickerson, E. Stenehjem, A. B. Kharbanda, J. Han, T. L. Spark, S. A. Irving, B. E. Dixon, O. Zerbo, C. E. McEvoy, S. Rao, C. Raiyani, C. Sloan-Aagard, P. Patel, K. Dascomb, A. C. Uhlemann, M. M. Dunne, W. F. Fadel, N. Lewis, M. A. Barron, K. Murthy, J. Nanez, E. P. Griggs, N. Grisel, M. K. Annavajhala, A. Akinseye, N. R. Valvi, K. Goddard, M. Mamawala, J. Arndorfer, D. H. Yang, P. J. Embi, B. Fireman, S. W. Ball and M. W. Tenforde (2023): Estimation of COVID-19 mRNA Vaccine Effectiveness and COVID-19 Illness and Severity by Vaccination Status During Omicron BA.4 and BA.5 Sublineage Periods. *JAMA Netw Open* 6: e232598. DOI: 10.1001/jamanetworkopen.2023.2598.
- Liu, F., C. Feng, S. Xu, Q. Wu, J. Tang, Y. Chen, R. Xu, F. Chen, N. Gao, Z. Xu, S. Gu, Y. Lan, H. Zhou, X. Hu and X. Wang (2022): An AAV vaccine targeting the RBD of the SARS-CoV-2 S protein induces effective neutralizing antibody titers in mice and canines. *Vaccine* 40: 1208-1212. DOI: 10.1016/j.vaccine.2022.01.030.
- Liu, M., F. J. van Kuppeveld, C. A. de Haan and E. de Vries (2023): Gradual adaptation of animal influenza A viruses to human-type sialic acid receptors. *Curr Opin Virol* 60: 101314. DOI: 10.1016/j.coviro.2023.101314.
- Liu, R., Z. Sheng, C. Huang, D. Wang and F. Li (2020): Influenza D virus. *Curr Opin Virol* 44: 154-161. DOI: 10.1016/j.coviro.2020.08.004.
- Long, J. S., B. Mistry, S. M. Haslam and W. S. Barclay (2019): Host and viral determinants of influenza A virus species specificity. *Nat Rev Microbiol* 17: 67-81. DOI: 10.1038/s41579-018-0115-z.
- Lotfinia, M., M. Abdollahpour-Alitappeh, B. Hatami, M. R. Zali and M. Karimipoor (2019): Adeno-associated virus as a gene therapy vector: strategies to neutralize the neutralizing antibodies. *Clin Exp Med* 19: 289-298. DOI: 10.1007/s10238-019-00557-8.

- Lovelace, P. and H. T. Maecker (2011):
Multiparameter intracellular cytokine staining.
Methods Mol Biol 699: 165-178. DOI: 10.1007/978-1-61737-950-5_8.
- Lu, X., T. M. Tumpey, T. Morken, S. R. Zaki, N. J. Cox and J. M. Katz (1999):
A mouse model for the evaluation of pathogenesis and immunity to influenza A (H5N1)
viruses isolated from humans.
J Virol 73: 5903-5911. DOI: 10.1128/JVI.73.7.5903-5911.1999.
- Ludwig, S., R. Zell, M. Schwemmler and S. Herold (2014):
Influenza, a One Health paradigm--novel therapeutic strategies to fight a zoonotic
pathogen with pandemic potential.
Int J Med Microbiol 304: 894-901. DOI: 10.1016/j.ijmm.2014.08.016.
- Maguire, C. A., L. Balaj, S. Sivaraman, M. H. Crommentuijn, M. Ericsson, L. Mincheva-
Nilsson, V. Baranov, D. Gianni, B. A. Tannous, M. Sena-Esteves, X. O. Breakefield and J.
Skog (2012):
Microvesicle-associated AAV vector as a novel gene delivery system.
Mol Ther 20: 960-971. DOI: 10.1038/mt.2011.303.
- Maines, T. R., A. Jayaraman, J. A. Belser, D. A. Wadford, C. Pappas, H. Zeng, K. M. Gustin,
M. B. Pearce, K. Viswanathan, Z. H. Shriver, R. Raman, N. J. Cox, R. Sasisekharan, J. M.
Katz and T. M. Tumpey (2009):
Transmission and pathogenesis of swine-origin 2009 A(H1N1) influenza viruses in ferrets
and mice.
Science 325: 484-487. DOI: 10.1126/science.1177238.
- Margine, I. and F. Krammer (2014):
Animal models for influenza viruses: implications for universal vaccine development.
Pathogens 3: 845-874. DOI: 10.3390/pathogens3040845.
- Margine, I., F. Krammer, R. Hai, N. S. Heaton, G. S. Tan, S. A. Andrews, J. A. Runstadler,
P. C. Wilson, R. A. Albrecht, A. Garcia-Sastre and P. Palese (2013):
Hemagglutinin stalk-based universal vaccine constructs protect against group 2 influenza
A viruses.
J Virol 87: 10435-10446. DOI: 10.1128/JVI.01715-13.
- Marks, P. W., P. A. Gruppuso and E. Y. Adashi (2023):
Urgent Need for Next-Generation COVID-19 Vaccines.
JAMA 329: 19-20. DOI: 10.1001/jama.2022.22759.
- Matlin, K. S., H. Reggio, A. Helenius and K. Simons (1981):
Infectious entry pathway of influenza virus in a canine kidney cell line.
J Cell Biol 91: 601-613. DOI: 10.1083/jcb.91.3.601.
- Matsuzaki, Y., N. Katsushima, Y. Nagai, M. Shoji, T. Itagaki, M. Sakamoto, S. Kitaoka, K.
Mizuta and H. Nishimura (2006):
Clinical features of influenza C virus infection in children.
J Infect Dis 193: 1229-1235. DOI: 10.1086/502973.
- McCarthy, K. R., L. J. Rennick, S. Nambulli, L. R. Robinson-McCarthy, W. G. Bain, G.
Haidar and W. P. Duprex (2021):
Recurrent deletions in the SARS-CoV-2 spike glycoprotein drive antibody escape.
Science 371: 1139-1142. DOI: 10.1126/science.abf6950.

- McCullers, J. A. (2016):
The Role of Punctuated Evolution in the Pathogenicity of Influenza Viruses.
Emerging Infections 10: 121-130.
- McIntosh, K., J. H. Dees, W. B. Becker, A. Z. Kapikian and R. M. Chanock (1967):
Recovery in tracheal organ cultures of novel viruses from patients with respiratory disease.
Proc Natl Acad Sci U S A 57: 933-940. DOI: 10.1073/pnas.57.4.933.
- McLean, G., J. Kamil, B. Lee, P. Moore, T. F. Schulz, A. Muik, U. Sahin, O. Tureci and S. Pather (2022):
The Impact of Evolving SARS-CoV-2 Mutations and Variants on COVID-19 Vaccines.
mBio 13: e0297921. DOI: 10.1128/mbio.02979-21.
- Medina, R. A., B. Manicassamy, S. Stertz, C. W. Seibert, R. Hai, R. B. Belshe, S. E. Frey, C. F. Basler, P. Palese and A. Garcia-Sastre (2010):
Pandemic 2009 H1N1 vaccine protects against 1918 Spanish influenza virus.
Nat Commun 1: 28. DOI: 10.1038/ncomms1026.
- Medzhitov, R. and C. Janeway, Jr. (2000):
Innate immunity.
N Engl J Med 343: 338-344. DOI: 10.1056/NEJM200008033430506.
- Meliani, A., F. Boisgerault, Z. Fitzpatrick, S. Marmier, C. Leborgne, F. Collaud, M. Simon Sola, S. Charles, G. Ronzitti, A. Vignaud, L. van Wittenberghe, B. Marolleau, F. Jouen, S. Tan, O. Boyer, O. Christophe, A. R. Brisson, C. A. Maguire and F. Mingozzi (2017):
Enhanced liver gene transfer and evasion of preexisting humoral immunity with exosome-enveloped AAV vectors.
Blood Adv 1: 2019-2031. DOI: 10.1182/bloodadvances.2017010181.
- Memoli, M. J., P. A. Shaw, A. Han, L. Czajkowski, S. Reed, R. Athota, T. Bristol, S. Fargis, K. Risos, J. H. Powers, R. T. Davey, Jr. and J. K. Taubenberger (2016):
Evaluation of Antihemagglutinin and Antineuraminidase Antibodies as Correlates of Protection in an Influenza A/H1N1 Virus Healthy Human Challenge Model.
mBio 7: e00417-00416. DOI: 10.1128/mBio.00417-16.
- Meng, B., S. A. Kemp, G. Papa, R. Datir, I. Ferreira, S. Marelli, W. T. Harvey, S. Lytras, A. Mohamed, G. Gallo, N. Thakur, D. A. Collier, P. Mlcochova, C.-G. U. Consortium, L. M. Duncan, A. M. Carabelli, J. C. Kenyon, A. M. Lever, A. De Marco, C. Saliba, K. Culap, E. Cameroni, N. J. Matheson, L. Piccoli, D. Corti, L. C. James, D. L. Robertson, D. Bailey and R. K. Gupta (2021):
Recurrent emergence of SARS-CoV-2 spike deletion H69/V70 and its role in the Alpha variant B.1.1.7.
Cell Rep 35: 109292. DOI: 10.1016/j.celrep.2021.109292.
- Merad, M., C. A. Blish, F. Sallusto and A. Iwasaki (2022):
The immunology and immunopathology of COVID-19.
Science 375: 1122-1127. DOI: 10.1126/science.abm8108.
- Mills, C. D., K. Kincaid, J. M. Alt, M. J. Heilman and A. M. Hill (2000):
M-1/M-2 macrophages and the Th1/Th2 paradigm.
J Immunol 164: 6166-6173. DOI: 10.4049/jimmunol.164.12.6166.
- Minskaia, E., T. Hertzog, A. E. Gorbalenya, V. Campanacci, C. Cambillau, B. Canard and J. Ziebuhr (2006):

Discovery of an RNA virus 3'->5' exoribonuclease that is critically involved in coronavirus RNA synthesis.

Proc Natl Acad Sci U S A 103: 5108-5113. DOI: 10.1073/pnas.0508200103.

Mitchell, M., H. J. Nam, A. Carter, A. McCall, C. Rence, A. Bennett, B. Gurda, R. McKenna, M. Porter, Y. Sakai, B. J. Byrne, N. Muzyczka, G. Aslanidi, S. Zolotukhin and M. Agbandje-McKenna (2009):

Production, purification and preliminary X-ray crystallographic studies of adeno-associated virus serotype 9.

Acta Crystallogr Sect F Struct Biol Cryst Commun 65: 715-718. DOI: 10.1107/S1744309109021460.

Monto, A. S., J. G. Petrie, R. T. Cross, E. Johnson, M. Liu, W. Zhong, M. Levine, J. M. Katz and S. E. Ohmit (2015):

Antibody to Influenza Virus Neuraminidase: An Independent Correlate of Protection.

J Infect Dis 212: 1191-1199. DOI: 10.1093/infdis/jiv195.

Morens, D. M., J. K. Taubenberger and A. S. Fauci (2023):

Rethinking next-generation vaccines for coronaviruses, influenzaviruses, and other respiratory viruses.

Cell Host Microbe 31: 146-157. DOI: 10.1016/j.chom.2022.11.016.

Moritzky, S. A., K. A. Richards, M. A. Glover, F. Krammer, F. A. Chaves, D. J. Topham, A. Branche, J. L. Nayak and A. J. Sant (2023):

The Negative Effect of Preexisting Immunity on Influenza Vaccine Responses Transcends the Impact of Vaccine Formulation Type and Vaccination History.

J Infect Dis 227: 381-390. DOI: 10.1093/infdis/jiac068.

Moriyama, M., C. Lucas, V. S. Monteiro, S.-C.-G. S. I. Yale and A. Iwasaki (2023):

Enhanced inhibition of MHC-I expression by SARS-CoV-2 Omicron subvariants.

Proc Natl Acad Sci U S A 120: e2221652120. DOI: 10.1073/pnas.2221652120.

Muecksch, F., H. Wise, B. Batchelor, M. Squires, E. Semple, C. Richardson, J. McGuire, S. Clearly, E. Furrer, N. Greig, G. Hay, K. Templeton, J. C. C. Lorenzi, T. Hatziioannou, S. Jenks and P. D. Bieniasz (2021):

Longitudinal Serological Analysis and Neutralizing Antibody Levels in Coronavirus Disease 2019 Convalescent Patients.

J Infect Dis 223: 389-398. DOI: 10.1093/infdis/jiaa659.

Muik, A., B. G. Lui, M. Bacher, A. K. Wallisch, A. Toker, C. I. C. Couto, A. Guler, V. Mampilli, G. J. Schmitt, J. Mottl, T. Ziegenhals, S. Fesser, J. Reinholz, F. Wernig, K. G. Schraut, H. Hefesha, H. Cai, Q. Yang, K. C. Walzer, J. Grosser, S. Strauss, A. Finlayson, K. Kruger, O. Ozhelvaci, K. Grikscheit, N. Kohmer, S. Ciesek, K. A. Swanson, A. B. Vogel, O. Tureci and U. Sahin (2022a):

Exposure to BA.4/5 S protein drives neutralization of Omicron BA.1, BA.2, BA.2.12.1, and BA.4/5 in vaccine-experienced humans and mice.

Sci Immunol 7: eade9888. DOI: 10.1126/sciimmunol.ade9888.

Muik, A., B. G. Lui, A. K. Wallisch, M. Bacher, J. Muhl, J. Reinholz, O. Ozhelvaci, N. Beckmann, R. C. Guimil Garcia, A. Poran, S. Shpyro, A. Finlayson, H. Cai, Q. Yang, K. A. Swanson, O. Tureci and U. Sahin (2022b):

Neutralization of SARS-CoV-2 Omicron by BNT162b2 mRNA vaccine-elicited human sera. Science 375: 678-680. DOI: 10.1126/science.abn7591.

Mukherjee, S., D. Bhattacharyya and A. Bhunia (2020):

Host-membrane interacting interface of the SARS coronavirus envelope protein: Immense functional potential of C-terminal domain.

Biophys Chem 266: 106452. DOI: 10.1016/j.bpc.2020.106452.

Muzio, M., N. Polentarutti, D. Bosisio, M. K. Prahladan and A. Mantovani (2000):

Toll-like receptors: a growing family of immune receptors that are differentially expressed and regulated by different leukocytes.

J Leukoc Biol 67: 450-456. DOI: 10.1002/jlb.67.4.450.

Muzyczka, N. and K. Berns (2001):

Fields Virology, edited by DM Knipe & PM Howley, New York: Lippincott, Williams and Wilkins.

Nakatsu, S., S. Murakami, K. Shindo, T. Horimoto, H. Sagara, T. Noda and Y. Kawaoka (2018):

Influenza C and D Viruses Package Eight Organized Ribonucleoprotein Complexes.

J Virol 92. DOI: 10.1128/JVI.02084-17.

Naso, M. F., B. Tomkowicz, W. L. Perry, 3rd and W. R. Strohl (2017):

Adeno-Associated Virus (AAV) as a Vector for Gene Therapy.

BioDrugs 31: 317-334. DOI: 10.1007/s40259-017-0234-5.

Naumer, M., F. Sonntag, K. Schmidt, K. Nieto, C. Panke, N. E. Davey, R. Popa-Wagner and J. A. Kleinschmidt (2012):

Properties of the adeno-associated virus assembly-activating protein.

J Virol 86: 13038-13048. DOI: 10.1128/JVI.01675-12.

NCBI. (2023, 2023).

Influenza Virus Resource.

Retrieved 25.08., 2023, from <https://www.ncbi.nlm.nih.gov/genomes/FLU/Database/nph-select.cgi?go=3>.

Nerome, R., Y. Hiromoto, S. Sugita, N. Tanabe, M. Ishida, M. Matsumoto, S. E. Lindstrom, T. Takahashi and K. Nerome (1998):

Evolutionary characteristics of influenza B virus since its first isolation in 1940: dynamic circulation of deletion and insertion mechanism.

Arch Virol 143: 1569-1583. DOI: 10.1007/s007050050399.

Neumann, G., M. T. Hughes and Y. Kawaoka (2000):

Influenza A virus NS2 protein mediates vRNP nuclear export through NES-independent interaction with hCRM1.

EMBO J 19: 6751-6758. DOI: 10.1093/emboj/19.24.6751.

Nextstrain. (2022, 10.09.2022).

Genomic epidemiology of SARS-CoV-2 with subsampling focused globally over the past 6 months.

Retrieved 25.08., 2022, from <https://nextstrain.org/ncov/gisaid/global/6m>.

Nguyen, T. Q., R. Rollon and Y. K. Choi (2021):

Animal Models for Influenza Research: Strengths and Weaknesses.

Viruses 13. DOI: 10.3390/v13061011.

Nicolson, S. C. and R. J. Samulski (2014):

Recombinant adeno-associated virus utilizes host cell nuclear import machinery to enter the nucleus.

J Virol 88: 4132-4144. DOI: 10.1128/JVI.02660-13.

Nieto, K. and A. Salvetti (2014):
AAV Vectors Vaccines Against Infectious Diseases.
Front Immunol 5: 5. DOI: 10.3389/fimmu.2014.00005.

Nimmerjahn, F. and J. V. Ravetch (2008):
Fcγ receptors as regulators of immune responses.
Nat Rev Immunol 8: 34-47. DOI: 10.1038/nri2206.

Noda, T. (2011):
Native morphology of influenza virions.
Front Microbiol 2: 269. DOI: 10.3389/fmicb.2011.00269.

Noda, T., H. Sagara, A. Yen, A. Takada, H. Kida, R. H. Cheng and Y. Kawaoka (2006):
Architecture of ribonucleoprotein complexes in influenza A virus particles.
Nature 439: 490-492. DOI: 10.1038/nature04378.

Nouailles, G., J. M. Adler, P. Pennitz, S. Peidli, L. G. Teixeira Alves, M. Baumgardt, J. Bushe, A. Voss, A. Langenhagen, C. Langner, R. Martin Vidal, F. Pott, J. Kazmierski, A. Ebenig, M. V. Lange, M. D. Muhlebach, C. Goekeri, S. Simmons, N. Xing, A. Abdelgawad, S. Herwig, G. Cichon, D. Niemeyer, C. Drosten, C. Goffinet, M. Landthaler, N. Bluthgen, H. Wu, M. Witznath, A. D. Gruber, S. D. Praktijnjo, N. Osterrieder, E. Wyler, D. Kunec and J. Trimpert (2023):
Live-attenuated vaccine sCPD9 elicits superior mucosal and systemic immunity to SARS-CoV-2 variants in hamsters.
Nat Microbiol. DOI: 10.1038/s41564-023-01352-8.

Ohmit, S. E., J. G. Petrie, R. T. Cross, E. Johnson and A. S. Monto (2011):
Influenza hemagglutination-inhibition antibody titer as a correlate of vaccine-induced protection.
J Infect Dis 204: 1879-1885. DOI: 10.1093/infdis/jir661.

Ohmit, S. E., J. C. Victor, J. R. Rotthoff, E. R. Teich, R. K. Truscon, L. L. Baum, B. Rangarajan, D. W. Newton, M. L. Boulton and A. S. Monto (2006):
Prevention of antigenically drifted influenza by inactivated and live attenuated vaccines.
N Engl J Med 355: 2513-2522. DOI: 10.1056/NEJMoa061850.

Okuno, Y., Y. Isegawa, F. Sasao and S. Ueda (1993):
A common neutralizing epitope conserved between the hemagglutinins of influenza A virus H1 and H2 strains.
J Virol 67: 2552-2558. DOI: 10.1128/JVI.67.5.2552-2558.1993.

Opitz, B., A. Rejaibi, B. Dauber, J. Eckhard, M. Vinzing, B. Schmeck, S. Hippenstiel, N. Suttorp and T. Wolff (2007):
IFNβ induction by influenza A virus is mediated by RIG-I which is regulated by the viral NS1 protein.
Cell Microbiol 9: 930-938. DOI: 10.1111/j.1462-5822.2006.00841.x.

Oran, D. P. and E. J. Topol (2020):
Prevalence of Asymptomatic SARS-CoV-2 Infection : A Narrative Review.
Ann Intern Med 173: 362-367. DOI: 10.7326/M20-3012.

Osterhaus, A. D., G. F. Rimmelzwaan, B. E. Martina, T. M. Bestebroer and R. A. Fouchier (2000):

Influenza B virus in seals.

Science 288: 1051-1053. DOI: 10.1126/science.288.5468.1051.

Palese, P. (2004):

Influenza: old and new threats.

Nat Med 10: S82-87. DOI: 10.1038/nm1141.

Palese, P., K. Tobita, M. Ueda and R. W. Compans (1974):

Characterization of temperature sensitive influenza virus mutants defective in neuraminidase.

Virology 61: 397-410. DOI: 10.1016/0042-6822(74)90276-1.

Parham, P. (2015):

The Immune System.

New York, Garland Science, Taylor & Francis Group, LLC.

Parkin, J. and B. Cohen (2001):

An overview of the immune system.

Lancet 357: 1777-1789. DOI: 10.1016/S0140-6736(00)04904-7.

Patel, R., M. Kaki, V. S. Potluri, P. Kahar and D. Khanna (2022):

A comprehensive review of SARS-CoV-2 vaccines: Pfizer, Moderna & Johnson & Johnson.

Hum Vaccin Immunother 18: 2002083. DOI: 10.1080/21645515.2021.2002083.

Paul-Ehrlich-Institut. (2022, 13.04.2022).

Zusammensetzung der Influenza-Virus-Impfstoffe für die Saison 2022/2023.

Sai-so-na-le In-flu-enza-Impf-stof-fe Retrieved 25.08., 2023.

Paules, C. and K. Subbarao (2017):

Influenza.

Lancet 390: 697-708. DOI: 10.1016/S0140-6736(17)30129-0.

Paules, C. I., H. D. Marston, R. W. Eisinger, D. Baltimore and A. S. Fauci (2017):

The Pathway to a Universal Influenza Vaccine.

Immunity 47: 599-603. DOI: 10.1016/j.immuni.2017.09.007.

Paules, C. I., S. G. Sullivan, K. Subbarao and A. S. Fauci (2018):

Chasing Seasonal Influenza - The Need for a Universal Influenza Vaccine.

N Engl J Med 378: 7-9. DOI: 10.1056/NEJMp1714916.

Peacock, T. P., D. H. Goldhill, J. Zhou, L. Baillon, R. Frise, O. C. Swann, R. Kugathasan, R. Penn, J. C. Brown, R. Y. Sanchez-David, L. Braga, M. K. Williamson, J. A. Hassard, E. Staller, B. Hanley, M. Osborn, M. Giacca, A. D. Davidson, D. A. Matthews and W. S. Barclay (2021):

The furin cleavage site in the SARS-CoV-2 spike protein is required for transmission in ferrets.

Nat Microbiol 6: 899-909. DOI: 10.1038/s41564-021-00908-w.

Peacock, T. P., C. M. Sheppard, E. Staller and W. S. Barclay (2019):

Host Determinants of Influenza RNA Synthesis.

Annu Rev Virol 6: 215-233. DOI: 10.1146/annurev-virology-092917-043339.

PEI. (2023, 15.04.2023).

Archiv "Saisonale Influenza Impfstoffe).

Retrieved 25.08., 2023, from <https://www.pei.de/DE/Arzneimittel/Impfstoffe/Influenza-grippe/influenza-node.html>.

Pekar, J. E., A. Magee, E. Parker, N. Moshiri, K. Izhikevich, J. L. Havens, K. Gangavarapu, L. M. Malpica Serrano, A. Crits-Christoph, N. L. Matteson, M. Zeller, J. I. Levy, J. C. Wang, S. Hughes, J. Lee, H. Park, M. S. Park, K. Ching Zi Yan, R. T. P. Lin, M. N. Mat Isa, Y. M. Noor, T. I. Vasylyeva, R. F. Garry, E. C. Holmes, A. Rambaut, M. A. Suchard, K. G. Andersen, M. Worobey and J. O. Wertheim (2022):
The molecular epidemiology of multiple zoonotic origins of SARS-CoV-2.
Science 377: 960-966. DOI: 10.1126/science.abp8337.

Perabo, L., D. Goldnau, K. White, J. Endell, J. Boucas, S. Humme, L. M. Work, H. Janicki, M. Hallek, A. H. Baker and H. Buning (2006):
Heparan sulfate proteoglycan binding properties of adeno-associated virus retargeting mutants and consequences for their in vivo tropism.
J Virol 80: 7265-7269. DOI: 10.1128/JVI.00076-06.

Piccoli, L., Y. J. Park, M. A. Tortorici, N. Czudnochowski, A. C. Walls, M. Beltramello, C. Silacci-Fregni, D. Pinto, L. E. Rosen, J. E. Bowen, O. J. Acton, S. Jaconi, B. Guarino, A. Minola, F. Zatta, N. Sprugasci, J. Bassi, A. Peter, A. De Marco, J. C. Nix, F. Mele, S. Jovic, B. F. Rodriguez, S. V. Gupta, F. Jin, G. Piumatti, G. Lo Presti, A. F. Pellanda, M. Biggiogero, M. Tarkowski, M. S. Pizzuto, E. Camerini, C. Havenar-Daughton, M. Smithey, D. Hong, V. Lepori, E. Albanese, A. Ceschi, E. Bernasconi, L. Elzi, P. Ferrari, C. Garzoni, A. Riva, G. Snell, F. Sallusto, K. Fink, H. W. Virgin, A. Lanzavecchia, D. Corti and D. Veasley (2020):
Mapping Neutralizing and Immunodominant Sites on the SARS-CoV-2 Spike Receptor-Binding Domain by Structure-Guided High-Resolution Serology.
Cell 183: 1024-1042 e1021. DOI: 10.1016/j.cell.2020.09.037.

Pillay, S., N. L. Meyer, A. S. Puschnik, O. Davulcu, J. Diep, Y. Ishikawa, L. T. Jae, J. E. Wosen, C. M. Nagamine, M. S. Chapman and J. E. Carette (2016):
An essential receptor for adeno-associated virus infection.
Nature 530: 108-112. DOI: 10.1038/nature16465.

Pincetic, A., S. Bournazos, D. J. DiLillo, J. Maamary, T. T. Wang, R. Dahan, B. M. Fiebiger and J. V. Ravetch (2014):
Type I and type II Fc receptors regulate innate and adaptive immunity.
Nat Immunol 15: 707-716. DOI: 10.1038/ni.2939.

Pinto, L. H. and R. A. Lamb (2006):
The M2 proton channels of influenza A and B viruses.
J Biol Chem 281: 8997-9000. DOI: 10.1074/jbc.R500020200.

Plante, J. A., Y. Liu, J. Liu, H. Xia, B. A. Johnson, K. G. Lokugamage, X. Zhang, A. E. Muruato, J. Zou, C. R. Fontes-Garfias, D. Mirchandani, D. Scharon, J. P. Bilello, Z. Ku, Z. An, B. Kalveram, A. N. Freiberg, V. D. Menachery, X. Xie, K. S. Plante, S. C. Weaver and P. Y. Shi (2021):
Spike mutation D614G alters SARS-CoV-2 fitness.
Nature 592: 116-121. DOI: 10.1038/s41586-020-2895-3.

Poon, L. L., D. C. Pritlove, E. Fodor and G. G. Brownlee (1999):
Direct evidence that the poly(A) tail of influenza A virus mRNA is synthesized by reiterative copying of a U track in the virion RNA template.
J Virol 73: 3473-3476. DOI: 10.1128/JVI.73.4.3473-3476.1999.

Pramanick, I., N. Sengupta, S. Mishra, S. Pandey, N. Girish, A. Das and S. Dutta (2021):

Conformational flexibility and structural variability of SARS-CoV2 S protein.
Structure 29: 834-845 e835. DOI: 10.1016/j.str.2021.04.006.

Qin, X., S. Li, X. Li, D. Pei, Y. Liu, Y. Ding, L. Liu, H. Bi, X. Shi, Y. Guo, E. Fang, F. Huang, L. Yu, L. Zhu, Y. An, C. A. Valencia, Y. Li, B. Dong and Y. Zhou (2022):
Development of an Adeno-Associated Virus-Vectored SARS-CoV-2 Vaccine and Its Immunogenicity in Mice.
Front Cell Infect Microbiol 12: 802147. DOI: 10.3389/fcimb.2022.802147.

Qing, K., C. Mah, J. Hansen, S. Zhou, V. Dwarki and A. Srivastava (1999):
Human fibroblast growth factor receptor 1 is a co-receptor for infection by adeno-associated virus 2.
Nat Med 5: 71-77. DOI: 10.1038/4758.

Rabinowitz, J., Y. K. Chan and R. J. Samulski (2019):
Adeno-associated Virus (AAV) versus Immune Response.
Viruses 11. DOI: 10.3390/v11020102.

Rajendran, M., R. Nachbagauer, M. E. Ermler, P. Bunduc, F. Amanat, R. Izikson, M. Cox, P. Palese, M. Eichelberger and F. Krammer (2017):
Analysis of Anti-Influenza Virus Neuraminidase Antibodies in Children, Adults, and the Elderly by ELISA and Enzyme Inhibition: Evidence for Original Antigenic Sin.
mBio 8. DOI: 10.1128/mBio.02281-16.

Rambaut, A., E. C. Holmes, A. O'Toole, V. Hill, J. T. McCrone, C. Ruis, L. du Plessis and O. G. Pybus (2020a):
A dynamic nomenclature proposal for SARS-CoV-2 lineages to assist genomic epidemiology.
Nat Microbiol 5: 1403-1407. DOI: 10.1038/s41564-020-0770-5.

Rambaut, A., N. Loman, O. Pybus, W. Barclay, J. Barrett, A. Carabelli, T. Connor, T. Peacock, D. L. Robertson and E. Volz. (2020b, 19.12.2020).
Preliminary genomic characterisation of an emergent SARS-CoV-2 lineage in the UK defined by a novel set of spike mutations.
on behalf of COVID-19 Genomics Consortium UK (CoG-UK) Retrieved 25.08., 2023, from <https://virological.org/t/preliminary-genomic-characterisation-of-an-emergent-sars-cov-2-lineage-in-the-uk-defined-by-a-novel-set-of-spike-mutations/563>.

Rangel-Moreno, J., D. M. Carragher, R. S. Misra, K. Kusser, L. Hartson, A. Moquin, F. E. Lund and T. D. Randall (2008):
B cells promote resistance to heterosubtypic strains of influenza via multiple mechanisms.
J Immunol 180: 454-463. DOI: 10.4049/jimmunol.180.1.454.

Rapti, K., V. Louis-Jeune, E. Kohlbrenner, K. Ishikawa, D. Ladage, S. Zolotukhin, R. J. Hajjar and T. Weber (2012):
Neutralizing antibodies against AAV serotypes 1, 2, 6, and 9 in sera of commonly used animal models.
Mol Ther 20: 73-83. DOI: 10.1038/mt.2011.177.

Rawle, F. C., B. B. Knowles, R. P. Ricciardi, V. Brahmacheri, P. Duerksen-Hughes, W. S. Wold and L. R. Gooding (1991):
Specificity of the mouse cytotoxic T lymphocyte response to adenovirus 5. E1A is immunodominant in H-2b, but not in H-2d or H-2k mice.
J Immunol 146: 3977-3984.

Raymond, D. D., S. M. Stewart, J. Lee, J. Ferdman, G. Bajic, K. T. Do, M. J. Ernandes, P. Suphaphiphat, E. C. Settembre, P. R. Dormitzer, G. Del Giudice, O. Finco, T. H. Kang, G. C. Ippolito, G. Georgiou, T. B. Kepler, B. F. Haynes, M. A. Moody, H. X. Liao, A. G. Schmidt and S. C. Harrison (2016):

Influenza immunization elicits antibodies specific for an egg-adapted vaccine strain. *Nat Med* 22: 1465-1469. DOI: 10.1038/nm.4223.

Rehman, S. U., L. Shafique, A. Ihsan and Q. Liu (2020):

Evolutionary Trajectory for the Emergence of Novel Coronavirus SARS-CoV-2. *Pathogens* 9. DOI: 10.3390/pathogens9030240.

Reich, S., D. Guilligay, A. Pflug, H. Malet, I. Berger, T. Crepin, D. Hart, T. Lunardi, M. Nanao, R. W. Ruigrok and S. Cusack (2014):

Structural insight into cap-snatching and RNA synthesis by influenza polymerase. *Nature* 516: 361-366. DOI: 10.1038/nature14009.

Richardson, S. I. and P. L. Moore (2021):

Targeting Fc effector function in vaccine design. *Expert Opin Ther Targets* 25: 467-477. DOI: 10.1080/14728222.2021.1907343.

Riera Romo, M., D. Perez-Martinez and C. Castillo Ferrer (2016):

Innate immunity in vertebrates: an overview. *Immunology* 148: 125-139. DOI: 10.1111/imm.12597.

RKI. (2021, 30.03.2021).

Pressemitteilung der STIKO zum AstraZeneca-Impfstoff (30.03.2021).

Retrieved 25.08., 2023, from <https://www.rki.de/DE/Content/Kommissionen/STIKO/Empfehlungen/AstraZeneca-Impfstoff-2021-03-30.html>.

RKI. (2022, 06.10.2022).

Wissenschaftliche Begründung der STIKO zur Auffrischimpfung von Personen ≥ 12 Jahren mit einem Omikron-BA.1- oder einem Omikron-BA.4/5-adaptierten bivalenten mRNA-Impfstoff.

Retrieved 25.08., 2023, from https://www.rki.de/DE/Content/Infekt/EpidBull/Archiv/2022/40/Art_02.html.

Rogers, G. N. and J. C. Paulson (1983):

Receptor determinants of human and animal influenza virus isolates: differences in receptor specificity of the H3 hemagglutinin based on species of origin.

Virology 127: 361-373. DOI: 10.1016/0042-6822(83)90150-2.

Roltgen, K., S. C. A. Nielsen, O. Silva, S. F. Younes, M. Zaslavsky, C. Costales, F. Yang, O. F. Wirz, D. Solis, R. A. Hoh, A. Wang, P. S. Arunachalam, D. Colburg, S. Zhao, E. Haraguchi, A. S. Lee, M. M. Shah, M. Manohar, I. Chang, F. Gao, V. Mallajosyula, C. Li, J. Liu, M. J. Shoura, S. B. Sindher, E. Parsons, N. J. Dashdorj, N. D. Dashdorj, R. Monroe, G. E. Serrano, T. G. Beach, R. S. Chinthrajah, G. W. Charville, J. L. Wilbur, J. N. Wohlstadter, M. M. Davis, B. Pulendran, M. L. Troxell, G. B. Sigal, Y. Natkunam, B. A. Pinsky, K. C. Nadeau and S. D. Boyd (2022):

Immune imprinting, breadth of variant recognition, and germinal center response in human SARS-CoV-2 infection and vaccination.

Cell 185: 1025-1040 e1014. DOI: 10.1016/j.cell.2022.01.018.

Romagnani, S. (1999):

Th1/Th2 cells.

Inflamm Bowel Dis 5: 285-294. DOI: 10.1097/00054725-199911000-00009.

Rosales, C. and E. Uribe-Querol (2013):

Fc receptors: Cell activators of antibody functions.

Advances in Bioscience and Biotechnology Vol.04No.04: 13. DOI: 10.4236/abb.2013.44A004.

Rossler, A., A. Netzl, L. Knabl, H. Schafer, S. H. Wilks, D. Bante, B. Falkensammer, W. Borena, D. von Laer, D. J. Smith and J. Kimpel (2022):

BA.2 and BA.5 omicron differ immunologically from both BA.1 omicron and pre-omicron variants.

Nat Commun 13: 7701. DOI: 10.1038/s41467-022-35312-3.

Rossman, J. S. and R. A. Lamb (2011):

Influenza virus assembly and budding.

Virology 411: 229-236. DOI: 10.1016/j.virol.2010.12.003.

Rota, P. A., T. R. Wallis, M. W. Harmon, J. S. Rota, A. P. Kendal and K. Nerome (1990):

Cocirculation of two distinct evolutionary lineages of influenza type B virus since 1983.

Virology 175: 59-68. DOI: [https://doi.org/10.1016/0042-6822\(90\)90186-U](https://doi.org/10.1016/0042-6822(90)90186-U).

Rotshild, V., B. Hirsh-Racah, I. Miskin, M. Muszkat and I. Matok (2021):

Comparing the clinical efficacy of COVID-19 vaccines: a systematic review and network meta-analysis.

Sci Rep 11: 22777. DOI: 10.1038/s41598-021-02321-z.

Roubidoux, E. K. and S. Schultz-Cherry (2021):

Animal Models Utilized for the Development of Influenza Virus Vaccines.

Vaccines (Basel) 9. DOI: 10.3390/vaccines9070787.

Routhu, N. K., N. Cheedarla, V. S. Bollimpelli, S. Gangadhara, V. V. Edara, L. Lai, A. Sahoo, A. Shiferaw, T. M. Styles, K. Floyd, S. Fischinger, C. Atyeo, S. A. Shin, S. Gumber, S. Kirejczyk, K. H. Dinno, 3rd, P. Y. Shi, V. D. Menachery, M. Tomai, C. B. Fox, G. Alter, T. H. Vanderford, L. Gralinski, M. S. Suthar and R. R. Amara (2021):

SARS-CoV-2 RBD trimer protein adjuvanted with Alum-3M-052 protects from SARS-CoV-2 infection and immune pathology in the lung.

Nat Commun 12: 3587. DOI: 10.1038/s41467-021-23942-y.

Rutigliano, J. A., S. Sharma, M. Y. Morris, T. H. Oguin, 3rd, J. L. McClaren, P. C. Doherty and P. G. Thomas (2014):

Highly pathological influenza A virus infection is associated with augmented expression of PD-1 by functionally compromised virus-specific CD8⁺ T cells.

J Virol 88: 1636-1651. DOI: 10.1128/JVI.02851-13.

Rydzynski Moderbacher, C., S. I. Ramirez, J. M. Dan, A. Grifoni, K. M. Hastie, D. Weiskopf, S. Belanger, R. K. Abbott, C. Kim, J. Choi, Y. Kato, E. G. Crotty, C. Kim, S. A. Rawlings, J. Mateus, L. P. V. Tse, A. Frazier, R. Baric, B. Peters, J. Greenbaum, E. Ollmann Saphire, D. M. Smith, A. Sette and S. Crotty (2020):

Antigen-Specific Adaptive Immunity to SARS-CoV-2 in Acute COVID-19 and Associations with Age and Disease Severity.

Cell 183: 996-1012 e1019. DOI: 10.1016/j.cell.2020.09.038.

Sahin, U., A. Muik, I. Vogler, E. Derhovanessian, L. M. Kranz, M. Vormehr, J. Quandt, N. Bidmon, A. Ulges, A. Baum, K. E. Pascal, D. Maurus, S. Brachtendorf, V. Lorks, J. Sikorski, P. Koch, R. Hilker, D. Becker, A. K. Eller, J. Grutzner, M. Tonigold, C. Boesler, C.

Rosenbaum, L. Heesen, M. C. Kuhnle, A. Poran, J. Z. Dong, U. Luxemburger, A. Kemmer-Bruck, D. Langer, M. Bexon, S. Bolte, T. Palanche, A. Schultz, S. Baumann, A. J. Mahiny, G. Boros, J. Reinholz, G. T. Szabo, K. Kariko, P. Y. Shi, C. Fontes-Garfias, J. L. Perez, M. Cutler, D. Cooper, C. A. Kyratsous, P. R. Dormitzer, K. U. Jansen and O. Tureci (2021): BNT162b2 vaccine induces neutralizing antibodies and poly-specific T cells in humans. *Nature* 595: 572-577. DOI: 10.1038/s41586-021-03653-6.

Samulski, R. J., L. S. Chang and T. Shenk (1987):
A recombinant plasmid from which an infectious adeno-associated virus genome can be excised in vitro and its use to study viral replication.
J Virol 61: 3096-3101. DOI: 10.1128/JVI.61.10.3096-3101.1987.

Samulski, R. J. and N. Muzyczka (2014):
AAV-Mediated Gene Therapy for Research and Therapeutic Purposes.
Annu Rev Virol 1: 427-451. DOI: 10.1146/annurev-virology-031413-085355.

Sant'Anna, T. B. and N. M. Araujo (2022):
Adeno-associated virus infection and its impact in human health: an overview.
Virology 19: 173. DOI: 10.1186/s12985-022-01900-4.

Schepens, B., D. De Vlieger and X. Saelens (2018):
Vaccine options for influenza: thinking small.
Curr Opin Immunol 53: 22-29. DOI: 10.1016/j.coi.2018.03.024.

Schmidt, A. G., M. D. Therkelsen, S. Stewart, T. B. Kepler, H. X. Liao, M. A. Moody, B. F. Haynes and S. C. Harrison (2015):
Viral receptor-binding site antibodies with diverse germline origins.
Cell 161: 1026-1034. DOI: 10.1016/j.cell.2015.04.028.

Scholey, J., J. M. Aburto, I. Kashnitsky, M. S. Kniffka, L. Zhang, H. Jaadla, J. B. Dowd and R. Kashyap (2022):
Life expectancy changes since COVID-19.
Nat Hum Behav 6: 1649-1659. DOI: 10.1038/s41562-022-01450-3.

Sederdahl, B. K. and J. V. Williams (2020):
Epidemiology and Clinical Characteristics of Influenza C Virus.
Viruses 12. DOI: 10.3390/v12010089.

Sekine, T., A. Perez-Potti, O. Rivera-Ballesteros, K. Stralin, J. B. Gorin, A. Olsson, S. Llewellyn-Lacey, H. Kamal, G. Bogdanovic, S. Muschiol, D. J. Wullimann, T. Kammann, J. Emgard, T. Parrot, E. Folkesson, C.-S. G. Karolinska, O. Rooyackers, L. I. Eriksson, J. I. Henter, A. Sonnerborg, T. Allander, J. Albert, M. Nielsen, J. Klingstrom, S. Gredmark-Russ, N. K. Bjorkstrom, J. K. Sandberg, D. A. Price, H. G. Ljunggren, S. Aleman and M. Buggert (2020):
Robust T Cell Immunity in Convalescent Individuals with Asymptomatic or Mild COVID-19.
Cell 183: 158-168 e114. DOI: 10.1016/j.cell.2020.08.017.

Senior, M. (2017):
After Glybera's withdrawal, what's next for gene therapy?
Nat Biotechnol 35: 491-492. DOI: 10.1038/nbt0617-491.

Sette, A. and S. Crotty (2021):
Adaptive immunity to SARS-CoV-2 and COVID-19.
Cell 184: 861-880. DOI: 10.1016/j.cell.2021.01.007.

- Shafqat, A., M. H. Omer, O. Ahmad, M. Niaz, H. S. Abdulkader, S. Shafqat, A. H. Mushtaq, A. Shaik, A. N. Elshaer, J. Kashir, K. Alkattan and A. Yaqinuddin (2022): SARS-CoV-2 epitopes inform future vaccination strategies. *Front Immunol* 13: 1041185. DOI: 10.3389/fimmu.2022.1041185.
- Sharma, J. M. (1997): The structure and function of the avian immune system. *Acta Vet Hung* 45: 229-238.
- Shinya, K., M. Ebina, S. Yamada, M. Ono, N. Kasai and Y. Kawaoka (2006): Avian flu: influenza virus receptors in the human airway. *Nature* 440: 435-436. DOI: 10.1038/440435a.
- Sipo, I., M. Knauf, H. Fechner, W. Poller, O. Planz, R. Kurth and S. Norley (2011): Vaccine protection against lethal homologous and heterologous challenge using recombinant AAV vectors expressing codon-optimized genes from pandemic swine origin influenza virus (SOIV). *Vaccine* 29: 1690-1699. DOI: 10.1016/j.vaccine.2010.12.037.
- Siu, Y. L., K. T. Teoh, J. Lo, C. M. Chan, F. Kien, N. Escriou, S. W. Tsao, J. M. Nicholls, R. Altmeyer, J. S. Peiris, R. Bruzzone and B. Nal (2008): The M, E, and N structural proteins of the severe acute respiratory syndrome coronavirus are required for efficient assembly, trafficking, and release of virus-like particles. *J Virol* 82: 11318-11330. DOI: 10.1128/JVI.01052-08.
- Smith, G. L., J. Z. Levin, P. Palese and B. Moss (1987): Synthesis and cellular location of the ten influenza polypeptides individually expressed by recombinant vaccinia viruses. *Virology* 160: 336-345. DOI: 10.1016/0042-6822(87)90004-3.
- Smith, K. F., M. Goldberg, S. Rosenthal, L. Carlson, J. Chen, C. Chen and S. Ramachandran (2014): Global rise in human infectious disease outbreaks. *J R Soc Interface* 11: 20140950. DOI: 10.1098/rsif.2014.0950.
- Sobhanie, M., Y. Matsuoka, S. Jegaskanda, T. Fitzgerald, R. Mallory, Z. Chen, C. Luke, J. Treanor and K. Subbarao (2016): Evaluation of the Safety and Immunogenicity of a Candidate Pandemic Live Attenuated Influenza Vaccine (pLAIV) Against Influenza A(H7N9). *J Infect Dis* 213: 922-929. DOI: 10.1093/infdis/jiv526.
- Soema, P. C., R. Kompier, J. P. Amorij and G. F. Kersten (2015): Current and next generation influenza vaccines: Formulation and production strategies. *Eur J Pharm Biopharm* 94: 251-263. DOI: 10.1016/j.ejpb.2015.05.023.
- Sondermann, P., A. Pincetic, J. Maamary, K. Lammens and J. V. Ravetch (2013): General mechanism for modulating immunoglobulin effector function. *Proc Natl Acad Sci U S A* 110: 9868-9872. DOI: 10.1073/pnas.1307864110.
- Song, P., W. Li, J. Xie, Y. Hou and C. You (2020): Cytokine storm induced by SARS-CoV-2. *Clin Chim Acta* 509: 280-287. DOI: 10.1016/j.cca.2020.06.017.
- Sonntag, F., K. Schmidt and J. A. Kleinschmidt (2010): A viral assembly factor promotes AAV2 capsid formation in the nucleolus.

Proc Natl Acad Sci U S A 107: 10220-10225. DOI: 10.1073/pnas.1001673107.

Spangrude, G. J., S. Heimfeld and I. L. Weissman (1988):
Purification and characterization of mouse hematopoietic stem cells.
Science 241: 58-62. DOI: 10.1126/science.2898810.

Srivastava, A., E. W. Lusby and K. I. Berns (1983):
Nucleotide sequence and organization of the adeno-associated virus 2 genome.
J Virol 45: 555-564. DOI: 10.1128/JVI.45.2.555-564.1983.

Srivastava, B., P. Blazejewska, M. Hessmann, D. Bruder, R. Geffers, S. Mael, A. D. Gruber and K. Schughart (2009):
Host genetic background strongly influences the response to influenza a virus infections.
PLoS One 4: e4857. DOI: 10.1371/journal.pone.0004857.

Staheli, P., O. Haller, W. Boll, J. Lindenmann and C. Weissmann (1986):
Mx protein: constitutive expression in 3T3 cells transformed with cloned Mx cDNA confers selective resistance to influenza virus.
Cell 44: 147-158. DOI: 10.1016/0092-8674(86)90493-9.

Starr, T. N., A. J. Greaney, S. K. Hilton, D. Ellis, K. H. D. Crawford, A. S. Dingens, M. J. Navarro, J. E. Bowen, M. A. Tortorici, A. C. Walls, N. P. King, D. Veasley and J. D. Bloom (2020):
Deep Mutational Scanning of SARS-CoV-2 Receptor Binding Domain Reveals Constraints on Folding and ACE2 Binding.
Cell 182: 1295-1310 e1220. DOI: 10.1016/j.cell.2020.08.012.

Steinhauer, D. A. (1999):
Role of hemagglutinin cleavage for the pathogenicity of influenza virus.
Virology 258: 1-20. DOI: 10.1006/viro.1999.9716.

Stieneke-Grober, A., M. Vey, H. Angliker, E. Shaw, G. Thomas, C. Roberts, H. D. Klenk and W. Garten (1992):
Influenza virus hemagglutinin with multibasic cleavage site is activated by furin, a subtilisin-like endoprotease.
EMBO J 11: 2407-2414. DOI: 10.1002/j.1460-2075.1992.tb05305.x.

R. K. Institut (2018):
Wissenschaftliche Begründung für die Empfehlung des quadrivalenten saisonalen Influenzaimpfstoffs, 2/2018
Epidemiologisches Bulletin, 19-28

Strobel, B., F. D. Miller, W. Rist and T. Lamla (2015):
Comparative Analysis of Cesium Chloride- and Iodixanol-Based Purification of Recombinant Adeno-Associated Viral Vectors for Preclinical Applications.
Hum Gene Ther Methods 26: 147-157. DOI: 10.1089/hgtb.2015.051.

Su, S., X. Fu, G. Li, F. Kerlin and M. Veit (2017):
Novel Influenza D virus: Epidemiology, pathology, evolution and biological characteristics.
Virulence 8: 1580-1591. DOI: 10.1080/21505594.2017.1365216.

Su, S., G. Wong, W. Shi, J. Liu, A. C. K. Lai, J. Zhou, W. Liu, Y. Bi and G. F. Gao (2016):
Epidemiology, Genetic Recombination, and Pathogenesis of Coronaviruses.
Trends Microbiol 24: 490-502. DOI: 10.1016/j.tim.2016.03.003.

- Summerford, C., J. S. Bartlett and R. J. Samulski (1999):
AlphaVbeta5 integrin: a co-receptor for adeno-associated virus type 2 infection.
Nat Med 5: 78-82. DOI: 10.1038/4768.
- Summerford, C. and R. J. Samulski (1998):
Membrane-associated heparan sulfate proteoglycan is a receptor for adeno-associated virus type 2 virions.
J Virol 72: 1438-1445. DOI: 10.1128/JVI.72.2.1438-1445.1998.
- Suzuki, T., A. Kawaguchi, A. Aina, S. Tamura, R. Ito, P. Multihartina, V. Setiawaty, K. N. Pangesti, T. Odagiri, M. Tashiro and H. Hasegawa (2015):
Relationship of the quaternary structure of human secretory IgA to neutralization of influenza virus.
Proc Natl Acad Sci U S A 112: 7809-7814. DOI: 10.1073/pnas.1503885112.
- Tan, G. S., F. Krammer, D. Eggink, A. Kongchanagul, T. M. Moran and P. Palese (2012):
A pan-H1 anti-hemagglutinin monoclonal antibody with potent broad-spectrum efficacy in vivo.
J Virol 86: 6179-6188. DOI: 10.1128/JVI.00469-12.
- Tang, Y. S., S. Xu, Y. W. Chen, J. H. Wang and P. C. Shaw (2021):
Crystal structures of influenza nucleoprotein complexed with nucleic acid provide insights into the mechanism of RNA interaction.
Nucleic Acids Res 49: 4144-4154. DOI: 10.1093/nar/gkab203.
- Tegally, H., E. Wilkinson, M. Giovanetti, A. Iranzadeh, V. Fonseca, J. Giandhari, D. Doolabh, S. Pillay, E. J. San, N. Msomi, K. Mlisana, A. von Gottberg, S. Walaza, M. Allam, A. Ismail, T. Mohale, A. J. Glass, S. Engelbrecht, G. Van Zyl, W. Preiser, F. Petruccione, A. Sigal, D. Hardie, G. Marais, N. Y. Hsiao, S. Korsman, M. A. Davies, L. Tyers, I. Mudau, D. York, C. Maslo, D. Goedhals, S. Abrahams, O. Laguda-Akingba, A. Alisoltani-Dehkordi, A. Godzik, C. K. Wibmer, B. T. Sewell, J. Lourenco, L. C. J. Alcantara, S. L. Kosakovsky Pond, S. Weaver, D. Martin, R. J. Lessells, J. N. Bhiman, C. Williamson and T. de Oliveira (2021):
Detection of a SARS-CoV-2 variant of concern in South Africa.
Nature 592: 438-443. DOI: 10.1038/s41586-021-03402-9.
- Terajima, M., J. Cruz, M. D. Co, J. H. Lee, K. Kaur, J. Wrammert, P. C. Wilson and F. A. Ennis (2011):
Complement-dependent lysis of influenza A virus-infected cells by broadly cross-reactive human monoclonal antibodies.
J Virol 85: 13463-13467. DOI: 10.1128/JVI.05193-11.
- Thompson, A. J., R. P. de Vries and J. C. Paulson (2019):
Virus recognition of glycan receptors.
Curr Opin Virol 34: 117-129. DOI: 10.1016/j.coviro.2019.01.004.
- Thulin, N. K. and T. T. Wang (2018):
The Role of Fc Gamma Receptors in Broad Protection against Influenza Viruses.
Vaccines (Basel) 6. DOI: 10.3390/vaccines6030036.
- Tong, D., M. Zhang, Y. Yang, H. Xia, H. Tong, H. Zhang, W. Zeng, M. Liu, Y. Wu, H. Ma, X. Hu, W. Liu, Y. Cai, Y. Yao, Y. Yao, K. Liu, S. Shan, Y. Li, G. Gao, W. Guo, Y. Peng, S. Chen, J. Rao, J. Zhao, J. Min, Q. Zhu, Y. Zheng, L. Liu, C. Shan, K. Zhong, Z. Qiu, T. Jin, S. Chiu, Z. Yuan and T. Xue (2023):

Single-dose AAV-based vaccine induces a high level of neutralizing antibodies against SARS-CoV-2 in rhesus macaques.

Protein Cell 14: 69-73. DOI: 10.1093/procel/pwac020.

Tong, S., Y. Li, P. Rivaller, C. Conrardy, D. A. Castillo, L. M. Chen, S. Recuenco, J. A. Ellison, C. T. Davis, I. A. York, A. S. Turmelle, D. Moran, S. Rogers, M. Shi, Y. Tao, M. R. Weil, K. Tang, L. A. Rowe, S. Sammons, X. Xu, M. Frace, K. A. Lindblade, N. J. Cox, L. J. Anderson, C. E. Rupprecht and R. O. Donis (2012):

A distinct lineage of influenza A virus from bats.

Proc Natl Acad Sci U S A 109: 4269-4274. DOI: 10.1073/pnas.1116200109.

Tong, S., X. Zhu, Y. Li, M. Shi, J. Zhang, M. Bourgeois, H. Yang, X. Chen, S. Recuenco, J. Gomez, L. M. Chen, A. Johnson, Y. Tao, C. Dreyfus, W. Yu, R. McBride, P. J. Carney, A. T. Gilbert, J. Chang, Z. Guo, C. T. Davis, J. C. Paulson, J. Stevens, C. E. Rupprecht, E. C. Holmes, I. A. Wilson and R. O. Donis (2013):

New world bats harbor diverse influenza A viruses.

PLoS Pathog 9: e1003657. DOI: 10.1371/journal.ppat.1003657.

Tornabene, P. and I. Trapani (2020):

Can Adeno-Associated Viral Vectors Deliver Effectively Large Genes?

Hum Gene Ther 31: 47-56. DOI: 10.1089/hum.2019.220.

Tosh, P. K., T. G. Boyce and G. A. Poland (2008):

Flu myths: dispelling the myths associated with live attenuated influenza vaccine.

Mayo Clin Proc 83: 77-84. DOI: 10.4065/83.1.77.

Trapani, I., P. Colella, A. Sommella, C. Iodice, G. Cesi, S. de Simone, E. Marrocco, S. Rossi, M. Giunti, A. Palfi, G. J. Farrar, R. Polishchuk and A. Auricchio (2014):

Effective delivery of large genes to the retina by dual AAV vectors.

EMBO Mol Med 6: 194-211. DOI: 10.1002/emmm.201302948.

Trempe, J. P. and B. J. Carter (1988):

Alternate mRNA splicing is required for synthesis of adeno-associated virus VP1 capsid protein.

J Virol 62: 3356-3363. DOI: 10.1128/JVI.62.9.3356-3363.1988.

Trimpert, J., D. Vladimirova, K. Dietert, A. Abdelgawad, D. Kunec, S. Dokel, A. Voss, A. D. Gruber, L. D. Bertzbach and N. Osterrieder (2020):

The Roborovski Dwarf Hamster Is A Highly Susceptible Model for a Rapid and Fatal Course of SARS-CoV-2 Infection.

Cell Rep 33: 108488. DOI: 10.1016/j.celrep.2020.108488.

Tumpey, T. M., A. Garcia-Sastre, J. K. Taubenberger, P. Palese, D. E. Swayne, M. J. Pantin-Jackwood, S. Schultz-Cherry, A. Solorzano, N. Van Rooijen, J. M. Katz and C. F. Basler (2005):

Pathogenicity of influenza viruses with genes from the 1918 pandemic virus: functional roles of alveolar macrophages and neutrophils in limiting virus replication and mortality in mice.

J Virol 79: 14933-14944. DOI: 10.1128/JVI.79.23.14933-14944.2005.

Turner, M. D., B. Nedjai, T. Hurst and D. J. Pennington (2014):

Cytokines and chemokines: At the crossroads of cell signalling and inflammatory disease.

Biochim Biophys Acta 1843: 2563-2582. DOI: 10.1016/j.bbamcr.2014.05.014.

Turvey, S. E. and D. H. Broide (2010):

Innate immunity.

J Allergy Clin Immunol 125: S24-32. DOI: 10.1016/j.jaci.2009.07.016.

Tuttle, A. H., V. M. Philip, E. J. Chesler and J. S. Mogil (2018):
Comparing phenotypic variation between inbred and outbred mice.
Nat Methods 15: 994-996. DOI: 10.1038/s41592-018-0224-7.

Uyeki, T. M., D. S. Hui, M. Zambon, D. E. Wentworth and A. S. Monto (2022):
Influenza.
Lancet 400: 693-706. DOI: 10.1016/S0140-6736(22)00982-5.

V'Kovski, P., A. Kratzel, S. Steiner, H. Stalder and V. Thiel (2021):
Coronavirus biology and replication: implications for SARS-CoV-2.
Nat Rev Microbiol 19: 155-170. DOI: 10.1038/s41579-020-00468-6.

Valkenburg, S. A., V. Venturi, T. H. Dang, N. L. Bird, P. C. Doherty, S. J. Turner, M. P. Davenport and K. Kedzierska (2012):
Early priming minimizes the age-related immune compromise of CD8(+) T cell diversity and function.
PLoS Pathog 8: e1002544. DOI: 10.1371/journal.ppat.1002544.

Van den Hoecke, S., K. Ehrhardt, A. Kolpe, K. El Bakkouri, L. Deng, H. Grootaert, S. Schoonoghe, A. Smet, M. Bentahir, K. Roose, M. Schotsaert, B. Schepens, N. Callewaert, F. Nimmerjahn, P. Staeheli, H. Hengel and X. Saelens (2017):
Hierarchical and Redundant Roles of Activating FcγR3s in Protection against Influenza Disease by M2e-Specific IgG1 and IgG2a Antibodies.
J Virol 91. DOI: 10.1128/JVI.02500-16.

van der Hoek, L., K. Pyrc, M. F. Jebbink, W. Vermeulen-Oost, R. J. Berkhout, K. C. Wolthers, P. M. Wertheim-van Dillen, J. Kaandorp, J. Spaargaren and B. Berkhout (2004):
Identification of a new human coronavirus.
Nat Med 10: 368-373. DOI: 10.1038/nm1024.

van Domselaar, R. and N. Bovenschen (2011):
Cell death-independent functions of granzymes: hit viruses where it hurts.
Rev Med Virol 21: 301-314. DOI: 10.1002/rmv.697.

van Riel, D., M. A. den Bakker, L. M. Leijten, S. Chutinimitkul, V. J. Munster, E. de Wit, G. F. Rimmelzwaan, R. A. Fouchier, A. D. Osterhaus and T. Kuiken (2010):
Seasonal and pandemic human influenza viruses attach better to human upper respiratory tract epithelium than avian influenza viruses.
Am J Pathol 176: 1614-1618. DOI: 10.2353/ajpath.2010.090949.

van Riel, D., V. J. Munster, E. de Wit, G. F. Rimmelzwaan, R. A. Fouchier, A. D. Osterhaus and T. Kuiken (2006):
H5N1 Virus Attachment to Lower Respiratory Tract.
Science 312: 399. DOI: 10.1126/science.1125548.

Vance, M. A., A. Mitchell and R. J. Samulski (2015):
AAV Biology, Infectivity and Therapeutic Use from Bench to Clinic.
Gene Therapy - Principles and Challenges. D. Hashad. Rijeka, IntechOpen.

Vanderven, H. A., S. Jegaskanda, B. D. Wines, P. M. Hogarth, S. Carmuglia, S. Rockman, A. W. Chung and S. J. Kent (2017):

Antibody-Dependent Cellular Cytotoxicity Responses to Seasonal Influenza Vaccination in Older Adults.

J Infect Dis 217: 12-23. DOI: 10.1093/infdis/jix554.

Veit, M., M. V. Serebryakova and L. V. Kordyukova (2013):

Palmitoylation of influenza virus proteins.

Biochem Soc Trans 41: 50-55. DOI: 10.1042/BST20120210.

Vidarsson, G., G. Dekkers and T. Rispiens (2014):

IgG subclasses and allotypes: from structure to effector functions.

Front Immunol 5: 520. DOI: 10.3389/fimmu.2014.00520.

Volz, E., V. Hill, J. T. McCrone, A. Price, D. Jorgensen, A. O'Toole, J. Southgate, R. Johnson, B. Jackson, F. F. Nascimento, S. M. Rey, S. M. Nicholls, R. M. Colquhoun, A. da Silva Filipe, J. Shepherd, D. J. Pascall, R. Shah, N. Jesudason, K. Li, R. Jarrett, N. Pacchiarini, M. Bull, L. Geidelberg, I. Siveroni, C.-U. Consortium, I. Goodfellow, N. J. Loman, O. G. Pybus, D. L. Robertson, E. C. Thomson, A. Rambaut and T. R. Connor (2021): Evaluating the Effects of SARS-CoV-2 Spike Mutation D614G on Transmissibility and Pathogenicity.

Cell 184: 64-75 e11. DOI: 10.1016/j.cell.2020.11.020.

Von Holle, T. A. and M. A. Moody (2019):

Influenza and Antibody-Dependent Cellular Cytotoxicity.

Front Immunol 10: 1457. DOI: 10.3389/fimmu.2019.01457.

Vreede, F. T., T. E. Jung and G. G. Brownlee (2004):

Model suggesting that replication of influenza virus is regulated by stabilization of replicative intermediates.

J Virol 78: 9568-9572. DOI: 10.1128/JVI.78.17.9568-9572.2004.

Walsh, E. E., R. W. Frenck, Jr., A. R. Falsey, N. Kitchin, J. Absalon, A. Gurtman, S. Lockhart, K. Neuzil, M. J. Mulligan, R. Bailey, K. A. Swanson, P. Li, K. Koury, W. Kalina, D. Cooper, C. Fontes-Garfias, P. Y. Shi, O. Tureci, K. R. Tompkins, K. E. Lyke, V. Raabe, P. R. Dormitzer, K. U. Jansen, U. Sahin and W. C. Gruber (2020):

Safety and Immunogenicity of Two RNA-Based Covid-19 Vaccine Candidates.

N Engl J Med 383: 2439-2450. DOI: 10.1056/NEJMoa2027906.

Wang, J., M. Liu, N. Ding, Y. Li, J. Shao, M. Zhu, Z. Xie and K. Sun (2018):

Vaccine based on antibody-dependent cell-mediated cytotoxicity epitope on the H1N1 influenza virus increases mortality in vaccinated mice.

Biochem Biophys Res Commun 503: 1874-1879. DOI: 10.1016/j.bbrc.2018.07.129.

Wang, Q., C. Yang, L. Yin, J. Sun, W. Wang, H. Li, Z. Zhang, S. Chen, B. Liu, Z. Liu, L. Shi, X. Liu, S. Guan, C. Wang, L. Qu, Y. Feng, X. Niu, L. Feng, J. Zhao, P. Li, L. Chen and N. Zhong (2023):

Intranasal booster using an Omicron vaccine confers broad mucosal and systemic immunity against SARS-CoV-2 variants.

Signal Transduct Target Ther 8: 167. DOI: 10.1038/s41392-023-01423-6.

Wang, Z., X. Deng, W. Zou, J. F. Engelhardt, Z. Yan and J. Qiu (2017):

Human Bocavirus 1 Is a Novel Helper for Adeno-associated Virus Replication.

J Virol 91. DOI: 10.1128/JVI.00710-17.

Watanabe, H., K. Numata, T. Ito, K. Takagi and A. Matsukawa (2004):

Innate immune response in Th1- and Th2-dominant mouse strains.

Shock 22: 460-466. DOI: 10.1097/01.shk.0000142249.08135.e9.

Webster, R. G., W. J. Bean, O. T. Gorman, T. M. Chambers and Y. Kawaoka (1992):
Evolution and ecology of influenza A viruses.
Microbiol Rev 56: 152-179. DOI: 10.1128/mr.56.1.152-179.1992.

Weitzman, M. D. and R. M. Linden (2011):
Adeno-associated virus biology.
Methods Mol Biol 807: 1-23. DOI: 10.1007/978-1-61779-370-7_1.

WHO. (2022a, 09.09.2022).
Influenza Laboratory Surveillance Information.
Retrieved 25.08., 2023, from <https://app.powerbi.com/view?r=eyJrljoiZTZkyODcyOTEtZjA5YS00ZmI0LWFKZGZGUtODIxNGI5OTE3YjM0IiwidCI6ImY2MTBjMGI3LWJkMjQtNGIzOS04MTBiLTNkYzI4MGFmYjU5MCIslmMiOjh9>

WHO. (2022b, 11.08.2022).
Tracking SARS-CoV-2 variants.
Retrieved 25.08., 2023, from <https://www.who.int/en/activities/tracking-SARS-CoV-2-variants/>.

WHO. (2023a, 30.03.2023).
COVID-19 vaccine tracker and landscape.
Retrieved 25.08., 2023, from <https://www.who.int/publications/m/item/draft-landscape-of-covid-19-candidate-vaccines>.

WHO. (2023b).
Estimating disease burden of influenza.
Retrieved 25.08., 2023, from <https://www.who.int/europe/activities/estimating-disease-burden-of-influenza>.

WHO. (2023c).
WHO Coronavirus (COVID-19) Dashboard.
Retrieved 25.08., 2023, from <https://covid19.who.int/>.

WHO (2023d):
WHO press conference on COVID-19 and other global health issues - 26 April 2023.

Woo, P. C., S. K. Lau, C. M. Chu, K. H. Chan, H. W. Tsoi, Y. Huang, B. H. Wong, R. W. Poon, J. J. Cai, W. K. Luk, L. L. Poon, S. S. Wong, Y. Guan, J. S. Peiris and K. Y. Yuen (2005):
Characterization and complete genome sequence of a novel coronavirus, coronavirus HKU1, from patients with pneumonia.
J Virol 79: 884-895. DOI: 10.1128/JVI.79.2.884-895.2005.

Woodcock, J. M., B. Zacharakis, G. Plaetinck, C. J. Bagley, S. Qiyu, T. R. Hercus, J. Tavernier and A. F. Lopez (1994):
Three residues in the common beta chain of the human GM-CSF, IL-3 and IL-5 receptors are essential for GM-CSF and IL-5 but not IL-3 high affinity binding and interact with Glu21 of GM-CSF.
EMBO J 13: 5176-5185. DOI: 10.1002/j.1460-2075.1994.tb06848.x.

Wu, F., S. Luo, Y. Zhang and Y. O. Hairui Wang Zhaofei Guo Chunting He Shuting Bai Penghui He Min Jiang Xiaoyan Chen Guangsheng Du Xun Sun (2022):

Single-shot AAV-vectored vaccine against SARS-CoV-2 with fast and long-lasting immunity.

Acta Pharm Sin B. DOI: 10.1016/j.apsb.2022.07.004.

Wu, N. C. and I. A. Wilson (2018):

Structural insights into the design of novel anti-influenza therapies.

Nat Struct Mol Biol 25: 115-121. DOI: 10.1038/s41594-018-0025-9.

Wu, W. W. and N. Pante (2009):

The directionality of the nuclear transport of the influenza A genome is driven by selective exposure of nuclear localization sequences on nucleoprotein.

Virology 6: 68. DOI: 10.1186/1743-422X-6-68.

Wu, Y., Y. Wu, B. Tefsen, Y. Shi and G. F. Gao (2014):

Bat-derived influenza-like viruses H17N10 and H18N11.

Trends Microbiol 22: 183-191. DOI: 10.1016/j.tim.2014.01.010.

Wu, Z., A. Asokan and R. J. Samulski (2006):

Adeno-associated virus serotypes: vector toolkit for human gene therapy.

Mol Ther 14: 316-327. DOI: 10.1016/j.ymthe.2006.05.009.

Wu, Z., H. Yang and P. Colosi (2010):

Effect of genome size on AAV vector packaging.

Mol Ther 18: 80-86. DOI: 10.1038/mt.2009.255.

Xiao, P. J. and R. J. Samulski (2012):

Cytoplasmic trafficking, endosomal escape, and perinuclear accumulation of adeno-associated virus type 2 particles are facilitated by microtubule network.

J Virol 86: 10462-10473. DOI: 10.1128/JVI.00935-12.

Xiao, X. and D. S. Dimitrov (2004):

The SARS-CoV S glycoprotein.

Cell Mol Life Sci 61: 2428-2430. DOI: 10.1007/s00018-004-4257-y.

Xie, Y., E. Xu, B. Bowe and Z. Al-Aly (2022):

Long-term cardiovascular outcomes of COVID-19.

Nat Med 28: 583-590. DOI: 10.1038/s41591-022-01689-3.

Xin, K. Q., M. Urabe, J. Yang, K. Nomiya, H. Mizukami, K. Hamajima, H. Nomiya, T. Saito, M. Imai, J. Monahan, K. Okuda, K. Ozawa and K. Okuda (2001):

A novel recombinant adeno-associated virus vaccine induces a long-term humoral immune response to human immunodeficiency virus.

Hum Gene Ther 12: 1047-1061. DOI: 10.1089/104303401750214276.

Xu, L., L. Bao, W. Deng, H. Zhu, T. Chen, Q. Lv, F. Li, J. Yuan, Z. Xiang, K. Gao, Y. Xu, L. Huang, Y. Li, J. Liu, Y. Yao, P. Yu, W. Yong, Q. Wei, L. Zhang and C. Qin (2013):

The mouse and ferret models for studying the novel avian-origin human influenza A (H7N9) virus.

Virology 10: 253. DOI: 10.1186/1743-422X-10-253.

Xu, R., R. McBride, C. M. Nycholat, J. C. Paulson and I. A. Wilson (2012):

Structural characterization of the hemagglutinin receptor specificity from the 2009 H1N1 influenza pandemic.

J Virol 86: 982-990. DOI: 10.1128/JVI.06322-11.

- Yan, R., Y. Zhang, Y. Li, L. Xia, Y. Guo and Q. Zhou (2020):
Structural basis for the recognition of SARS-CoV-2 by full-length human ACE2.
Science 367: 1444-1448. DOI: 10.1126/science.abb2762.
- Yang, J., Y. Gong, C. Zhang, J. Sun, G. Wong, W. Shi, W. Liu, G. F. Gao and Y. Bi (2022):
Co-existence and co-infection of influenza A viruses and coronaviruses: Public health
challenges.
Innovation (Camb) 3: 100306. DOI: 10.1016/j.xinn.2022.100306.
- Yang, Y. T. and C. A. Evans (1961):
Hypothermia in mice due to influenza virus infection.
Proc Soc Exp Biol Med 108: 776-780. DOI: 10.3181/00379727-108-27064.
- Yang, Z. R., Y. W. Jiang, F. X. Li, D. Liu, T. F. Lin, Z. Y. Zhao, C. Wei, Q. Y. Jin, X. M. Li,
Y. X. Jia, F. C. Zhu, Z. Y. Yang, F. Sha, Z. J. Feng and J. L. Tang (2023):
Efficacy of SARS-CoV-2 vaccines and the dose-response relationship with three major
antibodies: a systematic review and meta-analysis of randomised controlled trials.
Lancet Microbe 4: e236-e246. DOI: 10.1016/S2666-5247(22)00390-1.
- Ye, Z. W., S. Yuan, K. M. Poon, L. Wen, D. Yang, Z. Sun, C. Li, M. Hu, H. Shuai, J. Zhou,
M. Y. Zhang, B. J. Zheng, H. Chu and K. Y. Yuen (2017):
Antibody-Dependent Cell-Mediated Cytotoxicity Epitopes on the Hemagglutinin Head
Region of Pandemic H1N1 Influenza Virus Play Detrimental Roles in H1N1-Infected Mice.
Front Immunol 8: 317. DOI: 10.3389/fimmu.2017.00317.
- Yin, W., Y. Xu, P. Xu, X. Cao, C. Wu, C. Gu, X. He, X. Wang, S. Huang, Q. Yuan, K. Wu,
W. Hu, Z. Huang, J. Liu, Z. Wang, F. Jia, K. Xia, P. Liu, X. Wang, B. Song, J. Zheng, H.
Jiang, X. Cheng, Y. Jiang, S. J. Deng and H. E. Xu (2022):
Structures of the Omicron spike trimer with ACE2 and an anti-Omicron antibody.
Science 375: 1048-1053. DOI: 10.1126/science.abn8863.
- Yoon, S. W., R. J. Webby and R. G. Webster (2014):
Evolution and ecology of influenza A viruses.
Curr Top Microbiol Immunol 385: 359-375. DOI: 10.1007/82_2014_396.
- Yurkovetskiy, L., X. Wang, K. E. Pascal, C. Tomkins-Tinch, T. P. Nyalile, Y. Wang, A. Baum,
W. E. Diehl, A. Dauphin, C. Carbone, K. Veinotte, S. B. Egri, S. F. Schaffner, J. E. Lemieux,
J. B. Munro, A. Rafique, A. Barve, P. C. Sabeti, C. A. Kyratsous, N. V. Dudkina, K. Shen
and J. Luban (2020):
Structural and Functional Analysis of the D614G SARS-CoV-2 Spike Protein Variant.
Cell 183: 739-751 e738. DOI: 10.1016/j.cell.2020.09.032.
- Zabaleta, N., U. Bhatt, C. Herate, P. Maisonnasse, J. Sanmiguel, C. Diop, S. Castore, R.
Estelien, D. Li, N. Dereuddre-Bosquet, M. Cavarelli, A. S. Gallouet, Q. Pascal, T. Naninck,
N. Kahlaoui, J. Lemaitre, F. Relouzat, G. Ronzitti, H. J. Thibaut, E. Montomoli, J. M. Wilson,
R. Le Grand and L. H. Vandenberghe (2022):
Durable immunogenicity, adaptation to emerging variants, and low-dose efficacy of an
AAV-based COVID-19 vaccine platform in macaques.
Mol Ther 30: 2952-2967. DOI: 10.1016/j.ymthe.2022.05.007.
- Zabaleta, N., W. Dai, U. Bhatt, C. Herate, P. Maisonnasse, J. A. Chichester, J. Sanmiguel,
R. Estelien, K. T. Michalson, C. Diop, D. Maciorowski, N. Dereuddre-Bosquet, M. Cavarelli,
A. S. Gallouet, T. Naninck, N. Kahlaoui, J. Lemaitre, W. Qi, E. Hudspeth, A. Cucalon, C.
D. Dyer, M. B. Pampera, J. J. Knox, R. C. LaRocque, R. C. Charles, D. Li, M. Kim, A.
Sheridan, N. Storm, R. I. Johnson, J. Feldman, B. M. Hauser, V. Contreras, R. Marlin, R.

H. Tsong Fang, C. Chapon, S. van der Werf, E. Zinn, A. Ryan, D. T. Kobayashi, R. Chauhan, M. McGlynn, E. T. Ryan, A. G. Schmidt, B. Price, A. Honko, A. Griffiths, S. Yaghmour, R. Hodge, M. R. Betts, M. W. Freeman, J. M. Wilson, R. Le Grand and L. H. Vandenberghe (2021):

An AAV-based, room-temperature-stable, single-dose COVID-19 vaccine provides durable immunogenicity and protection in non-human primates.

Cell Host Microbe 29: 1437-1453 e1438. DOI: 10.1016/j.chom.2021.08.002.

Zaki, A. M., S. van Boheemen, T. M. Bestebroer, A. D. Osterhaus and R. A. Fouchier (2012): Isolation of a novel coronavirus from a man with pneumonia in Saudi Arabia.

N Engl J Med 367: 1814-1820. DOI: 10.1056/NEJMoa1211721.

Zebedee, S. L. and R. A. Lamb (1988):

Influenza A virus M2 protein: monoclonal antibody restriction of virus growth and detection of M2 in virions.

J Virol 62: 2762-2772. DOI: 10.1128/JVI.62.8.2762-2772.1988.

Zhang, A., H. D. Stacey, M. R. D'Agostino, Y. Tugg, A. Marzok and M. S. Miller (2022):

Beyond neutralization: Fc-dependent antibody effector functions in SARS-CoV-2 infection.

Nat Rev Immunol: 1-16. DOI: 10.1038/s41577-022-00813-1.

Zhao, C. and J. Pu (2022):

Influence of Host Sialic Acid Receptors Structure on the Host Specificity of Influenza Viruses.

Viruses 14. DOI: 10.3390/v14102141.

Zhao, S., J. Ke, B. Yang, F. Tan, J. Yang, C. P. Lin, H. Wang and G. Zhong (2022):

A protective AAV vaccine for SARS-CoV-2.

Signal Transduct Target Ther 7: 310. DOI: 10.1038/s41392-022-01158-w.

Zheng, M., J. Luo and Z. Chen (2014):

Development of universal influenza vaccines based on influenza virus M and NP genes.

Infection 42: 251-262. DOI: 10.1007/s15010-013-0546-4.

Zhong, L., X. Zhou, Y. Li, K. Qing, X. Xiao, R. J. Samulski and A. Srivastava (2008):

Single-polarity recombinant adeno-associated virus 2 vector-mediated transgene expression in vitro and in vivo: mechanism of transduction.

Mol Ther 16: 290-295. DOI: 10.1038/sj.mt.6300376.

Zhou, P., X. L. Yang, X. G. Wang, B. Hu, L. Zhang, W. Zhang, H. R. Si, Y. Zhu, B. Li, C. L. Huang, H. D. Chen, J. Chen, Y. Luo, H. Guo, R. D. Jiang, M. Q. Liu, Y. Chen, X. R. Shen, X. Wang, X. S. Zheng, K. Zhao, Q. J. Chen, F. Deng, L. L. Liu, B. Yan, F. X. Zhan, Y. Y. Wang, G. F. Xiao and Z. L. Shi (2020a):

A pneumonia outbreak associated with a new coronavirus of probable bat origin.

Nature 579: 270-273. DOI: 10.1038/s41586-020-2012-7.

Zhou, R., K. K. To, Y. C. Wong, L. Liu, B. Zhou, X. Li, H. Huang, Y. Mo, T. Y. Luk, T. T. Lau, P. Yeung, W. M. Chan, A. K. Wu, K. C. Lung, O. T. Tsang, W. S. Leung, I. F. Hung, K. Y. Yuen and Z. Chen (2020b):

Acute SARS-CoV-2 Infection Impairs Dendritic Cell and T Cell Responses.

Immunity 53: 864-877 e865. DOI: 10.1016/j.immuni.2020.07.026.

Zhou, X., X. Zeng, Z. Fan, C. Li, T. McCown, R. J. Samulski and X. Xiao (2008):

Adeno-associated virus of a single-polarity DNA genome is capable of transduction in vivo.

Mol Ther 16: 494-499. DOI: 10.1038/sj.mt.6300397.

Zhu, N., D. Zhang, W. Wang, X. Li, B. Yang, J. Song, X. Zhao, B. Huang, W. Shi, R. Lu, P. Niu, F. Zhan, X. Ma, D. Wang, W. Xu, G. Wu, G. F. Gao, W. Tan, I. China Novel Coronavirus and T. Research (2020):

A Novel Coronavirus from Patients with Pneumonia in China, 2019.
N Engl J Med 382: 727-733. DOI: 10.1056/NEJMoa2001017.

Zhu, Z., E. Fodor and J. R. Keown (2023):

A structural understanding of influenza virus genome replication.
Trends Microbiol 31: 308-319. DOI: 10.1016/j.tim.2022.09.015.

Zinkernagel, R. M. and P. C. Doherty (1997):

The discovery of MHC restriction.
Immunol Today 18: 14-17. DOI: 10.1016/s0167-5699(97)80008-4.

Zohar, T. and G. Alter (2020):

Dissecting antibody-mediated protection against SARS-CoV-2.
Nat Rev Immunol 20: 392-394. DOI: 10.1038/s41577-020-0359-5.

Zost, S. J., K. Parkhouse, M. E. Gumina, K. Kim, S. Diaz Perez, P. C. Wilson, J. J. Treanor, A. J. Sant, S. Cobey and S. E. Hensley (2017):

Contemporary H3N2 influenza viruses have a glycosylation site that alters binding of antibodies elicited by egg-adapted vaccine strains.
Proc Natl Acad Sci U S A 114: 12578-12583. DOI: 10.1073/pnas.1712377114.

Zuallaert, J., F. Godin, M. Kim, A. Soete, Y. Saeys and W. De Neve (2018):

SpliceRover: interpretable convolutional neural networks for improved splice site prediction.
Bioinformatics 34: 4180-4188. DOI: 10.1093/bioinformatics/bty497.

Zuo, J., A. C. Dowell, H. Pearce, K. Verma, H. M. Long, J. Begum, F. Aiano, Z. Amin-Chowdhury, K. Hoschler, T. Brooks, S. Taylor, J. Hewson, B. Hallis, L. Stapley, R. Borrow, E. Linley, S. Ahmad, B. Parker, A. Horsley, G. Amirthalingam, K. Brown, M. E. Ramsay, S. Ladhani and P. Moss (2021):

Robust SARS-CoV-2-specific T cell immunity is maintained at 6 months following primary infection.
Nat Immunol 22: 620-626. DOI: 10.1038/s41590-021-00902-8.

9 Appendix

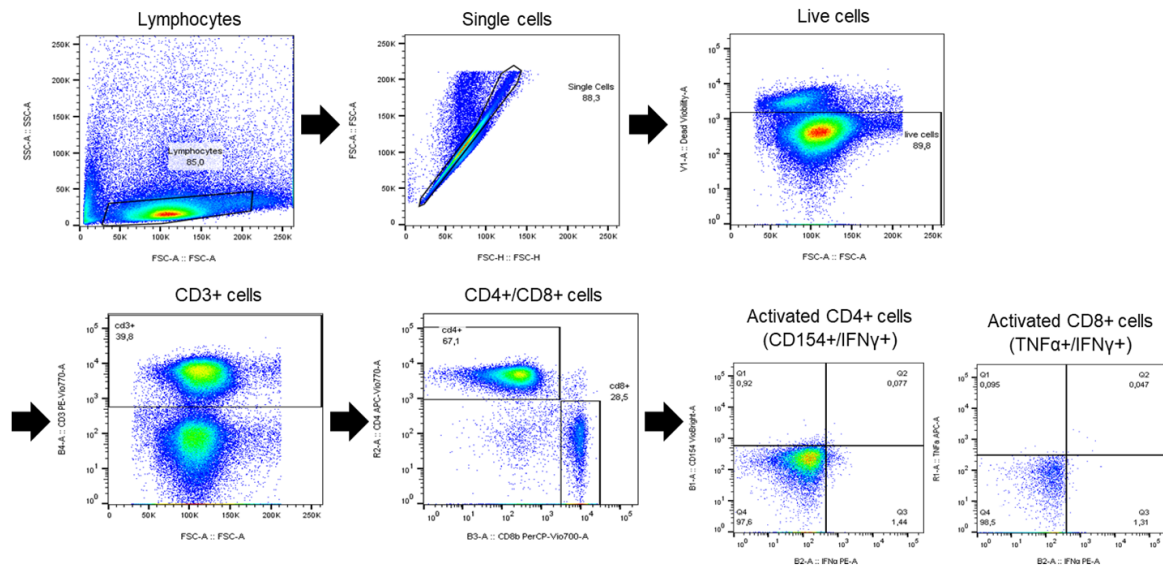


Figure 43: Gating strategy for intracellular cytokine staining for CD4 and CD8 T-cells
 For the intracellular cytokine staining, labelled splenocytes were gated as follows: first, the lymphocyte population was gated, then single cells and live cells. Live cells were gated for surface markers CD3, and the population was then separated into CD4⁺ and CD8⁺ cells. CD4 cells were analyzed for activation markers CD154 and IFN γ and CD8 cells for TNF α and IFN γ

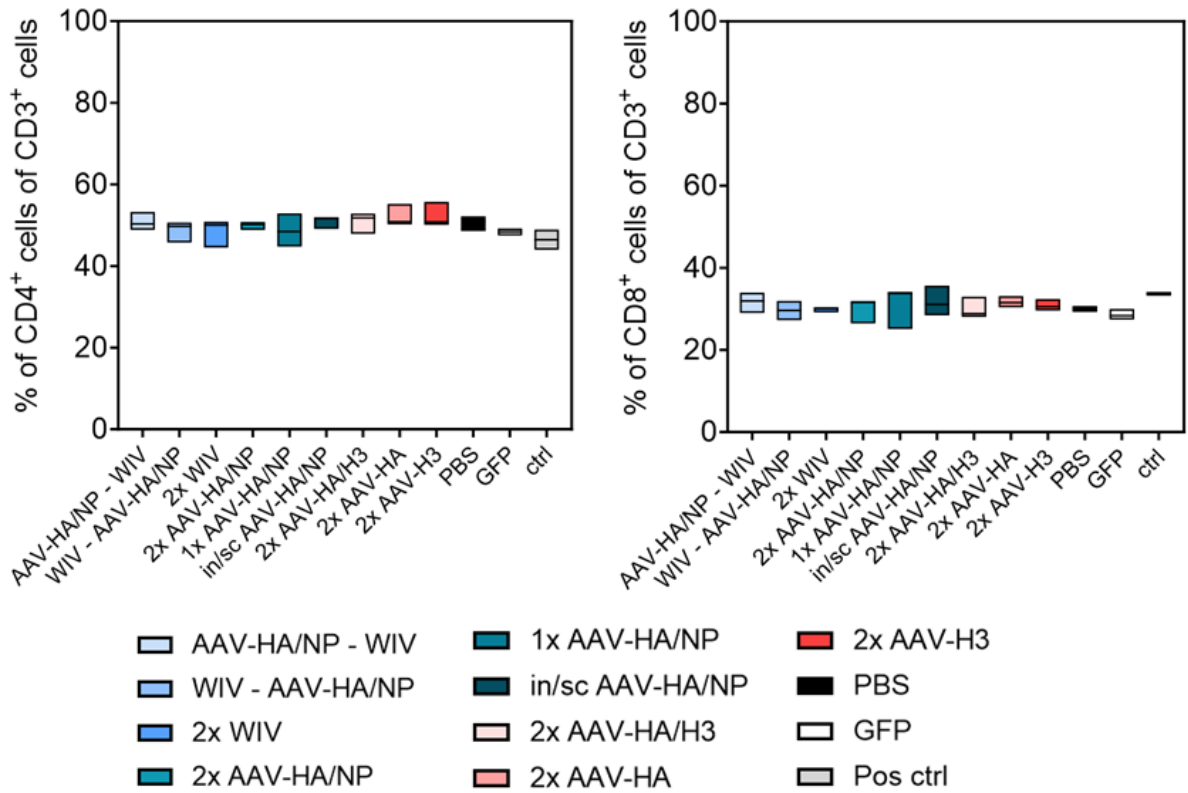


Figure 44: Fractions of CD4⁺ and CD8⁺ cells of CD3⁺ cells in mice immunized with influenza A antigens

Displayed are the fractions of CD4⁺ or CD8⁺ cells of CD3⁺ cells in the mice immunized with influenza A antigens.

Positions from 1 till 60
 Consensus sequence MKAILIVLLYFAAALGQDLPGNDNDADTLCIGYHANNSTDTVDTVLEKNVTVTHSVNLL
 CAA24269 A/Aichi/2/1968 (H3N2) -MKTII.A.S.I.CL.....STA...L.H..VNGTL.K.ITDDQIE..NATE.V
 ACP41953 A/California/07/2009 (H1N1)V...T..T.-----N.....
 BAR86308 A/Puerto Rico/8/1934 (H1N1) ...N.L...C.L.....I.....

Positions from 61 till 120
 Consensus sequence EDSHNGKLCCKNPHRILDGIAPHLGKCNIAGWLLGNPECDPLFPAESWSYIVETPKSDNG
 CAA24269 A/Aichi/2/1968 (H3N2) QS.ST..I.N.....D.TLIDA...D.H..-V.QN.T.DLF...RS.AFSN
 ACP41953 A/California/07/2009 (H1N1) ..K.....R.V.....I.....ES.ST.S.....S....
 BAR86308 A/Puerto Rico/8/1934 (H1N1)R-----K.....Q.....L.VR.....N.E..

Positions from 121 till 180
 Consensus sequence ICYPGDFIDYEELREQLSSVSSFERFEIFPKESSWPNHQNKGVTAACKHAGASSFYKNL
 CAA24269 A/Aichi/2/1968 (H3N2) -...Y.VP..AS...-L.A.SGTL.FITEGFT.TGVT...-GSN...RPG.G.FSR.
 ACP41953 A/California/07/2009 (H1N1) T.....T.....S.....P.....K.....
 BAR86308 A/Puerto Rico/8/1934 (H1N1)NT.-.....S.E.K....R..

Positions from 181 till 240
 Consensus sequence IWLTKKGGSPYPLKKSYPNDKKGKVLVWGIHHPSTSAEQQSPLYQNADAYVFGTSRYNK
 CAA24269 A/Aichi/2/1968 (H3N2) N...S.ST..V.NVTMP.NDNFDK.YI.....NQ..T...VQ.SGR.T.S.R.SQQ
 ACP41953 A/California/07/2009 (H1N1) ..V...N...S.....D.....S...S.
 BAR86308 A/Puerto Rico/8/1934 (H1N1) L...E.E.....N..V.K.....PN.K...N...EN...S.V..N..R

Positions from 241 till 300
 Consensus sequence KFIPEIAERPVKVRDQAGRMNYWTLVKPGDKIIFEANGNLIAPRYAFAMERGAGSGIIS
 CAA24269 A/Aichi/2/1968 (H3N2) T.I..N.GS..W..GLSS.ISI...I.....VLVINS.....GY.K.-TGR.S.MR.
 ACP41953 A/California/07/2009 (H1N1) ..K...I.....E.....T...T...V.....N.....
 BAR86308 A/Puerto Rico/8/1934 (H1N1) R.T.....L...T.....M...LS..F...T..

Positions from 301 till 360
 Consensus sequence DAPIHDCNTECQTPKGAJNSLFPQNIHPITIGACPKYVKSAKLRLATGLRNIPSIQSRG
 CAA24269 A/Aichi/2/1968 (H3N2) ...DT.IS..I..N.S.P.DK...VNK..Y.....QNT.K...M..V.EK.T..
 ACP41953 A/California/07/2009 (H1N1) .T.V...T.....T.....K.....T.....
 BAR86308 A/Puerto Rico/8/1934 (H1N1) N.SM.E...K...L...S...Y...V...E...R...MV.....

Positions from 361 till 420
 Consensus sequence LFGAIAGFIEGGWTGMIDGWYGYHHQNEQGSYAADLKSTQNAIDEITNKVNRVIEKME
 CAA24269 A/Aichi/2/1968 (H3N2)N...E.....FR...SE.T.Q.....A...Q.NG.L.....T..
 ACP41953 A/California/07/2009 (H1N1)V.....S.....T
 BAR86308 A/Puerto Rico/8/1934 (H1N1)Q.....NG.....T.....I

Positions from 421 till 480
 Consensus sequence QFTAVGKEFNELEKRIENLNKKVDDGFLDIWTYNAELVLLLENERTLDFHDSNVKNLYEK
 CAA24269 A/Aichi/2/1968 (H3N2) K.HQIE...S.V.G..QD.E.Y.E.TRI.L.S.....A...QH.I.LT..EMNK.F..
 ACP41953 A/California/07/2009 (H1N1)H.....Y.....
 BAR86308 A/Puerto Rico/8/1934 (H1N1)K...M.....

Positions from 481 till 540
 Consensus sequence VRSQLKNNAKEIGNGCFEFYHKCDNACMESVRNGTYDYPKYSEEAKLNREEIDGVKLESG
 CAA24269 A/Aichi/2/1968 (H3N2) T.R..RE..E.M.....KI.....I..I.....HDV.RD..LN..FQ.K..E.K..
 ACP41953 A/California/07/2009 (H1N1)T...K.....T
 BAR86308 A/Puerto Rico/8/1934 (H1N1) .K.....E.....S.....KV.....M

Positions from 541 till 581
 Consensus sequence GIYQILAIYSTVASSLVLVVSLGAI SFWMCSNGSLQCRICI
 CAA24269 A/Aichi/2/1968 (H3N2) YKDW..W.SFAISCF.LC..L..F.-M.A.QR.NIR.N...
 ACP41953 A/California/07/2009 (H1N1) R.....
 BAR86308 A/Puerto Rico/8/1934 (H1N1)L.....

Figure 45: Hemagglutinin amino acid sequences of influenza A viruses H1N1 Cal/7/09pdm and PR8 and H3N2 Aichi/2/1968

Amino acid sequence comparison of the hemagglutinin (HA) protein of the H1N1 influenza A viruses (IAV) Cal/7/09pdm and PR8 and the H3N2 IAV Aichi/2/1968 from the influenza virus database by NCBI (Bao et al. 2008; NCBI 2023).

```

Positions from 1 till 60
  Consensus sequence      MASQGTKRSYEQMETDGERQNATEIRASVGMIGGIGRFYIQMCTELKLSDEYEGRLIQNS
AFM71861 A/Aichi/2/1968 (H3N2) .....D.....
AGI52470 A/California/08/2009 (H1N1) .....G.....D.....R.....D.....
AGR63055 A/Puerto Rico/8/1934 (H1N1) .....

Positions from 61 till 120
  Consensus sequence      LTIERMVLSAFDERRNKYLEEHPISAGKDKPKKTGGPIYRRVDGKWMRELILYDKEEIRRIW
AFM71861 A/Aichi/2/1968 (H3N2) .....K.....R.....V.....
AGI52470 A/California/08/2009 (H1N1) I.....V.....
AGR63055 A/Puerto Rico/8/1934 (H1N1) .....N.....

Positions from 121 till 180
  Consensus sequence      RQANNDDATAGLTHMMIWHSNLNDATYQTRALVRTGMDPRMCSLMQGSTLPRRSGAAG
AFM71861 A/Aichi/2/1968 (H3N2) .....T.....
AGI52470 A/California/08/2009 (H1N1) .....E.....I.....
AGR63055 A/Puerto Rico/8/1934 (H1N1) .....

Positions from 181 till 240
  Consensus sequence      AAVKGVGTMVMELIRMIKRGINDRNFWRGENGRKTRIAAYERMCNILKGFQTAAQRAMMD
AFM71861 A/Aichi/2/1968 (H3N2) .....S.....
AGI52470 A/California/08/2009 (H1N1) .....IA.....R.....V.....
AGR63055 A/Puerto Rico/8/1934 (H1N1) .....V.....K.....

Positions from 241 till 300
  Consensus sequence      QVRESRNPNGAEIEDLIFLARSALILRGSVAHKSCLPACVYGPVAVASGYDFEREGYSLVG
AFM71861 A/Aichi/2/1968 (H3N2) .....K.....
AGI52470 A/California/08/2009 (H1N1) .....L.....H.....
AGR63055 A/Puerto Rico/8/1934 (H1N1) .....F.....T.....

Positions from 301 till 360
  Consensus sequence      IDPFKLLQNSQVYSLIRPNENPAHKSQLVWMACHSAAFEDLRVLSFIRGCTKVI PRGKLS
AFM71861 A/Aichi/2/1968 (H3N2) .....N.....S.....
AGI52470 A/California/08/2009 (H1N1) .....V.....M.....S.....K.....
AGR63055 A/Puerto Rico/8/1934 (H1N1) .....R.....K.....L.....

Positions from 361 till 420
  Consensus sequence      RGVQIASNENMETMESSTLELRSRYWAIRTRSGGNTNQQRASAGQISVQPTFSVQRNLFP
AFM71861 A/Aichi/2/1968 (H3N2) .....DA.....A.....
AGI52470 A/California/08/2009 (H1N1) .....V.....N.....N.....K.....
AGR63055 A/Puerto Rico/8/1934 (H1N1) .....I.....

Positions from 421 till 480
  Consensus sequence      DRATIMAAFNGNTEGRTSDMRTEIIRMMESAKPEDLSFQGRGVFELSDEKAANPIVPSFD
AFM71861 A/Aichi/2/1968 (H3N2) .KP.....T.....A.....G.....EM.....R.....
AGI52470 A/California/08/2009 (H1N1) E...V...S...N...V...T...
AGR63055 A/Puerto Rico/8/1934 (H1N1) ..T.....R.....V.....S.....

Positions from 481 till 498
  Consensus sequence      MSNEGSYFFGDNAEEYDN
AFM71861 A/Aichi/2/1968 (H3N2) .....
AGI52470 A/California/08/2009 (H1N1) .....S
AGR63055 A/Puerto Rico/8/1934 (H1N1) .....

```

Figure 46: Nucleoprotein amino acid sequences of influenza A viruses H1N1 Cal/7/09pdm and PR8 and H3N2 Aichi/2/1968

Amino acid sequence comparison of the nucleoprotein (NP) protein of the H1N1 influenza A viruses (IAV) Cal/7/09pdm and PR8 and the H3N2 IAV Aichi/2/1968 from the influenza virus database by NCBI (Bao et al. 2008; NCBI 2023).

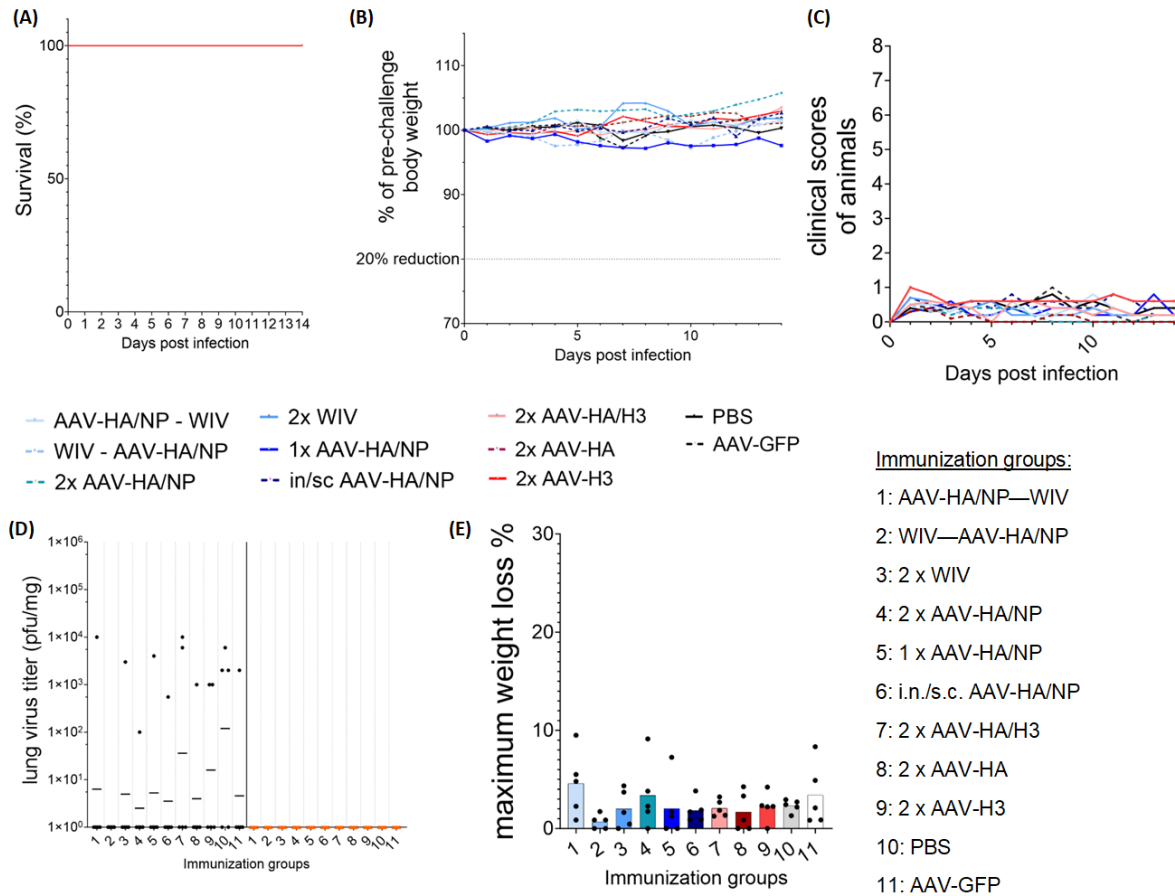


Figure 47: Data on first PR8 challenge

Data on PR8 challenges were summarized in Figure 27, Figure 28, and Figure 29. Displayed here are the separate data of the first PR8 challenge with 8×10^1 pfu/mouse **(A)** Kaplan-Meier plot **(B)** relative weight loss **(C)** clinical score development **(D)** lung viral titers at 3 days post infection (black) or the respective end point of the animal (orange) **(E)** maximum weight loss

(A): Mantel-Cox test analysis, groups compared to control groups; (B): mean body weight of individual animals in one group relative to the pre-challenge body weight \pm SD; (E): symbols represent individual animals, bars: mean; (D): geometric mean, symbols represent individual animals, black: 3 days post infection, orange: individual end point or 14 days post infection; (C): mean of daily clinical scores of individual animals in the groups.

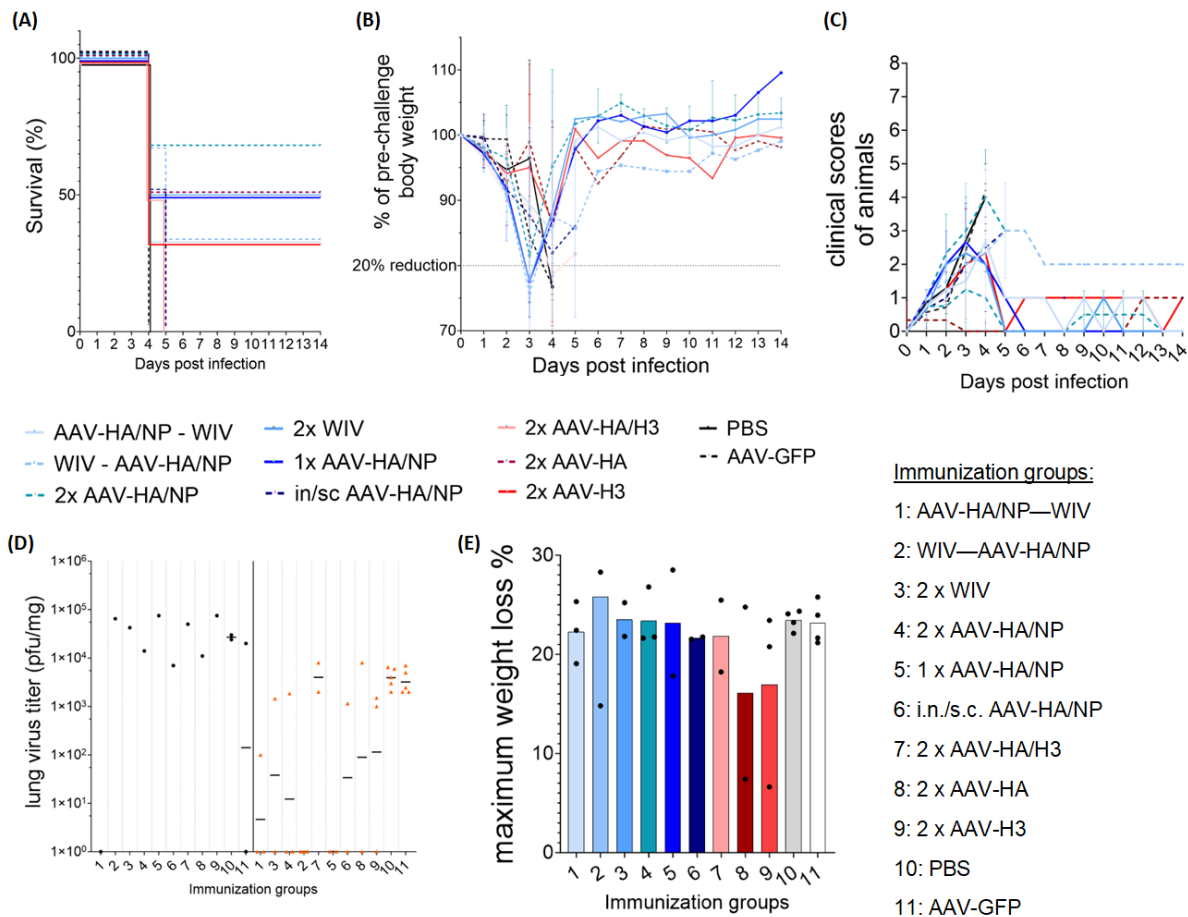


Figure 48: Data on second PR8 challenge

Data on PR8 challenges were summarized in Figure 27, Figure 28, and Figure 29. Displayed here are the separate data of the first PR8 challenge with 5×10^2 pfu/mouse

(A) Kaplan-Meier plot **(B)** relative weight loss **(C)** clinical score development **(D)** lung viral titers at 3 days post infection (black) or the respective end point of the animal (orange) **(E)** maximum weight loss

(A): Mantel-Cox test analysis, groups compared to control groups; (B): mean body weight of individual animals in one group relative to the pre-challenge body weight \pm SD; (E): symbols represent individual animals, bars: mean; (D): geometric mean, symbols represent individual animals, black: 3 days post infection, orange: individual end point or 14 days post infection; (C): mean of daily clinical scores of individual animals in the groups.

10 List of Publications

10.1 Oral Presentations

- **Stelzer S**, Krüger M, Meyer T, Dorner BG, Dorner MB, Wolff T (30.09.2020) Design and immunogenicity evaluation of Adeno-associated virus (AAV) – vectors containing the SARS-CoV-2 receptor-binding domain (S-RBD). *Robert Koch Conference*, Berlin, Germany (virtual meeting)
- **Stelzer S**, Krüger M, Meyer T, Dorner BG, Dorner MB, Wolff T (30.10.2020) Design and immunogenicity evaluation of Adeno-associated virus (AAV) – vectors containing the SARS-CoV-2 receptor-binding domain (S-RBD). *19th Workshop of the Study Group “Immunobiology of Viral Infections” of the Society for Virology (GfV)*, virtual meeting
- **Stelzer S**, Krüger M, Meyer T, Dorner BG, Dorner MB, Wolff T (28.10.2021) Design and immunogenicity evaluation of Adeno-associated virus (AAV) – vectors containing the SARS-CoV-2 receptor-binding domain (S-RBD). *Robert Koch Conference*, Berlin, Germany (virtual meeting)

10.2 Poster Presentations

- **Stelzer S**, Krüger M, Meyer T, Dorner BG, Dorner MB, Wolff T (15./16.10.2020) Design and immunogenicity evaluation of Adeno-associated virus (AAV) – vectors containing the SARS-CoV-2 receptor-binding domain (S-RBD). *Zoonoses 2020 - International Symposium on Zoonoses Research*, virtual meeting
- **Stelzer S**, Krüger M, Meyer T, Dorner BG, Dorner MB, Wolff T (24.-26.03.2021) Design and immunogenicity evaluation of Adeno-associated virus (AAV) – vectors containing the SARS-CoV-2 receptor-binding domain (S-RBD). *30th Annual Meeting of the Society for Virology*, virtual meeting
- **Stelzer S**, Krüger M, Meyer T, Dorner BG, Dorner MB, Wolff T (13.10.2021) Design and immunogenicity evaluation of Adeno-associated virus (AAV) – vectors containing the SARS-CoV-2 receptor-binding domain (S-RBD). *Autumn School of the German Society for Immunology*, Merseburg, Germany

11 Acknowledgements/Danksagung

Mein besonderer Dank gilt PD Dr. Thorsten Wolff für die Überlassung des spannenden Themas für diese Dissertation. Ohne es zu Beginn zu wissen, wurde es mir ermöglicht, im Rahmen der Pandemie an einem solch wichtigen Aspekt der letzten Jahre zu arbeiten. Ich bedanke mich für die Möglichkeiten, die mir eröffnet wurden und für die Betreuung, sowie die fachlichen Diskussionen.

Weiterhin möchte ich Prof. Dr. Gruber für die Betreuung der Promotion von Seiten des Fachbereichs Veterinärmedizin der Freien Universität Berlin herzlich danken.

Dem Tierpflege-Team des RKI spreche ich meinen großen Dank aus, ohne dessen Arbeit diese Arbeit nicht möglich gewesen wäre. Besonders möchte ich Jenny danken, die selbst an Wochenend- und Feiertagsterminen jederzeit bereitstand, mir bei den aufwändigen Arbeiten im Tierhaus zu helfen. Ohne deinen Einsatz wäre vieles so nicht möglich gewesen! Annette Dietrich möchte ich für ihre große Unterstützung bei der Planung und Durchführung meiner Arbeiten danken. Last but not least möchte ich mich auch bei den Mäusen, die in dieser Arbeit eingesetzt wurden, bedanken.

Nancy danke ich dafür, dass sie stets ein offenes Ohr für meine Fragen hatte, und mir immer so ausführlich und geduldig geholfen und mich unterstützt hat.

Den RKI Kolleg*innen Maren Krüger, Tanja Meyer und Brigitte und Martin Dorner aus ZBS3 danke ich für die Unterstützung bei den ersten Immunisierungsexperimenten mit dem AAV-S-RBD Vektor und der Durchführung des Multiplex Assays. Lars Möller aus ZBS4 danke ich für die EM-Bilder.

Meinen Kolleg*innen aus FG17 danke ich für die gemeinsame Zeit, auch wenn die Pandemie gemeinsame Aktivitäten sehr eingeschränkt hat. Danke trotzdem, für die schöne gemeinsame Zeit. Besonders möchte ich mich bei Gudrun bedanken. Ohne deine immerwährende Unterstützung bei allen Angelegenheiten hätte ich oft nicht gewusst, was zu tun ist! Danke für dein immer offenes Ohr! Christin und Jessi, sowie auch Marlina, Barbara, Jean-Marc und Matthias möchte ich für die Unterstützung im Labor und für die vielen netten Gespräche danken, die auch zu manch einem Denkanstoß geführt haben.

Mein grenzenloser Dank gilt meiner Familie, die mich immer in allen meinen Wünschen und Unternehmungen unterstützt hat, egal wie unkonventionell eine Idee grade mal wieder war. Ihr habt mir immer zu verstehen gegeben, dass ich alles erreichen kann, was ich will und dass nur ich selbst mir Grenzen setzen kann. Ohne euch wäre ich nicht da, wo ich nun bin. Wie gerne hätte ich dies noch mit dir, Papa, geteilt!

Der wichtigste Mensch in diesen letzten Jahren war und ist mein Uwe. Ich danke dir so sehr dafür, dass du immer an meiner Seite warst, alles ausgehalten und mich immer unterstützt hast! Du bist mein größter Cheerleader! Ohne dich wäre ich so viel öfter an meine Grenzen gestoßen und hätte meine Motivation schwerer wiedergefunden. Danke, dass du da bist!

12 Funding Sources

The project and all resources, including the funding for the doctoral student, were financed by the Robert Koch Institute.

13 Conflict of Interest

In the context of this work, there are no conflicts of interest due to contributions from third parties.

14 Rights and permissions

Licenses for figures from other publications:

Figure 2: 5612601141984 (Elsevier license, date: August 19th, 2023)

Figure 3: 5612610384597 (Springer Nature license, date: August 19th, 2023)

Figure 4 A: 5612610614593 (Springer Nature license, date: August 19th, 2023)

Figure 4 B + C: allowed to use for non-commercial purposes (such as scientific publications; see reference)

Figure 6: 5612610769987 (Springer Nature license, date: August 19th, 2023)

Table 2: CC BY 4.0, the original table was cut behind the description of subunit 1

Figure 9: CC BY 4.0 with attribution to nextstrain.org

Figure 10: CC BY 4.0

Figure 14: 5612620195053 (Elsevier license, date: August 19th, 2023)

Figure 42: CC0 1.0 DEED from outbreak.info

Provided license numbers for the reuse of figures from original publications in figures 2, 3, 4 A, 6 and 14 have been provided by the respective publishers and are only valid for their use in this dissertation.

The CC BY 4.0 license is a creative commons license, which allows to copy and redistribute, as well as to remix or transform the material, as long as the appropriate attributions are provided, and changes have been indicated. The CC0 1.0 DEED license indicates that the work has been dedicated to the public domain and can be used and modified without permission. More information is provided under the following link: <https://creativecommons.org/licenses>.

15 Declaration of independence

I hereby certify that I have prepared this thesis independently. I assure that I have used only the sources and aids indicated.

Intellectual property of other authors has been marked accordingly. I also declare that I have not applied for an examination procedure at any other institution and that I have not submitted the dissertation in this or any other form to any other faculty as a dissertation.

Berlin, 10.04.2024

Sandra Stelzer